# Defining the neural correlates of pain and analgesia in health and disease

Melvin Nnanyelu Mezue

St Hugh's College & Nuffield Department of Clinical Neurosciences

University of Oxford

A thesis submitted in partial fulfilment for the degree of

*Doctor of Philosophy*

Trinity Term 2013

# Defining the neural correlates of pain and analgesia in health and disease

**Melvin Nnanyelu Mezue**

*St Hugh's College, University of Oxford*

A thesis submitted in partial fulfilment for the degree of Doctor of Philosophy

Trinity Term 2013

## Abstract

Chronic neuropathic pain affects up to 8% of the United Kingdom population and is a difficult condition to manage. It is established and maintained through many mechanisms, including central sensitisation (CS) in the spinal cord and brainstem. Neuropathic pain manifests as spontaneous pain, sensory loss and evoked hypersensitivity. The development of novel treatments for neuropathic pain is challenging, in part due to inadequate experimental models of clinically relevant pain. The use of functional magnetic resonance imaging (fMRI) techniques for imaging acute and increasingly tonic states enables the assessment of the neural correlates of evoked hypersensitivity and persistent pain, with the goal of developing appropriate biomarkers to test new therapies. This thesis develops novel techniques for the assessment of ongoing pain states and their modulation by therapies.

We first identified a suitable human experimental model of CS using topical capsaicin, and an fMRI pipeline for the investigation of supraspinal involvement in pain hypersensitivity. In a placebo-controlled study, we then demonstrated the improved sensitivity of fMRI above subjective reports in detecting the efficacy of a known analgesic as compared to an ineffective active compound in a small cohort. To translate this to the more clinically relevant symptom of spontaneous pain, we developed and validated the use of a multi-inversion time pseudo-continuous arterial spin labelling (ASL) imaging and analysis pipeline for the neural assessment of tonic states and the absolute quantification of cerebral blood flow (CBF).

Current evidence from structural and functional studies suggests a direct role for the posterior insula cortex in the encoding of nociception and pain. Using the ASL pipeline, we found that only a CBF change in the posterior insula region was correlated with the changing perception of persistent capsaicin-induced pain, and in a separate experiment showed that suppression of CBF in this region by gabapentin was related to the drug's suppression of subjective pain perception. We also demonstrated in a cohort of phantom limb patients that pain relief resulting from transcranial direct current stimulation of the deprived sensorimotor cortex is neurally represented by a decrease in posterior insula CBF.

In a separate study, we showed that baseline CBF in the periaqueductal grey can predict individuals who are most vulnerable to pain and hypersensitivity following the induction of capsaicin-related CS.

Taken together, these findings suggest that fMRI can be used as a tool to assess the efficacy of established and novel analgesics, with the midbrain reticular formation and posterior insula cortex being prime candidates as biomarkers of CS mechanisms and persistent pain respectively. Relatedly, ASL-fMRI may also be an effective technique for evaluating individuals' susceptibility to pain following inflammation or injury.

# Acknowledgements

I've left this until the very end because it is the most important section of the thesis and has allowed me to reflect back on the relationships that have made these past three years so fulfilling and enjoyable.

I thank the Almighty for guiding and protecting me through my journey thus far.

To Irene Tracey, it's hard to ask for a better role model, as an individual, scientist and supervisor. Thank you for teaching me to love research, and for believing in an unproven medical student.

I greatly appreciate the support of many wonderful scientists without whom I would still be learning how to pronounce FMRIB:

To Jon Brooks for teaching me to use UNIX and guiding me through my first experiments.

To Vishvarani Wanigasekera, without whom a large part of the work in this thesis would not have been possible; thank you for teaching me to be thorough and meticulous in my approach.

To Tamar Makin, who as well as being a worryingly insightful scientist, reminds me daily of the importance of speaking one's mind.

To Falk Eippert, who has been a great friend and is probably the most humble yet brilliant researcher I know.

To Andy Segerdahl, for being a great colleague and friend.

To Tom Okell, Mike Kelly, Michael Chappell, Stuart Clare, Yazhuo Kong, Eugene Duff and Charlie Stagg whose patient support with technical matters was invaluable.

To all my other amazing collaborators, especially Anushka Soni, Sanne Kikkert, and John Farrar.

To colleagues and mentors in the LPC, thank you for your support, both scientifically and financially. And to the Wellcome Trust, for funding my time in Oxford.

To all the great friendships formed within FMRIB, through football and beyond. Thank you all for making this a memorable experience.

To SS, without whose foresight and forwarded email I would never have started a DPhil.

Lastly, to my parents Angela and Wilfred for your immeasurable sacrifices. And to my brother Bryan, and sisters Phyllis and Pamela. Thank you for setting the bar and believing in me to reach it.

# Contents

# List of Abbreviations

| | |
|---|---|
| **AAT** | Arterial Arrival Time |
| **ACC** | Anterior Cingulate Cortex |
| **ANOVA** | Analysis of Variance |
| **ASL** | Arterial Spin Labelling |
| **BBR** | Boundary Based Registration |
| **BET** | Brain Extraction Tool |
| **BOLD** | Blood Oxygenation Level Dependent |
| **CASL** | Continuous Arterial Spin Labelling |
| **CBF** | Cerebral Blood Flow |
| **CNS** | Central Nervous System |
| **CS** | Central Sensitisation |
| **CSF** | Cerebrospinal Fluid |
| **DLPFC** | Dorsolateral Prefrontal Cortex |
| **DMA** | Dynamic Mechanical Allodynia |
| **dPIN** | Dorsal Posterior Insula Cortex |
| **DPMS** | Descending Pain Modulatory System |
| **EEG** | Electroencephalography |
| **EPI** | Echo Planar Imaging |
| **FAST** | FMRIB Automated Segmentation Tool |
| **FEAT** | FMRIB Expert Analysis Tool |
| **FICCS** | FMRI in conjunction with a CS model |
| **FLIRT** | FMRIB Linear Registration Tool |
| **FMRI** | Functional Magnetic Resonance Imaging |
| **FNIRT** | FMRIB Non-linear Registration Tool |
| **FOV** | Field of View |
| **FSL** | FMRIB Software Library |
| **GABA** | $\gamma$-Amino Butyric Acid |
| **GLM** | General Linear Modelling |
| **GRAPPA** | Generalised Autocalibrating Partially Parallel Acquisition |
| **HRF** | Haemodynamic Response Function |
| **ICC** | Intraclass Correlation Coefficient |
| **M1** | Primary Motor Cortex |
| **MNI** | Montreal Neurological Institute |
| **MPFC** | Medial Prefrontal Cortex |
| **MRF** | Mesencephalic Reticular Formation |
| **MT** | Magnetisation Transfer |

| | |
|---|---|
| **NCF** | Nucleus Cuneiformis |
| **NRS** | Numerical Rating Scale |
| **NSAID** | Non-Steroidal Anti Inflammatory Drug |
| **OFC** | Orbitofrontal Cortex |
| **OGP** | Ongoing Pain |
| **PAG** | Periaqueductal Grey |
| **pASL** | Pulsed Arterial Spin Labelling |
| **pCASL** | Pseudo-continuous Arterial Spin Labelling |
| **PET** | Positron Emission Tomography |
| **PLD** | Post Labelling Delay |
| **PLP** | Phantom Limb Pain |
| **PNM** | Physiological Noise Modelling |
| **rAIN** | Rostral Anterior Insula Cortex |
| **RETROICOR** | Retrospective Image Correction |
| **RF** | Radiofrequency |
| **ROI** | Region of Interest |
| **RVM** | Rostral Ventromedial Medulla |
| **SD** | Standard Deviation |
| **SEM** | Standard Error of the Mean |
| **SI** | Primary Somatosensory Cortex |
| **SII** | Secondary Somatosensory Cortex |
| **SMA** | Supplementary Motor Area |
| **SMPH** | Secondary Mechanical Punctate Hyperalgesia |
| **SNR** | Signal to Noise Ratio |
| **SSNRI** | Selective Reuptake Inhibitors of Serotonin and Noradrenaline |
| **STT** | Spinothalamic Tract |
| **TCA** | Tricyclic Antidepressants |
| **TDCS** | Transcranial Direct Current Stimulation |
| **TE** | Echo Time |
| **TI** | Inversion Time |
| **TR** | Repetition Time |
| **TRPV** | Transient Receptor Potential Vanilloid |
| **TSNR** | Temporal Signal to Noise Ratio |
| **VAS** | Visual Analogue Scale |
| **WDR** | Wide Dynamic Range |
| **wsCV** | Within Subject Coefficient of Variation |
| **V1** | Primary Visual Cortex |
| **VLPFC** | Ventrolateral Prefrontal Cortex |

# List of Figures

# List of Tables

# Chapter 1

# Introduction

## 1.1 Motivation

Chronic pain, which is defined by the International Association for the Study of Pain (IASP) as pain persisting beyond 3 months (IASP, 1986), is a major health issue affecting up to 20% of the adult population (Breivik et al., 2006). As a result, the financial implications on economic output in the developed world are vast- estimated at $635 billion annually in the USA alone (Institute of Medicine, 2011). Underlying these figures is the difficulty in managing chronic pain conditions. In particular, neuropathic pain, defined as pain caused by a lesion or disease to the somatosensory system (Jensen et al., 2011), can be more difficult to treat than other types of pain (McQuay, 2002).

Research into the neurobiological factors underlying the pain experience has increased in the past few decades. Due to limitations in investigative methods, most such work has been in non-primates, which lack analogous higher cortical structures to primates, and in which the inherently subjective pain experience is difficult to measure. Nonetheless these preclinical studies have generated a rich literature defining the pathway of pain perception from the peripherally encoding neurons (nociceptors) to the cortex. Over the past two decades, the development of non-invasive neuroimaging methods has propelled

the investigation of central pain mechanisms in man. Although inferences from such data can be challenging, it has enabled the assessment of pain states more comparable to the clinical condition and now allows us to examine the endogenous and exogenous modulation of pain processing, in view of developing better treatments. In this section we will review the literature on pain neurophysiology, as is pertinent to the development and management of neuropathic pain.

## 1.2 From nociception to pain

IASP define pain as "an unpleasant sensory and emotional experience associated with actual or potential tissue damage, or described in terms of such damage". Nociception is defined as "the neural process of encoding noxious stimuli" (IASP, 2011). As indicated by these descriptions, there can be a disparity between peripheral nociceptive inputs triggered by tissue damage, and the perception of pain. Thus, pain is a conscious experience, which often but does not always arise from nociception. This thesis will largely focus on pain that is ongoing and consequential to external peripheral noxious stimulation. We begin by defining the processes by which nociceptive inputs are encoded, transmitted, perceived and modulated by the nervous system.

### 1.2.1 Peripheral encoding

Signal transduction begins with noxious stimulation at the nociceptor (Sherrington, 1906). These primary sensory neurons can be classified by their response characteristics, modality sensitivities and receptor profiles. Nociceptors innervating somatic and visceral structures can be high-threshold mechano-receptors or polymodal nociceptors (Steeds, 2009). Mechanoreceptors respond to pressure, vibration and touch, while polymodal nociceptors respond to temperature and chemical stimuli (including endogenous

ligands such as substance P and bradykinin). Some polymodal nociceptors respond to irritants such as capsaicin and to heat via specific sensors in the Transient Receptor Potential Vanilloid (TRPV) receptor family (Caterina et al., 1999, 1997).

### 1.2.2 Signal transmission

Signal transmission occurs from the periphery to the spinal cord, from the spinal cord to the brainstem and subcortical structures, and finally on to cortical structures.

Two main nociceptor classes are thinly myelinated A fibres and the more common unmyelinated C-fibres (Millan, 1999; Ringkamp et al., 2013). A$\delta$ fibres are intermediate conducting (>2m/s) and are functionally subdivided into types I and II based on their thermal response thresholds (Ringkamp et al., 2013). Type I fibres are mechano-heat-sensitive with high heat thresholds (>53°C) to short stimuli, while type II fibres are largely mechanically insensitive and have lower heat thresholds (39-41°C). These fibres depolarize rapidly to elicit a brief, sharp and well-localised 'first pain' response, which serves as an immediate warning signal. C-fibres are slow conducting (<2m/s) and mediate a diffuse and maintained burning sensation in a 'second pain' response, which alerts the body to persisting threats. C-fibres can be subdivided into peptidergic nociceptors (which express substance P, calcitonin gene-related peptide and tyrosine kinase A receptors, and have cutaneous and visceral targets) and non-peptidergic nociceptors (which bind to lectin IB4 and mainly innervate the epidermis of the skin) (Hunt and Rossi, 1985; Snider and McMahon, 1998; Taylor et al., 2009). Noxious stimulation at the peripheral terminal of the nociceptor leads to depolarisation of these neurons. However, in man, pain thresholds are higher than the activation thresholds for individual nociceptors, suggesting an important role for central mechanisms of spatial and temporal summation in pain signalling (Millan, 1999).

### 1.2.3 Spinal cord

Peripheral nociceptors have their cell bodies in the dorsal root ganglion and differentially synapse at the dorsal horn of the spinal cord via central terminals. A$\delta$ fibres terminate in laminas I, V and VI while C-fibres synapse in laminas I, II and V of the dorsal horn (Millan, 1999; Price et al., 2003). Peptidergic C-fibres largely terminate more superficially, synapsing with lamina I neurons and interneurons in outer lamina II, while non-peptidergic nociceptors synapse with interneurons in the inner aspect of lamina II (Snider and McMahon, 1998). This disparity in fibre distribution may reflect a difference in the functions of these nociceptor subclasses (Todd, 2010). This view is supported by a recent study suggesting a double dissociation in modality-specific thermal or mechanical nocifensive responses between distinct C-fibre populations (Cavanaugh et al., 2009).

At this first synapse within the central nervous system (CNS), nociceptors terminate on spinal projection neurons, via complex circuits involving excitatory and inhibitory interneurons (Todd, 2010). Second-order projection neurons are characterised by their electrophysiological responses to cutaneous stimuli into wide dynamic range (WDR) neurons or nociceptive specific (NS) neurons (Price et al., 2003). WDR neurons form the majority of nociceptive neurons in deep layers of the dorsal horn. They respond to a broad range of stimulus intensities in a highly discriminative manner and also receive synaptic input from the large diameter mechanoreceptive A$\beta$ primary afferent neurons (Price et al., 2003). NS neurons are present in both superficial and deep layers, have a small receptive field, and respond predominantly to high threshold noxious stimuli.

Plasticity at the level of the spinal cord is thought to be the crucial central mechanism of post-injury pain hypersensitivity (see below). Projection neurons expressing neurokinin (NK-1) receptors are necessary for the increased response to noxious stimulation (hyperalgesia) seen in neuropathic injury, however their role may not be related to the action

of substance P on these receptors (Hill, 2000).

### 1.2.4 Ascending nociceptive pathways

Multiple ascending tracts relay nociceptive input from the dorsal horn to supraspinal structures (Dostrovsky and Craig, 2013). These include: direct projections to the thalamus (via the spinothalamic tract [STT] and trigeminothalamic tract); direct projections to homeostatic control regions in the medulla and brainstem (via spinomedullary and spinobulbar projections), possible direct projections to the hypothalamus and ventral forebrain (via the spinohypothalamic tract [SHT]); and indirect pathways to the forebrain through the brainstem (via the post-synaptic dorsal column system and the spinocervicothalamic pathways).

The STT is the most studied pathway and is thought to be most closely associated with pain (Craig, 2003; Willis, 1985). It originates from three distinct regions in the spinal gray matter, crosses the spinal commissure within one or two segments rostral to the cells of origin, and ascends the contralateral spinal cord in two separate bundles. The lateral spinothalamic tract arises mainly from the superficial dorsal horn and primarily projects NS neurons while the anterior spinothalamic tract arises mainly from the deeper laminae and primarily projects WDR neurons. Both projections terminate in various regions of the brainstem (including the periaqueductal gray [PAG]) and various thalamic nuclei, from which they are connected to cortical targets including the insula cortex, anterior cingulate cortex (ACC), primary somatosensory cortex (SI) and secondary somatosensory cortex (SII).

Spinobulbar projections have a similar neuronal distribution to STT cells in the dorsal horn and project to brainstem regions including the PAG, parabrachial nucleus (PB),

noradrenergic cell groups, and the brainstem reticular formation (Dostrovsky and Craig, 2013; Wiberg et al., 1987). Together with the direct spinohypothalamic projections, this pathway is important in providing nociceptive relay via the PB to the hypothalamus, amygdala and other forebrain and cortical limbic structures important in the emotional regulation of pain (Bernard and Besson, 1990).

### 1.2.5 Cortical representation and perception

Early views on supraspinal contributions to pain perception posited that pain was a predominantly subcortical phenomenon. Lesions and electrical stimulation of the cortex during surgery were thought not to affect pain perception (Head and Holmes, 1911; Penfield and Boldrey, 1937), leading to conclusions that cortical involvement was minimal. However, these early studies investigated cortical injuries or focal stimulation (during epilepsy surgery) without appreciation for the multifaceted nature of cortical involvement in pain processing. Following the development of integrative pain theories that highlighted the relevance of emotional and motivational components (Melzack and Casey, 1968), convergent evidence began to suggest the importance of cortical influences. Recent studies have since demonstrated that pain can be elicited by focal lesions or stimulation of cortical brain regions (Garcia-Larrea, 2012). Importantly, the advent of modern human brain imaging techniques (functional magnetic resonance imaging [fMRI] and positron emission tomography [PET]) in the early 1990s enabled the investigation of the brain's contribution to pain experience (Apkarian et al., 2013). Such studies have consistently revealed several brain areas where the brain response to acute pain increases blood flow. These regions include most commonly the thalamus, SI, SII, insula cortex, ACC, and prefrontal cortex, but also the amygdala, PAG, cerebellum and hippocampus (Apkarian et al., 2005; Stephenson and Arneric, 2008; Treede et al., 1999). This large network of cortical and subcortical involvement is thought to reflect the multi-dimensional

nature of the pain experience. There is strong evidence that interactions between structures in this network are influenced by cognitive, emotional and motivational factors - as might have been predicted by the importance of these factors in individuals' subjective perception of pain (Tracey and Mantyh, 2007; Wiech and Tracey, 2009). Recent evidence further suggests that a common signature for acute experimental physical pain, reflecting activation in a network of structures, can be defined using algorithmic methods (Wager et al., 2013). Despite this, the precise mechanisms by which pain emerges, from a convergence of nociceptive inputs to the neural signature recorded using brain imaging, remain largely unknown.

The neural representation of pain perception is thought to reflect two distinct but overlapping pathways of nociceptive processing: the sensory-discriminative and affective-motivational components previously proposed by Melzack and Casey (1968). Current evidence suggests the importance of the rostral ACC and anterior insula in pain affect related to both nociceptive (neurogenic) and non-nociceptive (psychogenic) sources (Raij et al., 2005; Rainville et al., 1997; Singer et al., 2004). These regions are functionally heterogenous structures within the limbic system, which are thought to interact with prefrontal and forebrain structures involved in cognitive and emotional regulation (Wiech et al., 2008). Conversely, the mid and posterior insula cortex and SII have been shown to be involved both in parametric modulation of pain intensity and its binary representation (Bornhövd et al., 2002; Coghill et al., 1999), while modality- and spatial-specific somatotopy of noxious stimuli has been shown in the somatosensory cortices and the posterior insula, suggesting their importance in stimulus localisation and discrimination (Baumgärtner et al., 2010; Bingel et al., 2004b; Brooks et al., 2005; Henderson et al., 2011). Interestingly, studies of spontaneous pain in chronic back pain patients have suggested an increased contribution of prefrontal mechanisms, particularly the medial prefrontal cortex, in intensity modulation as compared to the insula cortex for evoked

pain (Baliki et al., 2006). This suggests a more significant role for affective systems in persistent and pathological pain states.

Although the concept of a singular 'pain cortex' appears elusive in light of the findings described above, recent convergent evidence, including the nociceptive somatotopic studies described above, suggests a role for the posterior insula and adjacent medial opercula region in specific nociceptive encoding (reviewed in Garcia-Larrea, 2012). Specifically, this region in primates receives the densest ascending STT projections of all cortical regions (Dum et al., 2009) and has recently been reported to receive topographically organised projections from the posterolateral thalamus (which itself receives somatotopically organised lamina I STT projections) (Craig, 2013). It is also systematically activated in a parametric and somatotopic manner by noxious stimuli as described above. Moreover, lesions in the posterior insula/SII are associated with selective pain and thermosensory deficits (Birklein et al., 2005; Greenspan et al., 1999) while electrical stimulation of the posterior insula has been shown to elicit discrete and topographically organised pain sensations in conscious humans (Mazzola et al., 2009; Ostrowsky et al., 2002).

The temporal integration of pain perception and activity in these spatially defined brain regions is best understood using tools such as electroencephalography (EEG) or magnetoencephalography (MEG), which provide improved temporal resolution over fMRI and PET. Studies measuring latencies of nociceptive-specific laser-evoked potentials (LEP) suggest that nociceptive input is first processed in the operculoinsula region in a pre-perceptual phase, before subsequent processing in the bilateral operculoinsula, SI and cingulate cortex, from which pain percept likely emerges (Garcia-Larrea et al., 2003; Iannetti et al., 2005a; Lee et al., 2009). Furthermore, there is evidence, from intracortical recordings, of early parallel processing of nociceptive inputs between sensory-discriminative and affective brain regions (Frot et al., 2008), suggesting the importance

of rapid integration of contextual information relating to pain, presumably to drive appropriate immediate behaviour.

As nociceptive inputs are transmitted up the central nervous system, they are modulated at various levels by endogenous factors. We will next consider the top-down modulation of nociceptive processing from supraspinal centres, and their relevance to the perception of pain.

## 1.3 Descending modulation of nociceptive processing

Ever since Sherrington (1906) noted increased nociceptive reflexes after rat spinal cord transection, it has been thought that descending spinal influences are involved in the processing of pain. However, investigation of the descending modulation of pain truly began following the seminal report showing that electrical stimulation of the midbrain periaqueductal grey matter (PAG) produced adequate analgesia in the rat to permit abdominal surgery without general anaesthetic (Reynolds, 1969). Several preceding studies had suggested the modulatory effect of supraspinal centres on non-specific sensory inputs in the spinal cord (Carpenter et al., 1965; Hagbarth and Kerr, 1954), while the gate control theory proposed by Melzack and Wall (1965) had purported that supraspinal influences affected nociceptive spinal excitability, though with no real evidence from animal or human studies.

In the decades following Reynolds' report, the PAG became an important region of study in the pain field and soon, animal behaviour studies began to report that stimulation of the region produced selective loss of nocifensive behaviour without any changes in responses to other non-noxious stimuli or in general alertness and movement (Mayer and Price, 1976). With the discovery of endogenous opioid activity sites, and the analgesic

effect of microinjection of opioids into the PAG (Yaksh and Rudy, 1978), it became clear that this region has a profound inhibitory role on the sensation of pain. Further, analgesia was produced with PAG stimulation in human chronic pain patients without any additional motor or sensory effects (Boivie and Meyerson, 1982), although this is uncommonly used now as a method of pain relief due to autonomic side effects. Research into the connections of the PAG identified other associated brainstem nuclei, which form a network that modulates nociceptive inputs at the spinal dorsal horn. Although early studies focused on the inhibitory effect of supraspinal modulation, it is now clear that this influence can be facilitatory as well as inhibitory. The dynamic balance between these two is altered in various psychological and pathological conditions, and disruption of this equilibrium may contribute to the development of chronic pain states (Heinricher et al., 2009). The PAG acts as a point of convergence between the cortical, forebrain, and spinal projections. Although many of the structures that provide these inputs have been independently identified to have a role in pain modulation, the ultimate perception of pain is likely to involve a complex integration of these inputs, accounting for a range of physical and contextual factors. This is supported by a range of studies using functional connectivity analyses where changes in coupling between cortical regions and the PAG produces analgesia in a range of contexts (Eippert et al., 2009; Petrovic, 2002; Tracey et al., 2002; Valet et al., 2004). See below for further discussion on the PAG.

### 1.3.1 Higher cerebral influences

In addition to work on the brainstem descending networks, it has become clear that there are important top down cerebral influences that result in pain modulation via changes in emotional and cognitive states from the limbic brain (Figure 1.1). In rodents, modulation of glutaminergic signalling in the anterior cingulate cortex and amygdala has been linked with the affective aspects of pain perception - assessed using conditioned place

aversion tests (Deyama et al., 2007b; Johansen and Fields, 2004). These reports support direct limbic involvement in the processing of the negative affective components of pain. In humans, the effects of attention, expectation and other psychological variables on pain have been examined with use of behavioural and functional imaging studies (Tracey, 2010; Wiech et al., 2008). Behaviourally, there is evidence that negative affect can increase or even decrease the perception of pain, with respect to the level of perceived threat- high threat can lead to stress-induced analgesia (Wiech and Tracey, 2009). Furthermore, chronic pain patients often find their problems exacerbated by mood disorders and there is a well-established link in chronic pain patients between depression and pain. Neuroimaging studies have allowed the investigation of the neural correlates underlying these behaviours. The value of such methods is perhaps most striking in the various studies that have investigated the neural correlates of the placebo effect- which has been shown to involve several opioid rich limbic and brainstem structures (Eippert et al., 2009; Petrovic, 2002; Wager et al., 2004). We will briefly discuss evidence for involvement of these and other important structures in the descending pain modulatory system.

### 1.3.2 Prefrontal cortex

The involvement of prefrontal structures in pain perception is complex and well documented but will only be addressed in brief in this section. It has been proposed that involvement of the ventrolateral prefrontal cortex (VLPFC) during cognitive modulation may have a role in changing the emotional context and subsequent perception of pain - a process known as reappraisal (Wiech et al., 2008) (Tracey, 2010). Activation in this region has been associated with voluntary attenuation of emotion (Ochsner et al., 2004; Phan et al., 2005), perceived control over pain (Salomons et al., 2007), belief related pain modulation (Wiech et al., 2008), and placebo analgesia (Petrovic et al., 2010). The

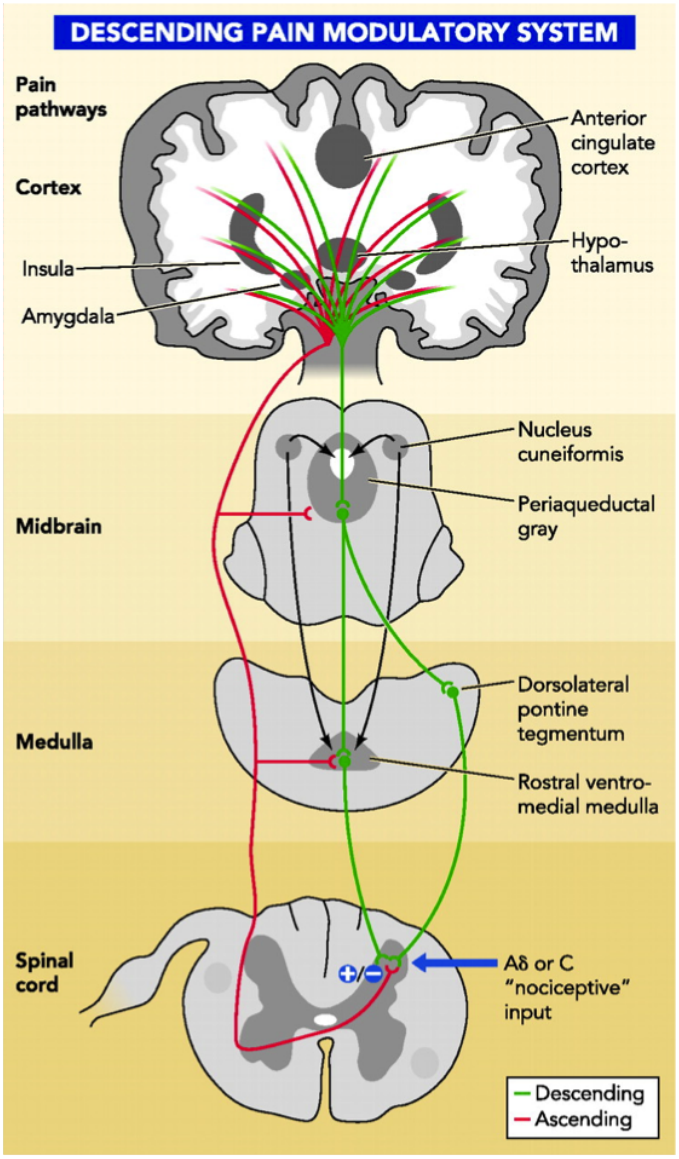


Figure 1.1: **The descending pain modulatory system**. From Bingel and Tracey, 2008

role of the VLPFC in emotional regulation may be effected through its connectivity with the anterior insula cortex (Mitchell, 2011; Peltz et al., 2011; Veit et al., 2012). The orbitofrontal cortex (OFC) is also involved in emotional processing but is associated with encoding of the reward value of stimuli and the anticipation of future outcome (Kahnt et al., 2010). Recent findings have highlighted that information from the OFC (together with the PAG) prior to pain stimulation accurately predicts the trial-by-trial perception of pain (Brodersen et al., 2012). Conversely, the dorsolateral prefrontal cortex (DLPFC) activity has been shown to negatively correlate with perceived pain, in association with disruption of thalamic-midbrain coupling by the left DLPFC and increased anterior insular connectivity with the right DLPFC (Lorenz et al., 2003). The role of the DLPFC in top-down pain inhibition is further supported by evidence that direct current stimulation of the region has some efficacy against experimental pain (Boggio et al., 2008). Yet others have reported a role for the medial prefrontal cortex (MPFC) in predicting pharmacological antihyperalgesic responses in healthy volunteers (Seifert et al., 2009), and pain chronification in back pain patients (via functional connections with the nucleus accumbens) (Baliki et al., 2012). Furthermore, these prefrontal regions have all been shown with white matter tract imaging to be structurally connected with midbrain structures important in descending pain modulation (Hadjipavlou et al., 2006). This provides a basis for direct cognitive modulation of pain perception.

### 1.3.3 Amygdala and limbic forebrain

The amygdala is a limbic structure, which is important in the processing of emotionally salient stimuli and the affective dimension of pain (Neugebauer et al., 2004; Phelps and LeDoux, 2005). The two key amygdala nuclei relevant for pain and anxiety processing are the basolateral nucleus (BLA) which processes information from the cortical and forebrain limbic areas, and the central nucleus (CeA) which receives nociceptive spe-

cific inputs from the spino-parabrachial system (Neugebauer et al., 2004). The BLA projects to the CeA, which in turn projects densely to the PAG. In rodents, morphine microinjection into the BLA has been shown to reduce glutaminergic excitation and so reduce nocifensive reflex behaviour in rats (Deyama et al., 2007b). Lesioning of the bed nucleus of the stria terminalis (which projects from the amygdala to hypothalamus) also suppressed conditioned place aversion, a measure of negative affect in rodents (Deyama et al., 2007a). The CeA also appears to have a key role in pain perception- it has been shown to undergo neuroplastic changes in a rodent model of chronic visceral pain (Han and Neugebauer, 2004). The CeA receives projections from the noradrenergic cell groups, which modulate negative affective responses to stress. A study by Demaya and colleagues (2010) reported that bilateral injections of a $\beta$-adrenoceptor antagonist into the CeA is selectively suppressive of visceral pain-induced aversive responses. This suggests that the CeA adrenoreceptors have a key role in modulating negative affective but not sensory components of visceral pain. In humans, neuroimaging studies have reported both increases and decreases in amygdala activity in response to pain, with peak activity in clinical studies located in the BLA region (reviewed recently in Simons et al., 2012). The amygdala has also been shown to be involved in opioid and cannabinoid analgesia in healthy human pain models (Lee et al., 2013; Wanigasekera et al., 2012). Importantly, the amygdala and limbic forebrain are heavily connected to the PAG and the brainstem nuclei, which are thought to be key drivers of supraspinal pain modulation. A number of these brainstem nuclei have been studied in conjunction with PAG-RVM network; those described below form an important but far from exhaustive selection.

### 1.3.4 Periaqueductal grey

The PAG receives inputs from the limbic cortical areas (anterior cingulate cortex and insular cortex), hypothalamus, amygdala (which receives inputs from the hippocampus

and neocortex), as well as from the ascending nociceptive fibres from the dorsal horn of the spinal cord (Fields et al., 2006). Of note, the nucleus accumbens in the ventral striatum, which is involved in reward processing and implicated in pain modulation, receives inputs from the BLA and projects indirectly to the PAG via the lateral hypothalamus. Other important brainstem inputs to the PAG include the pontomedullary reticular formation, the nucleus cuneiformis (which is adjacent to the PAG and also receives spinal dorsal horn inputs), the locus coeruleus (LC) and other brainstem noradrenergic nuclei (Herbert and Saper, 1992). The main projection of the PAG is to the rostral ventromedial medulla (RVM) to which it is reciprocally connected, but there are also projections to the noradrenergic cell groups (which in turn project to the spinal dorsal horn), and smaller rostral projections to the medial thalamus and orbitofrontal cortex (Fields et al., 2006). This complex array of connections allows top-down control of nociception as well as feedback modulation. The PAG is cytoarchitectonically heterogenous with its ventrolateral and dorsolateral portions contributing differently to pain modulation. Importantly the PAG (together with the ACC, amygdala and RVM) contains a high level of opioid receptors, and its involvement in endogenous pain modulation is directly linked to the opioid responsiveness of its cells. In human neuroimaging studies, the PAG has been shown to be active in pain perception, sensitisation, and placebo/nocebo responses (reviewed recently by Linnman et al. (2012)).

### 1.3.5 Rostral ventromedial medulla

The RVM is a functionally defined area in the midline pontomedullary reticular region of the brainstem, which is thought to be the main common output for descending pro- and anti-nociceptive signals. The RVM contains the midline serotonergic nucleus raphe magnus and is closely related to the adjacent ventrolateral reticular formation. Both medial and lateral parts of the RVM have to be blocked to completely stop descending

inhibitory effects from PAG stimulation (Sandkühler and Gebhart, 1984) emphasising the role of this region as a final output. The RVM receives inputs from the PAG, nucleus cuneiformis (NCF), adjacent reticular nuclei, A5 and A7 noradrenergic cell groups in the dorsolateral pons, and some ascending spinal nociceptive inputs (although these are mainly via the NCF and adjacent reticular nuclei). It also receives direct projections from higher limbic cortical regions including the CeA, hypothalamus and prefrontal cortices. The RVM projects to both deep and superficial layers of the dorsal horn to directly modulate the excitability of the nociceptive neurons, via 5HT spinal receptors or otherwise. Although 5HT spinal receptors may be either facilitatory or inhibitory to nociceptive signalling depending on receptor subtype (Suzuki et al., 2004), the RVM's serotonergic projections likely affect 5HT1A spinal receptors, which are thought to be antinociceptive (Viisanen and Pertovaara, 2010). Early evidence showed that microstimulation or opioid microinjection into the RVM produced profound and selective analgesia comparable to that seen in the PAG (Yaksh and Rudy, 1978). Conversely, anatomical lesions or pharmacological inactivation of the RVM abolishes the analgesic effect of PAG stimulation (Fields et al., 1991). This supported the role of the PAG-RVM system as an inhibitor of nociception and the RVM as the final supraspinal relay point. However, a series of reports from Zhuo & Gebhart showed that low intensity electrical stimulation of the RVM can facilitate the tail-flick nocifensive reflex at the same sites where inhibition can also be produced (Zhuo and Gebhart, 1990, 1992, 1997). Furthermore focal microinjection of the neuropeptide cholecystokinin (CCK) into the RVM has been shown to be pronociceptive and hyperalgesic (Heinricher and Neubert, 2004). The RVM has also been shown to be important in hyperalgesia and maintenance of spontaneous pain in some neuropathic and inflammatory models but seems to be selective for certain inputs only (De Felice et al., 2011; Heinricher et al., 2009; Porreca et al., 2002; Wang et al., 2013). Neuroimaging of the brainstem in humans has revealed regions of the mesencaphalic and pontine reticular formation to be important in post-injury pain sen-

sitisation (see below) (Lee et al., 2008; Zambreanu et al., 2005). These studies together suggest that descending control from the RVM can be facilitatory as well as inhibitory to nociception.

The neural basis of such complex modulation as seen in the RVM can be understood by considering an earlier key study by Fields and colleagues (1983) which categorised two subsets of RVM neurons based on their state changes in association with nocifensive withdrawal. ON cells are abruptly active while OFF cells are suddenly silent in association with the nocifensive reflex (NEUTRAL cells appeared unaffected and so were classified by exclusion). OFF cells were first identified as the crucial cell class in inhibition signalling as disinhibition of these cells by GABA blockade was sufficient to produce behavioural antinociception (Heinricher and Tortorici, 1994). Opiate drugs are thought to exert their effects by causing continuous activation of OFF cells- their action in the basolateral nucleus of the amygdala appears to recruit OFF cells in the RVM (McGaraughty and Heinricher, 2002). ON cells proved more difficult to characterise but were later confirmed as the facilitating output cells of the RVM when their selective activation was shown be adequate to produce hyperalgesia in lightly anaesthetised rats (Neubert et al., 2004). Stimulation of higher centres such as the ventromedial orbital cortex and the dorsomedial nucleus of the hypothalamus also appeared to activate ON cells and produce hyperalgesia (Heinricher et al., 2009). The role of NEUTRAL cells, if any, is unclear as they are unresponsive during nocifensive reflexes, acute inflammation or to pharmacological stimulation. Nonetheless, it has been suggested that these cells may be recruited to become ON or OFF cells in chronic pain states; this idea is given weight by the fact that a considerable number of these cells are serotonergic while no ON or OFF cells appear to be (Heinricher et al., 2009). Serotonergic RVM cell populations have a slow and steady discharge suggesting a role in tonic spinal modulation (Mason, 1997). These neurons also respond to noxious tail heat independently of ON

or OFF cells suggesting that these cell groups do not share physiological functions (Gao and Mason, 2000). The role of pain facilitation can be understood as advantageous in promoting recuperative behaviours and enhancing vigilance when a threat is possible but not imminent. This is comparable to the importance of the suppression of pain in prioritising survival or escape in stressful or dangerous situations.

### 1.3.6 Dorsal pontomesencephalic formation

The dorsal pontomesencephalic formation includes the nucleus cuneiformis (NCF) and parabrachial nucleus (NPB). The NCF/PBN region receives major inputs from lamina I of spinal and trigeminal horns as well as smaller inputs from the deeper laminae of the spinal cord. Its projections are mainly to the RVM, thus creating a spinal-bulbar-spinal loop thought to mediate facilitation or inhibition at the dorsal horn (Suzuki et al., 2004). Although most fibres from the formation terminate in the RVM, there is also a minor projection of noradrenergic neurons from the region of the ventral NPB and adjacent Kolliker-Fuse nucleus directly to the dorsal horn, which may serve as a parallel pathway mediating suppression of nociceptive inputs (Haws et al., 1989). The discovery of ON and OFF cells in a region of the NCF/NBP that was shown to suppress nocifensive behaviour in rats on microstimulation suggests that input into the RVM from this region may be important in pain modulation (Haws et al., 1989). Activity in this area has also been shown in an fMRI study to be correlated with RVM activity in visceral pain, which supports the view of a brainstem-spinal loop modulating nociceptive inputs (Dunckley et al., 2005).

The nucleus cuneiformis (NCF) itself is immediately ventrolateral of the PAG and has been identified as an important part of the pain modulation network, owing to its inputs from the prefrontal cortex, hypothalamus and amygdala, strong association with the ad-

jacent PAG and projection to the nucleus raphe magnus of the RVM. These put the NCF in a prime position to receive autonomic, executive and affective information with which it can bidirectionally modulate pain perception. Together with the deep layers of the superior colliculus, the NCF is thought to have a role in the sensory-motor integration of pain processing (Zemlan and Behbehani, 1988). Recent findings demonstrated that microinjection of morphine into the NCF produces analgesia in rats and that the nucleus' antinociceptive influence is via tonic glutaminergic input modulated by the NMDA receptor (Haghparast et al., 2007). Further evidence showed that the majority of neurons in the NCF exhibited monophasic excitatory single unit firing during the formalin test, and that this was suppressed by subcutaneous morphine injection and reinstated by naloxone administration (Haghparast et al., 2010). These studies suggest that the NCF acts as an important gateway for the endogenous inhibition of nociception, modulated by endogenous glutaminergic and opioid receptors. In humans, an fMRI study by Zambreanu and colleagues (2005) identified the NCF as a major region of brainstem activation in a healthy volunteer model of hyperalgesia.

### 1.3.7 Locus coeruleus and noradrenergic nuclei

The dorsolateral pontine tegmentum noradrenergic neurons are important contributors to the modulation of pain- these include the locus coeruleus (LC) and the A5 and A7 noradrenergic cell groups (Fields et al., 2006). The locus coeruleus (LC) is the most studied of this group. The LC is a principally noradrenaline producing nucleus found on the floor of the fourth ventricle at the dorsal region of the rostral pons. The nucleus has an important role in stress and anxiety behaviour modulation and mediates arousal via its widespread excitatory effects in the brain. The presence of noradrenergic receptors and terminals in the region of the dorsal horn where small nociceptive fibres terminate was one of the first suggestions that this class of monoamines are particularly important in

the modulation of nociceptive signalling (Proudfit, 1988). It has been shown that electrical or chemical stimulation of the LC produces descending antinociception by inhibiting nociceptive activity in dorsal horns (Jones and Gebhart, 1988). The LC receives major excitatory afferents from the ventrolateral medullary reticular formation and inhibitory afferents from the dorsomedial rostral medulla, as well as smaller inputs from the posterior hypothalamus, mesencephalic reticular formation and some forebrain regions (Luppi et al., 1995). In particular, a projection from the central nucleus of the amygdala may be important in allowing emotional pain to trigger noradrenergic responses. The LC projects widely to the forebrain and sensory brainstem nuclei, and provides noradrenergic innervation to spinal cord neurons- mostly in the ventral horn but also in the dorsal horn (Proudfit and Clark, 1991). The LC is also activated in experimentally induced inflammation, where it attenuates the development of hyperalgesia (Tsuruoka and Willis, 1996). These observations suggest that noradrenergic neurons have important inhibitory effects, both as contributors to the PAG-RVM system and as an independent descending anti-nociceptive pathway.

### 1.3.8 Summary

The evidence outlined above suggests that active regulation by various excitatory and inhibitory CNS circuits, gated by brainstem structures, can decrease or increase pain perception, dependent on a number of cognitive, mood or contextual factors. Disruptions of these circuits at the supraspinal or spinal level can contribute to abnormal and pathological pain amplification.

## 1.4 Response to injury- peripheral and central sensitisation

The sections above largely describe pathways and events related to nociceptive processing in the normal state. Of particular relevance to chronic pain are changes resulting from inflammation or nerve injury. In this section, we will briefly explore peripheral and spinal mechanisms thought to underlie the development of persistent pain and hypersensitivity following injury to the nervous system.

A common feature of the nervous system is its ability to modify its properties in response to inputs- termed plasticity. In this vein, activity dependent plasticity following noxious stimulation of nociceptors manifests in several forms (von Hehn et al., 2012; Woolf and Salter, 2000).

In the periphery, nociceptive neurons reversibly decrease their thresholds as a result of transducer protein changes following activation (autosensitisation) or excitability of terminal membranes by exposure to inflammatory mediators and neurotrophic factors (heterosensitisation) (Andrew and Greenspan, 1999a; Woolf and Salter, 2000). As a result of this peripheral sensitisation, subsequent stimuli to the same nociceptive fibres initiate action potentials more readily and so identical inputs are perceived to be more painful (primary hyperalgesia).

In the spinal dorsal horn, plasticity following nociceptive input can result in the phenomena of wind-up and central sensitisation. Wind-up refers to the temporal summation of inputs, where repeated low frequency inputs lead to a progressive increase in action potential discharge over the course of the stimuli (Mendell and Wall, 1965; Sivilotti et al., 1993). Of far greater clinical import is central sensitisation (CS); this refers to

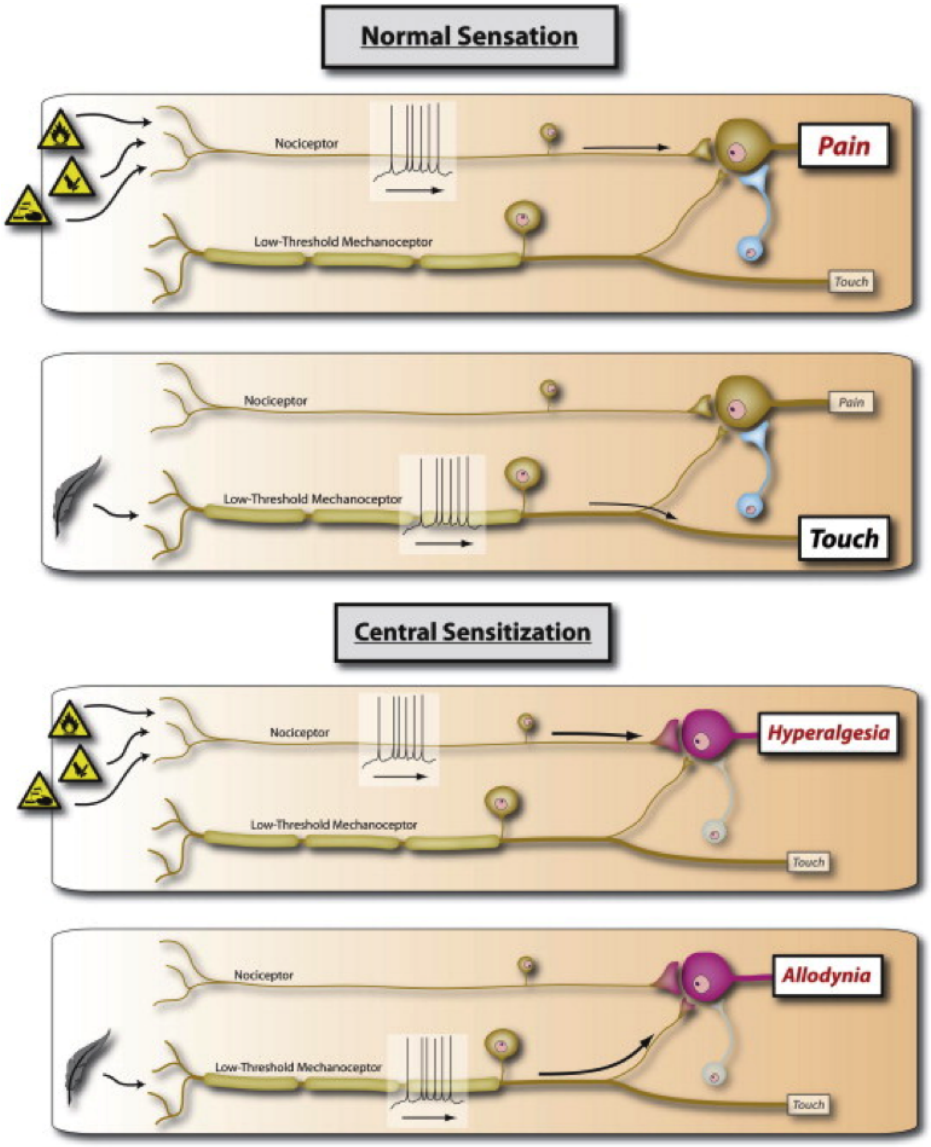


Figure 1.2: **Mechanisms of central sensitisation.** Adapted from Woolf (2011). Central sensitisation results in (1) reduction of thresholds, (2) increase in responsiveness, (3) expansion of receptive fields of dorsal horn neurons. This lead to the phenotype of hyperalgesia (increased pain to a normally painful input) and allodynia (pain to a normally innocuous input) shown above.

use-dependent synaptic plasticity (increased synaptic strength) resulting in increased excitability and responsiveness of spinal neurons (Woolf, 1983; Woolf and Salter, 2000) (Figure 1.2). Facilitation of excitatory synaptic responses, depression of inhibition, and the consequent increased 'gain' and enlargement of receptive fields arise secondary to activation of intracellular cascades by the initiating input. These changes outlast the initiating input or are sustained by a very low level of peripheral drive. Importantly they are not limited to the activated synapse (homosynaptic) but also spread to adjacent synapses (heterosynaptic). This leads to increased responsiveness beyond the injured tissue (secondary hyperalgesia) and facilitates pain responses to low-threshold, normally innocuous inputs (allodynia) (LaMotte et al., 1991). Although experimental CS is typically initiated by C-fibre afferents, mechanical allodynia is mediated by low threshold A$\beta$ fibres (Torebjörk et al., 1992) while hyperalgesia is mediated by A$\delta$ fibres (Ziegler et al., 1999); this underscores the heterosynaptic nature of clinically relevant dorsal horn changes.

CS is thought to be a major mechanism in the development of inflammatory and neuropathic pain conditions; this notion is supported by long-standing evidence of hyperalgesia and allodynia amongst these patient groups (Baron, 2006; Rasmussen et al., 2004; Woolf, 2011). Genetic contributions and molecular interactions between neurons, glia and inflammatory mediators, which underlie the development of sensitisation and hypersensitivity are complex and beyond the scope of this thesis. However, these molecular components have provided important therapeutic targets aimed at reducing such pain (McKelvey et al., 2013; von Hehn et al., 2012).

Several preclinical and human studies have indicated that CS and spontaneous neuropathic pain are maintained by descending supraspinal facilitation, largely from the RVM and associated structures (De Felice et al., 2011; Lee et al., 2008; Porreca et al.,

2002; Suzuki et al., 2004; Wang et al., 2013). In the first part of this thesis, we use an accepted human experimental model of CS in healthy volunteers to assess the use of neural CS biomarkers as a surrogate for testing analgesic efficacy in neuropathic pain. In the next section, we will address the epidemiology, treatment and current investigative methods for neuropathic pain conditions, with a view to understanding our experimental approach.

## 1.5 Neuropathic pain

Chronic pain conditions are heterogenous but can be broadly classified as nociceptive, inflammatory or pathological (including neuropathic and dysfunctional syndromes) (Woolf, 2010) (Figure 1.3). Nociceptive pain is associated simply with detection of noxious stimuli and serves to alert to potential danger. Inflammatory pain is caused by immune responses to injury, generates hypersensitivity, and is adaptive such that healing occurs following tissue damage if the source of inflammation is removed. Pathological pain on the other hand involves maladaptive processes where the hypersensitive state is maintained independent of any initiating lesion or disease.

Of these, neuropathic pain poses a particularly significant clinical problem. Although few epidemiological studies have directly addressed its scope, a survey has estimated a prevalence of 8% for chronic neuropathic pain (>3 months duration) from a cohort of 3000 patients registered to family practices in three UK cities (Torrance et al., 2006). Such pain is often more severe and harder to treat than nociceptive pain, particularly given its poor response to traditional analgesics such as opioids (McQuay, 2002). As a result, it is associated with a poorer quality of life than other types of chronic pain (Jensen et al., 2007; McDermott et al., 2006). Neuropathic pain conditions are also vastly heterogenous with different aetiologies, presentations and putative mechanisms. It

is now accepted that a mechanism-based classification of these conditions is appropriate, ideally with correlates to clinical signs and symptoms (Finnerup and Jensen, 2006). This necessitates development of adequate tools to define these mechanisms, and therapeutic interventions to target them.

### 1.5.1 Basis of current treatments

Neuropathic pain therapies aim to modify the nervous system. While there are a large number of treatment options, few have consistently demonstrated efficacy while many are costly and have significant side effects. In this section we will focus on up-to-date pharmacological recommendations for treatment proposed from an evidence base of randomised controlled trials (Dworkin et al., 2007).

Stepwise management of neuropathic pain involves patient assessment and diagnosis; initiation of first line therapies (alone or in combination); patient evaluation for non-pharmacological treatments; frequent reassessment and trial of second and third line therapies if appropriate.

Recommended first line treatments include some anti-depressants (tricyclic antidepressants [TCA] and selective reuptake inhibitors of serotonin and noradrenaline [SSNRI]), anti-epileptics (calcium channel $\alpha 2\delta$ ligands- pregabalin and gabapentin) and topical lidocaine (a sodium channel blocker) (Dworkin et al., 2007). Antidepressants inhibit monamine uptake at synaptic terminals; their analgesic effect may involve an increase in serotonin and noradrenaline levels, both important neurotransmitters in the endogenous inhibition network (Sawynok et al., 2001). Calcium channel $\alpha 2\delta$ ligands bind to presynaptic voltage-gated calcium channels in the dorsal horn, reducing the release of excitatory neurotransmitters (Dooley et al., 2007). Efficacy for both classes has largely

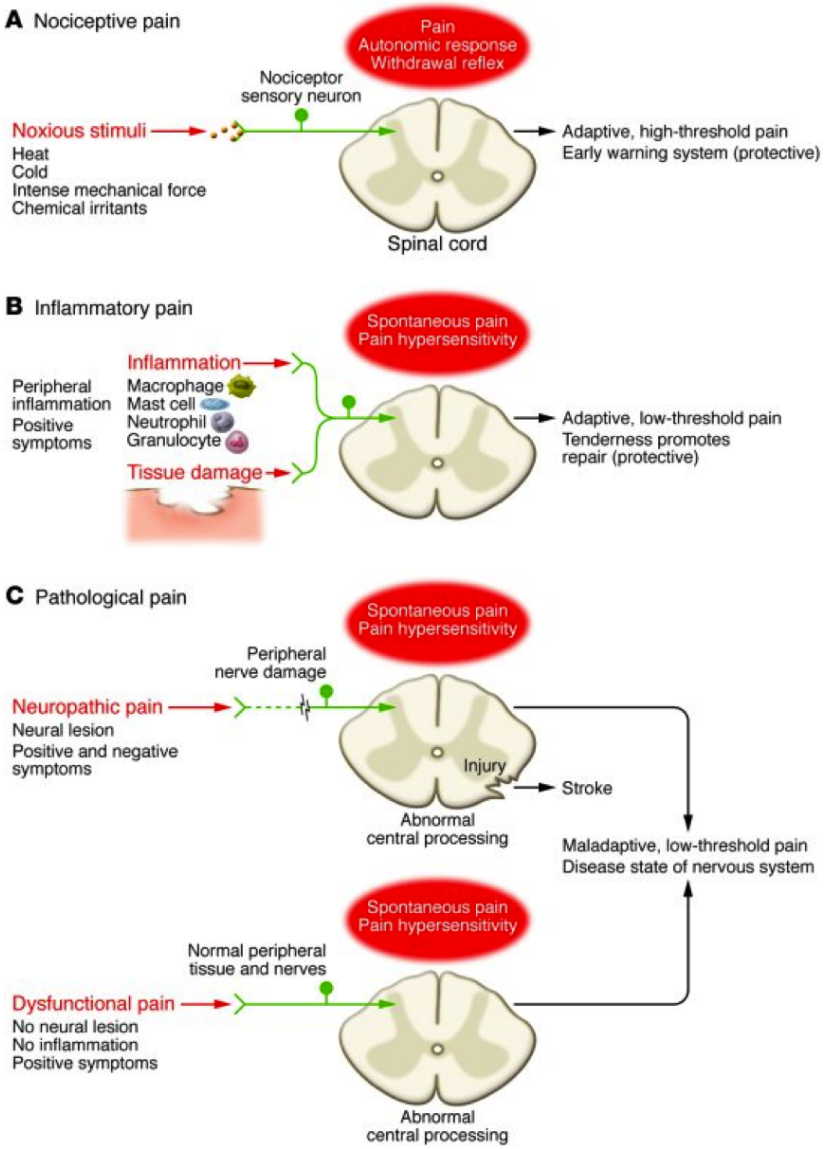


Figure 1.3: **Classifications of pain.** From Woolf (2010).

been shown in postherpetic neuralgia (PHN) and painful diabetic neuropathy (DPN), although there is some evidence of broader efficacy for the antiepileptics (Finnerup et al., 2010). Topical lidocaine is indicated in PHN, allodynia and localised peripheral neuropathies. In cases of trigeminal neuralgia, the antiepileptic carbamezapine is generally also recommended as a first-line therapy- it may act by inhibiting sodium channels and reducing neuronal discharge in a use dependent manner (Kuo et al., 1997).

General recommendations for second line treatments include opioid analgesics and tramadol ($\mu$-opioid agonist), although these can also be considered a first-line therapy in cases of acute neuropathic pain, episodic exacerbations or neuropathic cancer pain (Dworkin et al., 2007). Third line treatments include drugs for which there is substantially less evidence of efficacy- some antiepileptics (e.g. lamotrigine), antidepressants (e.g. citalopram), N-methyl-d-aspartate (NMDA) antagonists (e.g. memantine) and high dose topical capsaicin.

Non-pharmacological treatments for neuropathic pain abound- these include psychotherapeutic and neurostimulatory (invasive and non-invasive) techniques (Xu et al., 2012). Given the growing knowledge of central mechanisms of pain, there is much promise for use of targeted neurostimulatory techniques in the management of intractable pain. While deep brain stimulation has shown efficacy in some of these patient groups (Boccard et al., 2013), it is limited by the side effects associated with surgery and non-pain specific stimulatory effects. Non-invasive neurostimulatory techniques including transcranial magnetic stimulation (TMS) and transcranial direct current stimulation (tDCS) may be viable options (Fregni et al., 2007). We assess this in Chapter 7, where we investigate the neural basis of tDCS therapy (the cheaper and safer of the two) in a chronic neuropathic patient cohort.

Despite these options, the number needed to treat (NNT) for first line therapies typically range between 3-5 for the most effective (Finnerup et al., 2010). There is a clear need for new efficacious pharmacological treatment options for neuropathic pain. In this thesis, we aim to validate the use of functional imaging as a tool for assessing analgesic potency in acute and persistent pain states. We will then test the use of such tools in the assessment of therapeutic efficacy both in healthy controls and in a group of chronic neuropathic pain patients. In the next section, we will outline the basis of some of the experimental methods that will underpin this investigation.

### 1.5.2 Experimental tools

#### Human experimental methods for evaluating pain

Most preclinical models of neuropathic pain are in rodents. These have been immensely valuable in elucidating the pathophysiological mechanisms of pain over the past few decades. However the predictive validity of these models for clinical efficacy of analgesics is disputed (Berge, 2011). As neuropathic pain by definition involves nerve damage, reversible models in healthy human volunteers are difficult to create. Human experimental models of central sensitisation, such as the use of intradermal or topical capsaicin, have provided a means to investigate symptoms of neuropathic pain (Lee et al., 2008). Capsaicin-induced central sensitisation (CS) mimics spontaneous pain, allodynia and hyperalgesia, which are common symptoms of neuropathic pain (Klein et al., 2005). The extensive preclinical knowledge regarding mechanisms of central sensitisation and their relevance to neuropathic pain provides an important background to its use as a marker for pharmacological modulation in healthy humans. Furthermore, as chronic pain patients are a difficult group to study- owing largely to their wide range of co-morbidities, studying central pain processing and its modulation in healthy volunteers provides less confounding yet important insights into potential therapies. To examine the clinical

relevance of our approach, we will also investigate the modulation of neuropathic pain in a specific cohort of phantom limb pain patients (see Chapter 7), where a putative mechanism can be directly targeted.

### Psychometric tools

Psychophysical evaluation of pain via subjective reports is the standard for assessing analgesic efficacy in the clinical setting. Following the separation of sensory-discriminative and affective-motivational components of pain, these tools have attempted to address both aspects distinctly. In this thesis we largely use two psychometric tools for assessing pain perception- the verbal numerical rating scale (NRS) and the visual analogue scale (VAS). The 11-point NRS scale (0-10) has been shown to be practical for assessing patient groups (Jensen et al., 1999). We also use an online VAS with anchors that define the sensations to be reported (e.g. 'not at all' and 'worst imaginable'). In both cases, we assess pain intensity and pain unpleasantness to capture both sensory and affective dimensions of the experience. Although the NRS can be easier to use offline, communication difficulties in the scanner environment make it less practical. The VAS is comparatively more studied and its scores are thought to be internally consistent and reproducible across sessions (Price et al., 1983; Rosier et al., 2002).

While these psychophysical measures are most pertinent to the patient's condition, they reflect a private and highly contextual experience that cannot easily be accessed by scientific methods. Furthermore, there is likely a non-direct relationship between pain experience and subjective report. Therefore neuroimaging provides a tool that allows more objective measurements of the physiological changes that underlie the subjective pain experience and subsequent report. It is important to state that functional imaging of pain experience is not simply a surrogate measure of pain report, as has often been misstated and misunderstood. It is a measure of the CNS processing that underpins the

multidimensional experience that is pain, from which a verbal report is derived using the psychometric measures mentioned above. The two are related but not equivalent and arguably functional imaging provides the richer measure as it captures much of the processing underpinning the perception.

### Neuroimaging principles

Over the past 15 years, neuroimaging has proven to be an important tool in furthering our knowledge of human central pain processing. Functional Magnetic Resonance Imaging (fMRI) in particular provides non-invasive objective physiological correlates of nociception and pain, which can enable in vivo assessment of brain function and its modulation (e.g. by therapy).

The principles of MRI are well established and will not be described in detail here (Huettel et al., 2008). In brief, fMRI exploits the electromagnetic properties of charged proton particles found in water. In the presence of an external magnetic field ($B_0$), these particles become aligned to the field creating a net magnetisation. These aligned particles can be excited into a high-energy state by use of a brief secondary radiofrequency (RF) pulse, which tilts the net magnetisation to be perpendicular to $B_0$. Decay of this transverse magnetisation back to equilibrium over time can be measured and depends on local magnetic field properties, such as field inhomogeneities. As a result, relaxation times differ depending on the $B_0$ field strength and tissue properties, allowing contrast to be generated. The time between RF excitation and data acquisition is known as the echo time (TE), while the time between cycles of excitation is known as the repetition time (TR). Image acquisition uses additional magnetic gradients, which cause localised shifts in frequency and phase that can be recorded mathematically in k-space. Rapid echo-planar imaging (EPI), which maps k-space in seconds following excitation, is most

commonly used (Mansfield and Maudsley, 1977). Data in k-space can be converted into an image by using an inverse Fourier transform.

The most commonly applied fMRI contrast technique is blood oxygen level dependent (BOLD) imaging. BOLD contrast measures the vascular response to neural activation (Ogawa et al., 1990); this incorporates changes in cerebral blood flow (CBF), cerebral blood volume (CBV) and oxygen metabolism. During activation, neurons consume oxygen carried by haemoglobin in circulating red blood cells- this triggers local increases in blood flow within a few seconds. It should be noted that the haemodynamic response to neural activations is highly non-linear- a small increase in metabolic demand leads to a relative oversupply of oxygenated blood. However the rapid increase in the relative concentration of oxyhaemoglobin (which is diamagnetic) to deoxyhaemoglobin (which is paramagnetic) changes the magnetic susceptibility (and hence transverse relaxation) of blood in the local area, enabling measurement of changes in blood delivery. Physiological interpretation of the BOLD signal is therefore dependent on the close coupling between neural activation and vascular changes, as mediated by glial cells (Attwell et al., 2010; Logothetis et al., 2001).

After image acquisition, the fMRI data is pre-processed before statistical analysis is performed. Pre-processing typically involves correction of head motion by aligning the image volumes to a single midbrain volume; correction for $B_0$ field inhomogeneities associated with EPI image acquisition; spatial smoothing to increase signal to noise ratio; and high-pass Gaussian-based temporal filtering to remove low-frequency drifts. For BOLD imaging, statistical analysis typically involves a convolution of an expected haemodynamic response with the voxel-wise timecourse of the data in a general linear model. This generates voxel-wise parameter estimates for the magnitude of signal response and error estimates for the model fitting. Statistical maps are registered to a standard brain

for between subject comparisons, thresholded and corrected for multiple comparisons across the whole brain using a range of methods (e.g. cluster based correction using random field theory (Worsley, 2001)). Region of interest approaches may be used in the case of a clear *a priori* hypothesis about effects on a specific brain area (Mitsis et al., 2008).

### fMRI for drug modulation of pain

A large number of fMRI studies have reported BOLD related changes in the acute pain state. Nonetheless, many of these pain-related changes are known to be non-specific to nociceptive processing and have been reported during imagined pain (Derbyshire et al., 2004), social rejection (Eisenberger et al., 2003) and empathy for pain (Singer et al., 2004). Various studies over the past 15 years have dissected the varying contributions of different active brain regions to the multidimentional pain experience (Bantick et al., 2002; Berna et al., 2010; Ploghaus et al., 1999; Wager et al., 2004; Wiech et al., 2008). More recently, some commentators have also suggested that the BOLD response to brief noxious stimuli may in part reflect non-specific encoding of stimulus saliency (Legrain et al., 2011; Mouraux et al., 2011). Despite this, the sensation of pain is distinctive and perceived differently from innocuous sensory stimuli. Further, ongoing pain is the dominant symptom in chronic neuropathic pain (Backonja and Stacey, 2004) and so its assessment with fMRI will likely enable more clinically relevant interpretations of the underlying neural mechanisms of chronic pain.

BOLD fMRI is optimised for high frequency tasks and so is sub-optimal for the investigation of ongoing pain states. As onset and maintenance of pain are likely dependent but separate processes that may recruit different brain networks, newer techniques such as arterial spin labelling (ASL)- which quantifies CBF over stable states, are a promising

alternative that may enable assessment of pain states that more closely resemble clinical reality. In this thesis, we will use both BOLD and ASL (described in detail in Chapter 4) to define the neural correlates of evoked and persistent pain. We will then investigate its modulation by pharmacological and non-invasive neurostimulatory methods in healthy volunteer and patient groups.

Pharmacological fMRI refers to the use of pharmacological agents to modify the physiological state as detected by fMRI. Such studies have been paired with evoked pain paradigms to investigate the influence of drugs on stimulus-related BOLD activity. The drug effects measured can be global or local, and neuronal or vascular in origin. Global changes often result from direct drug effects on cardiorespiratory variables or on the vasculature (Wise and Tracey, 2006). Monitoring cardiorespiratory variables and use of well-designed paradigms that include a control task can help to evaluate global effects of no interest. Quantitative measurements of absolute CBF (e.g. ASL) also allow comparisons of global CBF changes between sessions. In Chapter 3 we will use an analgesic, which has been shown not to have a global effect in a previous study (Iannetti et al., 2005b); we further confirm this by calculating global CBF changes induced by the drug in Chapter 6.

## 1.6 Thesis outline

There is a pressing need to develop new therapies for the management of neuropathic pain. Functional MRI enables the investigation of central mechanisms of pain, which can uncover targets for new treatments. This thesis aims to validate the use of fMRI as a tool for testing analgesic efficacy against evoked and persistent pain.

By assessing preclinical and human evidence about central mechanisms of hypersensi-

tivity, we formed hypotheses about possible sites of analgesic action against a model of central sensitisation.

Chapter 2 optimises tools that allow us to image supraspinal sites where we expect to see modulation. We also validate the use of the topical capsaicin model as a model of hypersensitivity and spontaneous pain in a crossover design.

In Chapter 3, we use these optimised tools to test the efficacy of two compounds against CS-induced hypersensitivity- one compound that is known to be effective in neuropathic pain, and another that has no demonstrated efficacy in neuropathic pain. We aimed here to validate the superior sensitivity of fMRI over subjective reports for assessing efficacy between these compounds.

Chapter 4 describes the arterial spin labelling technique and assesses the reliability of an updated sequence and associated novel analyses methods for imaging resting and long activation (e.g. persistent pain) states, over week and month time frames.

As there are few studies that have investigated the neural correlates of persistent pain in healthy volunteers, Chapter 5 defines this using a controlled paradigm design.

In Chapter 6, we use the techniques developed in Chapter 4 and evidence from Chapter 5 to assess the endogenous and pharmacological modulation of the perception and neural representation of persistent pain.

Chapter 7 uses the validated method for assessing efficacy in persistent pain to test the use of tDCS as a novel therapy in a cohort of phantom limb patients.

Chapter 8 concludes by discussing the significance of our findings and possible directions for future work.

# Chapter 2

# Optimising Subcortical Brain Imaging and Defining a Pain Model for Investigating Central Sensitisation

The studies described in this thesis aim to employ Functional Magnetic Resonance Imaging (fMRI) in understanding the development and modulation of central sensitisation (CS) and persistent pain in the brain. Of special interest in this regard are the brainstem and several subcortical brain structures which are typically difficult to image.

In the two studies described in this chapter, we aimed to define optimal BOLD fMRI parameters to image the regions relevant to CS-induced pain. We investigated the application of such techniques as high-resolution imaging, physiological modelling and ultra high field imaging in the context of various pain paradigms. We also tested the reliability of a model of mechanical hyperalgesia and spontaneous pain to validate its use in crossover designs. The findings from this chapter helped to define the protocols used in the forthcoming chapters.

## 2.1 Experiment 1

This study establishes an optimised protocol for brainstem fMRI during nociceptive stimulation. By comparing two high resolution acquisition sequences, with and without physiological noise modelling (PNM), we aimed to establish the benefit of PNM and the feasibility of high resolution imaging for assessing activity in small brainstem and subcortical nuclei.

### 2.1.1 Introduction

The brainstem is a difficult region to image, owing to the small size and close proximity of relevant nuclei that requires high spatial resolution for functional localisation, and the effects of coarse motion (cardiac, respiratory and cerebrospinal fluid [CSF]) on the regional magnetic susceptibility (Harvey et al., 2008). Three key issues that arise from this are the difficulty of image registration accuracy between subjects, the importance of high resolution imaging for localising these small structures and the influence of physiological artefacts on the temporal signal in inferior brain regions.

Despite these issues, a number of studies have highlighted the feasibility and importance of pain imaging in the brainstem by identifying the neural correlates of somatic and visceral pain in brainstem nuclei using various pain models (Dunckley et al., 2005; Lee et al., 2008; Zambreanu et al., 2005) including central sensitisation (CS).

In this study, we tested the importance of physiological noise modelling for pain imaging of the brainstem and associated subcortical regions, while employing updated three-stage and boundary-based registration (Greve and Fischl, 2009) techniques in the FMRIB Software Library (FSL) pipeline. We assessed the effect of varying acquisition orientation and echo-planar image (EPI) phase-encode direction on the fMRI signal and BOLD

activity in pain relevant brainstem regions. We further compared the sequences by examining their relative ability to discriminate between the adjacent cuneate and gracile medullary nuclei, which encode vibrotactile stimuli to the finger and toe respectively.

#### 2.1.1.1 Physiological noise correction

FMRI acquisitions are compromised by fluctuations in the cardiac and respiratory cycle- coarse motion results from pulsatile activity of blood vessels and CSF, as well as changes in intracranial pressure (Birn et al., 2006; Poncelet et al., 1992; Shmueli et al., 2007). As a result of their proximity to these causes of gross motion, inferior brain regions such as the brainstem show high temporal signal variability, spatio-temporal blurring of the BOLD signal and bulk magnetic susceptibility changes (Limbrick-Oldfield et al., 2012; Raj et al., 2001).

Various correction methods have been introduced to account for these artefacts. In particular, for 2D-echo planar imaging readouts, retrospective image correction (RETROICOR) using independent physiological measures has been shown to improve functional task-related BOLD activity (Birn et al., 2006; Glover et al., 2000; Shmueli et al., 2007). This method is more effective than k-space correction for spatially localised cardiac fluctuations (Glover et al., 2000) and does not necessitate offline image reconstruction (as with k-space correction). Furthermore, unlike cardiac gating methods (Zhang et al., 2006), retrospective image correction models both respiratory and cardiac fluctuations, and avoids the disadvantage of a variable acquisition rate, which can reduce efficiency.

RETROICOR was first developed for whole-brain fMRI (Glover et al., 2000) and removes structural noise by assigning a cardiac and respiratory phase to each slice of the imaging data- depending on the slice acquisition order and acquisition time. The effects of

these phases are modelled using a basis set of 4 Fourier terms. A modified version of RETROICOR- the Physiological Noise Model (PNM) has been employed in brainstem (Brooks et al., 2008; Harvey et al., 2008; Limbrick-Oldfield et al., 2012) and spinal studies to also account for the interactions between cardiac and respiratory cycles and low frequency heart rate fluctuations (an additional source of low frequency noise) (Chang et al., 2009). These interactions have also been shown to correlate with CSF pulsations in the spinal cord (Friese et al., 2004). Removing structural noise by including these regressors in the general linear modelling of functional data (to a finger-tapping motor task) can improve the likelihood of detecting true effects and rejecting false positives (Harvey et al., 2008). The technique is shown to be particularly effective in reducing inter-subject signal variance.

Despite the clear benefits of noise correction in the context of non-pain paradigms, phasic pain stimuli are often associated with stimulus related motion. As such there is potential that in modelling out motion and physiological parameters, some true positive activity is also removed and BOLD activity is not improved. In the study below, we implemented the PNM in a pain paradigm within the general linear model, avoiding the loss of degrees of freedom associated with implementation in pre-processing. We verified that the PNM stabilises the brainstem signal time-course (reduce signal variance) and also improves task-related BOLD parameters in the context of painful stimuli.

#### 2.1.1.2 Orientation selection for high-resolution imaging

Pain studies investigating brainstem structures have varied in their use of axial (Iannetti et al., 2005b; Zambreanu et al., 2005) or coronal (Dunckley et al., 2005) acquisition orientations, but to our knowledge none has systematically compared both acquisition methods. Axial sequences typically have an anterior-posterior (y-plane) phase-encode

direction while coronal sequences encode in the medio-lateral (x-plane) direction. One potential benefit of encoding in the y-plane is that any distortions are symmetrical between both hemispheres and may have a decreased overall effect on BOLD signal in brainstem structures- which are often in the midline and can activate bilaterally to pain stimuli (Lee et al., 2008). In light of this, we tested which orientation most ably overcomes these distortions by quantifying regional signal-to-noise ratios (SNR) and task-related signal changes in relevant regions.

Pain relevant brainstem structures- including the periaqueductal grey, nucleus cuneiformis, rostral ventromedial medulla and locus coeruleus, have their largest dimension in the rostro-caudal direction (Naidich et al., 2009). This suggests that using an axial sequence with high in-plane resolution and larger slice thickness would be able to combine better localisation with good signal acquisition in these areas. We tested such an axial sequence ($1.5x1.5x3mm^3$) against a more standard 2mm isotropic coronal sequence acquisition, which while having larger voxel volumes (and more signal) does not incorporate these potential structure-specific benefits.

#### 2.1.1.3 Registration

The compact nature of brainstem nuclei increases the importance of registration accuracy. Conventional functional neuroimaging analyses typically involve registration of images from a functional space to a standard space to facilitate between-group comparisons. This typically involves a two-step process where a whole-brain functional image is registered to a higher quality structural image (typically T1-weighted) and the structural image is then registered to a standard brain (e.g. Montreal Neurological Institute). Both transformation matrices are then concatenated and applied to the functional data. In the context of brainstem imaging, limited field of view (FOV) acquisitions are often used to

allow higher resolution images to be acquired for activity localisation. In these cases, an additional registration step is added, where the limited FOV functional image is initially registered to a whole brain EPI from the same session. Here we used this three-step registration process within the FSL analysis pipeline (www.fmrib.ox.ac.uk/fsl).

Boundary based registration is an improved technique which optimises alignment of input images to a reference by maximising the intensity gradient across the tissue boundaries (Greve and Fischl, 2009). As the technique must separate tissue types in the reference image, it requires adequate resolution and quality of the reference image. While this technique has been developed for cortical registration, we employed it in the second registration step between a whole brain EPI image and the subject's structural image to improve brainstem and overall brain alignment.

### 2.1.2 Aim

This study aimed to improve our ability to image the brainstem and associated subcortical structures using tactile and painful stimuli in a non-CS state. We aimed to optimise acquisition parameters and registration techniques for high-resolution brainstem imaging at 3T, using physiological noise modelling to minimize regional susceptibility effects. By comparing axial and coronal sequences, we also intended to investigate which orientation most ably overcomes phase-encode specific EPI distortions that commonly affect data acquisition in the brainstem region.

### 2.1.3 Methods

#### 2.1.3.1 Subjects

6 healthy volunteers (3 male, 3 female, mean age: 26 (SD 2.17)) participated in this study after giving informed consent. Participants were right-handed non-smokers with no history of chronic pain conditions, free of acute illnesses and on no regular medication.

#### 2.1.3.2 Study protocol and stimulation paradigm

The study involved one fMRI scanning session per subject. Subjects received 2 sets of painful (thermal and punctate) and vibrotactile stimuli; one using an axial 1.5x1.5x3 $mm^3$ sequence and another using a coronal 2x2x2 $mm^3$ sequence. These sets took place in a pseudo-randomised order. The image resolutions were chosen to complement the shapes and sizes of the relevant brainstem nuclei (Naidich et al., 2009), given SNR limits for 3T imaging. A brainstem-focused acquisition was used (see Fig 2.2) to allow for a more robust examination of activity in pain-relevant nuclei at high resolution within reasonable TR and stimulus repetition limitations.

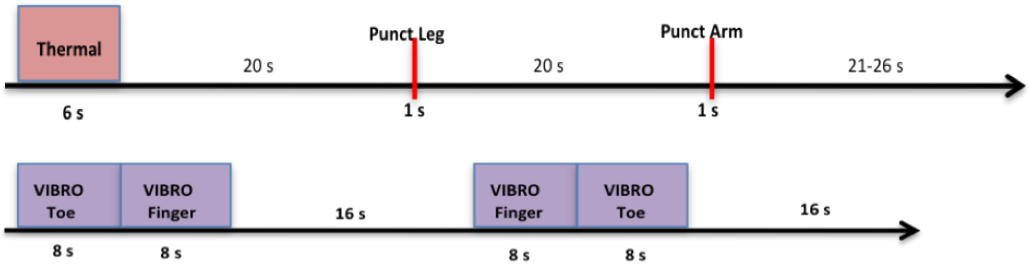


Figure 2.1: **Stimulus paradigm for pain & vibrotactile runs.** For the pain run, subjects received a thermal stimulus every 63-70 seconds, with punctate stimuli to the right arm and leg delivered at 20-second intervals within this time-frame. Vibrotactile runs included two adjacent stimulus blocks delivered pseudo-randomly to the toe and finger, and interspersed by 16-second intervals.

In the pain run, subjects received 15 thermal stimuli to the right volar forearm delivered with a MEDOC Pathway CHEPS device, and thresholded at 6/10 on an 11-point verbal pain rating scale (0-10; 0 no pain, 10 worst pain imaginable). The thermal stimuli were separated by two punctate stimuli delivered pseudo-randomly between the right forearm and right lower leg (antero-medial aspect) using a 512mN punctate probe (Fig 2.1). Subjects were asked after each experiment to give an average verbal rating of their thermal pain and to report any change in punctate sensation.

In the vibrotactile run, subjects received 20 blocks of vibrotactile stimuli to the right index finger and the right hallux delivered pseudo-randomly at 30Hz via a Piezo-electric vibration device (PI Ceramic, Lederhose, Germany).

For all scans, physiological noise data was collected using a pneumatic belt and a pulse oximeter (9500 Multigas Monitor MR Equipment, Bay Shore, NY), together with volume triggers from the scanner. All data was recorded using an MP150 system (BIOPAC Systems, Inc., Goleta, CA) at a sample rate of 100Hz. Experimental stimulation was controlled by a computer running PainGain (FMRIB Stimulus Presentation System) and visual prompting by a computer running Presentation (version 16.0; Neurobehavioral Systems, Albany, CA).

#### 2.1.3.3 fMRI data acquisition paradigm

All imaging data was acquired using a 3T Siemens Verio MRI scanner (Siemens Medical Systems, Erlangen, Germany). A 32 channel receiver head-only RF coil was used with a birdcage RF head coil for pulse transmission and signal reception. Functional scans for pain and vibrotactile runs were acquired with a partial-brain gradient-echo, echo-planar imaging (EPI) sequence (matrix 96x96, phase partial Fourier 7/8, echo time (TE)=30 ms,

repetition time (TR)= 2s, GRAPPA with acceleration factor 2). For the axial sequence, 21 contiguous 3-mm thick axial slices were acquired with an in-plane resolution of 1.5 x 1.5 $mm^2$. For the coronal sequences, 20 contiguous 2-mm thick coronal slices were acquired with an in-plane resolution of 2 x 2 $mm^2$. 483 and 329 volumes corresponding to 15 minutes and 10 minutes of scanning time were acquired for the pain and vibrotactile runs respectively. The field of view (FOV) of each acquisition is illustrated in Figure 2.2. For each subject, a single volume whole-brain EPI image per scan (1 axial and 1 coronal image per subject, same acquisition parameters as above), and a T1-weighted 1x1x1 $mm^2$ structural image were acquired for registration. Field maps were acquired to correct for regions of field inhomogeneity.

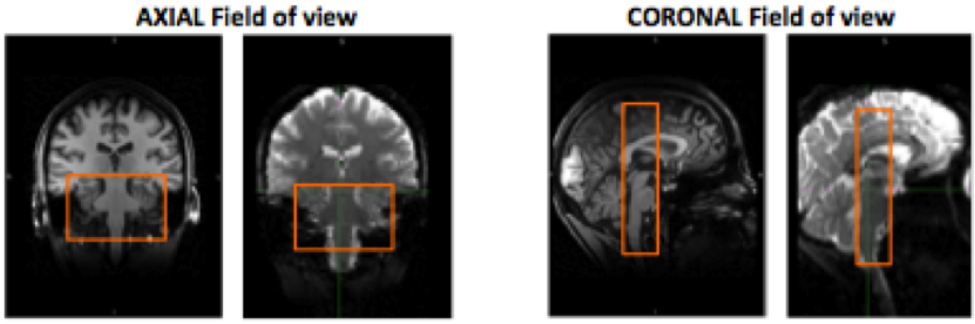


Figure 2.2: **Acquisition fields of view** Overlaid on structural (left) and functional (right) images.

#### 2.1.3.4 Data Analysis

Analysis of all imaging data was performed using FMRIB Software Library (FSL) version 5.01 (http://fmrib.ox.ac.uk/fsl) (Jenkinson et al., 2002). Preprocessing of functional data included motion correction using MCFLIRT (Jenkinson et al., 2002), spatial smoothing (full width at half maximum = 1.5mm), high-pass temporal filtering and application of BET (brain extraction tool) (Smith, 2002).

Physiological noise regressors were computed using a custom MatLab (MathWorks, Natick, MA) script (Brooks et al., 2008). A physiological noise model based on Retrospective Image Correction (RETROICOR) (Glover et al., 2000) was applied to the motion corrected time-series. Cardiac and respiratory phases were calculated from the acquisition time for each slice and physiological measurements recorded during BOLD image acquisition (Brooks et al., 2008; Harvey et al., 2008; Kong et al., 2012); respiratory phase was assigned using a histogram equalised transfer function to account for respiratory timing and amplitude. Next a Fourier series was constructed using the determined phases in order to independently model the cardiac and respiratory effects- this consisted of 8 cardiac sine/cosine terms and 8 respiratory sine/cosine terms, giving sixteen regressors. An additional sixteen multiplicative sine/cosine terms modelled the interaction between cardiac and respiratory effects. A heart rate and a respiratory ventricular trace regressor were also calculated from the cardiac and respiratory traces respectively giving a total of 34 slice-dependent physiological noise regressors. These regressors were then included in the general linear model (GLM) using FEAT (Limbrick-Oldfield et al., 2012) to test for responses to pain and vibrotactile stimulation tasks.

Each EPI image was first registered to a whole brain EPI image using FLIRT (Jenkinson and Smith, 2001), then to the individual subject's T1-weighted structural image using boundary-based registration (BBR) (Greve and Fischl, 2009). The image was then registered to a standard 1mm MNI brain for between-subject comparisons using FNIRT (Andersson et al., 2007).

Individual subject responses to stimuli were modelled in the GLM using convolved task blocks with a single gamma haemodynamic response function. Temporal derivatives of the stimuli were included to account for differences in individual HRF functions. Motion and physiological regressors were added as noise confounds in the GLM. The functional

acquisitions for all 6 subjects were entered into a fixed effects linear model analysis at a group level to give an average activation pattern. Z-score images were generated at a threshold of Z=1.8 with corrected cluster significance of $p \leq 0.05$ (Worsley, 2001) or displayed as an uncorrected statistical map at $p \leq 0.01$.

Temporal signal to noise ratio (TSNR) was used to assess the stability of the fMRI signal in brainstem regions. TSNR was calculated using hand-drawn anatomical masks of brainstem regions (see Fig 2.4), referenced from Duvernoy's Brainstem Atlas (Naidich et al., 2009), and the anatomical mask of the brainstem generated from the Montreal Neurological Institute (MNI) standard brain and thresholded such that only regions which had at least a 70% of being part of the brainstem were included (i.e. $p>0.7$). The leftover variance of each functional image (after modelling out activation and physiological noise) was square rooted to give a standard deviation image. This was then divided into the mean functional image to give a voxelwise map of the tSNR in the brainstem region. Voxels in this image were averaged in relevant masks to give the regional tSNR values for each of the functional acquisitions. A higher tSNR value indicates better signal stability.

### 2.1.4 Results

#### 2.1.4.1 Psychophysics

Before each thermal stimulation block, thermal pain was thresholded at 6/10. Following the block of thermal stimulation, subjects reported an average rating for all thermal stimuli within the block. Averaged across all subjects (mean ± standard deviation) this rating was 5.5/10 (±0.84) for the axial acquisitions and 5.3/10 (±1.03) for the coronal acquisitions, with no significant difference between the two acquisitions (paired t-test: $p=0.77$). Subjects reported no change in punctate sensation over the experimental run.

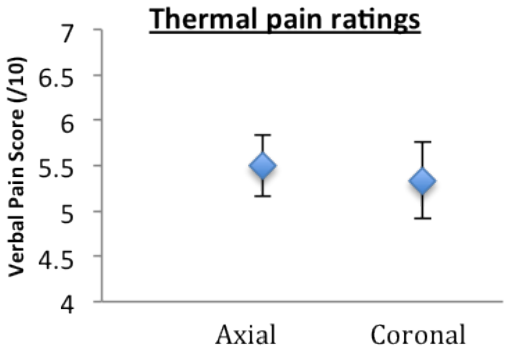


Figure 2.3: Thermal verbal pain ratings between axial and coronal acquisition runs. n=6. Error bars represent standard error of the mean (SEM).

#### 2.1.4.2 Temporal Signal to Noise Ratio

Temporal signal to noise ratio (tSNR) across the brainstem region, before physiological noise modelling (PNM), is illustrated in Fig 2.4. Higher tSNR values are seen in the axial sequence compared to the coronal sequence across most regions of the brainstem. Both sequences show higher tSNR values in deeper brainstem regions than in outer regions, adjacent to ventricles and blood vessels.

As expected, PNM improves tSNR across the brainstem for both axial and coronal sequences. Both sequences also show greater PNM related tSNR increases in peripheral brainstem regions compared to deeper regions, with axial acquisitions showing greater increases than coronal acquisitions (Fig 2.4). When this improvement is assessed in the brainstem's three structural divisions (midbrain, pons and medulla), the greatest PNM increase is seen in the medulla for both sequences- there is a larger proportion of voxels with >5% improvement (Fig 2.4). The axial sequence shows greater PNM improvements in the midbrain and pons than the coronal sequence, with the opposite effect in the medulla.

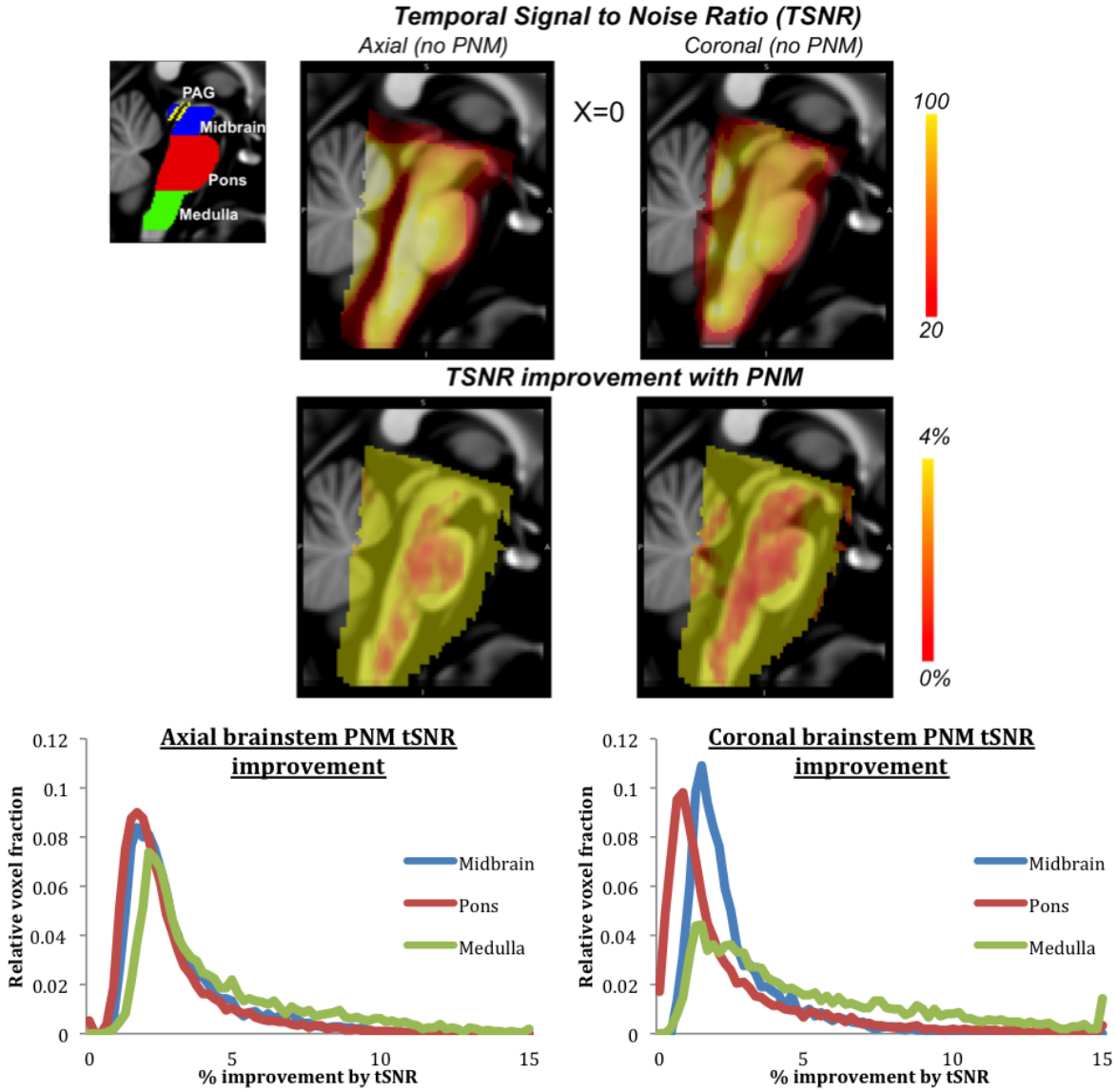


Figure 2.4: Regional differences in temporal signal to noise ratio (tSNR) are shown in the top image (n=6, pain runs only). Improvement in tSNR is shown in the middle row. The graphs show percentage tSNR improvement by PNM by fraction of voxels in each brainstem region-normalised to regional voxel number. Anatomical regional masks are shown in the top left image.

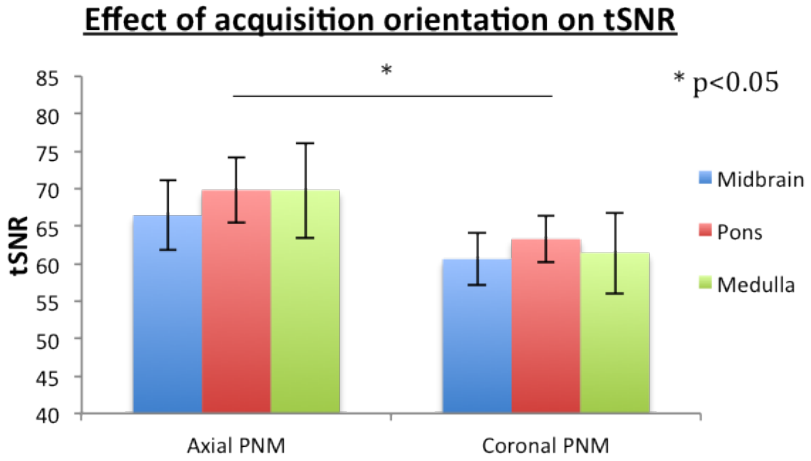


Figure 2.5: Shows tSNR differences between Axial and Coronal sequences in various brainstem regions (n=6, pain runs only; regional masks shown in Fig 2.4). Error bars represent SEM.

TSNR values after PNM are quantified in Fig 2.5. In a comparison across the whole brainstem, there is significantly higher tSNR for axial acquisitions (paired t-test, p=0.042). Independent samples t-tests comparing each brainstem region between axial and coronal acquisitions showed axial tSNR is significantly higher than coronal tSNR in the pons (paired t-test, 2 tailed, p=0.037), and trends in the same direction for the midbrain (p=0.079) and medulla (p=0.118) (Fig 2.5). Within both axial and coronal acquisitions, there is no significant difference between tSNR in the different brainstem regions.

#### 2.1.4.3 BOLD effect

*Pain run*

Suprathreshold activity is present for both acquisitions only with boundary-based registration. However, in Fig 2.6 we illustrate uncorrected activity (p<0.01) for better visual comparison between suprathreshold and near threshold voxels.

Both axial and coronal acquisitions show activation of pain-relevant nuclei in the brainstem region including the periaqueductal grey (PAG) to thermal and punctate stimuli

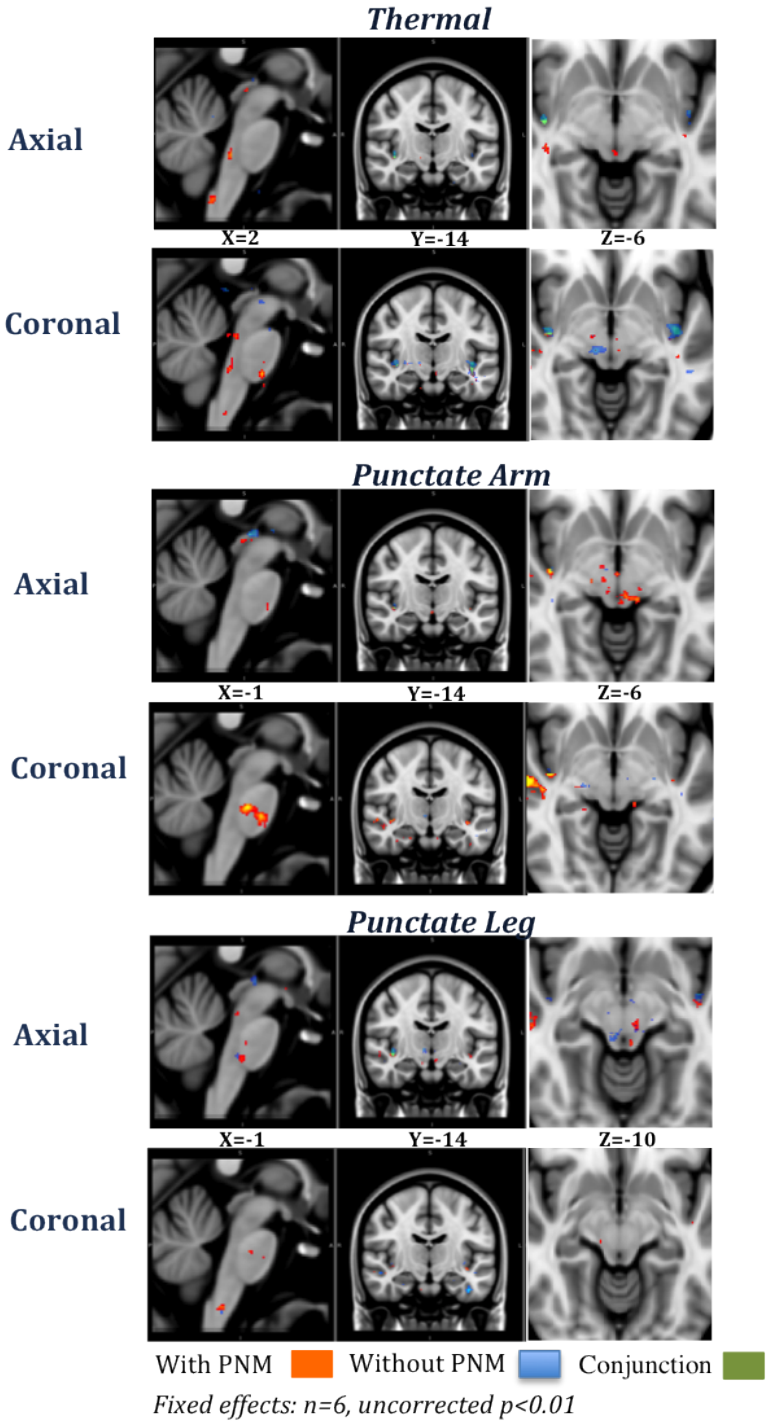


Figure 2.6: Activation to painful stimulation overlaid on an MNI standard brain. Top: thermal stimuli. Middle: punctate to R arm. Bottom: punctate to R leg. Images are displayed in radiological convention.

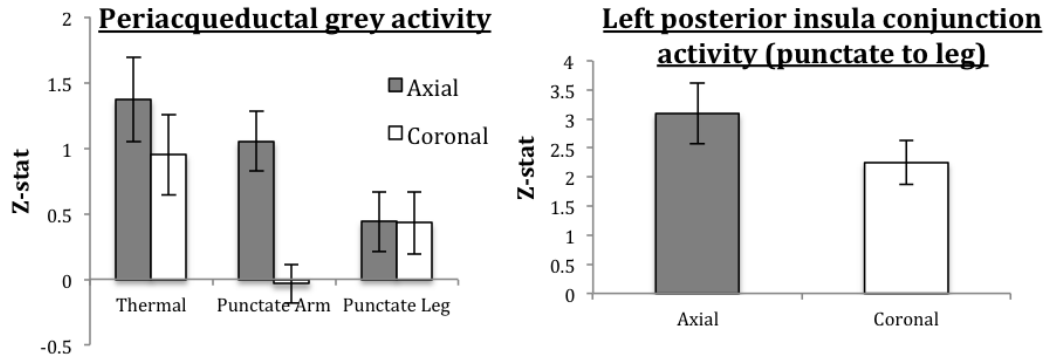


Figure 2.7: BOLD activity (after PNM) to pain stimuli compared in axial and coronal acquisitions- within the anatomical PAG (left) and in a conjunction mask (n=6, fixed effects model, Z=1.8, p<0.05 cluster corrected) within the contralateral posterior insula (right). Error bars represent SEM.

and rostral ventromedial medulla (RVM) to thermal stimuli (Fig 2.6). These activations are improved by PNM (Fig 2.6).

Axial acquisitions are shown to be more effective at revealing PAG activity (shown in all three pain conditions) when compared to coronal acquisitions (no PAG activity) (Fig 2.6). When z-scores are compared, there is greater PAG activity in the axial acquisition for all conditions (Fig 2.7). Outside of the brainstem, we also test a conjunction region of suprathreshold activity (Fixed effects; cluster corrected, Z=1.8, p<0.05) in the contralateral posterior insula and show that there is greater BOLD activity with the axial acquisition (Fig 2.7).

*Vibrotactile run*

Activity to vibrotactile stimuli did not survive cluster correction at a group level (Z=1.8, p<0.05)- not surprising given the small size of the sensory nuclei, low stimulus input and low subject number, but is appropriately visualised in Fig 2.8 (uncorrected p<0.01). Given the clear improvement in tSNR and relevant BOLD activity demonstrated above,

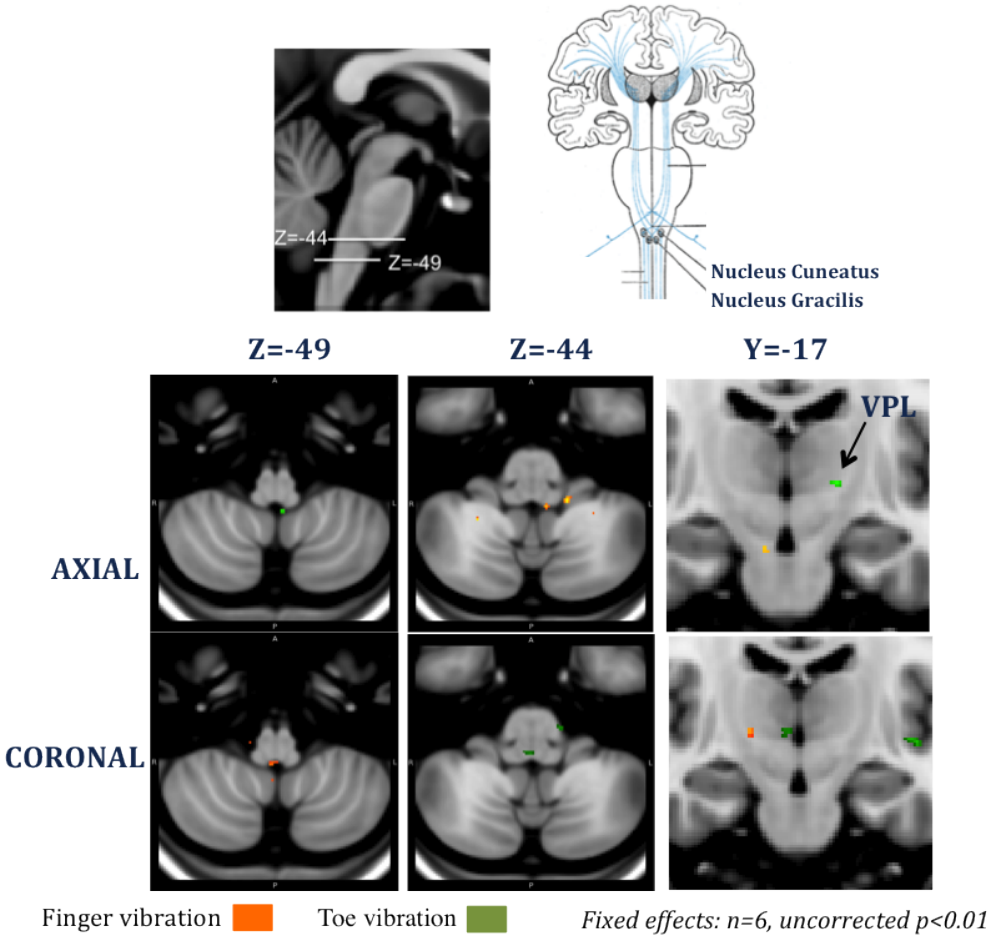


Figure 2.8: BOLD activity (after PNM) to vibrotactile stimuli (toe- green, finger- orange) compared in axial and coronal acquisitions (uncorrected $p<0.01$). Schematic on top right shows location of dorsal column nuclei (adapted from Gray's Anatomy (1918)). VPL- ventral posterolateral nucleus of the thalamus. Images are displayed in radiological convention.

the results shown here are only following PNM.

Both acquisitions show poor localisation of the cuneate and gracile nuclei when referenced with a detailed brainstem atlas (Naidich et al., 2009) (Fig 2.8). However, for the axial sequence, activation to toe vibration is appropriately more infero-medial when compared to activation to finger vibration. The axial acquisition also shows contralateral activation of the ventral posterolateral nucleus of the thalamus to toe vibration. The coronal acquisition shows ipsilateral activation of the same nucleus to finger vibration.

### 2.1.5 Discussion

Our results suggest that an axial high-resolution acquisition with physiological modelling and boundary-based registration is optimal for brainstem imaging

Temporal signal to noise ratio (tSNR) values reflect the change in signal to noise over an experimental timecourse, as influenced by thermal noise and other sources of timecourse variation. Physiological noise modelling (PNM), by removing structured noise, showed a trend of improving tSNR in both axial and coronal images across all regions of the brainstem (Fig 2.4). The medulla appeared to benefit more from PNM than other brainstem regions with the greatest voxel fraction showing >5% improvement. This reproduces a similar result shown by Harvey and colleagues (2008) and supports the use of PNM for stabilising functional signal from the rostral ventromedial medulla- a key structure in the descending modulation of pain. Greater tSNR improvements with PNM in the medulla and peripheral brainstem regions may be explained by their increased exposure to coarse motion from blood flow and CSF. For most conditions, this improved tSNR was shown to translate to improved functional visualisation of pain relevant BOLD activity in the PAG and RVM (Fig 2.6).

Following PNM, axial sequences were shown to have significantly higher tSNR in the pons (and to trend strongly in the same direction in the midbrain) when compared to coronal sequences (Fig 2.5). This is despite the axial prescription having a lower volume (6.75 $mm^3$ for axial, 8 $mm^3$ for coronal), supporting the use of the higher resolution voxels. This suggests that lower overall signal in higher resolution imaging can be traded for improved signal to noise by use of an optimised axial sequence that may reduce signal dropout in key brainstem areas.

A key limitation of this study is that we were unable to directly compare signal acquisition between the two sequences due to differing voxel sizes. However the results suggest that the benefits of decreased distortion and dropout with the axial sequence outweigh the theoretical decrease in signal acquisition from the reduced voxel volume. We therefore propose that normalising voxel volumes would further improve axial tSNR in the brainstem in comparison to coronal tSNR.

The axial 1.5x1.5x3 $mm^3$ acquisition showed improved activation (cluster volume and Z-statistics) to pain stimuli in the midbrain PAG when compared to the coronal 2x2x2 $mm^3$ acquisition (Fig 2.6 and Fig 2.7). The PAG as with other brainstem nuclei, while small in size, has its maximal length rostro-caudally. As such, higher in-plane resolution and greater slice thickness of the axial sequence may support greater BOLD signal acquisition in these nuclei despite the smaller voxel size. In addition, the EPI distortions seen in axial acquisitions are symmetrical in the acquired anterior-posterior phase-encode direction, which can reduce distortion and signal dropout within the midline PAG.

A drawback of the axial sequence is its reduced coverage of cortical areas compared to the coronal sequence. However, we showed that functional activity in an overlapping cortical region (posterior insula) is not compromised and may be improved by use of

the higher resolution axial sequence (Fig 2.7), supporting its use for larger coverage acquisitions. Although the field of view (FOV) for the sequences used in this study were limited to optimise brainstem acquisition, the generalizability of the technique for a larger axial FOV is important. This enables optimised simultaneous acquisition of functional activity from cortical, subcortical and brainstem regions, and allows testing of functional connectivity between these regions.

Results from the vibrotactile run suggest that 3T high-resolution imaging does not enable us to distinguish between two small adjacent nuclei in such a small cohort. However, uncorrected ($p<0.01$) activity in the region of the sensory nuclei suggested that significant BOLD-related neural activity in the gracile and cuneate nuclei might be revealed with higher subject numbers. The use of an axial orientation in acquisition, in addition to PNM and boundary-based registration appeared to improve localisation of medullary functional activity and better reveal a labelled-line subcortical correlate of the vibration stimulation in the contralateral ventral posterolateral thalamus.

The majority of pain imaging studies focusing on the brainstem have used sequences with in-plane resolutions of $3x3mm^2$ or lower (Dunckley et al., 2005; Lee et al., 2008; Zambreanu et al., 2005); these results suggest that using an axial sequence with a higher in-plane resolution may be useful in isolating activation from the small nuclei in the region.

Physiological noise modelling was shown to be beneficial for increasing true positive fMRI signal in pain-relevant brainstem areas and we propose that it may be useful in any such pain study involving these regions. Modelling out regressors that may have some stimulus correlation (e.g. changes in breathing with pain stimulation) may also remove some true signal from the data and as such the use of PNM should be well

evaluated, particularly with less robust experimental designs. However, we showed that the overall effect of PNM is to improve both signal-to-noise ratio stability and functional activation in the context of a simple pain paradigm.

## 2.2 Experiment 2

This study uses the optimised parameters from Experiment 1 to test the use of the capsaicin model and ultra high field imaging in investigating central sensitisation. We compare brain activity in a sensitised and sham state before comparing the use of a 3T scanner to a 7T scanner for identifying the neural correlates of punctate hyperalgesia in the brainstem and subcortical areas.

### 2.2.1 Introduction

Our results from study one indicated that the use of physiological noise, boundary-based registration and high-resolution axially oriented sequences are beneficial for pain imaging in the human brainstem. However, the pain model used in that experiment was for acute pain and is not suitable to investigate neuropathic pain and its causes. Neuropathic pain symptoms include secondary mechanical hyperalgesia, allodynia and ongoing pain, all of which can be induced by the ethically allowed capscaicin-induced central sensitisation model (Baron, 2006).

Here we tested the utility of the topical capsaicin model of central sensitisation- its reproducibility within a one-week time frame and its neural correlates. We further tested the incremental benefit of ultra high field (7T) imaging over high field (3T) in investigating subcortical activity with such paradigms.

#### 2.2.1.1 A healthy human model of central sensitisation

Following peripheral injury, there is a heightened behavioural response to heat and mechanical noxious stimulation within the injured area (primary hyperalgesia) due to local release of inflammatory mediators and subsequent sensitisation of peripheral nociceptors

(Ali et al., 1996).

In addition to this, an increased response to mechanical noxious stimulation in the area surrounding the injury but not directly innervated by the same group of neurons (secondary hyperalgesia), and a painful response to innocuous stimulation (allodynia) can also develop. This response is termed central sensitisation (CS) and is characterised by an increase in spinal dorsal horn neuronal excitability, which far outlasts the initial nociceptive input (Ji et al., 2003; Woolf, 1983).

In order to study pain responses secondary to injury, and the mechanism of central sensitisation, safe and reversible human models of hyperalgesia and allodynia have been developed (Klein et al., 2005). Foremost among these is the capsaicin model. The capsaicin model mimics the post-injury spontaneous and evoked pain phenotype most often seen in post-herpetic neuralgia, peripheral nerve injury and complex regional pain syndromes (Maier et al., 2010). However, it must be noted that capsaicin does not provide a direct model of neuropathic pain because it does not account for the consequences of nerve damage (e.g. sensory loss), which are common in many neuropathic pain conditions. Furthermore the evoked sensory perturbations typically measured in this model vary from the ongoing neuropathic pain that patients mainly complain of and which are primary outcome measures in randomised controlled trials for analgesic efficacy. As with most human surrogate models of neuropathic pain, the capsaicin model mimics sensory symptoms of both neuropathic and nociceptive pain. Therefore findings from the use of such a model are pertinent but not specific to neuropathic pain (Klein et al., 2005). Nonetheless, the benefits of studying the underlying mechanisms of CS in a homogenous, healthy and drug-free population compensates for the difficulty of immediate clinical translation due to these differences from the true neuropathic pain phenotype.

Capsaicin application has been reliably used as a model of mechanical punctate hyperalgesia, dynamic mechanical allodynia and spontaneous pain (Kilo et al., 1994; Liu et al., 1998; Zambreanu et al., 2005)- cardinal expressions of central sensitisation (Woolf, 2011). Capsaicin is a pungent alkaloid found in chillies and when applied cutaneously binds to transient receptor potential vanilloid receptor 1 (TRPV1) on peripheral C-fibre nociceptor terminals (Caterina and Julius, 2001). The mechanism by which it produces hyperalgesia and allodynia has been studied extensively (LaMotte et al., 1991; Lee et al., 2008; Magerl et al., 1998; Ziegler et al., 1999) and is thought to involve the sensitisation of central second- and third-order mechano-receptive neurons.

Capsaicin can be applied intradermally or topically. Intradermal application leads to brief but severe burning pain lasting minutes, after which there is mechanical hyperalgesia for up to 3 hours. When topically applied to normal skin, a mild to moderate (varying based on capsaicin concentration) burning sensation develops after 30-40 minutes and is maintained in addition to mechanical hyperalgesia until the cream is removed. Mechanical stimulation is delivered using punctate probes, which give a sharp sensation by specifically activating mechanoreceptors without also activating A$\beta$ tactile afferents (Treede et al., 2002). A somedic brush can also be used to elicit mechanical allodynia through activation of low threshold mechano-sensitive A$\beta$ fibres (Kilo et al., 1994). After large doses (8%) or prolonged administration, capsaicin can also lead to desensitisation of sensory neurons (Bevan and Szolcsányi, 1990), lending to its use in the treatment of neuropathic pain conditions (Derry et al., 2009). In healthy volunteers permanent damage may be avoided with inter-session intervals of at least a week (Karrer and Bartoshuk, 1991).

The neural correlates of central sensitisation and capsaicin-induced hyperalgesia have been investigated previously with both animal and human data supporting the specific

importance of descending brainstem activity in the maintenance of spinal excitability (Lee et al., 2008; Suzuki et al., 2002; Zambreanu et al., 2005). We use the topical capsaicin model here and in the later chapters to model tonic, ongoing pain and prolonged hyperalgesia as seen in nerve/tissue injury and the subsequent centrally sensitised state (Woolf, 2011). We use 1% capsaicin concentration and apply it for at least an hour before testing. The moderate concentration is to allow adequate induction of sensitisation while avoiding rapid desensitisation and the time frame is similar to what is used by Zambreanu and colleagues (2005) in a heat/capsaicin sensitisation model. While spontaneous pain in the topical model may confound the mechanistic interpretation of behavioural and neural correlates of hyperalgesia, its similarity with the neuropathic pain phenotype- where spontaneous pain is the most common symptom (Woolf and Mannion, 1999), improves its validity as a model. As such, results from this model may be more translatable to patient populations.

#### 2.2.1.2 Ultra-high field imaging for pain paradigms

The advent of ultra-high field (7 Tesla and above) fMRI in humans provides many potential benefits beyond the use of clinical strength (1.5 Tesla and 3 Tesla) MRI scanners (Yacoub et al., 2001). Both the magnitude of magnetic signal and ratio of thermal noise are proportional to the static ($B_0$) field. As a result, SNR at 7T is theoretically more than over twice that at 3T (Yacoub et al., 2001). Further, the T2* effect and subsequent signal change at a given susceptibility difference is also proportional to the static field. Together with the SNR increase, this means that contrast to noise ratio (CNR) is several times improved at ultra-high field. These factors allow imaging at a higher resolution to become more feasible and consequently fMRI signal can be more localised to the grey matter by avoiding partial volume effects associated with imaging large regions with mixed vascular compositions (Yacoub et al., 2003).

Despite these gains, there are also increased geometrical EPI distortions ($B_0$ field inhomogeneities increase linearly with field strength) and susceptibility artefacts (due to faster T2/T2* relaxation) at higher field. These effects are particularly evident in inferior brain regions where sharp tissue/non-tissue boundaries are present. Due to these limitations, the majority of ultra-high field imaging studies have used limited brain coverage acquisitions with localised shimming to improve image quality. However, the use of multi-channel receive-coils and parallel imaging has enabled whole brain acquisition at 7T without significantly compromising on efficiency or spatial resolution (De Martino et al., 2011).

To date, only a single published study has directly compared the use of high field and ultra-high field imaging in the context of imaging the human pain state (Hahn et al., 2013). The authors reported increased activity to electrical stimulation in the PAG at 7T when compared to 3T, although they used a brainstem-specific analysis strategy and report uncorrected voxel-level statistics ($p<0.001$). Importantly, the authors do not control for the varying effects of physiological noise at different field strengths (see below). We here aimed to investigate the utility of 7T imaging as compared to 3T in evaluating CS-related brainstem and subcortical brain activity in the context of a typical whole-brain image acquisition and analysis. We collected physiological data for noise modelling and $B_0$ field maps to measure field inhomogeneities and correct the related image distortion (Jezzard and Balaban, 1995).

#### 2.2.1.3 Physiological noise correction at ultra-high field

While the theoretical increase in fMRI contrast is linear to field strength, the increased ratio of physiological to thermal noise at higher fields (Krueger and Glover, 2001) may diminish some of this benefit (Fera et al., 2004). This makes physiological noise correc-

tion particularly important at ultra-high field. However, increasing the resolution and reducing signal at ultra-high field has been shown to reduce the ratio of physiological to thermal noise such that the higher sensitivity from the increased field strength still equates to better SNR overall (Triantafyllou et al., 2005).

In this study, we imaged at a 2mm isotropic resolution for both 3T and 7T. At the same resolution, we expected the influence of physiological noise to be higher at 7T and therefore applied the physiological noise model (PNM) to all our analyses as detailed from experiment 1.

### 2.2.2 Aim

In this study, we aimed to re-establish the behavioural and neural representation of the capsaicin model of hyperalgesia, confirm its reproducibility and verify its utility in investigating modulation of the sensitised state. Further we established the incremental benefit of ultra-high field (7T) over traditional high field imaging (3T) in the context of modulating this model of central sensitisation. This guided subsequent studies by determining how this model is employed for healthy human imaging. This study also aimed to elucidate the neural processing of lateralised pain by using identical stimuli in identical sites on both body sides- this part of the investigation will not be discussed in this thesis.

### 2.2.3 Methods

#### 2.2.3.1 Subjects

Twelve healthy volunteers (6 male, 6 female mean age: 26(S.D=4.2) participated in this study after giving informed consent. Participants were right-handed with no history

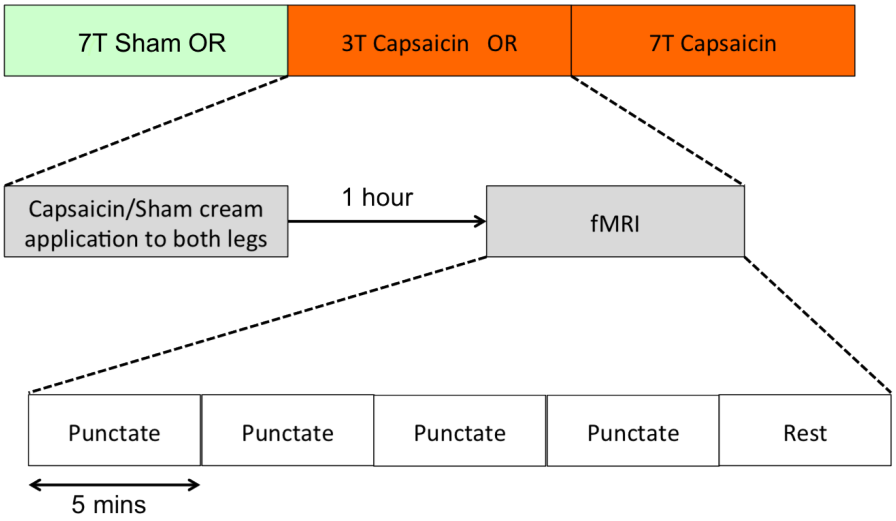


Figure 2.9: **Experimental design.** Subjects attended one of three sessions where they received 1% capsaicin cream to both legs 1 hour before fMRI scanning. Subjects received punctate stimuli with a force of 128mN and 512mN to both right and left legs (4 runs), and a resting scan.

of chronic pain conditions, free of acute illnesses and on no regular medication. Eight subjects had previously experienced capsaicin application in an experimental setting- these were all more than 3 months prior.

#### 2.2.3.2 Study protocol and stimulation paradigm

All subjects participated in a three-way crossover study. The study visits were pseudo-randomised, separated by 1-2 weeks and followed an identical pattern (Fig 2.9).

During each visit, a designated 4x4 $cm^2$ area was marked out on the antero-medial aspect of each subject's lower left and right legs, at least 14cm above the medial malleolus. In the first visit only, subjects' responses to a 128mN and 512mN punctate probe were first tested at least 2cm outside the designated area. Subjects then received either 1% capsaicin cream or sham cream to the designated area on both lower legs simultaneously. Two visits involved active 1% capsaicin cream and subjects were scanned at 3T or at 7T.

One visit involved sham cream and subjects were scanned at 7T. Room temperatures were controlled in all visits to decrease variability in the capsaicin response (Liu et al., 1998).

1 hour after capsaicin/sham cream application, subjects underwent four functional scans which involved punctate stimulation to a secondary area- at least 2cm away from the designated application area (with the capsaicin cream left on the skin). The punctate stimulation and secondary mechanical punctate hyperalgesia (SMPH) were elicited to either leg using two punctate probe forces (128 mN and 512mN), giving a nociceptive/low pain condition and a high pain condition. As such, the four stimulation runs were- 128mN punctate to the right leg (1R), 128mN punctate to the left leg (1L), 512mN punctate to the right leg (5R) and 512mN punctate to the left leg (5L), The order of these stimulation runs was pseudo-randomised. Each stimulation run included 15 punctate stimuli, applied for one second with a jittered inter-stimulus interval of 14-24 seconds to reduce subject expectation and improve BOLD sampling efficiency.

During each session, subjects used a computerised visual analogue scale (VAS) to rate their ongoing pain (0-100; no pain, extremely painful) before each stimulus run, and their ongoing pain, average punctate intensity (0-100; not intense, extremely intense) and average punctate unpleasantness (0-100; not unpleasant; extremely unpleasant) after each stimulus run. Average ratings were taken from repeated stimuli to help to control for the experimenter-error in stimulus delivery.

Following the stimulation runs, subjects also undertook a resting state scan- for which they kept their eyes fixated on a cross and rated their ongoing pain before and after the scan, as well as a structural scan. Anxiety has been shown to be associated with changes in behavioural and neural pain responses (Ploghaus et al., 2001). As such subjects also

completed a trait anxiety questionnaire at the start of the first session, and a state anxiety questionnaire just prior to the first functional scan in every session.

#### 2.2.3.3 fMRI data acquisition paradigm

Imaging data was acquired using a 3T Siemens Verio MRI scanner and a 7T Siemens MRI scanner (Siemens Medical Systems, Erlangen, Germany). For the 3T, a 32 channel receiver head-only RF coil was used with a birdcage RF head coil for pulse transmission and signal reception. For the 7T, a multi-element receive and transmit head coil was used. Functional scans were acquired with a whole-brain gradient-echo, echo-planar imaging sequence (3T: TE=30ms, TR= 4s; 7T: TE=25ms, TR=4s). For both scanner sequences, 61 contiguous 2-mm isotropic axial slices were acquired. 91 volumes, corresponding to 5 minutes of scan time, were acquired for the each stimulation/rest run. Slice orientation was adjusted for each subject to minimise inferior brain artefacts. Structural images [MPRAGE] (3T: T1-weighted 1mm isotropic; 7T: T2-weighted 1mm isotropic) and field map images were acquired for registration and bias field unwarping.

Physiological data was acquired using a pneumatic belt and a pulse oximeter (9500 Multigas Monitor MR Equipment, Bay Shore, NY). Data was recorded using an MP150 system (BIOPAC Systems, Inc., Goleta, CA) at a sample rate of 100Hz. Subject response registration was via a computer running Presentation (version 16.0; Neurobehavioral Systems, Albany, CA). Skin conductance responses (SCR) were recorded with MRI-safe electrodes attached to the hypothenar of the subject's left hand. The electrodes were attached to the same dermatome (C8) to control for potential recording differences between dermatomes.

#### 2.2.3.4 Data analysis

*Psychophysics*

Pain ratings and anxiety scores were assessed using IBM SPSS Statistics, version 18 (IBM, Armonk, NY, USA). Secondary mechanical punctate hyperalgesia (SMPH) was defined as an increase in the average punctate intensity rating on both legs by at least a factor of two between the pre-capsaicin and post-capsaicin stimuli and a pain score greater than 10/100 (painful range). The effects of session and stimulation run were assessed using repeated measures analyses of variance (ANOVA).

*Imaging*

Analysis of all imaging data was performed using FMRIB Software Library (FSL) version 5.01 (http://fmrib.ox.ac.uk/fsl). Preprocessing of functional data included motion correction using MCFLIRT (Jenkinson et al., 2002), spatial smoothing (full width at half maximum = 4mm), high-pass temporal filtering, application of BET (brain extraction tool) (Smith, 2002). Field map images were unwarped using PRELUDE and applied to functional images using FUGUE during pre-processing to reduce distortion artefacts.

Physiological noise regressors were computed and modelled as described in Experiment 1 (Brooks et al., 2008). Input functions related to the punctate stimuli and the VAS rating tasks were modelled in the GLM using convolved task blocks with a single gamma haemodynamic response function. Temporal derivatives of the stimuli were included to account for differences in individual HRF functions. Variables relating to the VAS rating response, motion, and physiological noise were added as noise confounds in the GLM. The first level functional results for each subject was entered into a fixed effects linear model analysis in a second level within subject design to compare between the different stimulation and scan conditions. A mixed effects linear model group analysis (FLAME 1+2) was performed to generate average activation patterns for each contrast

and condition across all 12 subjects. Z-score images were generated at a threshold of Z=2.3 with corrected cluster significance of $p \leq 0.05$ (Worsley, 2001).

EPI images were registered to the individual subject's T1-weighted structural image (collected at 3T) using FLIRT (Jenkinson et al., 2002) and boundary-based registration (BBR) (Greve and Fischl, 2009). The image was then registered to a standard 2mm MNI brain for between-subject comparisons using FNIRT (Andersson et al., 2007).

### 2.2.4 Results

#### 2.2.4.1 Psychophysics

Trait anxiety scores are low for all subjects (Fig 2.10). State anxiety scores are not significantly different between the three sessions ($F(2,10)=1.588$, $p=0.257$) (Fig 2.10).

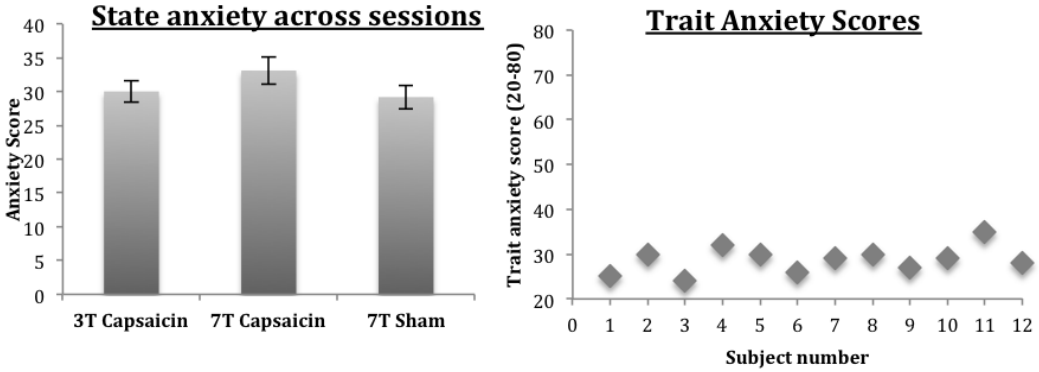


Figure 2.10: State Anxiety scores between sessions (left). n=12. Error bars represent standard error of the mean (SEM). Trait anxiety scores for each individual subject (right).

11 subjects fulfilled the criteria for SMPH for both sessions (Table 2.1). 3 subjects also exhibit SMPH during the sham session- this is surprising and may have resulted from the intrinsic variability in subjective ratings as the pre-capsaicin/sham scores were

Table 2.1: **Punctate intensity ratings for each subject and each session.** Subjects were stimulated in a secondary area (>2cm from capsaicin/sham application site). Pre-capsaicin ratings are for session 1 only. 3T- bold; 7T- italic. Average intensity rating for all runs. Mean (standard deviation).

| Subject number | Pre-capsaicin/ sham | 1st capsaicin visit | 2nd capsaicin visit | Sham visit |
|---|---|---|---|---|
| 01 | *0 (0)* | *0 (0)* | **0 (0)** | *0 (0)* |
| 02 | *3.3 (2.1)* | *10.8 (5.7)* | **22.5 (7.5)** | *3.5 (1.7)* |
| 03 | *0 (0)* | *32.3 (25.9)* | **31.3 (13.7)** | *0 (0)* |
| 04 | *0 (0)* | *28.8 (14.2)* | **5.5 (4)** | *1.8 (2.8)* |
| 05 | **14.5 (19)** | **41.8 (11.4)** | *41 (9.4)* | *11.3 (11.6)* |
| 06 | *8.3 (7.6)* | *40.3 (10.9)* | **34.5 (9.3)** | *20.5 (10.3)* |
| 07 | **2.5 (0.6)** | **46.8 (12.8)** | *54.5 (12.9)* | *4.8 (3.4)* |
| 08 | **4.5 (5.4)** | **57.8 (11)** | *63 (11.8)* | *20.5 (19.5)* |
| 09 | **8.3 (3.9)** | **44 (6.6)** | *21 (2.4)* | *16.8 (2.1)* |
| 10 | **0.5 (1)** | **20 (15.7)** | *45.8 (13.5)* | *2 (2.2)* |
| 11 | **1.3 (1.5)** | **14.3 (3.4)** | *20 (9.1)* | *4 (2.4)* |
| 12 | *0.8 (1)* | *71 (14.1)* | **18.8 (13.7)** | *6.3 (5)* |

taken only during the first session. In paired t-tests comparing the first and second capsaicin visits, there is no significant difference in average punctate intensity ratings in the region of SMPH (p=0.49) or OGP ratings (p=0.48). Test-retest correlations between both visits were significant for SMPH intensity (r=0.69, p=0.014) and OGP (r=0.79, p=0.002). The coefficient of repeatability was 39.8 for SMPH intensity and 32.6 for spontaneous pain (Bland and Altman, 1986).

In a 4-way repeated measure ANOVA comparing VAS scores, rating period (pre-stimuli and post-stimuli), session (3T Capsaicin, 7T Capsaicin, 7T Sham) and stimulation run (1R, 1L, 5R, 5L), there is a main effect of session ($F(2,10)=16.238$, p=0.001) and of rating period ($F(1,11)=10.347$, p=0.008) on spontaneous/ongoing pain. Pairwise comparisons adjusted for multiple comparisons (Bonferonni's correction) show that subjects experience significantly less spontaneous/ongoing pain during the sham cream session,

when compared to the 3T capsaicin session ($p<0.001$) and the 7T capsaicin session ($p=0.001$) (Fig 2.11). Subjects also experience significantly more pain post-stimuli than pre-stimuli ($p=0.008$).

There is no main effect of stimulation run ($F(3,9)=0.648$, $p=0.604$) on spontaneous/ongoing pain scores (Fig 2.11).

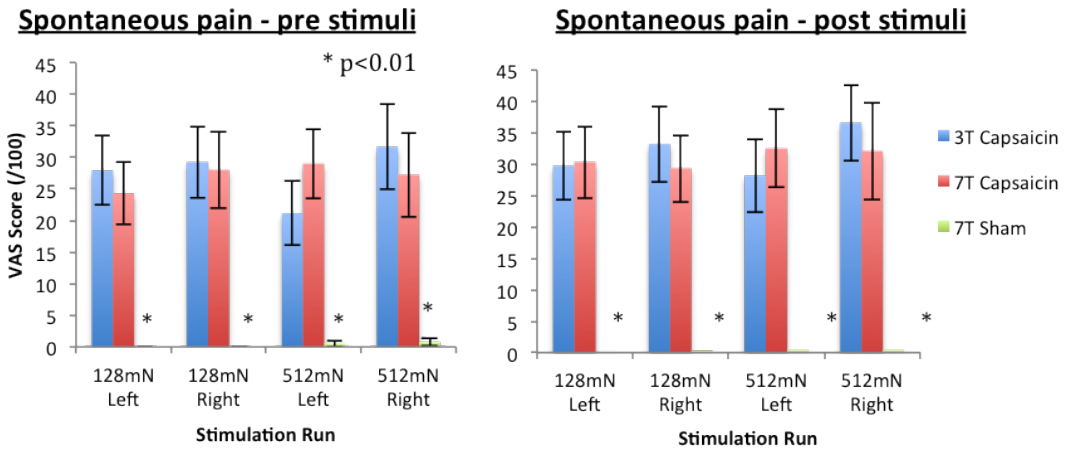


Figure 2.11: Average pre-stimuli (left) and post-stimuli (right) spontaneous/ongoing pain scores for different sessions and stimulation runs. n=12. Error bars represent SEM.

In a repeated measure ANOVA, there is a significant effect of session ($F(2,10)=17.559$, $p=0.001$) and run ($F(3,9)=5.585$, $p=0.019$) on punctate intensity scores (Fig 2.12). There is no interaction between run and session ($F(6,6)=0.737$, $p=0.64$). Pairwise comparisons (Bonferonni corrected) show that subjects report significantly less punctate intensity in the sham session when compared to the 3T capsaicin ($p=0.001$) and 7T capsaicin ($p=0.001$) sessions. Subjects also report increased punctate intensity in the 512mN left run when compared to the 128mN left ($p=0.22$) and 128mN right ($p=0.19$) runs.

In a separate repeated measure ANOVA testing effects of stimulation run and session on punctate unpleasantness, there is only a significant effect of session ($F(2,10)=15.641$, $p=0.001$) on unpleasantness scores (Fig 2.12). Pairwise comparisons (Bonferonni corrected) show that subjects experience significantly less punctate unpleasantness in the sham session when compared to the 3T capsaicin ($p=0.001$) and 7T capsaicin ($p=0.002$) sessions. There is no main effect of stimulation run ($F(3,9)=1.895$, $p=0.201$) and no interaction between session and run ($F(6,6)=0.247$, $p=0.943$).

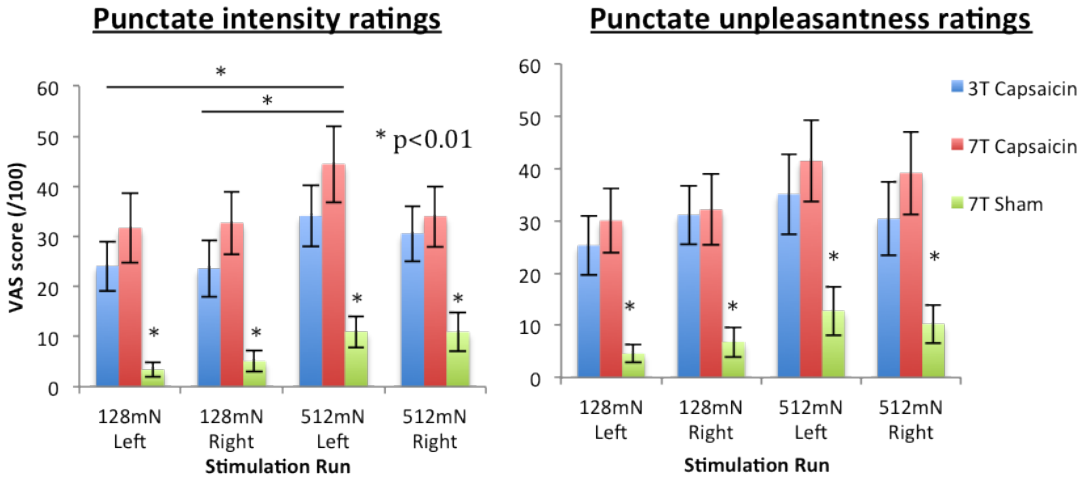


Figure 2.12: Punctate intensity (left) and unpleasantness (right) ratings for different sessions and stimulation runs. n=12. Error bars represent SEM.

#### 2.2.4.2 fMRI correlates of Capsaicin Induced Hyperalgesia

All 11 subjects who exhibited SMPH during the 7T capsaicin session were included into a group analysis comparing the 7T capsaicin session with the 7T sham session (Fig 2.13). We show that there is significantly stronger neural activation in the hyperalgesic state when compared to a control state (not controlled for perception) within several pain

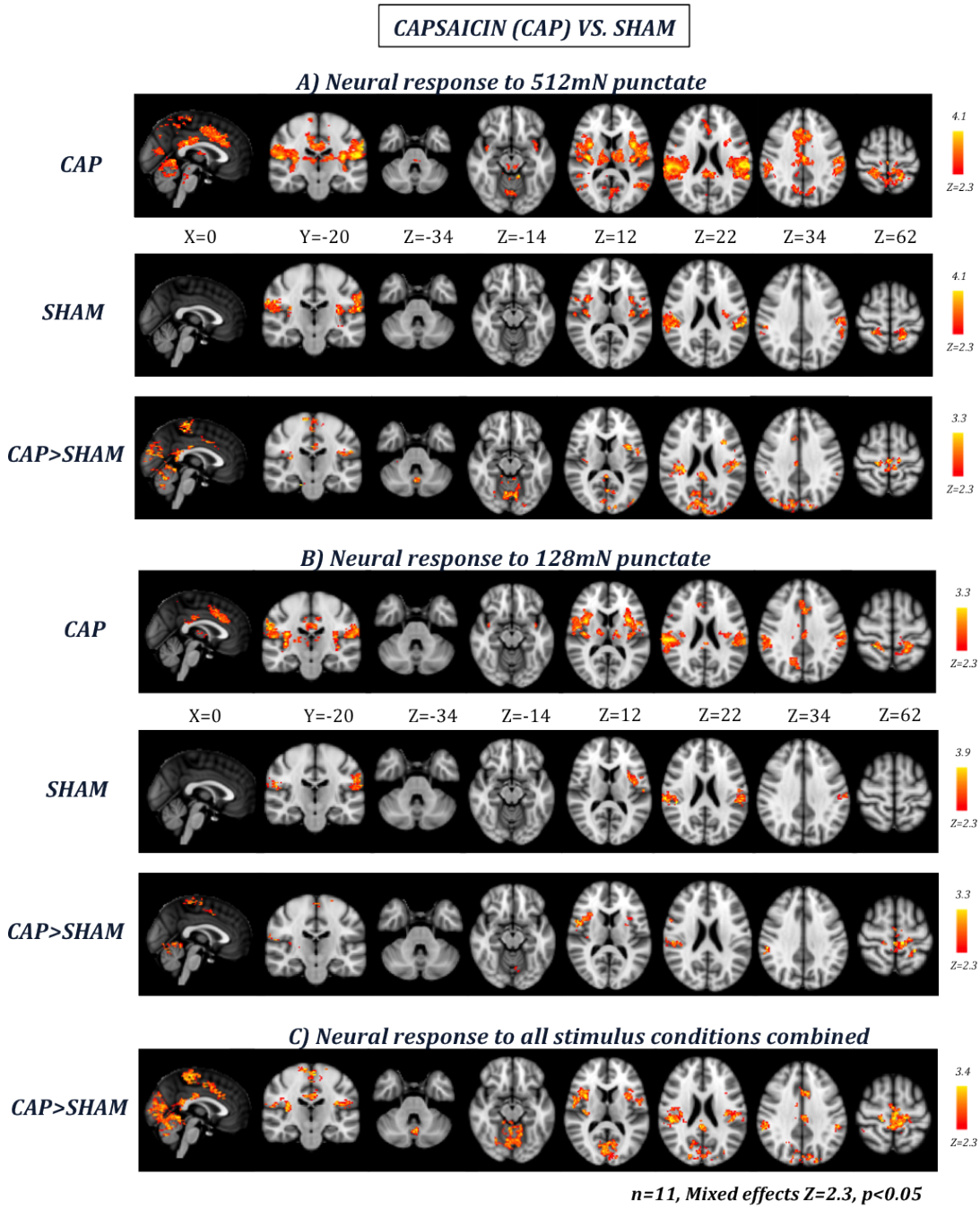


Figure 2.13: Group averaged activation maps (at 7T) showing neural correlates of capsaicin-induced mechanical hyperalgesia to 512mN punctate (A), 128mN punctate (B) and all stimuli combined (C). All images are in radiological convention (MNI coordinates are shown).

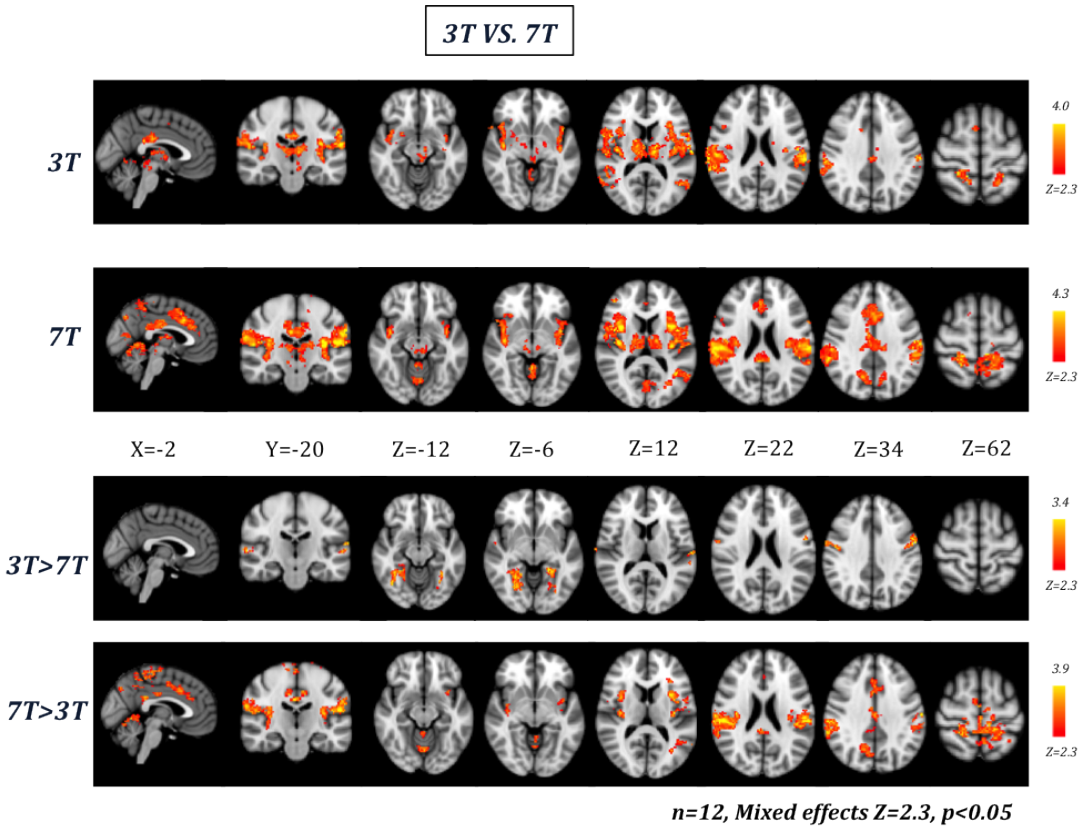


Figure 2.14: Comparison of neural representation of capsaicin-induced mechanical hyperalgesia (to all stimuli combined) between 3T and 7T. All images are in radiological convention (MNI coordinates are shown).

Table 2.2: **Peak z-scores in anatomical regions of interest** Shows peak z-scores in hyperalgesia-responsive regions of interest between 3T and 7T. Anatomical masks were derived from the Harvard-Oxford Structural Atlases (incorporated in FSLview) or hand-drawn with reference from a detailed brainstem atlas (see Fig 2.4). ACC, Anterior cingulate cortex; PAG, periaqueductal grey.

| | **Peak z-score** | | | |
|---|---|---|---|---|
| **Brain region** | 3T Left | 3T Right | 7T Left | 7T Right |
| SI | 4.50 | 4.39 | 4.60 | 4.58 |
| SII | 5.87 | 4.65 | 6.17 | 7.40 |
| Posterior insula | 4.63 | 4.24 | 4.94 | 4.97 |
| Anterior nsula | 4.06 | 4.25 | 4.11 | 4.26 |
| ACC | 3.77 | | 4.88 | |
| Thalamus | 4.69 | 4.35 | 3.99 | 3.79 |
| PAG | 3.33 | | 3.25 | |

relevant brain regions including the periacqueductal grey (PAG), primary somatosensory cortex (SI), secondary somatosensory cortex (SII), anterior cingulate cortex (ACC) and insula cortex (Fig 2.13C).

In a comparison of neural responses to SMPH between a control and capsaicin state, the use of a higher force probe (Fig 2.13A) reveals more brain regions than the use of a lower force probe (Fig 2.13B).

#### 2.2.4.3 Benefits of Ultra-High Field imaging for pain paradigms

All subjects were included in a group analysis comparing the 3T capsaicin session with the 7T capsaicin session (Fig 2.14 and Table 2.2). Both the 3T and 7T reveal a similar pattern of BOLD increases to SMPH. There is significantly stronger BOLD activation in several cortical pain-relevant areas (SI, SII, ACC and insula cortex) at 7T as compared to 3T (Fig 2.14 and Table 2.2).

Both field strengths reveal subcortical and brainstem activity (ventral tegmental area, PAG, nucleus cuneiformis) in the hyperalgesic state but there is no significant difference between the two. Furthermore Table 2.2 suggests that for a whole-brain coverage sequence, there is no difference in z-stats in subcortical (thalamus) and brainstem (PAG) areas between 3T and 7T.

### 2.2.5 Discussion

Our findings suggest that the topical capsaicin model of hyperalgesia and spontaneous pain is reliable and reproducible. We also showed that the use of an ultra-high field 7T MRI scanner significantly improves hyperalgesia-related BOLD activation in cortical areas but is comparable to a 3T scanner for subcortical and brainstem activation. It should be noted that this early experiment was done when the 7T scanner had just been installed; therefore, the sequence and various MR parameters (e.g. TE) were not necessarily optimised for the 7T and brainstem.

#### 2.2.5.1 Psychophysics - a reliable model of punctate hyperalgesia and spontaneous pain

We demonstrated that recruitment is feasible using this model as 11 of the 12 subjects recruited developed secondary mechanical punctate hyperalgesia when compared to the baseline ratings from the first session. Secondary mechanical hyperalgesia and spontaneous pain are also maintained in all runs (Fig 2.11 and Fig 2.12), suggesting that with the capsaicin cream left on the skin, subjects reach and maintain a stable hyperalgesia response in the 1-2 hour post-application time-frame. A comparison of post-application SMPH and spontaneous pain ratings showed a main effect of session, suggesting that the topical capsaicin method is reliable for inducing hyperalgesia and central sensitisa-

tion. However given that some subjects also developed hyperalgesia during the sham session, we suggest that pre-capsaicin intensity ratings should be taken in every session to better assess the intrinsic week-to-week variability in baseline ratings, and thus the development of hyperalgesia. Furthermore, by using multiple ratings for each stimulation run, we can use an average of the ratings to better account for subject rating error, in addition to experimenter error.

In studies investigating analgesic efficacy, treatment sessions may be separated by weeks. Various studies have investigated the reproducibility of pain stimuli in the non-sensitised state (Goddard et al., 2004; Rosier et al., 2002; Yarnitsky et al., 1996). Our results suggest that the between subject reproducibility of the behavioural secondary mechanical hyperalgesic response within a one or two week timeframe is reasonable- for all subjects who develop hyperalgesia in the capsaicin sessions, there was no significant difference between the intensity measures from the two capsaicin sessions. This suggests that this model of behavioural hyperalgesia can be used to test modulation of central sensitisation in a crossover design study. While the test-retest correlation is strong for the subjective ratings, within-subject test-retest reliability is more accurately assessed using a Bland-Altman plot (Bland and Altman, 1986), which tests absolute variation between measures. The corresponding coefficient of repeatability of the post-capsaicin SMPH VAS ratings is high (39.8), suggesting that a rating of 50/100 has a 95% chance of being between 10.2 and 89.8 the following week, if the pain stimulus remains the same. This high level of variability is comparable to what has been reported for thermal stimulation (coefficients of 3.8-4.7 on a 0-10 VAS scale range) (Yarnitsky et al., 1996). These session-to-session differences did not occur in a systematic fashion that may be indicative of residual skin de-sensitisation to capsaicin over the interval period (Table 2.1) and were likely due to session-related differences in the level of sensitisation, experimenter-related errors in stimulus delivery and subject-related errors in scale usage and ratings. A number of these

factors can also be mitigated by controlling for local temperature- which can influence capsaicin sensitisation, using an average of repeated stimulus ratings and taking baseline ratings in each session as described prior. Measuring the change in VAS ratings between the non-sensitised and sensitised state within each session, rather than only ratings in the sensitised state, would control for some of the differences related to session-specific rating ability of subjects.

Spontaneous pain report was also shown to be reproducible between subjects across time- no significant difference between capsaicin sessions (Fig 2.11), supporting its use in our later studies (Chapters 5 and 6) on the tonic pain state. Interestingly, punctate stimulation appeared to interact with ongoing pain, with increased ongoing pain reported after the stimulation. This is likely because the residual pain sensation from the punctate stimuli is difficult for subjects to separate from the background spontaneous pain in the short interval between ratings used. It would be appropriate to avoid using ongoing pain measurements immediately following a pain stimulation run.

#### 2.2.5.2 Neural correlates of hyperalgesia

We reported neural responses to hyperalgesia in similar regions to what has been previously described in models of topical and intradermal capsaicin (Fig 2.13) (Lee et al., 2008; Zambreanu et al., 2005). In particular, the neural response to SMPH with the 512mN probe showed suprathreshold activity in regions of the mesencephalic pontine reticular formation (MPRF)- which has been shown to be specifically involved in maintenance of central sensitisation (Lee et al., 2008). Furthermore, the contrast between capsaicin and sham revealed suprathreshold activity in more pain areas (includes anterior and posterior cingulate cortices) to the 512mN than the 128mN probe (Fig 2.13). It is evident that the use of a stronger probe allows better examination of relevant struc-

tures in a smaller cohort. These considerations led us to conclude that the use of 512mN probe would be appropriate to study modulation of central sensitisation in this topical capsaicin model.

The BOLD activity to all stimuli comparing capsaicin and sham sessions (Fig 2.13C) revealed activation in the caudal PAG. This involvement of the brainstem descending pain modulatory pathway in central sensitisation has been well established in animal and human studies (Lee et al., 2008; Suzuki et al., 2002). We showed here that the topical capsaicin model can be used to study the relevance of this pathway in central sensitisation in humans.

#### 2.2.5.3 Benefits of ultra-high field imaging

We demonstrated that regional activation patterns to hyperalgesia are similar between the 3T and 7T acquisitions (Fig 2.14). The lack of an obvious benefit in subcortical/brainstem regions at 7T is likely due to its early use and non-optimisation of the sequence parameters necessary for coping with the additional challenges of imaging structures like the brainstem at 7T. The use of such a cortical-optimised sequence might have resulted in increased EPI distortions and signal dropout at higher field strength in inferior subcortical brain regions. Improvements in distortion correction, dynamic shimming, MR parameter optimisation, signal detection and co-localisation at ultra-high field will be important for ultra-high field applications in the brainstem. However, this will require significant development and time; therefore, as it does not form the basis of my thesis and the data from the 3T was of sufficiently high quality, we concluded that the use of the 3T scanner was most suitable to examine the neural correlates of capsaicin-induced hyperalgesia in the brainstem and subcortical structures at this stage.

## 2.3 Summary

The two experiments described in this chapter provide important insights into the tools that can be used to study central sensitisation and its relevance in neuropathic pain in humans.

Our results suggest that the topical capsaicin model is suitable for investigating this mechanism. We also optimised imaging tools and parameters for investigating central sensitisation and propose the use of a 3T scanner with physiological noise correction, an axial image-acquisition orientation, boundary-based registration and $B_0$ field map correction. The chapter following describes our use of these tools to investigate the modulation of the centrally sensitised state.

# Chapter 3

# Validating Analgesic Efficacy Using Functional Imaging in a Model of Central Sensitisation

In the previous chapter, we established optimal imaging parameters and an appropriate human model for testing brainstem activity to nociceptive stimuli. Here, we use these tools to investigate the modulation of brainstem and cortical activity by pharmacological agents. We hypothesise that we can use neural activity in the brainstem as a biomarker to test drug efficacy in the context of central sensitisation.

## 3.1 Introduction

The development of new analgesics for neuropathic pain is hindered by the poor translation of their efficacy in animal models to patients, with the neurokinin1 (NK1) antagonist and the anticonvulsant, lamotrigine, as prime examples of such translational failure. Some reasons for this include difficulty in producing suitable animal models of clinical pain, differences in ligand physiology and receptor distribution between species, poor central nervous system drug penetration, insufficient receptor occupancy at the target and an over-reliance on subjective rating scores in clinical trials.

The case of the NK1 antagonist effectively underlines some of the limitations in the current pipeline for analgesic development. As the antagonist for the substance P receptor, it was an obvious ligand target for drug development. But while NK1 knockouts and use of NK1 antagonists led to attenuation of behavioural and electrophysiological responses to noxious stimuli in animals, the compound failed to show any analgesic effects in human clinical trials (Hill, 2000). This is despite demonstrably adequate systemic exposure of the drug, sufficient penetration into the central nervous system and suitable receptor occupancy (Bergström et al., 2004). A key persisting challenge that could speak to this lack of efficacy is the translation of pain as measured in animal models to the clinical pain experience (Blackburn-Munro, 2004). This notwithstanding, there is good evidence that animal pain models are retrospectively predictive of efficacy of some compounds routinely used in treatment of neuropathic pain (Whiteside et al., 2008); therefore, the problem is that too many 'false positives' are produced in the animal studies and some filter is required to better select the compounds more likely to have pharmacodynamic efficacy as well as analgesia. Such a gap between animal models and clinical trials can be filled by use of translational studies. One goal of such studies may be to improve measured end-points in animal pain models, aligning them more closely with clinical reality. Importantly, the use of human surrogate pain models (such as the capsaicin model) can also help to verify the mechanistic effects of novel compounds by identifying and testing relevant biomarkers (Whiteside et al., 2008).

### 3.1.1 Objective brain biomarkers of pain

Measurement of pain responses in humans currently relies on subjective pain reports, which provide minimal information about the underlying mechanism of nociceptive processing and pain. While these are widely accepted and argued to be definitive measures of pain perception, they are largely context-dependent and readily influenced by many

factors unrelated to the physical injury. This leads to large within- and between-subject differences (Chizh et al., 2008). As a result, sizeable subject numbers are needed to detect analgesic efficacy, reflecting unsustainable monetary and time investments for pharmaceutical companies. The use of more objective markers of nociceptive activity, as demonstrated with fMRI, has several advantages in the context of drug discovery. Unlike subjective ratings, these markers can be used in animal models and so allow more direct translation between preclinical and clinical phases. This allows investigation of the overlap in basic mechanisms underpinning animal and human pain models, which can vary even within aetiologically or phenotypically defined groups. Furthermore, by focusing on mechanistic pathophysiological markers rather than context-modulated pain reports, the use of such biomarkers may also be more sensitive to treatment efficacy in small patient groups- pharmacodynamic efficacy can be determined irrespective of subjective report providing key data to support the drug's continued development.

In short, while pain remains an inherently subjective experience, the use of neuroimaging in a translational phase of drug discovery, in conjunction with an objective brain biomarker of nociceptive and pain processing mechanisms, may be important in identifying which drugs to progress on to large-scale patient trials (Borsook et al., 2006) (Chizh et al., 2008) (Wartolowska and Tracey, 2011) (Wise and Preston, 2010).

### 3.1.2 Topical capsaicin as a human surrogate model of neuropathic pain

The use of a human surrogate model of neuropathic pain together with neuroimaging can facilitate the investigation of on-target effects of a novel compound. As demonstrated in Chapter 2 and supported by other studies, the acute topical capsaicin model of central sensitisation (CS) mimics some ongoing and positive sensory symptoms of neuropathic

pain, including secondary mechanical punctate hyperalgesia (SMPH) (Klein et al., 2005). Patients with pain and hyperalgesia show a similar incidence in hyperalgesia and shift in stimulus-response function as healthy subjects after capsaicin, suggesting that capsaicin-induced hyperalgesia is a valid surrogate model of neurogenic hyperalgesia (Iannetti et al., 2005b; Magerl et al., 1998). While the model precludes sensory loss and cannot be directly translated to clinical populations, it may provide some guidance towards drug efficacy against the positive sensory symptoms of neuropathic pain in the context of CS. Moreover, SMPH in the capsaicin model of CS has been shown to specifically involve the mesencephalic pontine reticular formation (Lee et al., 2008)- a region containing several important nuclei in the descending pain modulatory system. This combination of factors allows us to test modulation of the behavioural and neural representation of SMPH in the capsaicin model by drugs with known or unknown efficacy in the clinic.

Validating the use of this model in testing pharmacological efficacy serves two purposes. Firstly, it provides evidence that the use of human surrogate models can be informative in novel drug discovery. This may be helpful in conditions where heterogeneity in patient populations, treatments and co-morbidities render patient studies unrealistic. Secondly, it provides support for the use of neuroimaging in testing mechanistic actions of novel drugs in small and specific cohorts of patients. This is vital in the neuropathic pain context as it can enable testing of drugs in phenotypically stratified patient populations and provide a crucial translational step between preclinical drug development and large-scale clinical trials.

### 3.1.3 Gabapentin and Ibuprofen for neuropathic pain

Before testing novel compounds, it is crucial to validate the use of the capsaicin model of CS with fMRI by testing its ability to detect behavioural analgesia and neural modulation

with compounds of known efficacy. Drugs licensed for use in neuropathic pain include pregabalin for central and peripheral neuropathic pain, topical lidocaine for postherpetic neuralgia (PHN), duloxetine for painful diabetic neuropathy and tramadol for moderate to severe pain (NICE, 2010). These drugs have demonstrated moderate efficacy across various neuropathic pain states - with a number needed to treat (NNT) in the range of 3-5 for the most effective (Finnerup et al., 2010). While the different drug classes appear to have similar efficacy, pregabalin is a recommended first line treatment for most neuropathic pain states (Dworkin et al., 2007; NICE, 2010). Gabapentin has a similar pharmacological profile to pregabalin and provides equivalent efficacy, though at higher doses (Bockbrader et al., 2010; Gilron, 2007). Due to its longer half-life and relative safety, gabapentin is suitable for studying experimental pain states and has been used accordingly (Iannetti et al., 2005b).

Gabapentin and pregabalin are both derivatives of the inhibitory neurotransmitter $\gamma$-aminobutyric acid (GABA), and bind to the $\alpha 2\delta$ subunit of voltage-gated calcium channels (Gee et al., 1996). Their mechanism of action against neuropathic pain has not been fully elucidated but may be through down-regulation of calcium channels and decreased excitatory neurotransmitter release in the postsynaptic dorsal horn (Dooley et al., 2007; Field et al., 2006).

Gabapentin's analgesic effect has been demonstrated in animal (Jun and Yaksh, 1998; Stanfa et al., 1997), patient (Rice et al., 2001; Serpell et al., 2002) and healthy subject (Dirks et al., 2002) studies. Importantly, it has been shown to have strong modulatory effects on synaptic transmission and the development of a central sensitised state (anti-hyperalgesic effects) (Curros-Criado and Herrero, 2007; Dirks et al., 2002; Iannetti et al., 2005b). More recently, post-hoc study analyses have suggested that pregabalin is efficacious in a subset of HIV neuropathy patients with severe punctate hyperalgesia

(Attal et al., 2011; Simpson et al., 2010). Given these findings, we propose to test the efficacy of gabapentin at modulating CS-related brainstem activity using fMRI.

To appropriately test the efficacy of gabapentin, we will use two negative controls: an analgesic drug without confirmed efficacy in neuropathic pain and an inactive placebo compound. The role of non-steroidal anti-inflammatory drugs (NSAIDs) in treatment of neuropathic pain has been debated in the literature. While there is limited evidence that topical indomethacin and aspirin may be associated with pain relief in postherpetic neuralgia, there is little to no evidence of similar efficacy for diclofenac or oral ibuprofen (Hempenstall et al., 2005; Vo et al., 2009). Furthermore, pre-emptive analgesia with ibuprofen appears not to inhibit the development of CS following third molar surgery (Bauer et al., 2012). Conversely, NSAIDs have been shown to be efficacious for acute and chronic nociceptive pain conditions (Derry et al., 2012; Roelofs et al., 2008). We therefore chose oral ibuprofen as an active negative control compound with the hypothesis that it will not modulate CS-related behaviour.

## 3.2 Aim

We aim to establish the utility of functional magnetic resonance imaging (FMRI) in conjunction with a central sensitisation (FICCS) model in healthy humans as an objective measure for selecting clinically effective drugs used in neuropathic pain. To do this, we rehearsed the paradigm using drugs with a known history. We induced CS using topical capsaicin after administering a drug that is known to be ineffective in neuropathic pain (ibuprofen), after a drug that is known to be effective in neuropathic pain (gabapentin) and after placebo administration. We then compared the intensity of punctate stimuli in the area of secondary hyperalgesia (SMPH) and brain activity induced by mechanical hyperalgesia between the three administrations. In summary, this study uses fMRI to

investigate how drugs of known efficacy affect the development of central sensitisation in the healthy human. We hypothesise that the capsaicin-induced increase in fMRI signal in the brainstem would be reduced by gabapentin when compared to placebo but not by ibuprofen.

## 3.3 Methods

### 3.3.1 Subjects

35 healthy subjects were recruited for this study. All participants gave written informed consent in accordance with the local ethics committee. Only subjects who developed SMPH and tolerated study procedures were included in the full study.

Inclusion criteria were as follows: age 18-60; in good health (American Society of Anaesthesiologists physical status 1); participant willing and able to give informed consent; development of SMPH after capsaicin application.

Exclusion criteria were: evidence of any relevant clinically significant disease on questioning or physical examination; history of any relevant and significant drug allergies (including allergies to chilli-peppers); report of having taken any prescribed or over the counter medications in the week prior to the study session that is considered to influence the effects of the study drug; report of having received any experimental drug within the past months prior to the first dosing day of the study; average alcohol consumption >3 units per day for men and >2 units per day for women; evidence of current recreational drug use on questioning, or positive drug urine analysis on pre-study screening; any contraindication to magnetic resonance imaging; pregnancy or breast-feeding.

### 3.3.2 Personality and Emotion Questionnaires

The perception of pain and pain relief can be influenced by a number of personality and emotion traits including anxiety, fear of pain, catastrophising, and individual behaviour to rewarding or aversive stimuli (Granot and Ferber, 2005; Wanigasekera et al., 2012). Evidence suggests that anxiety and catastrophising can heighten pain perception while fear of pain can increase pain thresholds (Rhudy and Meagher, 2000; Sullivan et al., 2001). Furthermore, trait reward responsiveness has been shown to predict expression of opioid analgesia while personality optimism-pessimism variables are shown to affect expectation-related treatment responding (Geers et al., 2005; Wanigasekera et al., 2012).

These traits were assessed here using a range of validated questionnaires- the Trait Anxiety Inventory (Spielberger, 1983), the Positive And Negative Affect Schedule (PANAS) (Crawford and Henry, 2004), the Pain Catastrophising Scale (PCS) (Sullivan et al., 1995), the Behaviour Inhibition System/Behaviour Activation System (BIS/BAS) scale (Carver and White, 1994), the Pain Sensitivity Questionnaire (PSQ) (Ruscheweyh et al., 2009), the Avoidance-Endurance Questionnaire (AEQ) (Hasenbring et al., 2009), and the revised Life Orientation Test (LOT-R) (Scheier et al., 1994)- which assesses individual optimism and pessimism orientation. Subjects completed these questionnaires at the start of the first visit.

### 3.3.3 Study visits

We completed a double blind, placebo-controlled, three-way crossover study. There were 3 randomised fMRI drug study sessions where subjects received a single oral dose of placebo (PL), ibuprofen (IB) 600mg or gabapentin (GB) 1200mg. Participants were in a centrally sensitised state for all drug study visits and the visits were separated by at least one week. The drug doses were chosen based on available literature on drug

bioavailability, pharmacokinetics and time to peak plasma and CSF levels (BNF, 2007; Davies, 1998; Rose and Kam, 2002). Our study design required both active drugs to reach effective concentrations within two hours and to maintain this for at least an hour following. Gabapentin has previously been administered effectively with a dose of 1800 mg *per os* in a similar experimental design (Iannetti et al., 2005b). We use a lower dose in this study to minimise side effects associated with its administration so as not to compromise experimental blinding.

The study visits followed an identical pattern (Figure 3.1). All subjects fasted for 6 hours before the study visit. On arrival, a urine analysis was undertaken to exclude the presence of unsolicited substances and subsequently subjects were given 4 tablets of the drug/placebo together with food (to minimise gastric side-effects of ibuprofen).

1 hour after drug administration, a concentric rectangle (4x4 $cm^2$) was drawn on the antero-medial aspect of the lower right leg (at least 14cm above the medial malleolus). Another rectangle of 4x2 $cm^2$ was outlined 3 cm directly below the upper rectangle- this defined the 'target area'. Tactile stimulation with a calibrated brush and mechanical stimulation with a non skin-penetrating punctate probe (512mN) (Ziegler et al., 1999) were tested in the target area.

1.5 hours after drug administration, subjects were asked to rate the amount of treatment related pain relief they expected in that session using a computerised visual analogue scale (VAS) (anchors- 'No Relief', 'Complete Relief') and how much confidence they had in this relief rating. Immediately following, 1% capsaicin was applied in the upper rectangle. The capsaicin cream stayed on during fMRI acquisition and was held in place on the leg using a sterile dressing. Room temperatures were controlled in all visits to decrease variability in the capsaicin response (Liu et al., 1998).

2.5 hours after drug administration (an hour after capsaicin application), functional (BOLD) scans were obtained while eliciting dynamic mechanical allodynia (DMA) using a calibrated brush and secondary mechanical punctate hyperalgesia (SMPH) using a punctate probe (512 mN). Arterial spin labelling (ASL) functional imaging data was acquired 20 minutes after scanning began and resting state data was acquired 30 minutes after scanning began (Figure 3.2).

3.5 hours after drug/placebo administration (after fMRI scanning), capsaicin was removed from the skin and a blood sample was taken from the subject to measure drug concentration in the plasma.

### 3.3.4 Baseline visits

Subjects also attended 2 separate additional control sessions.

In the first baseline screening session (BL), which took place before the drug sessions, subjects underwent a baseline scanning session with no drug or capsaicin. This scan session followed an identical protocol to the drug visits and aimed to test subject baseline responses in a non-sensitised state and ability to tolerate the scanner environment. Following the scan, subject responsiveness to capsaicin and ability to develop SMPH and DMA was tested. DMA was defined as unpleasantness or pain to tactile brush stimulation of the skin in the target area 45 minutes after capsaicin application. SMPH was defined as the presence of a significantly increased pain sensation to repeated mechanical punctate stimulation of the target skin area 45 minutes after capsaicin application, as compared to before capsaicin application. Based on the discussion of the results from Chapter 2, we established that using repeated stimuli with ratings to each individual stimulus could help to control for the experimenter-error in stimulus delivery as well as

subject-error in reporting.

In a second control session (CAP), which took place after the drug sessions, subjects were scanned with the same protocol after receiving capsaicin but no drug. This tested baseline responses in a centrally sensitised state with no pain relief expectation.

### 3.3.5 Mood and psychological assessments

Changes in mood and anxiety have been shown to have an influence on pain perception and its neural correlates (Berna et al., 2010; Ploghaus et al., 2001). Furthermore, gabapentin has been trialled as a mood stabiliser and may have an effect on mood ratings in some patient populations (Sokolski et al., 1999). As such, we quantify these variables multiple times (1- pre-drug, 2- pre-capsaicin, 3- pre-scan) over the timecourse of the study visits (see Figure 3.1). Mood is measured using the 16-item Bond-Lader VAS (Bond et al., 1974) while anxiety is assessed using the State Anxiety Inventory (Spielberger, 1983).

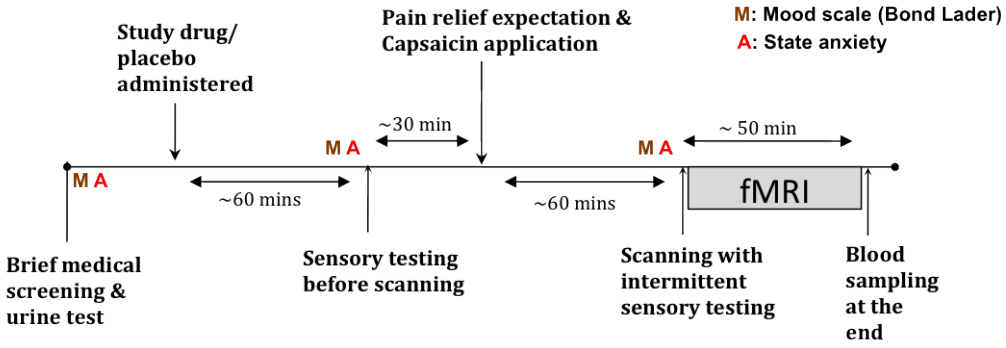


Figure 3.1: **Study design**

### 3.3.6 Stimulation paradigm

Tactile brush stimulation included 15 identical 6-second long stimuli, including three 2-second strokes across the leg in the medio-lateral direction. The inter-stimulus interval (ISI) was jittered between 28 and 46 seconds (average 38 seconds). Mechanical punctate stimulation included 18 identical 1-second stimuli with an ISI of 28 and 32 seconds (average 30 seconds). Successive punctate stimuli were applied to different regions of the stimulation region to minimise sensitisation of the skin. Both punctate and brush stimuli were applied by the same experimenter for all study sessions to reduce experimenter-related variability. Subjects were instructed to keep their eyes open and fixate on a cross during stimulation.

Subjects rated perception using an online computerised VAS displayed on a projector screen. Each scale was projected for 6 seconds. Average unpleasantness and pain intensity of the brush stimulation was rated 12 seconds and 18 seconds after the final brush stimulation- VAS anchors were 'Not unpleasant', 'Extremely unpleasant', and 'Not painful', 'Extremely painful' respectively. Punctate stimulus intensity was rated 12-seconds after every mechanical punctate stimulus using a VAS with anchors 'Not intense', 'Extremely intense'. Average unpleasantness to punctate stimuli was rated at the end of each run- 18 seconds after the final punctate stimulus.

ASL and resting data was acquired while subjects kept their eyes open and fixated on a cross. Spontaneous/ongoing pain ratings were acquired at 5 timepoints during scanning (see Figure 3.2). The VAS anchors were 'No pain', 'Severe pain'.

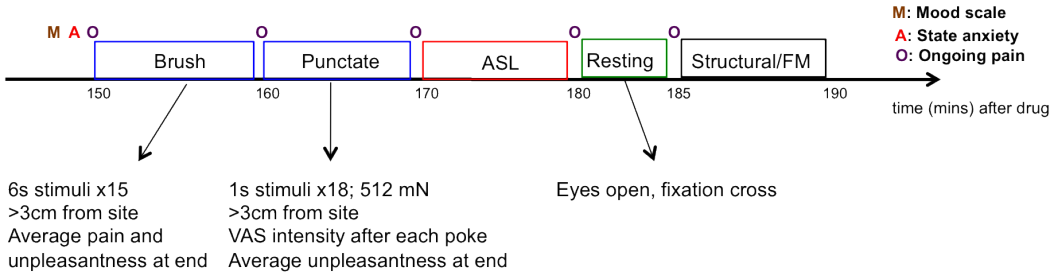


Figure 3.2: **fMRI scan paradigm.** ASL, arterial spin labelling. FM, field map

### 3.3.7 fMRI scanning protocol

During each session, fMRI was performed on a 3T Siemens Verio MRI scanner (Erlangen, Germany) fitted with 32 channel receiver head-only radio-frequency coil. Experimental event timing is summarised in Figure 3.2. Response registration was controlled by a computer running Presentation (version 16.0; Neurobehavioral Systems, Albany, CA).

Functional scans for tactile, mechanical and resting runs were acquired with a whole-brain gradient-echo, echo-planar imaging (EPI) sequence (echo time (TE)=30 ms; 46 contiguous 3-mm thick axial slices; field of view 192x192 $mm^2$; matrix 64x64) with an in-plane resolution of 3 x 3 $mm^2$). For the tactile and mechanical sequences, repetition time (TR) was 3s with 200 volumes, corresponding to 10 minutes of scanning time. For the resting state scan, TR was 2.41s (44 contiguous slices) with 128 volumes, corresponding to 5 minutes of scanning time. Functional scans utilised parallel imaging (GRAPPA) with an acceleration factor (iPAT) of 2.

Arterial spin labelling (ASL) data was acquired using a pseudo-continuous multiple inversion time quantitative sequence (label duration= 1.4s; post inversion delays [TI]= 1.6, 1.8, 2, 2.2, 2.4 ms; TE= 13ms; 28 contiguous 4.6mm slices; field of view 240x240 $mm^2$; matrix 64x64). TR for each tag/control image was 3.75s, with 150 volumes, cor-

responding to 10 minutes of scanning time. The tagging plane was defined anatomically for each individual subject at the carotid arteries (approximately 6cm below the circle of Willis).

For all scans, physiological noise data was collected using respiratory bellows and a pulse oximeter, together with volume triggers from the scanner. All data was recorded using an MP150 system (BIOPAC Systems, Inc., Goleta, CA) at a sample rate of 100Hz. A T1-weighted, 1x1x1 $mm^3$ structural image was collected in the BL visit only, for registration and overlay of brain activation. $B_0$ field maps (FM) (FOV and matrix identical to EPI) were also acquired to correct for regions of field inhomogeneity.

### 3.3.8 Data analysis

Arterial spin labelling scans and data from the baseline sessions are analysed and discussed in subsequent chapters.

Psychophysical statistical analysis, including analysis of variance (ANOVA) tests were implemented using IBM SPSS Statistics, version 18 (IBM, Armonk, NY, USA). Paired t-tests were performed to compare between the measured variables and post-hoc correction for multiple comparisons was performed using *Bonferroni* adjustments. Datasets were tested for normality using the Shapiro-Wilk test. For our correlation analyses, we excluded outlying variables by calculating Cook's distance (Cook and Dennis, 1977) and using a cutoff of 4/N to remove datapoints with disproportionally large residuals (where N is the number of subjects) (Bollen and Jackman, 1990).

Imaging data analyses were performed using FMRIB Software Library (FSL) version 5.01. Spatial smoothing in pre-processing was at FWHM 5. Physiological noise regres-

sors were computed using a custom MATLAB script (see Chapter 2 Methods) and were then included in a general linear model (GLM) using FEAT.

### 3.3.9 BOLD image analysis

Motion correction of raw data was performed using MCFLIRT (Jenkinson et al., 2002). Registration to structural and standard space was carried out using BBR (Greve and Fischl, 2009), FLIRT (Jenkinson and Smith, 2001) and FNIRT (Andersson et al., 2007). Field map correction was implemented to account for field inhomogeneities when registering to the unbiased structural image. Input functions related to the brush stimuli, punctate stimuli and the VAS rating tasks were modelled in the GLM using convolved task blocks with a single gamma haemodynamic response function. Temporal derivatives of the stimuli were included to account for differences in individual HRF functions. VAS rating, motion parameters and physiological noise regressors were added as GLM confounds. Z-score images were generated at a threshold of $Z = 2.3$ with corrected cluster significance of $p \leq 0.05$ (Worsley, 2001). The functional acquisitions for all 24 subjects were entered into a mixed effects linear model analysis (FLAME 1+2) at a group level.

For illustration of BOLD signal change, functional masks were generated from a 5mm sphere around the peak voxel in the midbrain, and from a cluster of activity in the posterior insula (PL>GB contrast) masked by an MNI anatomical insula mask, which was divided at the long insula gyrus to isolate the posterior portion of the insula and thresholded at $p>0.5$. Parameter estimates were extracted from the relevant BOLD acquisitions using *Featquery* and masks generated in MNI standard space. Region of interest (ROI) analyses were performed using a non-parametric permutation method with the Randomise tool integrated within FSL (Hayasaka and Nichols, 2003). Test statistics were generated from the GLM design using threshold-free cluster enhancement

(TFCE) and corrected to a p-value $< 0.05$.

### 3.3.10 Sensitivity analysis

To investigate the relative sensitivities of psychophysical reports and fMRI in detecting drug efficacy, we used up to 1000 subject permutations at selected subject numbers (n= 12, 16, 18, 22) to assess the likelihood of obtaining a significant difference between the PL-GB and IB-GB comparisons, with a p-value of less than 0.05. This was performed both for SMPH intensity and for cortical BOLD activity using extracted parameter estimates from specified anatomical regions for both contrasts. For the comparison of BOLD activity in the contralateral posterior insula, we use an MNI defined anatomical mask of the insula as described in the section above (thresholded at p>0.5). For comparison in the contralateral secondary somatosensory cortex (SII), we used an anatomical mask from the Juelich Histological Atlas- encompassing opercula 1, 3 and 4 (thresholded at p>0.5), which have been implicated in chronic neuropathic pain (Friebel et al., 2011). Probabilities were computed using MATLAB.

## 3.4 Results

35 healthy subjects were recruited and 24 subjects (11 male, 13 female, mean age: 24 [SD $\pm$ 4.08]) completed the study. 7 subjects were excluded, as they did not develop SMPH in the initial baseline screening session. One subject was excluded as the pain intensity from the capsaicin application was intolerable. Three further subjects were excluded due to neurological abnormalities on scanning, a positive urine analysis for use of recreational drugs and contraindications to MRI scanning. All 24 subjects developed SMPH while at least 18 subjects also developed DMA (Table 3.1).

Table 3.1: **SMPH and DMA developed in baseline session (BL) (post capsaicin - pre capsaicin scores) for individual subjects.** For all subjects, intensity scores were significantly higher ($p<0.05$) post capsaicin than pre capsaicin. VAS scores rated from 0-100 with anchors (Not intense/unpleasant; Extremely intense/unpleasant). pINT punctate intensity. pUNP punctate unpleasantness. bPAIN brush pain. bUNP brush unpleasantness. $ missing data

| Subject | pINT post-pre | pUNP post-pre | bPAIN | bUNP |
|---|---|---|---|---|
| 1 | 23.06 | 62 | $ | 33 |
| 2 | 10.89 | 23 | $ | $ |
| 3 | 37.61 | 36 | 45 | 37 |
| 4 | 29.06 | 19 | $ | $ |
| 5 | 25.33 | 19 | 31 | 39 |
| 6 | 38.28 | 52 | 22 | 39 |
| 7 | 17.00 | 32 | 40 | 33 |
| 8 | 20.89 | 45 | 0 | 0 |
| 9 | 23.44 | 45 | 28 | 56 |
| 10 | 24.94 | 31 | 0 | 0 |
| 11 | 11.22 | 21 | 6 | 1 |
| 12 | 14.11 | 37 | 23 | 18 |
| 13 | 7.28 | 12 | 8 | 11 |
| 14 | 36.22 | 39 | 10 | 19 |
| 15 | 16.61 | 44 | 9 | 37 |
| 16 | 10.72 | 20 | 11 | 3 |
| 17 | 33.56 | 73 | 47 | 73 |
| 18 | 12.83 | 25 | 11 | 10 |
| 19 | 37.56 | 35 | 12 | 6 |
| 20 | 25.08 | 32 | 0 | 0 |
| 21 | 15.44 | 36 | 40 | 56 |
| 22 | 21.22 | 53 | 26 | 17 |
| 23 | 64.67 | 50 | $ | $ |
| 24 | 21.67 | 68 | 21 | 39 |

### 3.4.1 Psychophysics

Psychophysical variables were compared across sessions using 3-way repeated measures analyses of variance. In the baseline (pre-drug) state and 60 minutes after dosing, there was no significant effect of session on psychological or mood assessments.

Prior to the start of fMRI acquisition in the scanner (150 minutes after dosing), there was an increase in the mental sedation score during the gabapentin session when compared to ibuprofen (*Bonferroni corrected* p=0.03) and placebo (*corrected* p= 0.03) sessions (Fig 3.3). There was no similar effect on physical sedation or any other psychological parameters. Subjects also reported an increased expectation of pain relief after receiving ibuprofen when compared to placebo (*corrected* p=0.03) (Fig 3.3).

There was a significant within-group effect of drug on the reported intensity of punctate hyperalgesia ($F[2,46]=30.017$, $p<0.001$). In a paired t-test, subjects reported secondary mechanical punctate hyperalgesia (SMPH) in the gabapentin session to be less intense than in the placebo session (*corrected* p=0.006) (Fig 3.4). Significance between ibuprofen and gabapentin did not survive post-hoc *Bonferroni* adjustment (*corrected* p=0.138) for multiple comparisons. Pairwise comparisons with post-hoc corrections comparing reported unpleasantness of punctate hyperalgesia between the 3 sessions did not reveal any significant differences (Pl/Gb *corrected* p=0.052, Pl/Ib *corrected* p=0.67, Ib/Gb *corrected* p=1).

A 3-way repeated measures ANOVA revealed a significant within-group effect of drug session on ongoing pain ratings ($F[2,46]=5.235$, $p<0.01$). Post hoc analyses with *Bonferroni* adjustment indicated that there are significant reductions in ongoing pain ratings (average of all timepoints) with gabapentin when compared to placebo (*corrected* p=0.046) or ibuprofen (*corrected* p=0.01) (Fig 3.4).

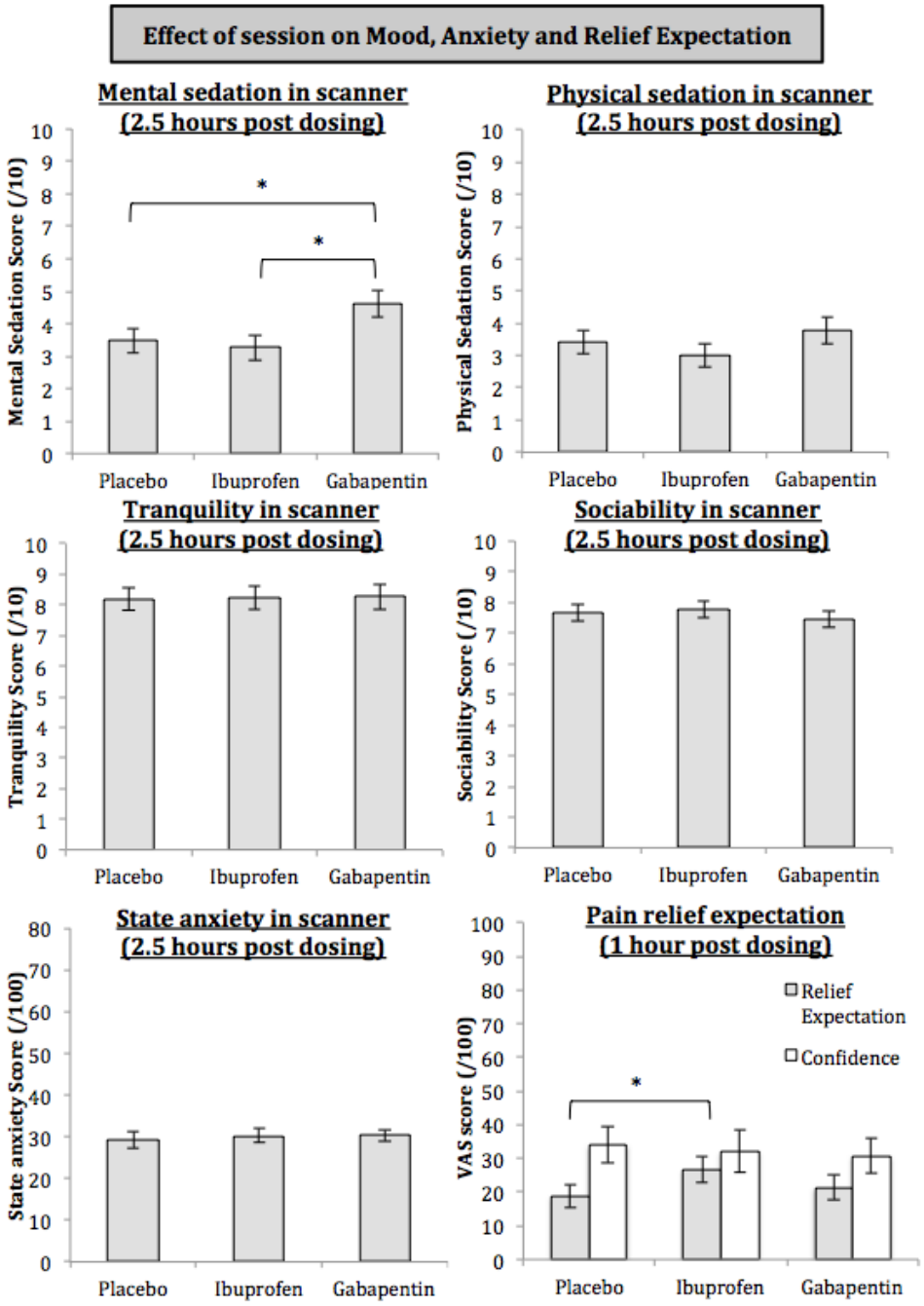


Figure 3.3: **Mood scores across session.** Gabapentin increases mental sedation scores when compared to placebo or ibuprofen (top right). Subjects reported more pain relief expectation in the ibuprofen session when compared to placebo (bottom right). * $p<0.05$, n=24.

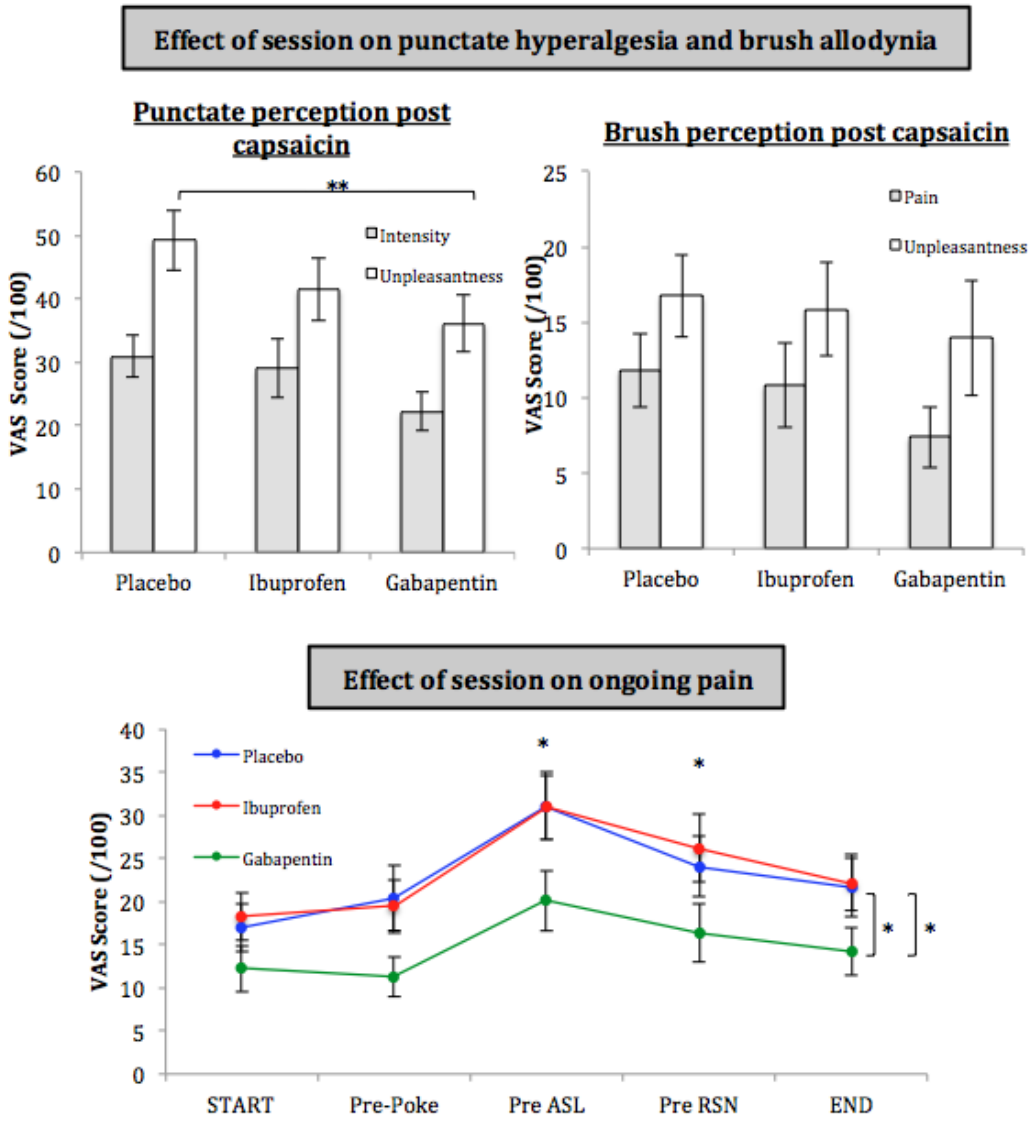


Figure 3.4: **Pain scores across session.** Gabapentin significantly reduces punctate intensity ratings when compared to placebo (top left), has no effect on allodynia (top right), but significantly decreases ongoing pain when compared to placebo or ibuprofen (bottom). n=24, * $p<0.05$, ** $p<0.01$

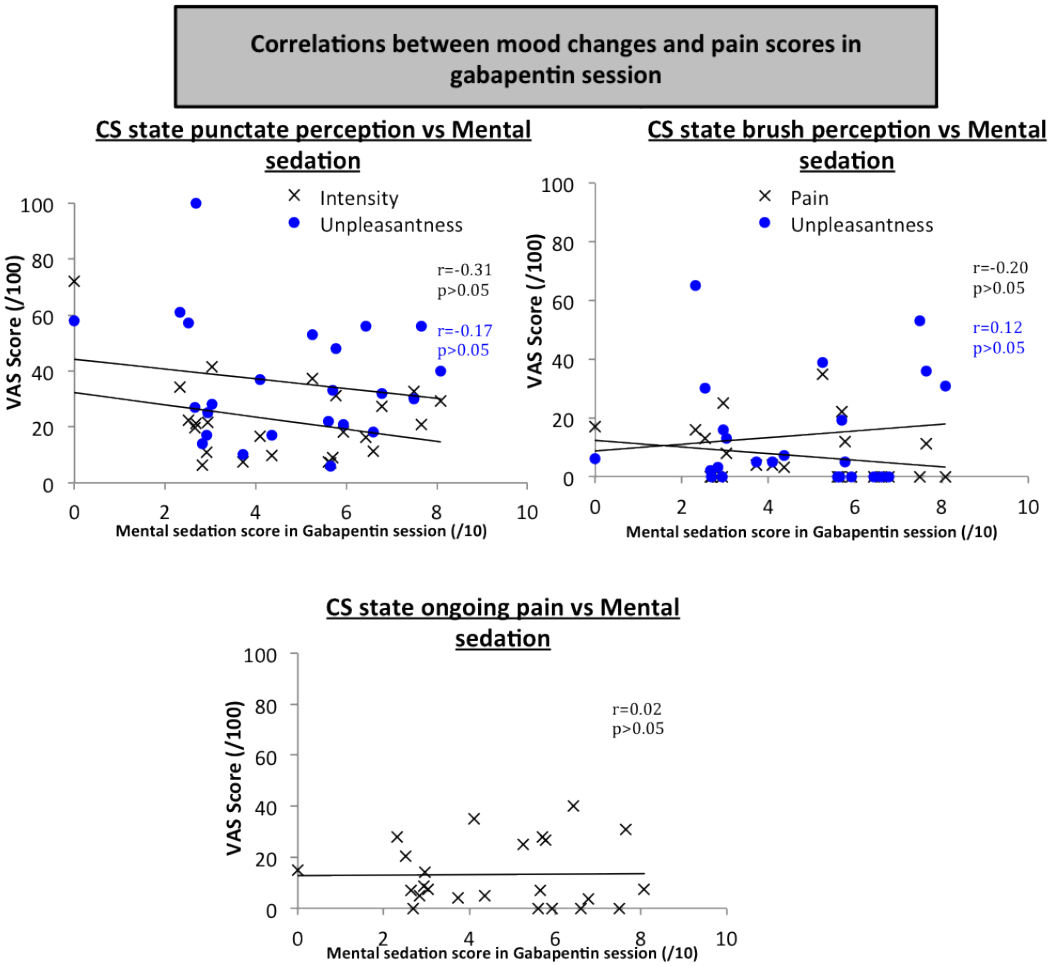


Figure 3.5: **Correlation between gabapentin session mental sedation scores and gabapentin session pain scores.** Mental sedation inside the scanner during the gabapentin session does not correlate with any of the pain related psychophysical variables measured at the same time. n=24. p>0.05.

To investigate the effects of the gabapentin modulation of mood scores on pain behavioural reports, we correlated mental sedation scores in the gabapentin session with pain ratings during the gabapentin session. There is no significant correlation between mental sedation scores and any of the pain rating variables (Fig 3.5).

### 3.4.2 fMRI

A repeated-measures ANOVA comparing the three sessions showed a significant effect of session on the BOLD signal to SMPH in the contralateral insula and secondary somatosensory cortex (SII) (Fig 3.6A).

In the CS-state whole-brain paired comparisons, gabapentin significantly decreased BOLD brain activity to SMPH in the contralateral insula and SII when compared to ibuprofen or placebo (Fig 3.6). There were no significant differences whole brain between ibuprofen and placebo, and no significant increases in BOLD activity by gabapentin.

Our *a priori* hypothesis indicated that brainstem activity to SMPH would be reflected in activity in the mesencephalic reticular formation (MRF) (Lee et al., 2008; Zambreanu et al., 2005). As such, we performed a region of interest (ROI) analysis of this region using an anatomical mask drawn on an MNI standard brain (Fig 3.7). The mask was defined using landmarks referenced from Duvernoy's Brainstem Atlas (Naidich et al., 2009). ROI analyses were performed using *Randomise* with threshold-free cluster enhancement and corrected to a p-value $< 0.05$.

ROI analysis revealed that gabapentin significantly decreased BOLD brain activity to SMPH in a region of the MRF when compared to ibuprofen ($p=0.016$) or placebo ($p<0.001$) (Fig 3.7). A distinct cluster is identified in the lateral mesencephalon ip-

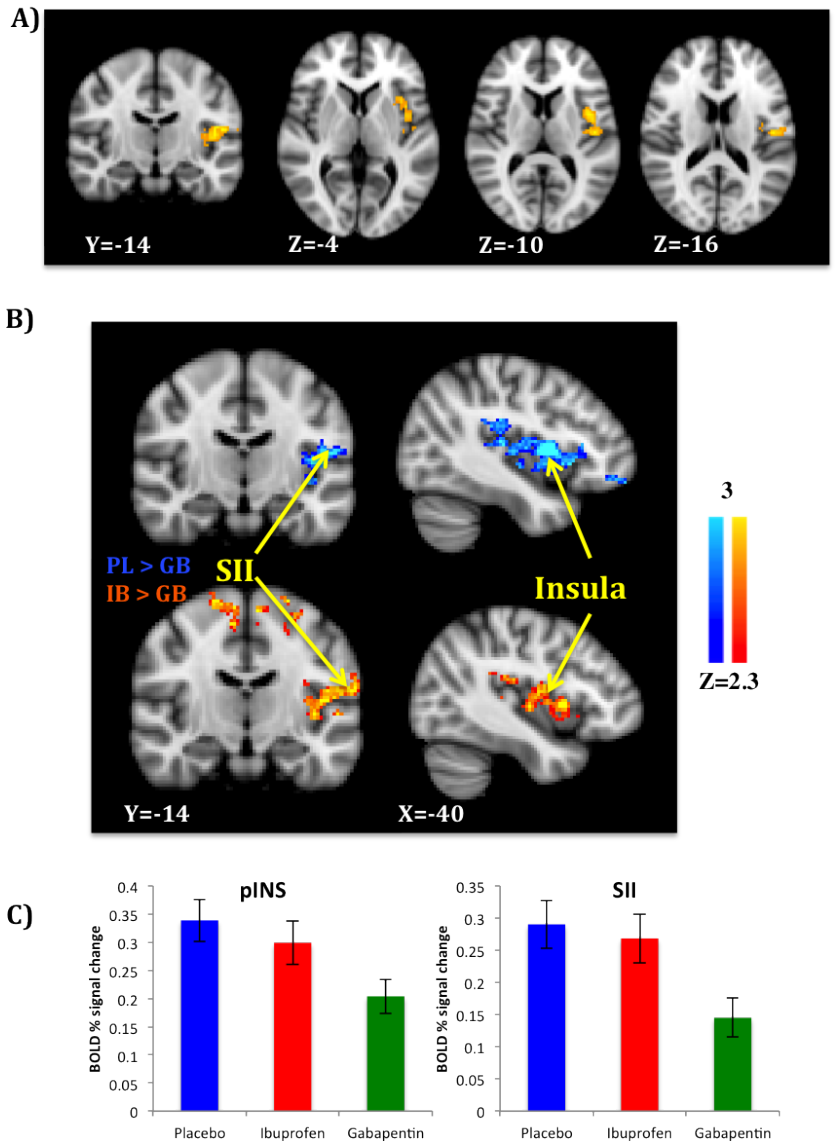


Figure 3.6: Top- F-test comparing all three conditions. Middle/Bottom shows brain areas where gabapentin significantly decreased brain activity to SMPH in a whole brain analysis when compared to placebo (middle) and ibuprofen (bottom). n=24, Mixed Effects: Z=2.3, p<0.05. [PL: placebo, IB: ibuprofen, GB: gabapentin, SII: secondary somatosensory cortex; pINS: posterior insula cortex]. Images are in radiological convention.

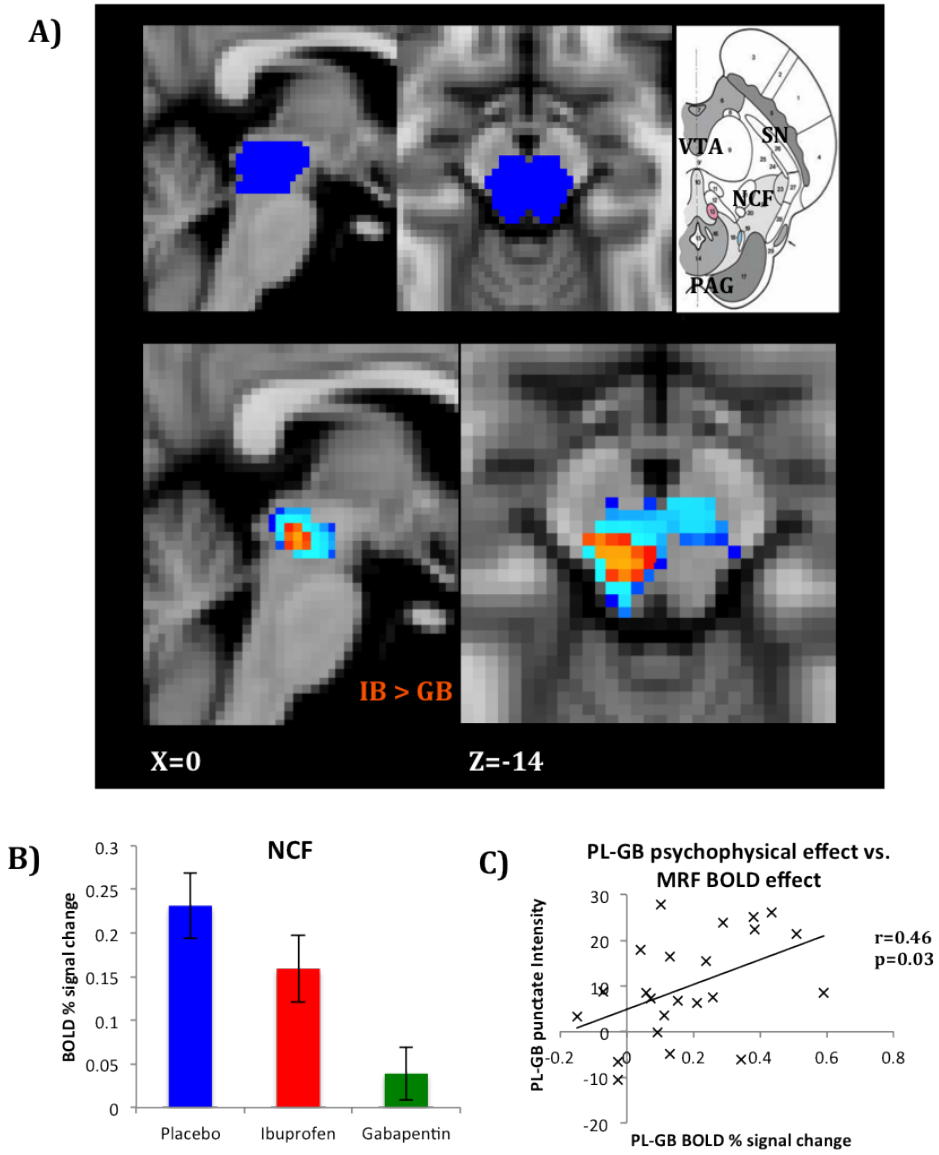


Figure 3.7: A) Pairwise t-test comparing SMPH-related BOLD changes in PL>GB (blue) and IB>GB (red) within a mesencephalic mask. Also shows the mesencephalic mask used (top left) and a corresponding midbrain axial slice modified from Duvernoy's brainstem atlas (top right). B) illustrates BOLD signal change in the overlapping functional region from the two contrasts shown in A, for each of the conditions. C) shows significant correlation between gabapentin suppression of MRF BOLD activity, and gabapentin analgesic effect as compared to placebo [PL: placebo, IB: ibuprofen, GB: gabapentin, NCF: nucleus cuneiformis, PAG: periaqueductal grey, SN: substantia nigra, VTA: ventral tegmental area]. Images in radiological convention.

silaterally, spanning to the midline dorsal raphe nucleus rostrally. This region is shown to reflect the ipsilateral nucleus cuneiformis (NCF) and contralateral red nucleus (RN) when compared with a detailed brainstem atlas (Fig 3.7).

We tested whether gabapentin's suppression of BOLD activity in the MRF is associated with its reduction in pain perception. We showed that BOLD reduction in the MRF between placebo and gabapentin is significantly explained by the reduction in punctate intensity induced by gabapentin ($r[21]=0.46$ $p=0.028$).

We further report that in the gabapentin session, there is no relationship between mental sedation scores and BOLD signal change extracted from functional masks in the posterior insula ($r[22]=0.17$, $p=0.47$), SII ($r[22]=0.1$, $p=0.64$) or NCF ($r[22]=0.04$, $p=0.85$).

### 3.4.3 Sensitivity analysis

To accurately quantify the relative sensitivities of psychophysics and cortical BOLD effects for evaluating the drug-modulated SMPH pain outcome, we tested the probability of a significant effect ($p<0.05$) of gabapentin with multiple subject permutations at pre-defined subject numbers (n=12, 16, 18, 22) (Table 3.2). We designated an >80% probability of significance as good evidence for a reproducible effect of significance. For the PL-GB contrast, SMPH-related BOLD signal change in the posterior insula is more predictive (>80% prediction probability at 12 subjects) than psychophysical reports of punctate intensity (>80% prediction probability at 16 subjects). For the IB-GB contrast, signal change in the posterior insula (at 22 subjects) and SII (at 18 subjects) were both predictive of gabapentin effect, while psychophysical reports did not show this effect in our cohort of 24 subjects.

Table 3.2: **Sensitivity of subjective reports and functional imaging for detecting gabapentin effect.** Figures show the probability of significance at the level of p<0.05 in pairwise comparisons, after 1000 permutations of subject data. Direction of effects shown is PL>GB and IB>GB. Numbers highlighted in red represent the first time there is >80% probability for each contrast for the relevant modality.

| N | Contrast | Punctate intensity | Left posterior insula | Left SII |
|---|---|---|---|---|
| 12 | Pl-Ib | 0.03 | 0.06 | 0.01 |
| | Pl-Gb | 0.58 | 0.876 | 0.53 |
| | Ib-Gb | 0.17 | 0.26 | 0.46 |
| 16 | Pl-Ib | 0.02 | 0.05 | 0.01 |
| | Pl-Gb | 0.86 | 1 | 0.797 |
| | Ib-Gb | 0.25 | 0.4 | 0.68 |
| 18 | Pl-Ib | 0.01 | 0.04 | 0 |
| | Pl-Gb | 0.96 | 1 | 0.91 |
| | Ib-Gb | 0.27 | 0.49 | 0.85 |
| 22 | Pl-Ib | 0 | 0.01 | 0 |
| | Pl-Gb | 1 | 1 | 1 |
| | Ib-Gb | 0.37 | 0.84 | 1 |

## 3.5 Discussion

In a small cohort of healthy subjects, we report that fMRI was able to detect suppression of CS-related brainstem activity by an analgesic effective in neuropathic pain when compared to that of an analgesic ineffective in neuropathic pain, where subjective psychophysical measures failed to show a significant difference between the 2 compounds for the corresponding pain stimulus.

### 3.5.1 Drug effect on behavioural report

Gabapentin is known to be effective in neuropathic pain while there is little evidence of a similar effect for ibuprofen. We corroborate this in our model, showing a reduction in ongoing pain and punctate intensity reports in the gabapentin session (when compared to placebo) but not in the ibuprofen session (when compared to placebo) (Fig 3.4). Further, our results suggest that while gabapentin also increases mental sedation, this is not associated with its analgesic effect (Fig 3.5).

Despite these clear effects, we are unable to distinguish between the efficacies of the two active treatments in our small cohort of subjects using behavioural reports of SMPH. This may be because the superior analgesic efficacy of gabapentin over ibuprofen is masked by auxiliary effects of the ineffective analgesic and/or inherent variability in the use of subjective reporting as an endpoint. Interestingly, we are able to distinguish this effect using ongoing pain as an endpoint. This may be because the spontaneous pain report is less prone to variability than evoked pain reports, which involve more experimenter-related error. Beyond this, gabapentin's effect on spontaneous pain may be more robust than its effect on evoked pain in the sensitised state.

### 3.5.2 Drug effect on cortical pain processing

We show that gabapentin decreases SMPH-related activity in brain regions, which are associated with pain processing (Apkarian et al., 2005). This supports previous findings with this model of central sensitisation, which show that gabapentin has anti-hyperalgesic effects in the cortex (Iannetti et al., 2005b). In our study, we further show that these cortical effects are evident when gabapentin is compared with an active analgesic, which is not effective in neuropathic pain.

Gabapentin has previously been shown at a higher dose, not to cause global changes in brain activity (Iannetti et al., 2005b). supporting a specific central analgesic role for the drug. Although ibuprofen freely crosses the blood-brain barrier (Parepally et al., 2006), we do not see any evidence of a similar central analgesic effect in our model, suggesting that the FICCS model can distinguish between the two treatments.

### 3.5.3 Drug modulation of brainstem reticular formation activity

Our study design allowed us to control for stimulus force but not pain perception between the drug conditions. Previous findings suggest that regions of the brainstem reticular formation are specifically activated in CS-related hyperalgesia in humans, after pain perception is controlled (Lee et al., 2008). Furthermore, in a similar study paradigm, the brainstem was revealed to be the only brain region to show an interaction between central sensitisation and gabapentin drug effect (Iannetti et al., 2005b). This region therefore provides a potential biomarker for anti-hyperalgesic activity induced by gabapentin.

Our results show that a region of the mesencephalic reticular formation (MRF) within the brainstem is modulated by gabapentin in the hyperalgesic state. This modulation is further shown to be associated with gabapentin's analgesic effect (Fig 3.7C). This region

includes the nucleus cuneiformis (NCF), which has been previously shown to be involved in CS-related hyperalgesia in humans (Lee et al., 2008; Zambreanu et al., 2005). The NCF receives inputs from lamina I dorsal horn neurons (Zemlan and Behbehani, 1988) and is a major source of input to the rostral ventromedial medulla (RVM), which has been shown in animal studies to have a role in the maintenance of central sensitisation (Gebhart, 2004; Porreca et al., 2002; Suzuki et al., 2002). These regions also possess a heterogeneous cytoarchitecture, with distinct ON and OFF cell populations allowing for bidirectional modulation of pain processing (Fields et al., 1983; Haws et al., 1989). Spino-bulbar-spinal circuits involving these brainstem regions and spinal dorsal horn neurons are known to contribute to the central sensitisation phenomenon (Suzuki et al., 2002). Given that gabapentin is thought to affect excitatory and inhibitory presynaptic spinal neurotransmission in the hyperalgesic state (Bayer et al., 2004), its indirect effect on the brainstem via activity in the spinal dorsal horn is highly plausible. Moreover, the prophylactic drug delivery method may inhibit presynaptic calcium channels, leading to reduced transmission from primary nociceptive afferents, and attenuating the subsequent development of central sensitisation. The reduction in activity in the MRF by gabapentin may therefore reflect a reduction in brainstem facilitatory influences induced by CS.

Importantly, this effect is distinguishable between gabapentin and ibuprofen, suggesting that fMRI can be used to identify an efficacious compound in a small cohort. This method also appears to be more sensitive than subjective reporting.

### 3.5.4 Relative sensitivity of fMRI and subjective ratings

Our sensitivity analyses suggest that in a central sensitised state, cortical BOLD activity is able to detect drug-related differences in pain processing before differences in its perception are captured using behavioural measures. When comparing gabapentin to

placebo, the BOLD activity readout appears to be slightly more sensitive at detecting gabapentin effects than subjective reports (12 subjects vs. 16 subjects). When considering a head-on comparison between the two analgesics, we are unable to detect a difference in subjective ratings to SMPH at 24 subjects, while we can detect the analgesic effect of gabapentin at 18 subjects using SII activity, and at 22 subjects using the posterior insula activity.

The reduced sensitivity of psychophysical reports likely results from the range of influences on the transition from nociception to pain perception. It is important to underline that the BOLD signal largely measures a physiological change. This is related to but does not directly reflect the individual's pain percept, which is further influenced by cognitive, attentional and emotional factors (Tracey and Mantyh, 2007). In light of this, our results suggest that the use of fMRI as a readout of this early mechanistic process may prove a more sensitive indicator of pharmacodynamic action (and potentially future analgesia) than subjective reports in the early testing of novel drug compounds. This may have relevance for future efforts when developing analgesics for neuropathic pain.

### 3.5.5 Conclusion

Despite the benefits of testing and validating these tools in healthy cohorts, we are limited by the use of an inadequate model of neuropathic pain. Future studies should aim to validate the use of fMRI in a similar fashion to test analgesic efficacy in patient cohorts. The heterogeneity in patient populations and the poor efficacy of most established analgesics in neuropathic pain populations means that such a study is likely best implemented in a subset of patients with a defined neuropathic pain profile, for which specific treatments are known to be effective. The group has recently completed such a study with considerable success (Wartolowska et al., in preparation 2013).

Moreover, in this study we use a pre-emptive treatment model. Although there is some preliminary evidence that gabapentinoid therapies are effective in the prevention of chronic post-surgical pain (Clarke et al., 2012), their efficacy has mainly been demonstrated in the pain state. As such, it will be important to validate the efficacy of these and other compounds in an fMRI model after establishing a pain phenotype.

The conjunction between fMRI and the capsaicin model, as used here, is additionally inadequate in its assessment of evoked pain rather than spontaneous pain, which is a more common symptom in neuropathy and is the primary efficacy endpoint in most clinical trials. As far as we can determine, no studies to date have assessed the neural correlates of ongoing pain in humans using the topical capsaicin model. In the following chapters, we investigate the use of an emerging fMRI tool to image tonic/spontaneous pain and its modulation using this model.

# Chapter 4

# Test-Retest Reproducibility and Optimisation of Multi-Inversion Time Pseudo-continuous Arterial Spin Labelling (PCASL) for the Imaging of Stable Neural States

A major aim of human pain neuroimaging research is to test models of experimental pain that are translatable to clinical pain syndromes. By nature, this necessitates the imaging of tonic and spontaneous pain, the predominant clinical manifestation. In this regard, arterial spin labelling is an exciting tool that allows direct imaging of cerebral perfusion in a non-invasive manner. In this chapter, we test the feasibility of a multi-inversion time pseudo-continuous ASL sequence for imaging resting and active states.

## 4.1 Introduction

Functional neuroimaging has emerged as an important non-invasive tool for exploring brain physiology and the principles underlying brain function. While several techniques have been developed, Blood Oxygen Level Dependent (BOLD) fMRI is by far the most commonly employed. BOLD fMRI has enabled the investigation of the neurophysiology

of acute pain conditions; however it is not well suited to imaging long activation states, as in tonic pain. Recent developments have facilitated the use of more quantitative fMRI tools for the investigation of tonic states and baseline conditions.

### 4.1.1 Limitations of BOLD imaging

BOLD fMRI has been an immensely beneficial tool in the investigation of brain function, including our understanding of mechanisms of human pain processing (Apkarian et al., 2005). BOLD fMRI images relative changes in vascular physiology by exploiting magnetic susceptibility differences between oxygenated and deoxygenated haemoglobin to create image contrast (see Introduction). Increased metabolic demand by active neurons results in local increases in cerebral blood flow (CBF), cerebral blood volume (CBV) and cerebral metabolic rate of oxygen (CMRO2), and decreases in oxygen extraction fraction (OEF). Therefore, the BOLD technique does not directly image neuronal activity, but rather is a correlate of decreasing deoxyhaemoglobin concentrations with increased metabolic demand- influenced by the aforementioned physiological factors (Bandettini et al., 1992; Kwong et al., 1992; Ogawa et al., 1990).

As a result of this non-linear relationship between neuronal activity and BOLD signal, BOLD results are reported statistically in arbitrary units and have no quantifiable physiological interpretation (Buxton et al., 2004). While the BOLD technique has higher signal-to-noise ratio (SNR) and temporal resolution than many other fMRI techniques, it still measures changes that occur far more slowly and over a larger region (largely in venous compartments) than the neuronal activity (Pfeuffer et al., 2002).

BOLD imaging also lends itself to magnetic susceptibility artefacts, particularly in areas with sharp air/tissue boundaries (discussed in Chapter 2) (Bandettini et al., 1992).

Although BOLD imaging has been used to image resting experimental states, it remains confounded by the fact that the BOLD response is affected by baseline perfusion and metabolic levels which are not directly measured and may change over the experimental time-course (Cohen et al., 2002). Furthermore, BOLD is susceptible to low frequency signal drift in the scanner, which is difficult to remove (Smith et al., 1999). As a result, SNR is low in BOLD acquisitions for experimental designs with low stimulus frequencies (long stimulus blocks) (Aguirre et al., 2002). These drift effects makes BOLD a suboptimal technique for studying the physiology of baseline states and their modification by long activation states (e.g. clinically relevant pain).

### 4.1.2 Quantifying physiological parameters

The measurement of quantifiable physiological parameters, such as CBF, CBV and oxygen consumption offer a more direct correlate of neuronal activity than the BOLD signal. The dynamic measurement of CBV and CMRO2 is possible but is currently hindered by such issues as poor SNR, low temporal resolution and inadequate models (Blockley et al., 2012; Uh et al., 2009). However the techniques for measurement of CBF are practical and have been suggested to show effects more localised to the relevant parenchyma than the BOLD effect (Pfeuffer et al., 2002; Tjandra et al., 2005). Changes in baseline CBF do not appear to affect the regional haemodynamic response measured by CBF change to a focal task (Li et al., 2000). Furthermore CBF and metabolism are closely coupled in stable states, enabling effective assessment of brain function using cerebral perfusion (Buxton and Frank, 1997; Fox and Raichle, 1986).

The dynamic measurement of cerebral blood flow has historically been achieved by use of diffusible and easily detectable tracers that are exogenously applied and measured in the relevant tissue of interest (Kety and Schmidt, 1945; Larson et al., 1987). This

idea is applied with use of radioactive or MRI tracers (which change the relaxation of blood/tissue) in various imaging modalities including positron emission tomography (PET), single-photon emission computed tomography (SPECT) and dynamic susceptibility contrast MRI (DSC-MRI). Perfusion imaging using these techniques in humans enabled the generation of kinetic models and bolus dispersion rates for existing tracers, which allow perfusion quantification (Meyer, 1989; Raichle et al., 1983). Such tools have been used to study brain perfusion in various pain states (Peyron et al., 2000). Unfortunately, the use of PET is limited by its high cost, use of ionising radiation and poor spatial resolution. DSC-MRI uses safer contrast agents and has improved temporal resolution over PET/SPECT, however the use of paramagnetic MRI tracers such as chelated gadolinium compounds remains invasive, requires an accurate estimation of regional perfusion (arterial input function) and only allow for a single contrast image as the compound can take hours to be removed from the body (Wible et al., 2009).

More recently, arterial spin labelling techniques have been developed, which use the tracer principle to magnetically label arterial water as an endogenous tracer (Detre et al., 2009; Williams et al., 1992). The immediate benefits of ASL are that it is non-invasive (no exogenous tracers injected) and fast (the tracer decays quickly with a relaxation rate far shorter than that of radioactive tracers). The rapid relaxation time allows repeatability of the technique but does mean that the technique has poor SNR in relation to other imaging techniques because only a small amount of labelled blood accumulates. ASL has been shown in functional studies to be reproducible and to reflect similar activation patterns as BOLD techniques, although with better specificity and co-localisation between subjects (less inter-subject variability) (Raoult et al., 2011; Tjandra et al., 2005). This 'endogenous tracer' neuroimaging method is attractive to both clinical and experimental (i.e. functional) studies in part because it offers the ability to complete multiple repeat scans (e.g. follow-up investigations, longitudinal designs, pharmacological trial design)

without cumulative risk to the subject. In conclusion, ASL provides an effective tool for rapid and safe estimation of blood flow in resting, task-related and pharmacological fMRI studies (Detre et al., 2009; Maleki et al., 2013; Wang et al., 2011). This is therefore potentially a powerful technique for the neuroimaging of tonic pain states and modulation of neuronal activity in chronic pain patients.

### 4.1.3 Imaging cerebral blood flow with arterial spin labelling

ASL imaging typically involves 3 key steps- (1) labelling/tagging of arterial water (creating arterial spin), (2) a delay for the tagged blood to reach the tissue of interest, and (3) imaging of the tissue of interest using a specified pulse sequence. At each one of these steps, there are multiple strategies available. The contribution of labelled spins is a small fraction of brain signal so a pair-wise subtraction of two adjacent images (tag minus control) is taken to generate a difference signal, which correlates with perfusion. This eliminates the low frequency drift seen in BOLD applications and enables imaging of long activation states (Wang et al., 2003). Perfusion estimation is quantified to physiological units (ml/100g/min) with measured or estimated values- T1 of blood and tissue, labelling efficiency and arterial transit time (Buxton et al., 1998).

There are various permutations of the ASL acquisition steps and analysis methods. I will briefly discuss these below, outlining what led to our choices for an optimal sequence.

#### Labelling

The major labelling techniques are pulsed ASL (pASL) and continuous ASL (CASL). We apply pseudo-continuous ASL (pCASL), which is a modification of the CASL technique.

CASL was the first technique developed (Williams et al., 1992) and acts by applying a single continuous long radiofrequency (RF) pulse to label blood as it passes through a particular plane (Kwong et al., 1995), typically in the inferior of the brain perpendicular to the brain's arterial supply. The pulse is applied with slice-selective gradients and inverts magnetisation of inflowing arterial blood by flow-driven adiabatic inversion. The fixed RF pulse removes magnetisation of stationary spins while the frequency gradient in the z-direction of the plane allows the inversion of moving spins (flowing blood)- given an appropriate constant blood velocity, the flowing spins experience a linearly varying magnetic field. As macromolecules in tissues have broad resonance frequencies, long RF pulses applied in the neck also invert spins in tissues of interest in the imaging plane due to off-resonance effects. These tissue-bound protons interact with free protons in the imaging plane (magnetisation transfer [MT]) and can confound measurement of the inflowing labelled blood (Williams et al., 1992). Several techniques have been applied to mitigate the effects of MT, but most have been inadequate or impractical, as they require a separate labelling coil (Talagala et al., 2004). In some cases, the tag image is subtracted from a control image where a non-brain region is tagged an equivalent distance away, to remove these MT effects. However, compensating for MT symmetrically across the whole brain is difficult and so the technique limits multi-slice acquisitions. As a result of the continuous nature of the RF pulses, CASL techniques yield better SNR than pASL techniques. Limitations of CASL include the requirement of special hardware for continuous RF irradiation, high signal absorption rate (SAR) and suboptimal labelling efficiency due to the long pulses. The CASL labelling efficiency is also very sensitive to blood velocity, motion and magnetic field inhomogeneities at the inversion plane.

pCASL provides a solution to the MT problem by delivering a train of successive pulses rather than a continuous pulse. The control image is also acquired with successive pulses, but with the phase of every other pulse shifted 180 degrees- every other pulse nullifies

the flip of the previous pulse, so the average B1 of pulses is zero. This results in both tag and control images receiving equivalent MT but with only the tag images having inverted blood during acquisition (Dai et al., 2008; Wu et al., 2007). This technique has provided an implementable strategy for multi-slice CASL based on compensating for the MT effects without additional hardware, while also limiting SAR and improving labelling efficiency as compared to CASL. pCASL can also be implemented on systems with only pulsed radiofrequency capability (most clinical systems) and so is more practical than CASL.

pASL mimics the injection of a bolus tracer- it acts by applying a short RF inversion pulse to a net volume of blood in a slab proximal to the tissue of interest, and allowing the inverted spins to flow into the relevant tissue microvasculature before imaging. A signal intensity difference is taken between tag and control images. The major pASL techniques are Flow-sensitive Alternating Inversion Recovery (FAIR) (Kim, 1995; Kwong et al., 1995) and Echo-planar Imaging with Signal Targeting by Alternating Radio-Frequency Pulses (EPISTAR) (Edelman and Chen, 1998); these vary in the location of the labelled slab over the tag and control images. As a result of the shorter pulse, pASL sequences are easier to implement and have been more widely used. While pASL provides high labelling efficiency, better temporal resolution and does not suffer from the same SAR limitations as CASL, it also generates lower SNR because of less overall tag time (Wong et al., 1998). More importantly, the difficulty of modelling the dispersion of the bolus tag means that true quantification of CBF is challenging as compared to pCASL.

Given these considerations, and based on previous direct comparisons between these techniques in our lab, we choose to use the pCASL technique for its combination of high SNR and high tagging efficiency, as well as the facility to quantify blood flow to absolute units (Wu et al., 2007).

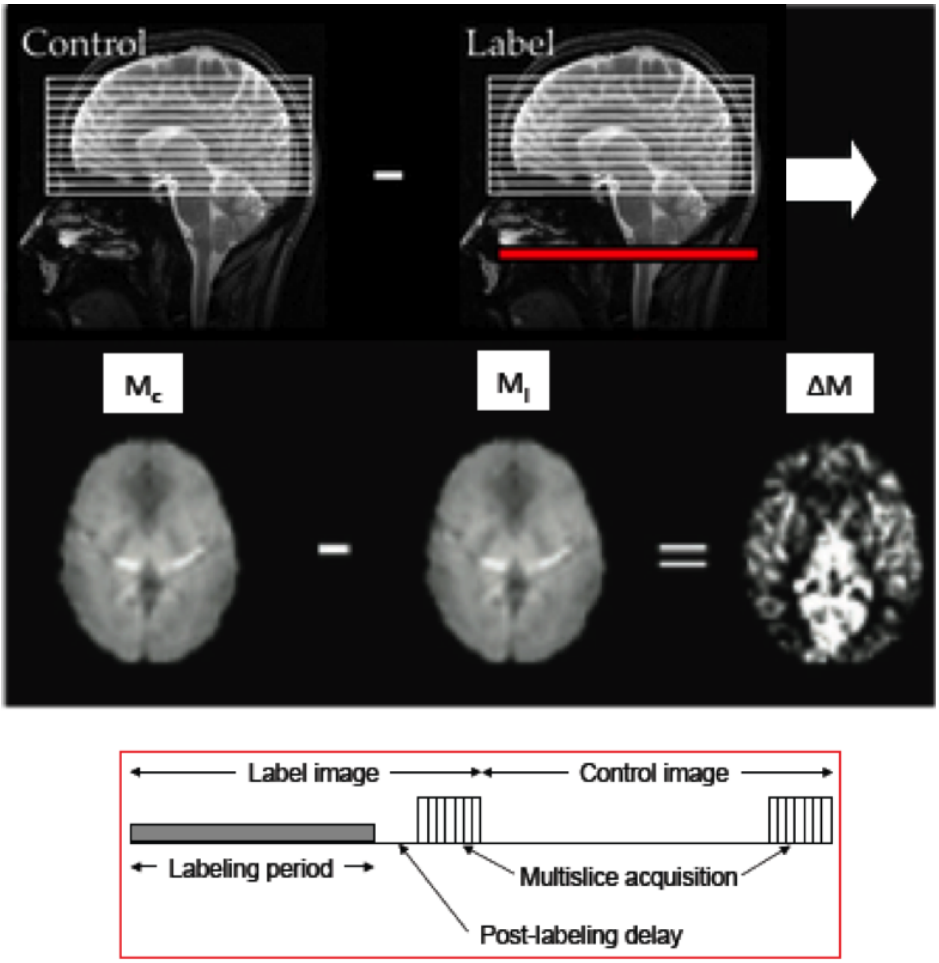


Figure 4.1: **A schematic of the pCASL acquisition technique.** Adapted from Donahue et al. (2012) and Petersen et al. (2006). Top: In label images, blood is labeled in the neck (red slab) before image acquisition. Control images ($M_c$) are subtracted from label images ($M_l$) to generate perfusion ($\Delta M$). Bottom: A set post-labeling delay between labeling period and acquisition is illustrated.

### Post-labelling delay (PLD) and Inversion time (TI)

The time between the blood labelling and image acquisition is known as the post-labelling delay (PLD) while the entire time from labelling to the start of image acquisition (tagging duration + PLD) is known as the inversion time (TI).

ASL data can be obtained with several repetitions of a single inversion time or with multiple inversion times (by changing the PLD). Although the sampling of multiple TIs can lead to a loss of SNR, it has the advantage of compensating for regional heterogeneity in arterial arrival time by allowing voxel-wise estimation of kinetic curves (Gallichan and Jezzard, 2009). The difference signal is measured as a function of time giving an accurate indication of peak signal from tagged blood. This facilitates signal estimation at a point where label decay is still minimal, improving regional SNR. Moreover, this method enables estimation of the arterial arrival time (AAT) in individual brain regions (MacIntosh et al., 2010) and can be used to model out macrovascular signal that can contaminate absolute CBF estimations in single-TI experiments (Chappell et al., 2010). As such, despite sacrifices in temporal resolution by the longer acquisition times, multi-TI ASL provides a more accurate estimation of absolute CBF.

### Image acquisition

ASL images are generally acquired using standard echo-planar imaging (EPI) techniques. Single-shot 3-dimensional gradient and spin-echo (3D-GRASE) sequences have also been used and are thought to boost SNR (Fernández-Seara et al., 2005). However unpublished data from our lab suggests that this can introduce non-physiological warp artefacts to the data (Segerdahl et al., 2011). ASL images also benefit from parallel imaging with a shorter echo time (Wang et al., 2005).

Therefore, in the studies described below we employ a 2D multi-slice EPI sequence with parallel imaging.

### Limitations of ASL

Despite the benefits outlined above, ASL is still a developing technique and has several shortcomings as compared to the more established BOLD technique.

A key drawback of the technique is the poor SNR in comparison to BOLD- this is due the comparatively low fraction of arterial blood to tissue in the brain and the small signal difference (1-2%) generated from perfusion subtraction (Ito et al., 2005). Consequently, the ASL signal can be significantly undermined by physiological noise and motion artefacts, which can also decrease labelling efficiency. Furthermore, despite being a more direct measure than BOLD, there is evidence that CBF and oxidative metabolism can uncouple in active states (Raichle et al., 1983). Whole brain acquisitions have also previously proved challenging because of the difficulty in controlling MT effects.

The importance of imaging long activation states in the pain context make overcoming these limitations a worthwhile endeavour. To minimise these effects, we use a pCASL sequence, which provides improved SNR, high labelling efficiency and controls for MT across the whole brain, in combination with a multi-TI approach for optimal absolute CBF estimation.

### Reliability of ASL techniques

The reliability of ASL quantitative CBF measures can be undermined by uncertainties surrounding arterial input functions, other kinetic assumptions and tissue parameters

such as blood equilibrium magnetisation (which is a direct scaling factor in quantification) (Petersen et al., 2010). However recent development efforts have enabled better application of ASL techniques in clinical and research settings, showing good reliability for repeated measures.

Both CASL and pASL techniques have been shown to be accurate and reproducible in the time frame of several weeks (Hermes et al., 2007; Petersen et al., 2010). When compared to pASL and CASL, pCASL is shown to be the least variable and also the least sensitive to site-specific differences (Chen et al., 2011; Gevers et al., 2011). Longitudinal repeatability of pCASL has also been validated for neurodevelopmental studies (Jain et al., 2012). A recent study assessing reproducibility of whole-brain pCASL 3D acquisitions suggests that pCASL with multiple PLDs may be more reliable for assessing CBF by accounting for heterogeneity in arterial transit time between subjects and different brain regions (Wu et al., 2013).

These aforementioned pCASL studies have used sequences with single inversion time acquisitions. The acquisition of data at multiple inversion times has been suggested to be a more accurate way to model out macrovascular noise than background suppression techniques (Chappell et al., 2010). Multi-TI pASL has been shown to correlate well with $H_2{}^{15}O$ PET in patients with carotid artery occlusion (Bokkers et al., 2010), while also accounting for the issue of variable bolus arrival time in perfusion estimation. However, to date no studies have assessed the within-session and between session reproducibility of a pCASL sequence modelling multiple PLDs. Given the potential relevance of this technique for longitudinal studies and assessment of drug efficacy or long acting cognitive and physiological states, we suggest this is an important initial investigation of the method with a view towards improving its experimental and clinical utility.

## 4.2 Aim

We assess the reproducibility of a multi-TI (6 inversion times) pCASL sequence for whole brain imaging, obtaining both within and across session measures at several time points. In each session, we acquire both resting and active task scans and test intraclass correlation coefficient (ICC) and within- subject coefficient of variation (wsCV) in the whole brain and in selected brain regions.

This technique has mainly been applied in the context of sequence development paradigms. Here, we aim to validate the use of the technique for the assessment of resting or long activation states, for application in longitudinal and crossover study designs. Furthermore, we assess novel tools for the analysis of such data, to improve the test-retest reliability of the measures.

## 4.3 Methods

### 4.3.1 Subjects

Eight healthy subjects (6 male, 2 female, age [mean $\pm$ s.e.m]= 28.3 $\pm$ 2.5) were recruited to participate in this study. Subjects were asked to abstain from caffeine for 6 hours prior to each session. In addition to routine screening for MRI contraindications, subjects were also screened to exclude any cerebrovascular disease, neurological/psychiatric disease, and use of medication that could interact with blood flow.

### 4.3.2 Study design

Subjects were scanned on three separate occasions, separated by one week and one month, respectively. Session 1 consisted of two repeat runs of the experimental protocol,

separated by a 30-minute rest period; while session 2 and 3 had only a single run. The protocol consisted of a 6-minute resting scan followed by a 6-minute OFF/ON visual-cued motor task (8Hz flashing checkerboard with combined finger-tapping)- alternating 1 minute ON and 1 minute OFF. The majority of scans took place between 8am and 12pm to minimise diurnal variation, which can affect CBF values (Parkes et al., 2004).


Figure 4.2: **A schematic of the experimental design used.** Session 1 consisted of two repeat runs of the experimental scans. Runs 1 and 2 were separated by a 20-min rest block. Session 2 was generally completed one week after Session 1. Session 3 was completed one month after Session 1. All scan sessions were identical in design.

### 4.3.3 MR data acquisition

All subjects were scanned using a Siemens 3T Verio whole-body MR scanner (Erlangen, Germany) equipped with a 32-channel head coil and a body coil. A time of flight MR angiography neck scan was acquired approximately 8cm below the circle of Willis to visualise the brain's feeding arteries. The labelling plane was placed parallel to the imaging slices, and perpendicular to the ascending carotid and vertebral arteries. The location of the plane was normalised to a point between the curvatures of the vertebral arteries, where all feeding arteries ran parallel in a transverse plane. $B_0$ shimming (Kim et al., 2002) was performed over the imaging region and the labelling plane to minimise off-resonance effects.

We use a pCASL acquisition sequence with background suppression as described in (Okell et al., 2013). Images were acquired in separate consecutive blocks, each composing 6 different post-labelling delays: 0.25, 0.5, 0.75, 1, 1.25, 1.5 (seconds). A labelling duration of 1.4 seconds was used. The selected inversion times are based on an optimal sampling schedule (OSS) design (Xie et al., 2008) and encompass a broad distribution of inversion times relative to single-TI experiments in the literature. Other imaging parameters were: single shot EPI, TR- 4s, TE- 13ms, Partial Fourier = $6/8^{ths}$, FOV 220x220 $mm^2$, matrix 64x64, 24 slices, slice thickness- 4.95mm. To keep repetition time constant while acquiring data at different TIs, a fill gap was added to the start of each TI acquisition where the PLD was below 1.5. For each scan, 96 volumes (control and tag) were acquired, corresponding to 6.4 minutes of scanning. Data was analysed as 8 separate epochs where each epoch represented a full set of control/tag images for all 6 TIs.

A reference calibration image of equilibrium magnetisation (no labelling or background suppression, TR=6s, all other parameters identical to pCASL scan) was also collected to enable the estimation of the equilibrium magnetisation of blood. A second calibration

image of the same prescription was collected using the body coil for signal detection. This body coil calibration scan was used to correct the PCASL data for the uneven sensitivity profile of the 32-channel head coil. A T1-weighted structural image was acquired for tissue segmentation and registration purposes. We additionally acquire a phase contrast angiography image (TR 72.9ms, TE 4.82ms, FOV 240x240 $mm^2$, matrix 128x128, slice thickness 5mm, flip angle 15 degrees, velocity encoding 100cm/s) in the same position as the labelling plane to assess blood flow velocity and inversion efficiency (Aslan et al., 2010), and corresponding $B_0$ field map images to correct for EPI distortion effects.

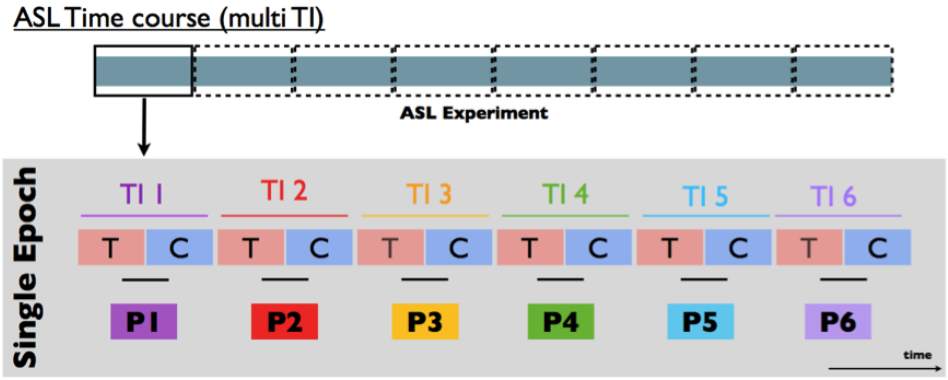


Figure 4.3: **A schematic of the multi-TI pCASL sequence for collection of one epoch of ASL data.** An epoch is defined as a single cycle of the TIs employed; where a 'tag-control' pair of images is collected for each TI (labeled 'T' and 'C'). Each 'tag-control' pair of images was then subtracted in the analysis preprocessing stages to generate relative perfusion images for each TI (labeled P1-P6 for each respective TI). The six relative perfusion images constituent of a single epoch were then processed using BASIL to generate an absolute CBF data point for that epoch.

### 4.3.4 Pre-quantification processing

Image processing was performed using FMRIB Software Library (FSL) tools (Jenkinson et al., 2012) (www.fmrib.ox.ac.uk/fsl). The pCASL raw images were stripped of non-brain structures using BET (Smith, 2002) and motion corrected using MCFLIRT

(Jenkinson et al., 2002).

The head coil calibration image was divided by the body coil image to generate a coil sensitivity map. This sensitivity map was applied to both the first reference image and the pCASL data before CBF quantification to correct for the uneven sensitivity profile of the 32-channel head coil.

Tissue segmentation was performed on each subject's high-resolution structural image using FAST (Zhang et al., 2001) to generate grey and white matter partial volume estimates (PVEs). These PVEs were thresholded to include regions with 50% and 1% inclusion probabilities respectively, then binarised and linearly transformed to the image acquisition space using FLIRT (Jenkinson and Smith, 2001).

### 4.3.5 Signal calibration to physiological units

Equilibrium magnetisation of blood ($M_{0,b}$) was estimated from the mean cerebrospinal fluid (CSF) magnetisation ($M_{0,csf}$) signal as previously described (MacIntosh et al., 2008). Briefly, a standard space ventricle mask was non-linearly registered (Andersson et al., 2007) to the subject's structural, linearly registered to the subject's image space, eroded to minimise partial volume effect, then used to extract the mean CSF signal from the reference image. The CSF signal was corrected for CSF T1 and T2* to determine $M_{0,csf}$. $M_{0,csf}$ was converted to $M_{0,b}$ by applying the known ratio of CSF to blood proton density. Final correction for blood T2* effects yielded the true value for $M_{0,b}$. We assumed an inversion efficiency of 0.88 for our calculations (Aslan et al., 2010); this value was verified by using the phase contrast image at the labelling plane to estimate blood velocity in the main feeding arteries.

PCASL perfusion images were divided by the effective $M_{0,b}$ and inversion efficiency to calibrate to physiological units (ml blood/ 100g tissue/ 60 seconds) before model fitting.

### 4.3.6 Quantification

A pairwise control minus tag subtraction was performed on the pCASL data to generate a perfusion image at each inversion time. The resultant voxel-wise concentration-time curves were fitted to the general kinetic model (Buxton et al., 1998) to estimate both CBF and arterial arrival time (AAT). Perfusion parameters were quantified using multi-component modelling with a Bayesian inference tool (BASIL) developed for this purpose (http://fsl.fmrib.ox.ac.uk/fsl/fslwiki/BASIL).

The BASIL algorithm uses a variational Bayes approach (Chappell et al., 2009), which is a probabilistic implementation of the more common non-linear least squares approach. A benefit of this approach is that it can incorporate prior information about known physiological parameters (e.g. T1, blood T1) and other varying parameters (labelling duration, post-label delays) to improve signal detection. The priors used are as described previously by Chappell and colleagues (2010). Flow crusher gradients were not used so vascular contributions to the perfusion signal were modelled out of the data (Chappell et al., 2010). BASIL outputs voxel-wise estimates of absolute CBF and AAT, as well as a corresponding voxel-wise variance/uncertainty map for each parameter.

Importantly, these parameters were estimated for each epoch of data (defined as a full set of inversion times), thus generating a time series of absolute CBF and AAT from each acquisition. 8 such epochs were generated from each scan.

### 4.3.7 Post-quantification processing

#### Resting data

The time-series of epochs generated for each scan was averaged using a mixed effects model, which accounted for the voxel-wise variance of the Bayesian fit. This generated a single CBF and AAT image for each scan, with a corresponding variance image. For comparisons, raw EPI images were registered first to each subject's structural image using BBR (Greve and Fischl, 2009), then non-linearly to the MNI standard brain using FNIRT (Andersson et al., 2007). Transformed quantified images were used for resting CBF and AAT extractions and comparisons described below.

#### Task data

The epochs were concatenated such that volumes alternated between a full rest block and a full visuomotor active block- i.e. for each 1 minute stimulation period, a single epoch of absolute CBF was generated. The resultant data timeseries (6 epochs- 3 rest and 3 task) were modelled using a GLM square design to generate a statistical map of brain regions responding to the visuomotor task. A significance map was generated with a cluster corrected Z threshold of 2.3 ($p<0.05$). Statistical images were transformed to standard space for group comparisons. A mixed effects model (FLAME 1+2) was used to assess group level effects. CBF values were extracted from grey matter (GM), white matter (WM) and region-defined voxels for each subject and session.

### 4.3.8 Statistical analysis

Within and across subject variation was calculated using IBM SPSS Statistics, version 18 (IBM, Armonk, NY, USA). This was assessed for grey matter (GM), white matter

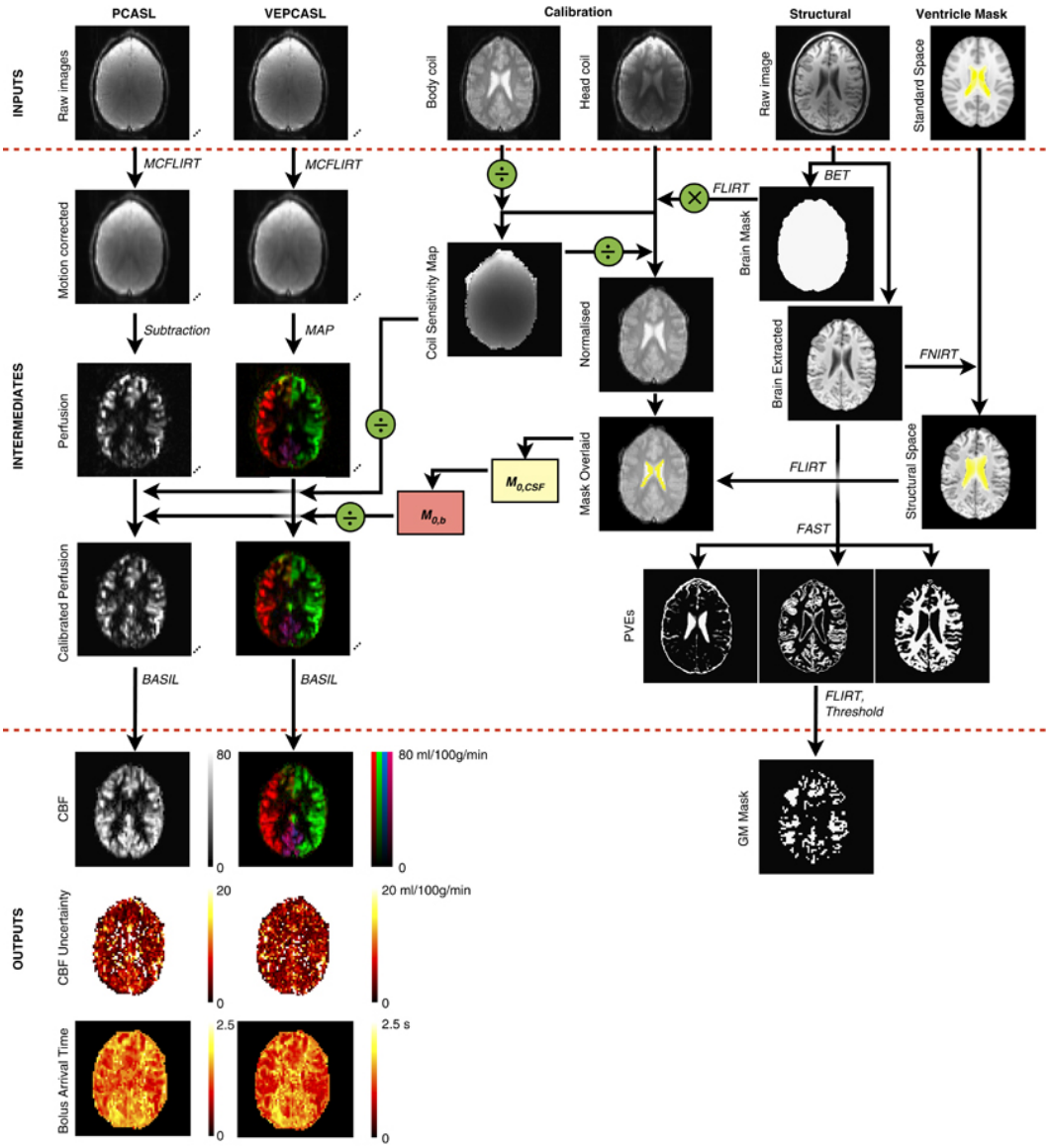


Figure 4.4: **A schematic of the analysis pipeline used for pCASL data**- adapted from Okell et al. (2013). We do not use Vessel-Encoded pCASL (VEPCASL) in this experiment but follow the pipeline as outlined for pCASL data, calibration data and structural/ventricle mask generation.

(WM), four major lobes (frontal, temporal, parietal, occipital) and a selection of brain regions bilaterally (insula cortex [INS], thalamus [THA], caudate [CAU] and putamen [PUT]) using masks generated from FAST (see pre-quantification processing), and the MNI Structural Atlas (thresholded at p>0.5, binarised).

Analyses of variance (ANOVA) and paired t-tests were performed to compare between the measured variables. Post-hoc correction for multiple comparisons was performed using *Bonferroni* adjustments. Normality testing was performed using the Shapiro-Wilk's test.

### 4.3.9 Repeatability of resting measures

We assessed repeatability of resting physiological variables using three separate methods:

We evaluated coefficients of variation (wsCV) and intraclass correlations (ICC); analyses of variance (with pairwise t-tests) between the CBF values extracted from regions of interest; and voxel-wise comparisons between the different conditions in the framework of a general linear model.

1) We calculated wsCV values from the ratio of the standard deviation of the difference between the repeated measures, to the mean of the repeated measures (Bland and Altman, 1996). A smaller wsCV number represents better reproducibility. Within- and across-session variation between subjects was quantified for CBF and AAT by calculating session-paired wsCV and ICC. We assessed intra-subject variation across session by calculating across-session wsCV using CBF values from the three sessions for each subject. These were averaged for all subjects to give a mean intra-subject wsCV. ICC measures the contribution of between subject variances to total variance. We calculated

two-way mixed single measures ICC in SPSS for absolute agreement between measures as described in (Shrout and Fleiss, 1979):

$$\mathrm{ICC}_{(3,1)} = \frac{(BMS-EMS)}{(BMS+(k-1)EMS)} \quad (1)$$

*(where BMS is between targets mean square, EMS is error mean square and k is number of repeat sessions)*

ICC values range from 0-1: we designate ICC values <0.4 as poor, 0.4-0.59 as fair, 0.60-0.74 as good, and >0.75 as excellent (Fleiss et al., 2003). These denotations do not account for confidence intervals so must be interpreted cautiously.

2) To investigate type I error inherent in the technique, we performed repeated-measures analyses of variance and paired comparisons (student paired t-tests) between session-wise and run-wise regional CBF values using SPSS. We used a 0.05 $\alpha$ threshold as evidence of good specificity of the technique.

3) Finally, we performed a voxel-wise analysis assessing differences between whole-brain CBF and AAT volumes by using GLM in a higher level FEAT analysis (www.fsl.ox.ac.uk/feat).

### 4.3.10 Repeatability of task measures

Type II error was assessed across all scan sessions by evaluating CBF percentage change between task and rest blocks in *a priori* defined anatomical masks for the primary visual motor cortices. We used a value of $\beta < 0.2$ as evidence of good sensitivity.

We assessed repeatability of task measures by performing analyses of variance and paired t-tests between run-wise and session-wise absolute CBF changes ($\Delta$CBF) from values

extracted from the visual cortex. For this we used a bilateral anatomical mask of the primary visual cortex from the Juelich Atlas (thresholded at p>0.5 and binarised). We also defined functional masks in the visual cortex and motor cortex by identifying the peak voxel from session-averaged activation maps (masked by standard Juelich Atlas anatomical masks), and defining a 5mm sphere around the peak voxel.

Finally we tested session-wise and task-wise reproducibility of the CBF change by performing a whole-brain voxel-wise analysis of variance between the sessions using FEAT.

### 4.3.11 Optimisation of inversion time selection

To assess the utility of our selection of inversion times in the context of single TI experiments, we calculate an optimisation metric ($\gamma$) that reflects how well CBF measures are observed across the whole brain.

For single-TI studies, in order for the measured signal to reflect CBF, the AAT must be shorter than the post-labelling delay- i.e. tagged blood must arrive at the region of interest before imaging. Because a fixed calculation is used to fit the peak magnetisation of arterial signal within a given voxel in multi-TI analysis, we can assess the ability of a given TI to accurately estimate CBF by comparing the estimated arrival time (AAT) to the delay time between tagging and imaging (PLD + slice acquisition time; slice dt).

$$\gamma = \text{AAT - (PLD + [z*slice dt])} \quad (2)$$

(where AAT - arterial arrival time; PLD - post labelling delay; z - number of slice acquired ascending from the most caudal; slice dt - acquisition time per slice)

Regions where $\gamma>0$ indicates when slice acquisition begins before the AAT; while $\gamma<0$ reflects areas within which acquisition occurs after AAT. We assume that the most optimized setting for SNR would be when the time it takes for arterial signal to arrive at a voxel is equal to the PLD (i.e. $\gamma = 0$). For CBF signal, the most optimised setting is where $\gamma \leq 0$ as this ensures adequate blood arrival. Calculation of the optimisation metric ($\gamma$) is useful as it informs selection of inversion times for whole-brain multi-TI studies. It also can be used to select an appropriate PLD for use in a single-TI ASL experiments to maximise signal in a given brain region. To illustrate this point, we plotted histograms for three key ROIs to visualise the range of $\gamma$ values for each TI used in the study (Figure 4.9).

### 4.3.12 Sample size calculation

A previous pCASL study, testing regional CBF responses to ongoing pain in patients, revealed CBF changes between 5-10% (Howard et al., 2011). We therefore performed a sample size calculation to estimate how many subjects would be needed to generate a 7.5% CBF signal change in pairwise within-session and across-session comparisons (Machin et al., 2011) using this sequence. We assumed an identical amount of sampling (scan acquisition length). Our estimates are taken for a unilateral region of the secondary somatosensory cortex, which has been shown to be relevant in neuropathic pain (Friebel et al., 2011) and to be modulated by gabapentin in a topical capsaicin model (see Chapter 3). We used the anatomical SII mask defined as in Chapter 3.

## 4.4 Results

Before reporting the absolute perfusion data, we tested the reliability of $M_{0,b}$ values generated for physiological calibration. We report that the wsCV for $M_{0,b}$ over week

and month repeat scans were 3.45% and 2.42%, respectively. The wsCV for all scan sessions was 2.77%.

### 4.4.1 Repeatability of resting state physiological measures

Average CBF and AAT values from all ROIs are shown in supplementary tables (see Appendix A). We observed heterogeneity in CBF and AAT between subjects and between regions. Bland Altman plots (with 95% confidence intervals) plotting mean CBF against difference in CBF values in the selected ROIs are in Figure 4.5. Intra- and inter-subject repeatability measures (wsCV and ICC) are shown for CBF in Table 4.1 and for AAT in Table 4.2. There is evidence of good to excellent reliability (ICC>0.6) and moderate to high reproducibility (wsCV<10%) for most measures.

Repeatability measures are shown to be stronger with shorter inter-scan intervals- for example wscV for GM CBF ranged from 3.17% within session to 9.67% for a month repeat scan while ICC ranged from 0.924 to 0.329 for the same periods. CBF and AAT reliability measures also showed heterogeneity between different ROIs- for CBF, the insula cortex (ICC: 0-0.608) and white matter (ICC: 0.205-0.825) showed the lowest reliability while the thalamus (wsCV 8.99-12.89%) and occipital lobe (wsCV 6.63-14.38%) showed the least reproducibility. AAT repeatability analyses showed uniformly lower wsCV values (<3%) in comparison to CBF indicating better reproducibility.

In 1x3 ANOVAs testing the effect of session on extracted CBF and AAT values, there was no significant difference between any of the tested regions (Suppl Table 4.3). There were no significant changes in AAT values between runs 1 and 2 in session 1 for all ROIs tested. However, we report an average CBF decrease of 10.4% in an anatomical mask of the thalamus between runs 1 and 2 (corrected p=0.028). No other brain regions tested

show within-session CBF changes.

In a voxel-wise ANOVA comparison of sessions, there was no significant effect of session on voxel-wise CBF across the whole brain (mixed effects, cluster corrected, Z=2.3). A paired t-test comparing within-session effects in session 1 showed clusters of significantly decreased CBF between run 1 and 2 in the bilateral thalami (Figure 4.6).

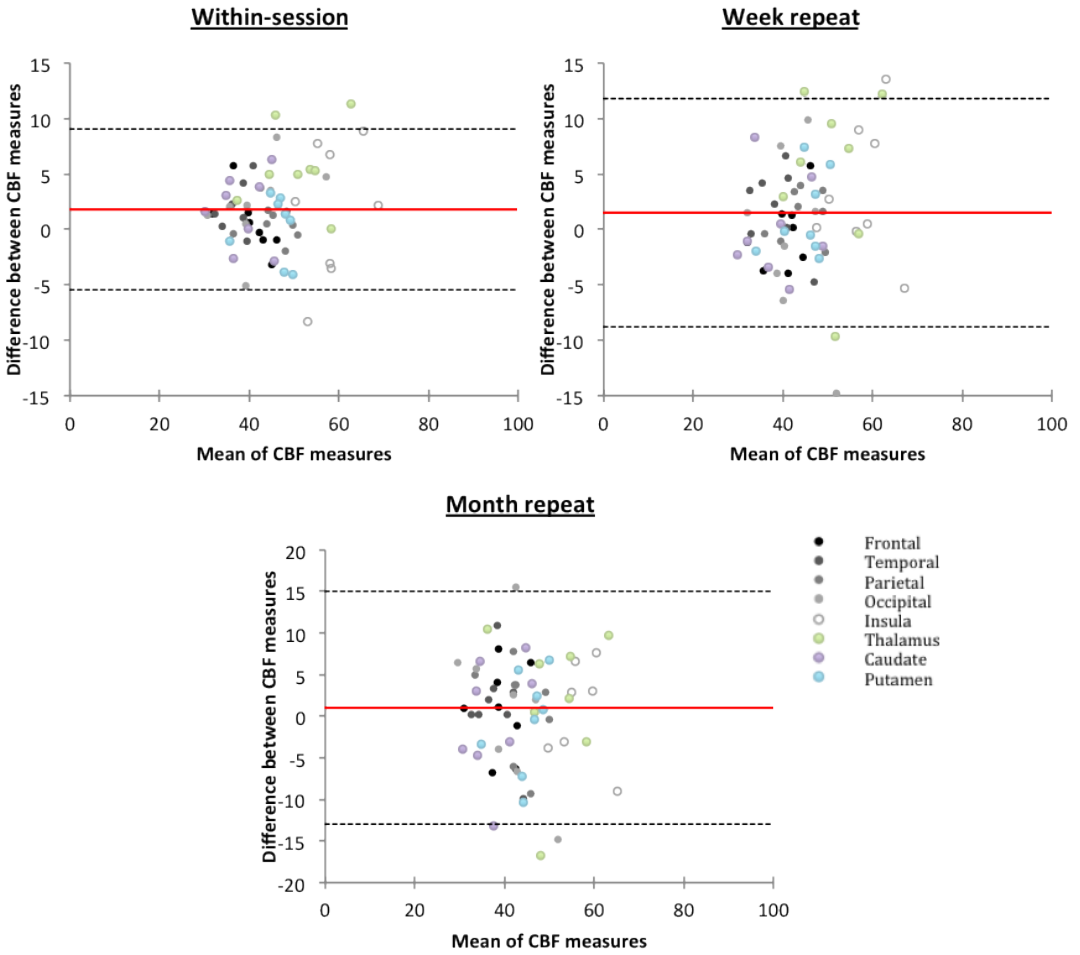


Figure 4.5: **Bland-Altman plots showing repeatability of CBF measures (ml/100g/min).** Red line denotes the bias from 0, top and bottom lines denote the 95% confidence intervals (bias ± 1.96 x SD). The difference between measures is always the first session - second session. Data shown represents absolute CBF values extracted from 8 representative brain regions for all 8 subjects.

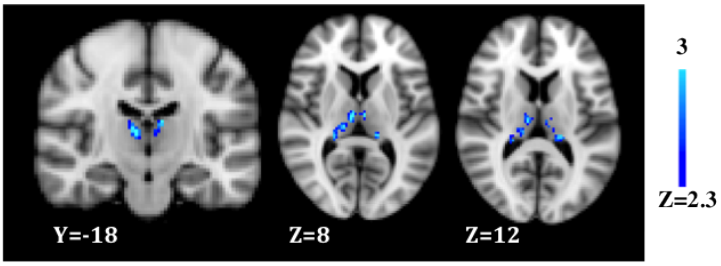


Figure 4.6: Brain regions showing a time dependent decrease in rCBF within-session (blue). (Mixed Effects; z>2.3, p<0.05; cluster corrected). No regions showed rCBF increases. Images are in radiological convention.

### 4.4.2 Repeatability of CBF response to active task

Figure 4.7 shows brain regions that respond significantly to the visuomotor task for all runs. For all task runs in all sessions, we report the power (1-$\beta$) for signal change (ON vs. OFF) in the anatomical V1 as greater than 0.9, and in functionally defined masks as $\sim$1. The mean task-induced percentage changes in CBF during ON vs. OFF blocks for each run and session are shown in Table 4.3.

Comparisons of extracted $\Delta$CBF within- and across-sessions showed no significant differences (p>0.05) in either the anatomical or functional ROIs (within-session Student T-test: p=0.75; between-session ANOVA: F=0.107, p=0.90).

Similarly, a GLM-based voxel-wise FEAT analysis revealed no significant differences in extent of CBF changes with task ON vs OFF either within or across sessions (mixed effects analysis; z>2.3; p<0.05, cluster corrected).

Table 4.1: **Measures of reproducibility: Absolute CBF.** Lower within subject coefficient of variation (wsCV) values reflect better reproducibility, values <20% are considered to be in the normal range for ASL data (Gevers et al., 2011). Intraclass correlation (ICC) values range from 0-1; we designate ICC values <0.4 as poor, 0.4-0.59 as fair, 0.60-0.74 as good, and >0.75 as excellent (Fleiss et al., 2003). * out of range; CBF, cerebral blood flow; GM, grey matter; WM, white matter; ROI, region of interest

| **CBF wsCV (%)** | | | | |
|---|---|---|---|---|
| ROI | Session repeat | Week repeat | Month repeat | All sessions |
| GM | 3.17 | 5.11 | 9.67 | 6.38 |
| WM | 4.59 | 6.77 | 11.06 | 7.40 |
| Frontal lobe | 4.62 | 5.13 | 9.06 | 6.56 |
| Temporal lobe | 4.98 | 7.06 | 9.60 | 6.13 |
| Parietal lobe | 2.75 | 3.96 | 9.28 | 6.48 |
| Occipital lobe | 6.63 | 11.31 | 14.38 | 11.03 |
| Insular cortex | 7.33 | 7.76 | 11.94 | 7.82 |
| Thalamus | 8.99 | 11.94 | 12.89 | 10.58 |
| Caudate | 6.30 | 8.10 | 12.49 | 9.19 |
| Putamen | 4.10 | 5.73 | 8.99 | 6.92 |

| **CBF Intraclass correlation** | | | | |
|---|---|---|---|---|
| ROI | Session repeat | Week repeat | Month repeat | All sessions |
| GM | 0.924 | 0.776 | 0.329 | 0.573 |
| WM | 0.825 | 0.651 | 0.205 | 0.490 |
| Frontal lobe | 0.869 | 0.804 | 0.493 | 0.635 |
| Temporal lobe | 0.856 | 0.725 | 0.335 | 0.603 |
| Parietal lobe | 0.932 | 0.874 | 0.549 | 0.697 |
| Occipital lobe | 0.870 | 0.450 | 0.435 | 0.504 |
| Insular cortex | 0.608 | 0.585 | * | 0.325 |
| Thalamus | 0.744 | 0.529 | 0.574 | 0.640 |
| Caudate | 0.805 | 0.824 | 0.460 | 0.677 |
| Putamen | 0.829 | 0.773 | 0.456 | 0.570 |

Table 4.2: **Measures of reproducibility: Arterial arrival time.** Lower within subject coefficient of variation (wsCV) values reflect better reproducibility, values <20% are considered to be in the normal range for ASL data (Gevers et al., 2011). Intraclass correlation (ICC) values range from 0-1; we designate ICC values <0.4 as poor, 0.4-0.59 as fair, 0.60-0.74 as good, and >0.75 as excellent (Fleiss et al., 2003). * out of range; AAT, arterial arrival time; GM, grey matter; WM, white matter; ROI, region of interest.

| **AAT wsCV (%)** | | | | |
|---|---|---|---|---|
| ROI | Session repeat | Week repeat | Month repeat | All sessions |
| GM | 1.24 | 1.36 | 1.65 | 1.12 |
| WM | 0.82 | 0.55 | 0.71 | 0.56 |
| Frontal lobe | 2.53 | 1.94 | 1.59 | 1.39 |
| Temporal lobe | 1.59 | 1.12 | 2.24 | 1.19 |
| Parietal lobe | 1.36 | 1.26 | 1.14 | 0.84 |
| Occipital lobe | 1.57 | 2.34 | 2.77 | 1.76 |
| Insular cortex | 1.27 | 1.80 | 1.86 | 1.69 |
| Thalamus | 1.73 | 1.74 | 1.46 | 1.08 |
| Caudate | 0.96 | 1.32 | 1.42 | 1.05 |
| Putamen | 1.86 | 1.29 | 1.77 | 1.47 |

| **AAT Intraclass correlation** | | | | |
|---|---|---|---|---|
| ROI | Session repeat | Week repeat | Month repeat | All sessions |
| GM | 0.800 | 0.623 | 0.552 | 0.657 |
| WM | 0.450 | 0.740 | 0.471 | 0.599 |
| Frontal lobe | 0.444 | 0.523 | 0.643 | 0.546 |
| Temporal lobe | 0.621 | 0.749 | 0.452 | 0.661 |
| Parietal lobe | 0.761 | 0.749 | 0.768 | 0.778 |
| Occipital lobe | 0.827 | 0.362 | 0.031 | 0.239 |
| Insular cortex | 0.716 | 0.230 | 0.198 | 0.180 |
| Thalamus | 0.475 | 0.503 | 0.688 | 0.676 |
| Caudate | 0.906 | 0.784 | 0.754 | 0.819 |
| Putamen | 0.716 | 0.814 | 0.699 | 0.691 |

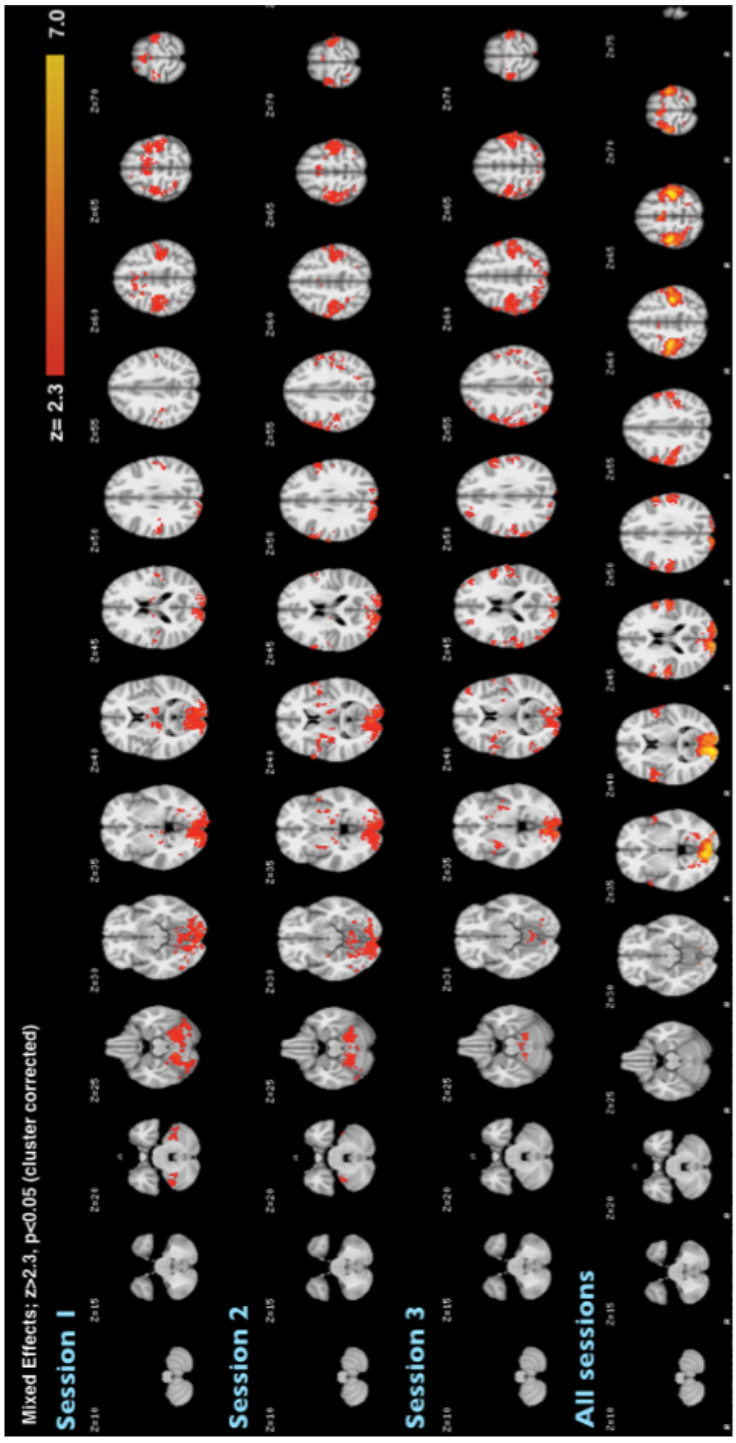


Figure 4.7: **Activation to visual-cued motor task.** Statistical maps represent voxels with suprathreshold activation across the group during the task ON compared to OFF blocks. (Mixed Effects; $z>2.3$, $p<0.05$; cluster corrected). A repeated measures ANOVA revealed no significant differences in hyperperfusion (or hypoperfusion) maps across repeat sessions. Each row represents group mean statistics maps for a given scan session (1-3 and all sessions combined). The whole brain volume is divided into axial slices (left to right; Z: 10 - 70) with a single image taken every 5 slices. Images are in radiological convention.

Table 4.3: **Reproducibility of activation within key ROIs during the functional task.** The table above displays the group mean absolute CBF change between ON and OFF BLOCKS (ON-OFF) and group mean percent changes, for within and across session comparisons. Absolute CBF was extracted from both the visual and motor cortices. For clarity, both anatomical and functional masks of V1 are included in the table.

| **Mean ΔCBF / % change (N=6)** | | | | |
|---|---|---|---|---|
| ROI | Run 1 | % | Run 2 | % |
| V1 | 12.07 | 39 | 12.05 | 43 |
| Functional V1 | 26.61 | 101 | 28.20 | 121 |
| Functional M1(left) | 16.09 | 67 | 13.18 | 53 |
| Functional M1(right) | 15.91 | 60 | 15.11 | 55 |

| **Mean ΔCBF / % change (N=7)** | | | | | | |
|---|---|---|---|---|---|---|
| ROI | Session 1 | % | Session 2 | % | Session 3 | % |
| V1 | 13.76 | 44 | 11.25 | 41 | 10.98 | 39 |
| Functional V1 | 25.96 | 115 | 25.78 | 121 | 22.97 | 100 |
| Functional M1(left) | 14.81 | 74 | 16.19 | 72 | 15.71 | 65 |
| Functional M1(right) | 15.35 | 65 | 17.34 | 73 | 16.83 | 65 |

### 4.4.3 Optimisation of inversion time selection

Figure 4.8 shows inversion time optimisation values ($\gamma$) mapped onto a standard brain for each individual inversion time selected. Most cortical regions have been adequately perfused by labelled blood with a PLD of 1, although many inferior regions are maximally perfused subsequent to this.

To quantify this, we plotted voxel fractions for three representative brain regions in Figure 4.9. Regional masks were generated from the Juelich, MNI, and Harvard-Oxford Subcortical Atlases respectively ($p>0.5$). We designate inversion times where most voxels have values close to zero as optimal for both SNR and CNR. For single-TI studies using such a protocol, we therefore suggest the optimal PLD selection to be 0.5 for the motor cortex, 0.25 for the insula and 1 for the amygdala.

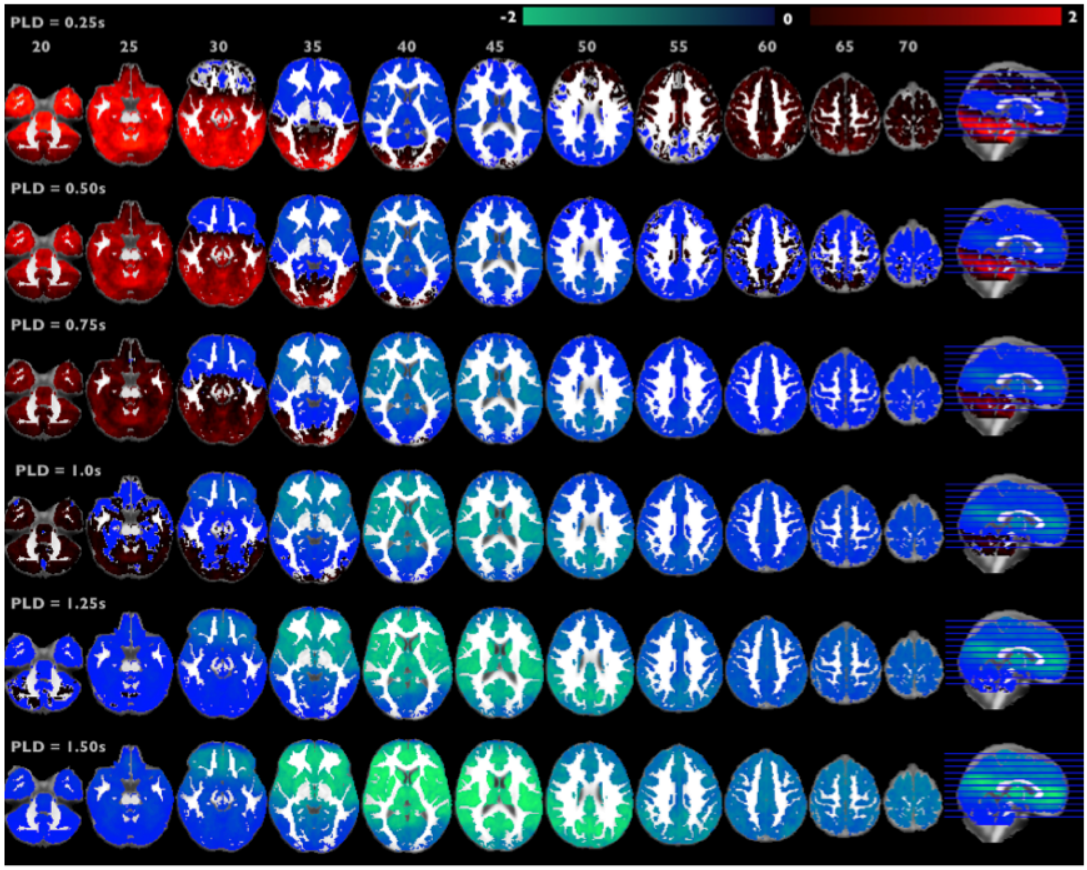


Figure 4.8: **Optimisation of TI selection based on region location.** The optimisation metric ($\gamma$) is mapped onto a standard brain (masked for grey matter) for each inversion time selected. Briefly, colour coding details the extent of optimisation for each PLD across the whole brain where the darker the colour, the greater the SNR benefit of a given TI (in the context of a single-TI study) at a given brain region (i.e. the closer $\gamma$ tends to zero). Blue ($\gamma$<0) indicates good CBF estimation, although a brighter blue ($\gamma$<<0) indicates reduced SNR benefit. Most cortical regions have been adequately perfused by labelled blood with a PLD of 1, although some inferior regions may be maximally perfused subsequent to this. The whole brain volume is divided into axial slices (left to right; Z: 10 - 70) at 5-slice intervals. All images are in radiological convention.

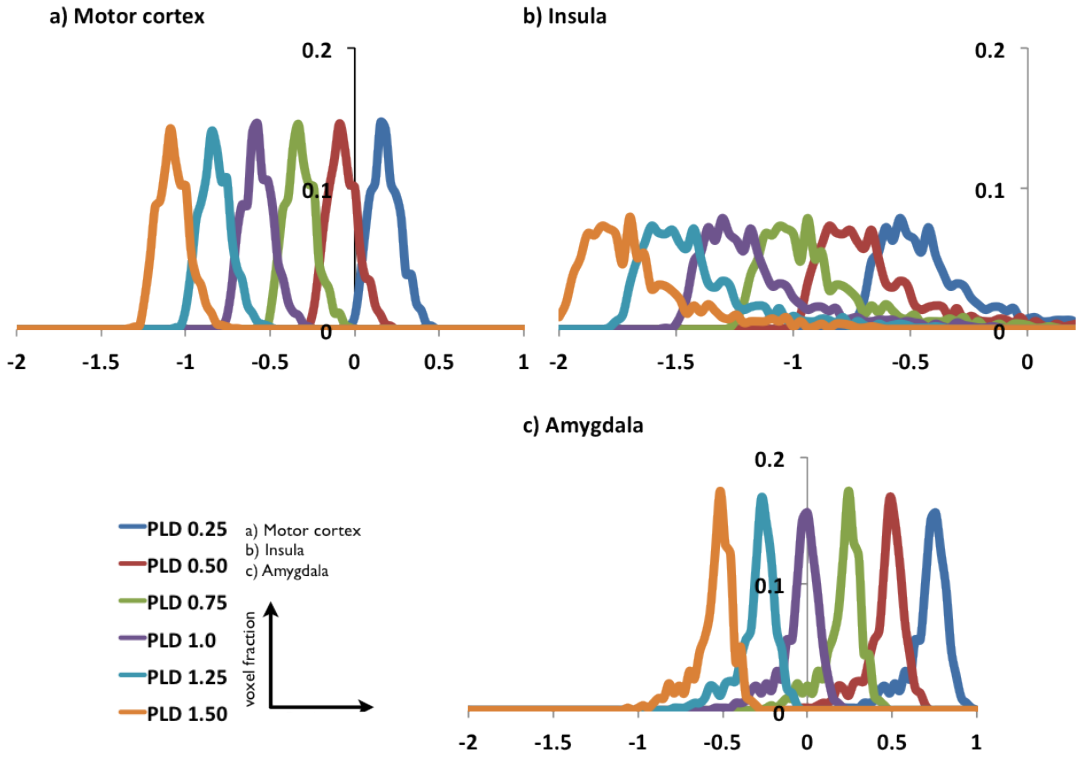


Figure 4.9: **Optimization of TI selection for specific ROIs.** The figure below displays histograms generated from the following ROIs: A) motor cortex; B) insular cortex; C) amygdala. Optimisation metric of TI selection ($\gamma$ as calculated in Methods) is plotted on the x-axis while voxel fraction is plotted on the y-axis. The coloured lines represent plots generated from each PLD used in the study (dark blue: PLD=0.25s; red: PLD=0.50s; green: PLD=0.75s; purple: PLD=1.0s; light blue: PLD=1.25s; orange: PLD=1.50s).

### 4.4.4 Sample size calculation

Following our verification of the technique's high sensitivity and high specificity, we assumed an $\alpha$ of 0.05 and $\beta$ of 0.2 for this calculation. We report that in an anatomical left SII mask, the sample sizes needed to generate a 7.5% CBF change in within-session, one-week and one-month crossover designs are 10, 10 and 38 respectively.

## 4.5 Discussion

The results from this study show that the multi-TI pCASL approach has high test-retest reliability as the data reveal strong consistency across subjects and sessions for key perfusion outcome measures (AAT and CBF). Specifically, we report low variation coefficients, high interclass correlation coefficients and good effect specificity in standard GLM-based analyses of the ASL data. Additionally, we successfully validated the reliability of this newly developed tool for assessment of functional tasks; a novel feature which has not been investigated for multi-TI pCASL imaging to our knowledge. Importantly, the results of this study give insight into optimal TI sampling schedules across different brain regions for healthy populations and provide key caveats for future investigations employing ASL to image absolute perfusion changes across whole brain volumes or within specific ROIs. In particular, our findings demonstrate the importance of acquiring data with multiple inversion times, as single inversion times may only be optimal for a select region.

### 4.5.1 Resting physiological measures are reliable and reproducible

Assessment of CBF across the whole brain shows both the wsCV(%) and the ICC measures to be reliably consistent across session repeats on the same day, a week and a

month later. However, these measures show slight depreciation in exact reproducibility as the duration between scan sessions increases.

Specifically, the data show good to excellent longitudinal reproducibility across most brain regions for both CBF (ICC= 0.776, wsCV= 5.11% for grey matter over 1 week) and AAT (ICC= 0.623, wsCV=1.36% for grey matter over 1 week). In general, within subject repeatability measures less than 20% are suggested to be in the normal range for ASL studies (Gevers et al., 2011). Previous reports show moderate to good longitudinal CBF reproducibility (ICC= 0.65, wsCV= 14% for grey matter) for pCASL over a 2-4 week period in a paediatric cohort (Jain et al., 2012); while other studies of week-repeat comparisons report whole brain/regional wsCV to be between 8-14% (Chen et al., 2011; Floyd et al., 2003). The data we report here are consistently within this range or show improved reliability (i.e. wsCV values are lower) when compared to previous investigations of the same session comparisons.

We find no differences in session-wise ANOVAs for extracted data and voxel-wise GLM analyses, suggesting high specificity for the technique across 1-week and 1-month comparisons. Interestingly, we show that in a within-session comparison where both runs are separated by 20 minutes, there is a significant decrease in thalamic CBF (Fig 4.6). The thalamus is a key relay centre and is an important shared anatomical substrate for both arousal and attentional processes (Portas et al., 1998). Given that subjects were lying in the scanner without attending to any task in the intervening period, we suggest that this reduction in thalamic CBF may reflect decreased attentional processing between the early and late scans. This is supported by a lack of significant differences between corresponding CBF responses to the functional task, where attention/arousal is better matched.

These data support the conclusion that the mean variation intrinsic to the technique is lower than what is associated with general physiology for within and between session comparisons. Therefore we conclude that the technique is reliable for use in longitudinal studies over similar time-frames; with the caveat that it is optimally suited for within session or more short-term crossover studies.

### 4.5.2 Reliability and sensitivity to functional changes in physiology

We find that the multi-TI pCASL approach is highly sensitive (power consistently >0.9 in an *a priori* defined anatomical mask) to functional CBF change in a salient visuomotor task (Fig 4.7). Importantly, in paired t-tests and ANOVAs on extracted CBF change and voxel-wise cluster corrected activation maps, there is no significant run-wise or session-wise difference between functional CBF responses to the task. This suggests that the sensitivity of the technique is reliable and that it can be used to test long (>1 minute) activation states in the context of multiple study visits. This has direct relevance for tonic pain studies with long stimulus durations.

### 4.5.3 Benefit of multi-TI approach to increase reliability

A recent study by Wu and colleagues (2013) highlights the importance of multiple PLD acquisitions to help account for AAT heterogeneity between subjects and brain regions. Although the acquisition length of the paradigm used in the current study is comparable to similar ASL investigations employing single TI pCASL sequences, the analysis of the multi TI data yields time courses constituent of only 8 epochs of absolute perfusion data (i.e. the multi TI approach necessitates far less averaging of ASL data over time). Considering this in the context of the subject- and region-wise AAT variability data discussed above, the multi TI approach improves the reliability and specificity of pCASL

to estimate absolute perfusion by accounting for bolus arrival time variability across the whole brain volume.

Interestingly, we also show that both CBF and AAT reliability decrease as repeat interval time increases. As was proposed previously (Hermes et al., 2007), this likely reflects physiological variability over long time periods rather than increases in measurement error. ICC values also show more variability than wsCV in this respect. It should be noted that while wsCV normalises to the mean and so is unbiased, ICC depends on the ratio of within- to between-subject variance; a feature that can vary significantly between sessions. Nonetheless, we report ICC values that are comparable or improved when considered in the context of previously published pCASL reproducibility studies (Jain et al., 2012; Wu et al., 2013).

### 4.5.4 Optimising inversion time selection

We perform an exploratory analysis of voxel-wise inversion time optimisation at each chosen PLD. A region is said to have an SNR-optimal inversion time selection if its AAT corresponds closely with the delay time from labelling to imaging ($\gamma$=$\sim$0) (Fig 4.8, 4.9). It should be noted that the optimisation values we report are specific to our sequence and protocol as they depend on variable scanner parameters (e.g. slice timing). We show that there is regional heterogeneity in optimisation across the brain (particularly in the superior-inferior domain) for different PLDs. However, most regions of the brain reach peak ASL signal within a 1-second PLD- this corroborates similar findings in healthy subjects using an adaptive sequential design (ASD) strategy that modifies the OSS regionally in real time (Xie et al., 2010).

These findings suggest that inversion time selection for single TI studies should be op-

timised depending on the region of interest. In the case of a whole-brain acquisition, a multi-TI approach may be better suited to accounting for regional heterogeneity. In the context of a functional experiment in a healthy cohort, arrival time is likely to decrease during regional activation, making a single TI approach suboptimal. In such studies, it may also be appropriate to narrow and centre the OSS range around 1 second, allowing better sampling of the kinetic curve or reduction of the number of PLDs and improved temporal resolution.

### 4.5.5 Limitations of the study

As with any such exploratory investigation, there a number of limitations we must address. Firstly, we tested a small cohort who we scanned multiple times using the same MRI scanner. While several studies have shown the reliability of other ASL techniques in multi-site studies (Gevers et al., 2011; Petersen et al., 2010), it will be important to validate this for functional tasks, in larger cohorts, and using a similar multi-TI pCASL approach. We also used healthy volunteers from a similar age group. It has been noted that various physiological parameters measured by ASL are influenced by age and other factors (Parkes et al., 2004). As such, it is important to optimise model assumptions for the relevant study group- e.g. by modifying labelling efficiency assumptions and inversion time selection in patient groups with cerebrovascular conditions or medication affecting blood flow (and hence blood arrival time).

Currently, modelling subject-specific physiological variation into the calculation of absolute CBF remains difficult given the multi-TI Bayesian inference approach used. However, tools able to account for intra-subject variability in CO2, blood pressure and cardiac cycle may account for variation in inversion efficiency (i.e. tagging of arterial blood) (Aslan et al., 2010) to improve pCASL reliability further.

### 4.5.6 Conclusion

The data presented here show that this technique is not only robust and reliable but is also a novel alternative to more commonly applied ASL approaches because of the added experimental flexibility the multi-TI approach offers. We are confident this approach will provide a powerful tool for low frequency functional activation studies, clinical diagnostic approaches and novel drug development paradigms- particularly when repeated within a week's time frame.

In the context of assessment of tonic pain responses, we propose the potential use of fewer inversion times to improve temporal resolution (and total number of averages) and in a narrower range ($\leq$1s) for optimal sampling of the kinetic curve in the relevant ranges for most brain areas.

Our preliminary sample size calculations suggest that we will need more than 10 subjects to reliably detect effects in pain relevant regions using the pCASL paradigm. Given the inadequacy of our effect size estimations (few studies have tested experimental pain responses with ASL), we decide to test up to 18 subjects.

# Chapter 5

# Investigating the Neural Correlates of Persistent Pain Using Arterial Spin Labelling and a Topical Capsaicin Model

In the previous chapter, we established the feasibility of imaging tonic activation states using arterial spin labelling (ASL). Here we test the use of the topical capsaicin model with ASL for imaging the development and maintenance of persistent pain. We aim to identify a set of brain regions, which respond to a tonic painful stimulus.

## 5.1 Introduction

Spontaneous pain is the most prevalent and irksome complaint in neuropathic pain (Backonja and Stacey, 2004). Despite this, most pre-clinical models of pain assess hypersensibility and responses to evoked stimuli. This is largely because of the challenge of adequate behavioural endpoints for spontaneous pain, which can be difficult to distinguish from fear and anxiety in animals (King et al., 2009; Mogil et al., 2010). Likewise, few human experimental models of neuropathic pain suitably evaluate spontaneous pain (Klein et al., 2005), while pain neuroimaging studies have largely used BOLD imaging,

which is better suited to high frequency tasks such as phasic stimuli. With the recent advent of reliable, non-invasive and quantitative tools for imaging stable states, their relevance for imaging pain states has began to be investigated (Maleki et al., 2013).

### 5.1.1 Imaging CBF changes in ongoing pain

While the exact dynamic relationship between neural function and CBF is not yet well known, considerable evidence suggests that imaging CBF alone offers a strong correlate of brain function (Attwell et al., 2010; Buxton and Frank, 1997). Over the past 2 decades, a number of studies have investigated the relationship between cerebral blood flow and neural pain pathways (Apkarian et al., 2005; Peyron et al., 2000). This has largely been through the use of $H_2{}^{15}O$ positron emission tomography (PET), but with recent advances in MRI techniques, ASL has emerged as a sensitive non-invasive option (Maleki et al., 2013; Owen et al., 2008).

Due to the difficulty of employing safe and maintained ongoing pain states in healthy subjects, few studies have investigated the neural correlates of persistent pain. Studies of cerebral blood flow changes with neuropathic pain have suggested both CBF increases and decreases in a number of brain areas. A consistent early finding in the imaging of spontaneous peripheral neuropathic pain was a decrease in cerebral perfusion in the thalamus, which was often lateralised and was reversed by treatment (Hsieh et al., 1995; Iadarola et al., 1995; Kishima et al., 2010). Similar effects have also been reported in central pain syndromes (Garcia-Larrea et al., 1999) and cancer pain (Di Piero et al., 1991). Although early commentators suggested that deafferentation of thalamic inputs were largely responsible for depressed thalamic metabolism, later findings have suggested that thalamic hypoperfusion when associated with pain, may be more related to neurophysiological mechanisms directly relevant to neuropathic pain (Garcia-Larrea et al.,

2006). Other suggested implications of thalamic hypoperfusion include desensitisation of peripheral neurons, increased efficiency of thalamo-cortical relay, or uncoupling of blood flow from metabolism in the persistent pain state (Iadarola et al., 1995). More recent studies using ASL have reported CBF increases in a number of regions typically activated to phasic stimuli (Howard et al., 2012; Wasan et al., 2011). In a recent study comparing a cohort of post-herpetic neuralgia patients to matched controls, Liu and colleagues (2013) report CBF increases in the insula and somatosensory cortex, which correlated with pain reports. One problem with this approach is that control subjects are not matched for pain sensation and other cognitive factors associated with having persistent pain, and as such it is difficult to make causal statements regarding the neural basis of the pain itself. Within-subject paradigms, which better account for this issue are more difficult to design in patient groups, as they require the patients to be assessed prior to injury or in a state of relief, which itself is difficult to achieve. Using such a design in a dental extraction model, Howard and colleagues (2011) report CBF increases in a wide range of pain related areas- including bilateral primary and secondary somatosensory cortices, insula, cingulate, thalamus, amygdala, hippocampus and brainstem. In this study, subjects were imaged in separate sessions prior to surgery and then postsurgically after they had developed ongoing pain of 30/100 on a VAS scale - unfortunately pain perception was not recorded during or after the scan so there was no evidence of a stable pain state during data acquisition.

Studies of tonic experimental pain also show a mixed picture with global CBF decreases (Coghill et al., 1998), regional increases (Owen et al., 2012, 2010) and regional decreases (Owen et al., 2010; Thunberg et al., 2005) in pain related areas all being reported. Interestingly, a distinction between early and late pain phases has been described in longer hypertonic saline (HS) models. For example, in a PET study investigating lower back HS infusion, Thunberg and colleagues (2005) report a CBF increase in the left insula 4 min-

utes after infusion, and bilateral insula CBF decreases 20 minutes after infusion- however this study was confounded by pain habituation in the study group. In a more recent ASL study investigating CBF time-courses, (Owen et al., 2010) demonstrate attenuation of initial CBF increases in the bilateral insula, thalamus and anterior mid-cingulate cortex over a 15-minute infusion period, despite relatively constant pain intensity ratings. In a follow-up study where a slow infusion (no initial bolus) of HS is used, the authors detect only CBF increases (in the bilateral insula and frontal gyri) (Owen et al., 2012). However, psychophysical results in this study suggest that subject pain reports had not plateaued before imaging took place and CBF responses were averaged over the entire infusion period. While CBF increases are readily attributed to increased regional cerebral metabolism, CBF decreases have been more difficult to explain and in some cases have been ascribed to changes in attention and sympathetic activation during pain (Coghill et al., 1998; Thunberg et al., 2005).

These findings suggest that CBF responses to tonic pain are highly paradigm specific. Some of the variability seen in these studies may be due to the types of stimuli used. Experimental models of tonic pain used in neuroimaging have typically been for muscular pain. To our knowledge, the single PET study investigating tonic pain in a human model of central sensitisation (subcutaneous capsaicin application) reported global CBF decreases in the pain state (Coghill et al., 1998). These studies also address tonic pain using stimuli that typically last no more than 20 minutes. This may be of particular relevance given that brain networks involved in the multifactorial pain experience may have varying contributions between acute and ongoing pain conditions (Baliki et al., 2006; Mouraux et al., 2011). Furthermore only one of the studies described has used a pCASL sequence while none have employed multi-inversion time acquisitions to quantify CBF. By using these new tools in a controlled pain paradigm, we aim to improve detection of CBF changes specific to the persistent pain state.

### 5.1.2 Capsaicin and spontaneous pain behaviour

Various pain modalities have been used to investigate tonic pain including heat (Lautenbacher et al., 1995), cold (Ruscheweyh et al., 2010), electrical (Geber et al., 2007) and mechanical stimuli (Andrew and Greenspan, 1999b). To elicit ongoing, spontaneous pain, chemical modalities such as capsaicin and mustard oil, hypertonic saline, and ischaemic models have been used most often (Owen et al., 2012; Sawynok et al., 2006). Many of these models are not ideal for investigating persistent pain because it is difficult to create a steady-state experience- there is significant habituation to the stimulus shortly after application (Greffrath et al., 2007; Rennefeld et al., 2010) or there are noteworthy risks associated with prolonged exposure.

The capsaicin model is attractive because its peripheral and central mechanisms of action have been well investigated in animals and humans (O'Neill et al., 2012). Capsaicin causes a persistent discharge of slow-conducting C-fibres (Koltzenburg et al., 1994), which can recover quickly allowing assessment of an ongoing pain experience without leading to irreversible tissue damage.

In Chapter 2, we show in a 1% topical capsaicin model that spontaneous pain scores, an hour after application, are stable within a 1hr session and are reproducible across-session (Fig 2.11). This model also provides a low stimulus frequency paradigm (sustained painful stimulus), which is more reflective of the clinical pain state and to which arterial spin labelling is well suited. An additional benefit is that the site of primary hyperalgesia or peripheral sensitisation reflects thermal allodynia and so pain perception can be modified by application of innocuous thermal stimuli (Drummond, 2001).

### 5.1.3 In search of a 'nociceptive cortex'

Although a number of brain regions have been associated with the tonic pain experience, as reviewed above, there remains no consensus regarding their specificity to nociception and the pain experience. The identification of a neural biomarker for nociception is of vital importance for validation of pain processing mechanisms and also potentially for use in drug discovery. Also, ongoing and tonic pain is the major symptom that chronic pain patients suffer and yet we know very little of its neural underpinnings. Although the processing of pain is a complex and integrated process involving several brain regions that perform many other functions, accumulating evidence over the years suggests that the dorsal posterior insula and adjacent opercula region may have a unique and specific role in the processing of nociceptive inputs (Craig, 2013; Garcia-Larrea, 2012).

## 5.2 Aim

We test neural responses to acute and persistent spontaneous pain using the topical capsaicin model and perfusion imaging with arterial spin labelling. At present, no studies have directly assessed experimentally induced responses to pain lasting beyond 20 minutes with perfusion imaging. While previous studies of tonic pain have largely used deep muscle pain models, we will test spontaneous cutaneous burning pain in the context of chemical injury and peripheral C-fibre sensitisation.

We aim to identify a neural network recruited and modulated by the experience of persistent pain. We hypothesise that these regions will overlap with brain regions previously shown to be relevant in preclinical studies and in evoked pain neuroimaging studies (Apkarian et al., 2005).

## 5.3 Methods

### 5.3.1 Subjects

Seventeen healthy subjects (11 female, 6 male, age [mean ± s.e.m.] = 24.1 ± 1.8) were recruited to participate in this study after screening to exclude any history of neurological conditions, regular use of medication, allergies to chilli and MRI contraindications. Subjects were asked to avoid caffeine for 6 hours prior to each session.

### 5.3.2 Study design

Subjects were scanned in two phases (separated by 30 mins) during the same visit.

In phase I, subjects were scanned with BOLD and ASL sequences at baseline before 1% capsaicin cream was applied to a 1x3in region on the antero-medial aspect of the lower right leg. The capsaicin cream was held in place with sterile dressing and layered with cloth to preserve heat. Immediately after capsaicin application, subjects were scanned for 24 minutes using a pCASL protocol. Online pain ratings with a visual analogue scale (VAS) (Anchors: No pain, Severe pain) were taken at 2.5 minute intervals during each of the pCASL scans- 3 times during the baseline (BL) block and 9 times during the longer (RAMP) phase. Subjects who had not reached a pain rating of 5/10 after the RAMP phase were scanned for an additional 7 minutes with the pCASL sequence. A 5-minute BOLD scan followed the pCASL scanning.

Following this, subjects were taken out of the MRI scanner and were monitored in a nearby temperature-controlled room for 30 minutes. During this phase, verbal pain ratings (using an 11-point numerical rating scale) were taken every 5 minutes. Subjects kept the leg with capsaicin elevated to simulate the conditions in the scanner.

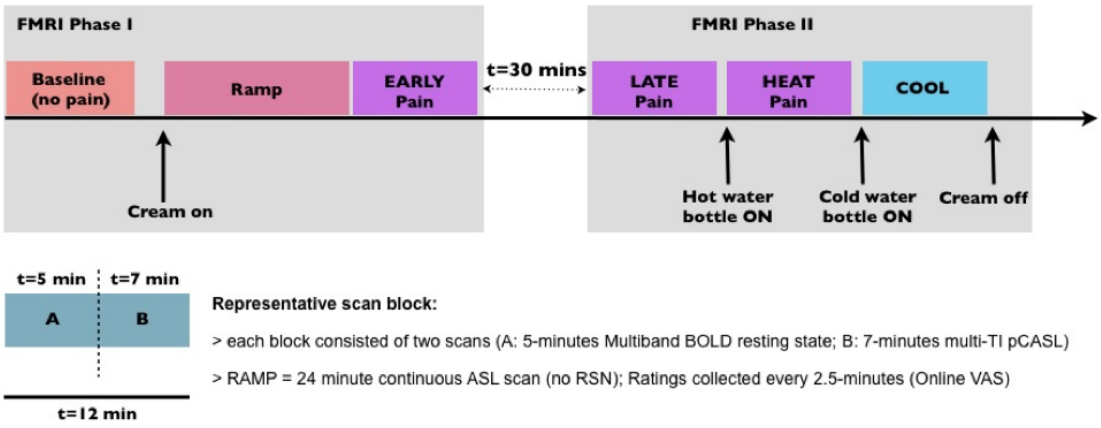


Figure 5.1: **Experimental paradigm.** Subjects were imaged in 5 scan blocks (Baseline [BL], Early Pain [EP], Late Pain [LP], Heat [HE] and Cool [CO]) and a RAMP period. Pain ratings were taken every 2.4 minutes.

Functional scanning in a second phase began approximately 30 minutes later. Here, subjects were scanned with both pCASL and BOLD sequences in a late pain block (LP), after application of a rubber hot water bottle to the capsaicin site (HE), and after application of a rubber icy cold water bottle to the capsaicin site (CO). The hot water was applied at a temperature of 38°C (as tested with an infrared thermometer), while the cold water temperature varied between 7-10°C. The water bottles were placed directly on top of the application region (in the case of the cold water bottle, it was separated from the skin by a thin layer of cloth to avoid injury). After this second phase, the capsaicin cream was removed.

In addition to online VAS pain ratings for each pCASL scan, subjects also verbally rated their pain (using an 11-point numerical rating scale) before and after each BOLD scan. For all scans, when not rating their pain, subjects were asked to fixate on a cross, which was displayed on a projector.

The external temperature of the right leg around the region of capsaicin application (2

cm medial to the application site) was monitored with an infrared thermometer at 5 time points: before capsaicin application, before the break, before application of the hot water bottle, before application of the cold water bottle and at the end of the second scan phase.

### 5.3.3 MR data acquisition

Scanning took place in a Siemens 3T Verio whole-body MR scanner (Erlangen, Germany), with a 32-channel head coil and body coil.

pCASL image acquisition procedure and parameters were identical to that described in Chapter 4 (TR- 4s, TE- 13ms, FOV 220x220 $mm^2$, matrix 64x64, 24 slices, slice thickness- 4.95mm, labelling plane- 10mm, TIs- 0.25, 0.5, 0.75, 1, 1.25, 1.5s). For the RAMP phase, 344 volumes were acquired corresponding to 24 minutes of scanning. For all other phases, 114 volumes were acquired corresponding to 7 minutes of scanning.

BOLD images were acquired using Multiband Echo-Planar Imaging (MB-EPI) (Feinberg et al., 2010; Moeller et al., 2010) with an acceleration factor of x6, enabling fast multi-slice acquisition and improving image temporal resolution. 230 volumes were acquired (TR 1.3s, TE 40ms, FOV 212x212 $mm^2$, matrix 106x106, 72 contiguous 2-mm axial slices) in each phase, corresponding to 5 minutes of scan time. A corresponding non-saturated reference scan was acquired for motion correction and registration purposes.

A T1-weighted structural image was acquired for each subject to allow registration and activation overlay.

### 5.3.4 Data processing

For the purposes of this thesis, we will only discuss the pCASL data analysis as was relevant to defining a network of active structures in the persistent pain state. pCASL images were pre-processed and quantified as described in Chapter 4. All CBF map outputs from quantification were registered to MNI space (see Chapter 4) and concatenated to generate a CBF time-course for the entire experimental period. For paired comparisons between scan blocks, averaged CBF maps were also generated for all scan blocks for each subject using a mixed effects model.

### 5.3.5 Statistical analyses

Statistical analyses were performed using IBM SPSS Statistics, version 18 (IBM, Armonk, NY, USA). A one-way ANOVA was used to assess the effect of time on pain ratings during the RAMP period. Corresponding pairwise t-tests were performed comparing ratings at each time point with zero (first time point). One-way analyses of variance were performed to assess the effect of scan block on averaged ratings and averaged grey matter CBF- pairwise t-tests were performed between all the scan blocks. In all cases, post-hoc correction for multiple comparisons was applied using *Bonferroni* correction.

To compare CBF changes between scan blocks before temperature modulation, a paired t-test was first performed between the baseline and early pain blocks using a mixed effects linear model. To investigate the overall effect of scan block on CBF over the entire experimental period, a one-way ANOVA was performed using FEAT- an F-test was then performed to compare all pain scans (EP, LP and HE) with baseline. Statistical significance was determined by performing cluster correction at a Z threshold of 2.3 and significance of $p<0.05$.

Representative average regional CBF changes over the experimental time-course were plotted against average pain ratings. For this CBF values were binned into 2.4-minute intervals to match the frequency of pain ratings. Regions of interest (ROIs) were defined as a conjunction between clusters of statistically significant CBF changes (from BL/EP and F contrasts described above), and anatomically defined regions from the Harvard-Oxford Cortical and Subcortical Atlases (binarised at $p>0.5$). In order to explore the relationship between regional CBF and pain ratings, a parametric correlation was performed between average pain ratings and ROI CBF time-courses. To assess the influence of pain ratings on voxel-wise CBF changes over the experimental time-course, a linear regression was performed between each subject's CBF time-course and corresponding pain ratings over the entire experiment. The corresponding subject-specific statistical maps were averaged using a mixed effects model. To identify regions highly correlated to pain perception, we used a cluster correction method at a Z threshold of 2.7 and significance of $p<0.05$.

## 5.4 Results

### 5.4.1 Pain scores

Pain ratings during the RAMP for each subject are shown in Figure 5.2. The increase in pain ratings after capsaicin is highly variable in phase and amplitude between subjects. The one-way ANOVA showed a main effect of time on pain ratings during the RAMP ($F[6]=4.201$, $p=0.046$). Pain ratings first become significantly different from zero (baseline) 10 minutes after capsaicin application (paired t-test, $p=0.019$).

Mean ongoing pain ratings over the entire experimental period are shown in Figure 5.3. Pain ratings during the EP block are not significantly different, indicating that subjects

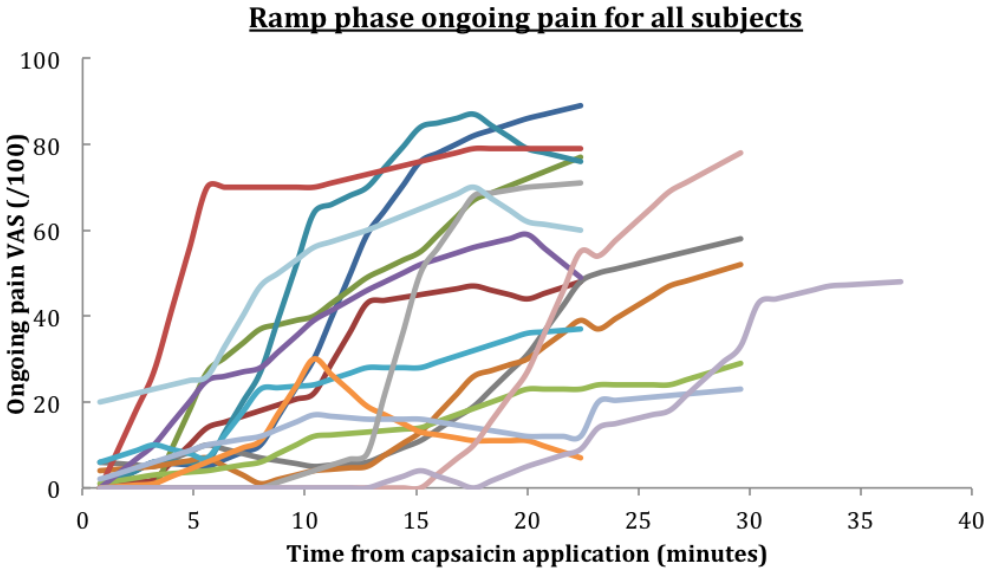


Figure 5.2: **Ramp and early phase ongoing pain for all subjects (represented by different colours).** Subjects ramp was variable in phase and amplitude. Subjects who had not reached a stable pain state or 5/10 in pain ratings were scanned for an additional session. One subject was scanned for two additional sessions for the same reasons. The final scan block (7.4 minutes) was taken as the early pain scan (EP) for each subject. One subject missing due to scanner data retrieval error.

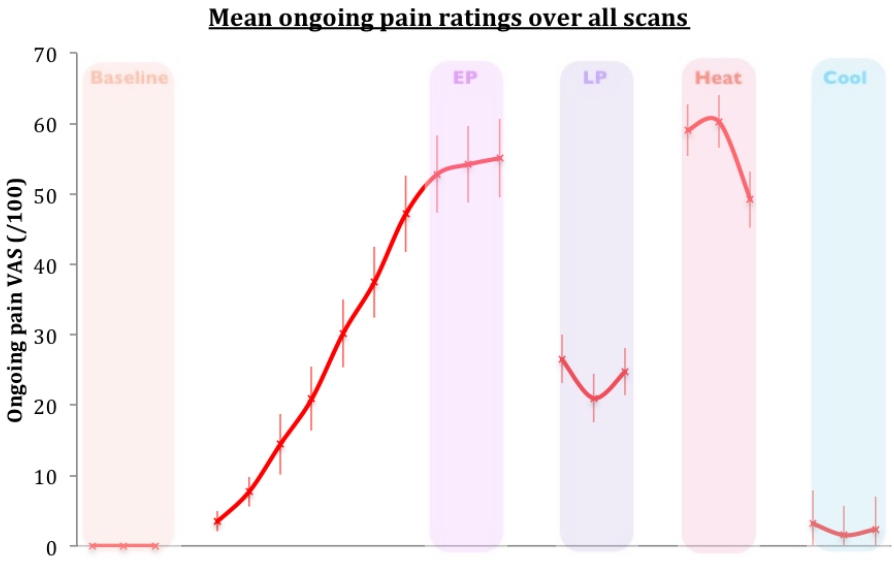


Figure 5.3: **Mean ongoing pain ratings over all scans.** Error bars represent SEM. EP Early pain; LP Late pain. EP is defined as final 7.4 minutes from Figure 5.2 for all subjects. Mean pain ratings from the preceding 15 minutes are also averaged and shown in this figure as the ramp period before EP.

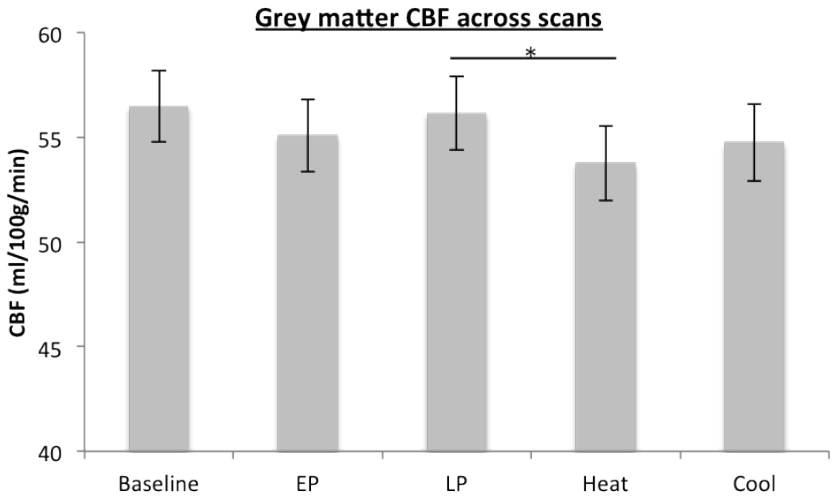


Figure 5.4: **Grey matter CBF across scans.** Main effect of scan (F[12]=4.892, p=0.014). EP., Early pain; LP., Late pain. * p<0.05

had reached a stable pain state. Results from a one-way ANOVA showed a main effect of session on ratings (F[12]=108.69, p<0.001). Pairwise comparisons are shown in Table 5.1. There is no significant difference between BL and CO pain ratings, or between EP and HE pain ratings. All other pairs are significantly different (see Fig 5.3).

### 5.4.2 Perfusion changes

A one-way ANOVA showed a significant effect of scan block on mean grey matter CBF (F[12]=4.892,p=0.014). Pairwise comparisons show a significant decrease in mean grey matter CBF in the HE block when compared to the LP block (p=0.031). There were no differences for all other comparisons (Fig 5.4).

Table 5.1: **Pairwise comparisons of pain ratings between scan blocks.** Student paired t-test. Post-hoc correction was performed using the Bonferroni method. Blocks: BL, baseline; EP, early pain; LP, late pain; HE, heat; CO, cool. * p<0.05.

| Session (I) | Session (J) | Mean Difference (I-J) | p-value |
|---|---|---|---|
| BL | EP | -49.844* | <0.001 |
| | LP | -20.802* | <0.001 |
| | HE | -56.146 | <0.001 |
| | CO | -2.438 | 0.762 |
| EP | BL | 49.844* | <0.001 |
| | LP | 29.042* | 0.008 |
| | HE | -6 | 1 |
| | CO | 47.406* | <0.001 |
| LP | BL | 20.802* | <0.001 |
| | EP | -29.042* | 0.008 |
| | HE | -35.344* | <0.001 |
| | CO | 18.365* | 0.002 |
| HE | BL | 56.146* | <0.001 |
| | EP | 6 | 1 |
| | LP | 35.344* | <0.001 |
| | CO | 53.708* | <0.001 |
| CO | BL | 2.438 | 0.762 |
| | EP | -47.406* | <0.001 |
| | LP | -18.365* | 0.002 |
| | HE | -53.708* | <0.001 |

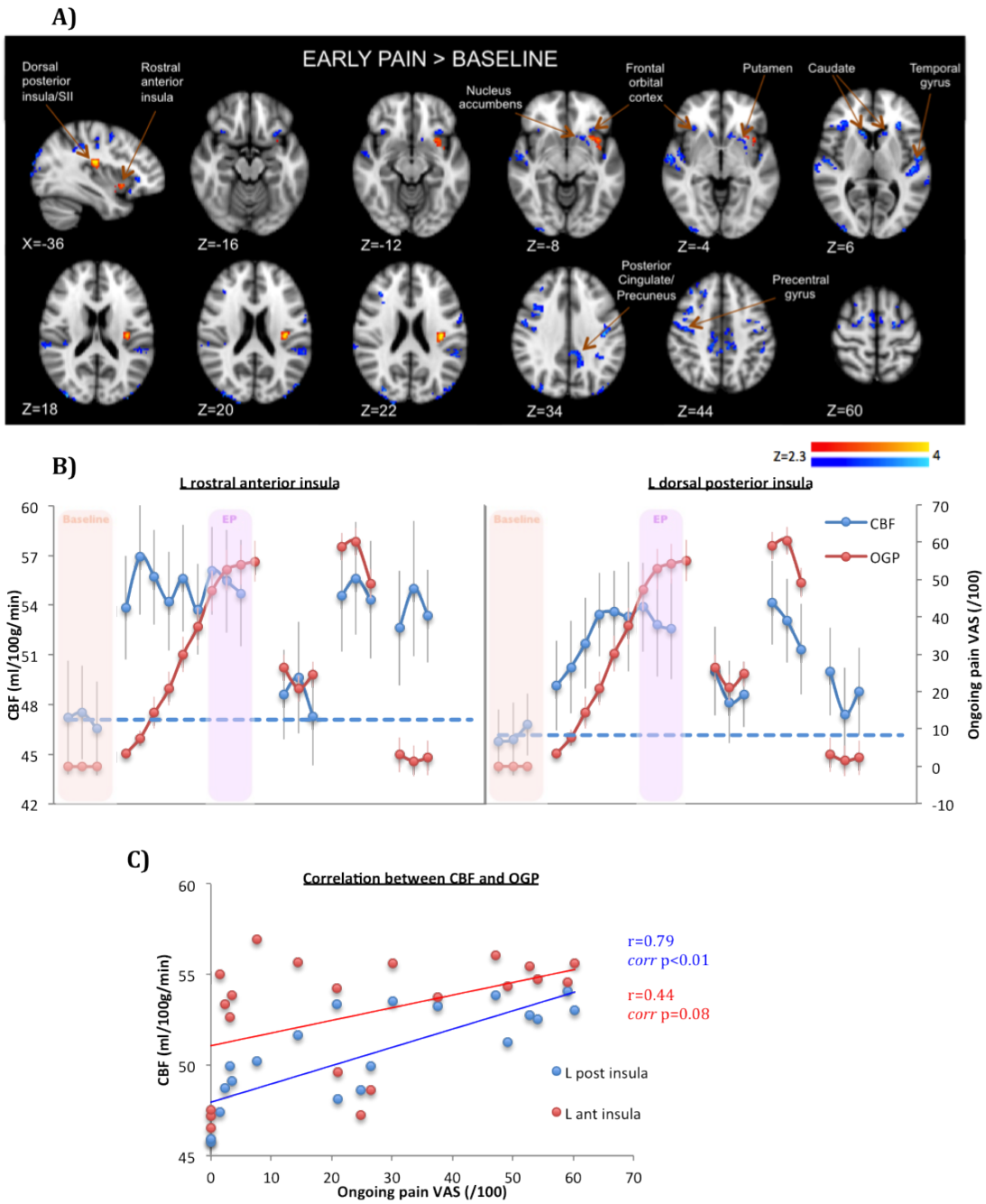


Figure 5.5: **CBF change induced by early persistent pain.** Mixed effects: Z=2.3, p<0.05 (A) Two clusters of increased activity are shown in the dorsal posterior insula and anterior insula cortex. Several clusters of decreased activity are shown across the brain (detailed in Table 5.2). Images are in radiological convention (B) CBF time-courses in a conjunction mask between suprathreshold clusters of increased activity in (A) and grey matter masks defined from the MNI Structural Atlas. The dotted blue line represents average baseline CBF in selected region. Ongoing pain (OGP) over the same time period is plotted on the secondary y-axis. (C) CBF values in the posterior insula correlate with pain perception over the entire experimental time-course

Table 5.2: **Clusters of increased and decreased CBF in the EP/BL contrast (see figure 5.5A).** Mixed effects cluster corrected Z=2.3 p<0.05. Anatomical labels were taken from the Harvard-Oxford Cortical and Subcortical Atlases within the FSLview tool. COG., centre of gravity; L., left; R., right; ant., anterior; post., posterior; trans., transverse; sup., superior; inf., inferior; mid., middle; cent., central; temp., temporal; SMA., supplementary motor area.

| | Volume ($mm^3$) | Anatomical Label | COG MNI coordinates | | | Peak z-score |
|---|---|---|---|---|---|---|
| | | | **X** | **Y** | **Z** | |
| ***CBF increases (EP>BL)*** | | | | | | |
| Cluster 1 | 728 | L. insula cortex | -34 | 11 | -9 | 4.36 |
| Cluster 2 | 936 | L. insula cortex | -35 | -20 | 20 | 3.34 |
| ***CBF decreases (EP<BL)*** | | | | | | |
| Cluster 1 | 968 | L. post. cingulate | -11 | -25 | 42 | 3.39 |
| Cluster 2 | 1024 | L. putamen | -19 | 14 | -2 | 3.18 |
| Cluster 3 | 1024 | R. caudate | 13 | 18 | 5 | 3.63 |
| Cluster 4 | 1032 | R. trans. temp. gyrus | 50 | -20 | 10 | 3.56 |
| Cluster 5 | 1056 | R. post. cingulate | 11 | -26 | 43 | 3.37 |
| Cluster 6 | 1096 | L. supramarg. gyrus | -40 | -39 | 39 | 3.35 |
| Cluster 7 | 1128 | L. inf. frontal gyrus | -32 | 26 | -3 | 3.61 |
| Cluster 8 | 1472 | R. SMA | 1 | 0 | 59 | 3.31 |
| Cluster 9 | 1504 | R. frontal orbital cortex | 36 | 29 | 1 | 3.67 |
| Cluster 10 | 1528 | L. lat. occipital cortex | -37 | -87 | 24 | 3.39 |
| Cluster 11 | 1552 | R. sup. frontal gyrus | 29 | 27 | 46 | 3.44 |
| Cluster 12 | 1936 | L. precentral gyrus | -46 | -11 | 36 | 3.77 |
| Cluster 13 | 2000 | L. sup. frontal gyrus | –29 | -1 | 52 | 4.19 |
| Cluster 14 | 2048 | L. post. cingulate | -5 | -43 | 32 | 3.25 |
| Cluster 15 | 2872 | R. lat. occipital cortex | 35 | -88 | 18 | 4.04 |
| Cluster 16 | 3096 | L. cent. opercular cortex | -51 | -27 | 10 | 3.56 |
| Cluster 17 | 3144 | R. sup. temp. gyrus | 59 | -16 | 2 | 3.73 |
| Cluster 18 | 6136 | R. mid. frontal gyrus | 40 | 0 | 43 | 4.21 |

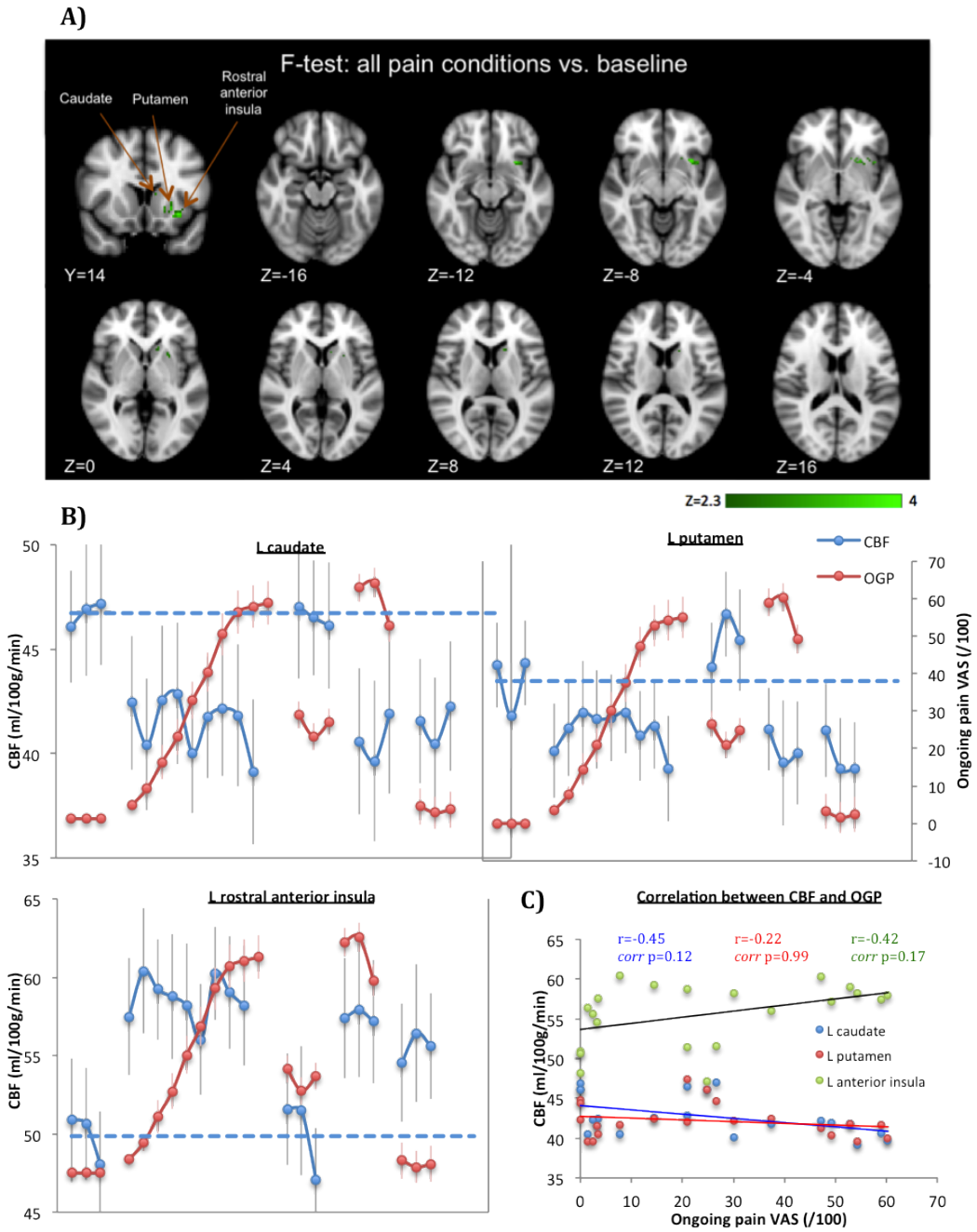


Figure 5.6: **Main effect of pain on CBF over experimental time-course (F-test).** Mixed effects: Z=2.3, p<0.05 (A) single cluster shown which includes the caudate nucleus, putamen and anterior insula cortex. Images are in radiological convention (B) CBF time-courses in a conjunction mask between suprathreshold activity in (A) and anatomical masks defined from the Harvard-Oxford Atlases. The dotted blue line represents average baseline CBF in selected region. Ongoing pain (OGP) over the same time period is plotted on the secondary y-axis.

Table 5.3: **Cluster of regions showing a significant CBF change to pain (see figure 5.6A**: F-test between pain and baseline in 1-way ANOVA. Mixed effects cluster corrected Z=2.3 p<0.05 (see figure 5.6A). Anatomical labels were taken from the Harvard-Oxford Cortical and Subcortical Atlases within the FSLview tool. COG., centre of gravity; L., left; R., right.

| | Volume ($mm^3$) | Anatomical Label | Peak z-score | | MNI coordinates | | |
|---|---|---|---|---|---|---|---|
| | | | | | **X** | **Y** | **Z** |
| Cluster 1 | 720 | | | *COG* : | -27 | 13 | -5 |
| | | L. insula cortex | 3.88 | | -30 | 14 | -8 |
| | | L. insula cortex | 3.80 | | -28 | 12 | -12 |
| | | L. insula cortex | 3.53 | | -40 | 12 | -6 |
| | | L. putamen | 3.33 | | -24 | 14 | -4 |
| | | L. caudate | 2.86 | | -14 | 18 | -8 |
| | | L. caudate | 2.85 | | -14 | 16 | 4 |

Activation maps showing regions of significantly increased or decreased CBF between BL and EP blocks are in Figure 5.5A. Statistical maps were overlaid on selected slices of the MNI brain. Orange pixels represent suprathreshold CBF increases while blue pixels represent CBF decreases. Clusters of suprathreshold CBF change are detailed in Table 5.2- cluster volumes, centre of mass MNI coordinates, peak Z-scores and anatomical labels (taken from the Harvard-Oxford Cortical and Subcortical Atlases in the FSLview toolbox) are specified. Pain related CBF increases were noted in two distinct clusters. The stronger cluster was in the contralateral (left) dorsal posterior insula (dpIN) and adjacent medial opercula region (mean CBF change ± s.e.m; 15 ±4.1% or 6.9 ±1.9 ml/100g/min). The second larger cluster was in the contralateral rostral anterior insula (raIN) (mean CBF change ± s.e.m; 19.7 ± 4% or 8.5 ±1.7 ml/100g/min). Both clusters are well localised within the described anatomical structures. Pain related CBF decreases were noted bilaterally in a large number of clusters including the caudate nuclei, putamen, nucleus accumbens, posterior cingulate cortex, superior temporal gyri and frontal gyri (Fig 5.5A, Table 5.2). There were no significant differences between BL and LP blocks (not shown).

To investigate modulation in the functional regions with increased activation during EP, mean absolute CBF was plotted over the experimental time-course together with the pain ratings (Fig 5.5B). On visual inspection, CBF in the dpIN appeared to track pain perception over the experimental time-course, while the raIN CBF change appeared to be binary. To test this, we performed a correlation analysis between CBF and pain ratings in both functional regions (Fig 5.5C). We report that in the dpIN, there is a significant correlation between CBF and pain ratings (corrected $p<0.001$). In the raIN, the correlation did not survive post-hoc correction (corrected $p=0.084$).

Results from an F-test comparing all pain conditions with baseline showed a single suprathreshold cluster encompassing the anterior cingulate cortex, putamen and caudate nucleus (Fig 5.6A, Table 5.3). CBF time-courses were plotted for the conjunction between this cluster and the respective anatomical masks (Fig 5.6B). Both putamen and caudate showed CBF decreases in high pain blocks. CBF in the putamen appears to overshoot the baseline when pain perception decreases in the LP block. The anterior insula showed an increase in CBF in high pain blocks. Activity in these regions was not correlated with pain ratings over the entire time-course (Fig 5.6C).

In a linear regression analysis, we determined regions of the brain that were correlated and anti-correlated with pain perception (Fig 5.7). A single suprathreshold cluster of activity was positively correlated with within-subject pain ratings in the dorsal posterior insula and adjacent opercula region. A separate cluster in the right dorsolateral prefrontal cortex was negatively correlated with pain perception.

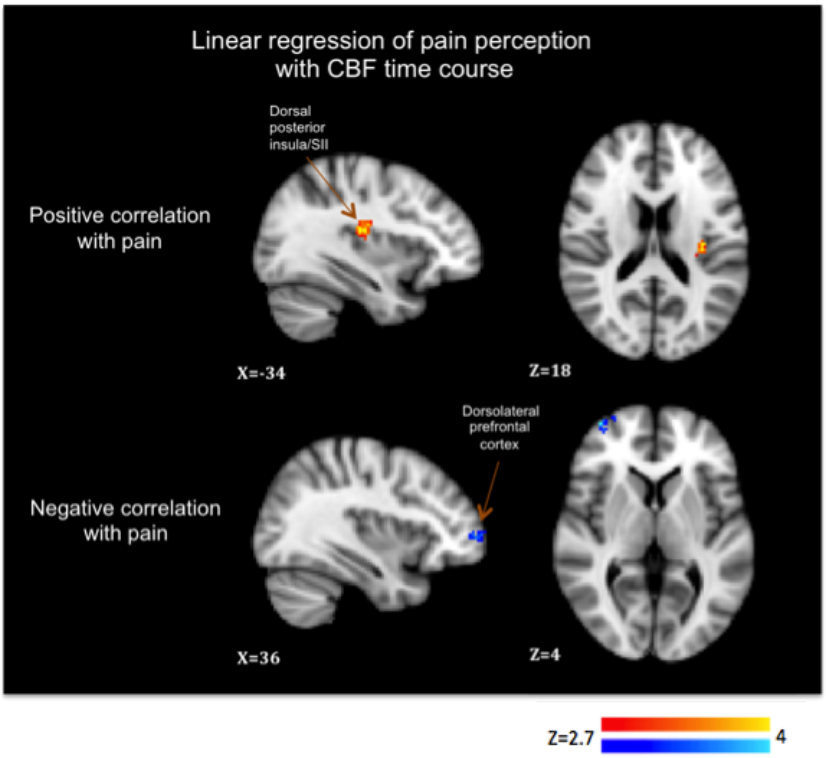


Figure 5.7: **Correlation between CBF and within-subject pain perception.** A cluster in the contralateral (left) dorsal posterior insula is positively correlated with pain perception while a cluster in the ipsilateral (right) dorsolateral prefrontal cortex is negatively correlated with pain perception. Mixed effects: Z=2.7, p<0.05 Images are in radiological convention.

## 5.5 Discussion

Using a topical capsaicin model of spontaneous pain and hyperalgesia, we examined the neural correlates of the persistent pain state. We used ASL to estimate absolute changes in CBF in response to persistent pain lasting for up to two hours. The heat-sensitivity of the capsaicin model allowed us to modulate pain perception using hot and cold water bottles. We report a distinct network of brain structures with increased or decreased activity in response to persistent pain. Importantly, we demonstrate that the contralateral dorsal posterior insula (and adjacent medial operculum) is the only brain region that is positively correlated with pain perception over the entire experimental period.

### 5.5.1 Behavioural changes

We report pain responses during the ramp phase of the experiment to be highly variable between subjects. This likely reflects inter-individual differences in cutaneous innervation (Gøransson et al., 2004) and the difficulty in matching dosing of the topical capsaicin cream between subjects- the outer layer of the epidermis acts as a significant diffusion barrier, making it difficult to estimate the amount of capsaicin that reaches the sensory receptors (Magnusson and Koskinen, 2000). Nonetheless, most subjects approached a plateau in pain perception within 23 minutes of 1% capsaicin application to the lower leg- this is in line with previous unpublished data from our lab. There is some evidence suggesting that capsaicin-induced spontaneous pain perception peaks within 10 minutes when applied to the face and rises continuously within a 30 minute period when applied to the ankle (Frot et al., 2004). However as the site, preparation, and dosing of capsaicin differ between this and our study, a direct comparison cannot be made. Given that the capsaicin spontaneous pain response is slow evolving and variable, we

perception matched the early pain scan block, using the 7 minutes during which each subject's pain perception was at its maximum (the preceding 15 minutes was defined as the RAMP phase). Using this approach, the mean pain perception across subjects was shown to be sinusoidal and to plateau at the EP block (Fig 5.3), suggesting that this was an appropriate time to image an early pain state.

We were successfully able to modulate pain perception during the study by using capsaicin cream, as well as hot and cold water bottles. Pain responses decreased significantly from the EP to the LP block. This was likely due to peripheral and centrally mediated habituation to the stimulus (Greffrath et al., 2007). Previous evidence indicates that heating the skin following capsaicin treatment can induce primary thermal hyperalgesia, while cooling decreases hyper-excitability of the C-fibres (Culp et al., 1989). In this way, we rekindled the heat pain back to the same magnitude as in the EP block using a hot water bottle, and finally we used the cold water bottle to switch the valence of the peripheral input to be non-painful (Fig 5.3; Table 5.1). These significant alterations allowed us to test for brain regions where perfusion was significantly modulated by pain perception.

### 5.5.2 Perfusion changes in the pain state

Previous studies using acute and persistent pain paradigms have reported large regions of CBF increase in the bilateral insula cortex (Apkarian et al., 2005; Maleki et al., 2013). Our findings indicate that in a slowly evolved capsaicin induced moderate pain state, there is significantly increased blood flow in localised regions of the contralateral rostral anterior insula (rAIN) and dorsal posterior insula (dPIN), which overlap with regions reported in previous studies (Table 5.2). We report two discrete and relatively small clusters, reflecting the more accurate localisation of parenchymal activity with the use

of arterial spin labelling as a quantitative measure of CBF (Pfeuffer et al., 2002; Tjandra et al., 2005). The functional relevance of these regions for pain perception has been debated over the past two decades. Current views suggest a role for the dorsal posterior insula in the encoding of sensory aspects of pain perception, while the anterior insula may have a less specific role in interoception and affective modulation (Craig, 2009; Garcia-Larrea, 2012; Raij et al., 2005). This functional segregation is supported by a wealth of evidence from primate tracer studies, human MRI tractography studies and functional connectivity analyses indicating that the posterior insula is functionally and structurally more connected to the primary somatosensory cortex while the anterior insula is more associated with the anterior cingulate cortex and prefrontal regions (Cerliani et al., 2012; Cloutman et al., 2012; Mesulam and Mufson, 1982; Mufson and Mesulam, 1982; Peltz et al., 2011). The role of the posterior insula in pain localisation and intensity encoding has been revealed by studies defining somatotopic pain representations in the region (Baumgärtner et al., 2010; Brooks et al., 2005), several reports of covariance between its activity and acute pain perception (Bornhövd et al., 2002; Coghill et al., 1999), and reports of increased pain tolerance following insula lesions (Greenspan et al., 1999). Moreover, independent of stimulus intensity, the posterior insula has been suggested to specifically reflect pain exclusive activations relevant to the qualitative change from innocuous to painful (Oertel et al., 2012). The anterior insula, on the other hand was shown in the same study to be activated by the stimulus irrespective of intensity or perception, suggesting a role in general sensory awareness. This is in line with current theories proposing the core function of the anterior insula to be detection of relevant stimuli and subsequent engagement of executive brain regions to ensure appropriate behaviour (Kurth et al., 2010; Menon and Uddin, 2010). In the pain imaging field, the anterior insula has been shown to have a role in pain anticipation, placebo responses, pain-related negative affect and short-term memory of pain perception (Albanese et al., 2007; Ploghaus et al., 1999; Ploner et al., 2011; Raij et al., 2005; Wager et al., 2004);

its function is thought to involve the integration of sensory and cognitive components to make perceptual decisions about pain (Brodersen et al., 2012; Wiech et al., 2010). In mice, lesioning of the anterior insula has also been suggested to indicate reduced pain affect as measured by facial expression correlates of spontaneous pain (Langford et al., 2010). Therefore our findings may indicate related but distinct aspects of the processing of persistent pain in the posterior and anterior insula. Of note, the rostral component of the anterior insula has been suggested to be functionally distinct from its caudal aspect, with the former more associated with the aversive representation of the clinical pain state (Schweinhardt et al., 2006). The use of more clinically relevant ongoing pain stimuli in this study may indicate a similar role for the rAIN in processing affective aspects of the persistent pain state.

We also report a more widespread and largely bilateral set of structures where there is a decrease in perfusion in the persistent pain state. This includes motor and basal ganglia structures, which have been implicated in sensory-motor integration (Borsook et al., 2010), and other structures previously reported to show decreases to a bolus hypertonic saline stimulus- including the posterior cingulate cortex, precuneus and temporal gyrus (Owen et al., 2010). These regions of decreased perfusion may therefore reflect both pain-relevant and stimulus independent changes associated with nociception and pain perception. The cumulative effect of regional hypoperfusion is larger than the hyperperfusion seen in the contralateral insula. This suggests that the brain response to persistent pain is dominated by decreased perfusion but includes a more localised increase in perfusion in brain areas that respond directly to the pain stimulus. This is further supported by the significant decrease in grey matter CBF from the late pain block to the more painful heat block (Fig 5.4).

Interestingly, we do not report any changes in thalamic CBF. This is surprising given

previous consistent findings of decreased thalamic perfusion in neuropathic pain (Hsieh et al., 1995; Iadarola et al., 1995), and evidence of a thalamic relay of spinothalamic inputs to higher cortical regions, including the insula (Craig, 2013). However, we reported in Chapter 4 that thalamic CBF is sensitive to drift changes when a single baseline is taken. This may be related to the role of the thalamus in integration of inputs that modulate attentional processing. Owen and colleagues (2010) also report that the bilateral thalamus showed the most rapid decrease to baseline following CBF increase to a bolus hypertonic saline stimulus. These findings suggest a complex relationship between thalamic activity, nociceptive activity and pain perception, for which a simple analysis approach is likely inadequate. Thalamic changes may be best investigated using a region of interest approach or with a crossover design that better controls for its role in non-pain specific attentional processing (see Chapter 6).

To mitigate the effects of attentional drift in the BL/EP contrast and to characterise neural structures that were consistently recruited in the pain state regardless of the level of pain or time of scan, we performed an F-test between the baseline block and all pain blocks. The only regions which survive this strict statistical correction were the contralateral rostral anterior insula (which is hyperperfused to pain), putamen and caudate (which are hypoperfused to pain). This underlines the importance of anterior insula activity in the conscious awareness of pain stimuli, irrespective of stimulus intensity or perception (Oertel et al., 2012). The role of the caudate and putamen in pain perception is less established, but has also been defined for acute and chronic pain states over the past few decades. In addition to putative direct and indirect nociceptive inputs to the basal ganglia, thalamo-cortical-striatal loops are suggested to be involved in the integration of motor, autonomic, cognitive and emotional aspects of pain (Borsook et al., 2010; Chudler and Dong, 1995). Some commentators have proposed that the basal ganglia acts by integrating multisensory information to enable selection of appropriate

actions or motor responses at the expense of others (Redgrave et al., 1999). Our findings may therefore reflect an inhibition of this processing in an experimental pain state where behavioural aversion from the stimulus is not an appropriate response. This is supported by evidence that lesions in the caudate nucleus impair avoidance behaviour from noxious stimuli in the macaque and that a population of caudate neurons are active during pain-avoidance behaviour (Koyama et al., 2000). A somatotopic representation of nociceptive-specific stimuli has also been identified in the contralateral putamen, providing spatial information that may form a basis for appropriate motor responses to such stimuli (Bingel et al., 2004a). Therefore the striatum and anterior insula may have direct involvement in the processing of persistent pain stimuli. The relevance of perfusion decreases in other neural structures to the early pain state remains to be addressed. The assessment of perfusion changes to a range of other tonic sensory stimuli may shed some light on this.

### 5.5.3 Correlation with pain perception

We investigated the relationship between within-subject pain perception and CBF changes to identify brain regions that may serve as biomarkers for nociception and pain perception. Using masks defined from functionally active regions in the BL/EP contrast, we tested the correlation of CBF change to pain perception over the experimental time-course (Fig 5.5C). We demonstrate that activity in the dorsal posterior insula is significantly correlated to pain perception while activity in the rostral anterior insula is not. To test for this effect across the whole brain, we performed a within-subject regression analysis looking for regions that track the change in perception. We report a significant and strong (peak z-score = 5.12) positive correlation between pain perception and CBF change in the contralateral dorsal posterior insula and adjoining medial opercula region. These findings suggest that only activity in the dorsal posterior insula is directly related

to the level of nociceptive input and subsequent pain perception. This result is especially pertinent in light of recent evidence suggesting a role for this region in the specific modulation of nociceptive and thermosensory inputs (Craig, 2013; Garcia-Larrea, 2012). There is evidence of conserved somatotopy of nociceptive inputs from the dorsal horn to the dorsal posterior insula, while direct stimulation of the posterior insula has been reported to elicit somatotopically organised pain responses (Craig, 2013; Mazzola et al., 2009). Studies using scalp recordings of laser-evoked potentials have also suggested that nociceptive-specific inputs are first processed in the operculoinsula region (Iannetti et al., 2005a; Lee et al., 2009). Taken together with our findings, these suggest that the posterior insula may represent an early cortical point of convergence for nociceptive inputs, and that its activity can be used as an objective readout of nociceptive input or pain perception.

Conversely, activity in the rostral anterior insula is not directly correlated with pain perception but appears to be binary- the region increases in activity as soon as the pain experience begins, and maintains that level of activity regardless of the pain level (Fig 5.5B, 5.6B). Importantly, in the cooling block where the sensory valence is switched and pain is extinguished, activity in the anterior insula remains stable. This supports the putative role of this region in the encoding of the significance of stimuli regardless of modality, rather than a direct or specific representation of pain perception (Craig, 2009; Wiech et al., 2010). The involvement of the insula in processing nociceptive stimuli may therefore progress from integration of primary interoceptive representations in the posterior region, to broader integration of subjective awareness in the anterior region.

We also report a cluster in the right dorsolateral prefrontal cortex (DLPFC) where perfusion change is negatively correlated to pain perception. The DLPFC is an important top-down driver of pain inhibition, through cortico-cortical and cortico-subcortical cir-

cuits. In a heat capsaicin pain paradigm, left DLPFC activity was shown to disrupt coupling between the midbrain and medial thalamus (which had been associated with pain unpleasantness), while right DLPFC activity was shown to reduce the association between bilateral anterior insula activity and subjective pain perception (Lorenz et al., 2003). Furthermore, atrophy of the bilateral DLPFC has also been reported in chronic back pain patients (Apkarian et al., 2004), while there is preliminary evidence of efficacy for non-invasive brain stimulation of the left DLPFC in healthy and chronic pain patient cohorts (Plow et al., 2012). Our findings corroborate the role of the DLPFC in pain inhibition- its activity is reduced when there is increased subjective pain perception. Further connectivity analyses will be important to define the networks through which this effect is manifest.

### 5.5.4 Conclusions

Our results suggest that persistent pain is represented in the brain by increased activity in a more localised set of structures than is defined for acute phasic pain. Increased activity in the anterior insula may reflect a higher cognitive representation of awareness of self, while decreased activity in the basal ganglia may reflect an inhibition of pain-related motor responses. Importantly, we show that perfusion change in the dorsal posterior insula is strongly correlated to pain perception within subjects. This may have direct relevance for its use as a surrogate objective readout for pain perception in pharmacological trials. To investigate this, the following chapter tests the use of ASL in the assessment of pharmacological efficacy as well as endogenous modulation of pain perception.

Further investigations will also be necessary to link these regions with the integrative functional networks underlying direct sensory or affective encoding of the persistent pain state.

# Chapter 6

# Physiological and Pharmacological Modulation of the Perception and Neural Representation of Persistent Pain

In the previous chapter, we established a neural basis for the representation of persistent pain, and its parametric modulation. A key subsequent application of these findings is to investigate the modulation of this representation by physiological inter-individual factors and pharmacological interventions. In this chapter we assess the influence of known endogenous and exogenous pain modulatory factors on the neural representation of persistent pain.

## 6.1 Experiment 1

The descending pain modulatory system (DPMS) has been well defined in animal studies over a number of decades (Heinricher et al., 2009). In man, electrical stimulation of various DPMS nuclei- including the periaqueductal and periventricular grey, has shown some efficacy against neuropathic pain (Boccard et al., 2013). However, investigation of the neural mechanisms underlying the balance between descending pain facilitation

and inhibition has proved challenging to study in the healthy human. This is partially because of the methodological challenges of quantifying neural activity in vivo in these deep subcortical structures. Here, we utilise arterial spin labelling to image resting cerebral blood flow in the DPMS in a baseline and a centrally sensitised (CS) state, in order to test its relationship with pain behaviour in healthy humans.

### 6.1.1 Introduction

Pain behaviour can vary greatly within and between individuals, making it difficult to identify those most at risk of severe and persistent pain. Tools that assess vulnerability to pain after injury are important in the perioperative setting and beyond. Functional MRI (fMRI) studies have investigated the role of pre-stimulus functional connectivity and multivariate pattern analysis in predicting responses to acute pain stimuli (Brodersen et al., 2012; Ploner et al., 2010). However, in the clinical setting, patients experience spontaneous pain and other complex sensory perturbations following sensitisation, which have not been addressed in such studies. The ability to assess susceptibility to persistent pain and the consequences of nerve injury is needed to fill this gap. Recent advances in neuroimaging have allowed the assessment of ongoing pain states in patients and healthy subjects.

The periaqueductal grey (PAG) and rostral ventromedial medulla (RVM) are key structures in the DPMS, with an ability to bi-directionally modulate pain perception. The PAG receives inputs from spinal and cortical networks and is intimately connected to various nuclei in the brainstem reticular formation (Yaksh and Rudy, 1978)- including the rostral ventromedial medulla (RVM), which projects to the spinal dorsal horn via facilitatory ON cells and inhibitory OFF cells (Fields et al., 1983). Amongst other functions, there is ample evidence for the PAG's role in human pain perception, analgesia,

placebo, and central sensitisation (Derbyshire and Osborn, 2009; Eippert et al., 2009; Linnman et al., 2012; Zambreanu et al., 2005). In various animal models, descending facilitation from the RVM has been shown to be essential for the maintenance of central sensitisation and spontaneous neuropathic pain (Porreca et al., 2002; Wang et al., 2013). It has been further suggested that the balance between facilitatory and inhibitory drive in the PAG-RVM system is a key determinant in the development of pathological pain states (Heinricher et al., 2009; Suzuki et al., 2004) - implying that a vulnerability might exist pre-injury that predisposes the development of persistent pain states. These findings have not been adequately challenged using human models of spontaneous pain and central sensitisation. Serendipitously, the validated arterial spin labelling (ASL) imaging technique facilitates quantification of resting cerebral blood flow (CBF) in the normal and sensitised states, and so enables us to evaluate the influence of basal PAG metabolism on pain susceptibility in a healthy population.

### 6.1.2 Aim

We used a multi inversion time pseudo-continuous arterial spin labelling (pCASL) fMRI approach- which enables effective estimation of absolute CBF in the midbrain and upper brainstem, together with a model of central sensitisation (CS) to investigate the relationship between inter-individual differences in PAG perfusion and pain vulnerability in a healthy population. We hypothesised that an increased basal facilitatory drive may be indicative of individuals vulnerable to pain injury.

### 6.1.3 Methods

The data described here was collected as described in the methods section of Chapter 3- baseline session (BL) and capsaicin sessions (CAP) only. These sessions are referred

to in this chapter by the order in which they were performed (BL= Session 1; CAP= Session 2)

#### 6.1.3.1 Subjects

24 healthy subjects (mean ± s.e.m. = 23.79 ± 0.83 years) participated in the study. All participants gave written informed consent in accordance with the local ethics committee. Only subjects who developed secondary mechanical punctate hyperalgesia (SMPH) and tolerated study procedures were included in the full study. One subject was excluded because of scanner related faults and incomplete data acquisition.

Subjects were screened to exclude past neurological or psychiatric conditions, reports of having taken any prescribed or over the counter analgesics in the week prior to the study session, and use of recreational drugs by way of a urine analysis. All subjects avoided caffeine for 6 hours and alcohol for 12 hours prior to each visit.

#### 6.1.3.2 Experimental design

All subjects attended 2 sessions separated by 2-11 months (4.73 ± 0.41 months) (Fig 6.1A). In the first session (S1), subjects underwent baseline scanning before capsaicin application. The scan paradigm included 20 minutes of functional BOLD imaging (which included 18 punctate stimuli to normal skin- see paradigm below) prior to 10 minutes of perfusion imaging (Figure 3.2). Following the scans, subject responsiveness to capsaicin and ability to develop secondary mechanical punctate hyperalgesia (SMPH) was tested offline. A concentric rectangle (4x4 $cm^2$) was drawn on the antero-medial aspect of the lower left leg (at least 14cm above the medial malleolus). Another rectangle of 4x2 $cm^2$ was outlined 3 cm from the first rectangle- this defined the 'target area' (Figure

6.1B). Mechanical stimulation was tested in the target area with a non-skin penetrating punctate probe (512mN) (Ziegler et al., 1999). SMPH was defined as the presence of a significantly increased pain sensation to repeated mechanical punctate stimulation of the target skin area 1 hour after capsaicin application as compared to before capsaicin application.

In the second session (S2), capsaicin was applied to the right leg in the same procedure as described above. 1 hour following capsaicin application, subjects' responsiveness to capsaicin was tested in an MRI scanner. Subsequently, they underwent 10 minutes perfusion imaging following the same protocol as in S1. This assessed blood flow in a centrally sensitised state.

All subjects attended 3 additional visits between S1 and S2 where they received capsaicin to the right leg after pre-emptive drug administration. Data from these visits was discussed in Chapter 3.

#### 6.1.3.3 Stimulation paradigm

Mechanical punctate stimulation included 18 identical 1-second stimuli with an ISI of 28 and 32 seconds (average 30 seconds). Successive punctate stimuli were applied to different regions of the stimulation region to minimise sensitisation of the skin. The same experimenter applied punctate stimuli for all study sessions to reduce experimenter-related variability. Subjects were instructed to keep their eyes open and fixate on a cross during stimulation.

Subjects rated perception using an online computerised VAS displayed on a projector screen. Each scale was projected for 6 seconds. Punctate stimulus intensity was rated

12-seconds after every mechanical punctate stimulus using a VAS with anchors 'Not intense', 'Extremely intense'. Average unpleasantness to punctate stimuli was rated at the end of the complete run of stimuli- 18 seconds after the final punctate stimulus.

ASL data was acquired while subjects kept their eyes open and fixated on a cross. There was no task in this period. Spontaneous/Ongoing pain ratings were acquired 45 minutes and 70 minutes after capsaicin application in S1; and 60 minutes and 100 minutes (before and after fMRI scanning) in S2. The VAS anchors were 'No pain', 'Severe pain'.

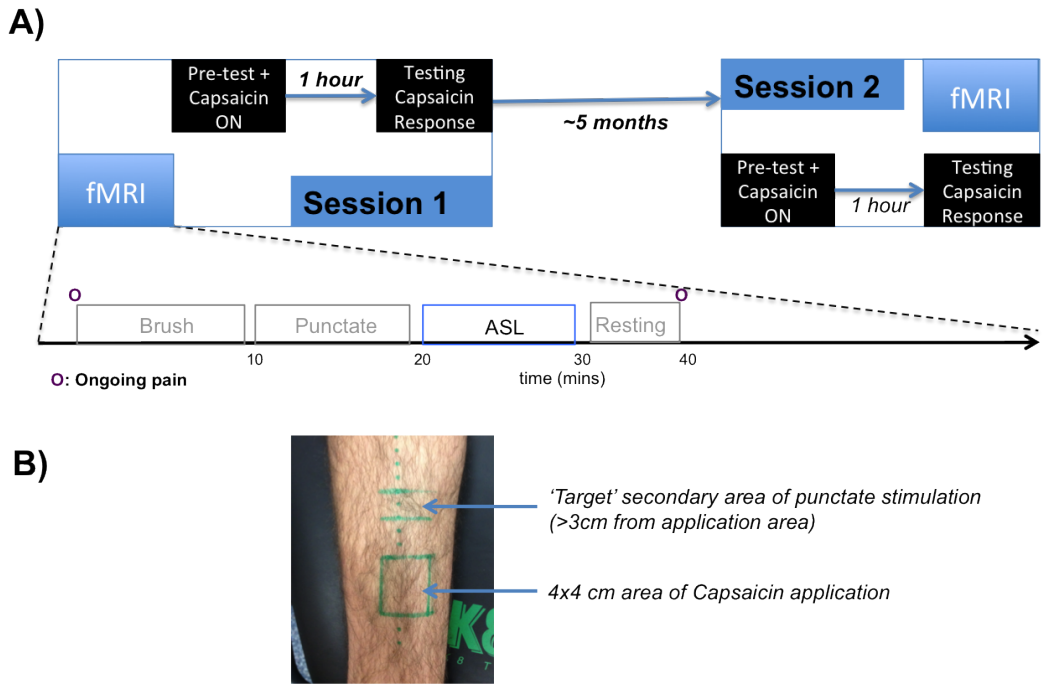


Figure 6.1: **Experimental procedure**, Site of capsaicin application and punctate stimulation. (a) In session 1 (S1), subjects were scanned in a baseline state before capsaicin testing. In session 2 (S2), subjects were scanned during capsaicin testing. (b) punctate stimulation was delivered in a 2x4cm target area >3cm from site of capsaicin application.

#### 6.1.3.4 fMRI scanning protocol

During each session, fMRI was performed on a 3T Siemens Verio MRI scanner (Erlangen, Germany) fitted with a 32 channel head-only gradient coil. Response registration was through a computer running Presentation (version 16.0; Neurobehavioral Systems, Albany, CA) and a button box controlled by the subject within the MRI scanner.

Arterial spin labelling data was acquired using a pseudo-continuous (pCASL) multiple inversion time quantitative sequence (labelling duration= 1.4 seconds; 5 post labelling delays [PLD]= 0.2, 0.4, 0.6, 0.8, 1 second(s); TE= 13ms; 28 contiguous 4.6mm slices; field of view 240x240 $mm^2$; matrix 64x64). A shorter range and smaller number of post-labelling delays enabled improved temporal resolution and increased sampling of the CBF signal in the appropriate TI range for most brain regions (see Figure 4.8 and Chapter 4 discussion). TR for each tag/control image was 3.75s, with 150 volumes, corresponding to 10 minutes of scanning time. The tagging plane was defined anatomically for each individual subject at the ascending brain-feeding arteries (approximately 6cm below the circle of Willis).

A T1-weighted, 1x1x1 $mm^3$ structural image was collected in the first session only, for registration and overlay of brain activation.

#### 6.1.3.5 Data analysis

Psychophysical statistical analyses, including correlation tests and t-tests were implemented using IBM SPSS Statistics, version 18 (IBM, Armonk, NY, USA). All tested variables were normally distributed (Shapiro-Wilk test: $p>0.05$) so correlations were analysed using the parametric Pearson's test. For validation in a smaller cohort of six subjects, we additionally used the non-parametric Spearman's test for correlation anal-

ysis. For each session, we define a hyperalgesia unpleasantness ($\Delta$UNP) score as the difference between average punctate unpleasantness ratings before and after capsaicin application.

Using stem and leaf plots, outliers were identified as cases falling more than 1.5x the interquartile range (IQR) away from the upper or lower limits of the IQR. These cases were removed from further correlation analyses.

#### 6.1.3.6 ASL data analysis

Imaging data analyses were performed using FMRIB Software Library (FSL) version 5.01 (Jenkinson et al., 2012).

pCASL data was perfusion-subtracted (control - tag), pre-processed (brain extraction and motion correction) using FSL tools and quantified using a Bayesian Inference Tool (BASIL) (Chappell et al., 2010). For each set of 5 tag/control-subtracted images (each with a different TI), BASIL iteratively calculated blood magnetization kinetics across all voxels for each inversion time, estimating blood arrival time and selecting the appropriate peak signal intensity. Magnetisation of blood was estimated from cerebrospinal fluid in a calibration image with an extended TR. This allowed conversion of signal intensity to physiological units. 15 epochs of quantified perfusion maps were generated and these were averaged within-session in a mixed effects model for variance-normalisation. This session-averaged CBF map was used in a group level mixed effects linear model (paired t-test) to compare the different conditions. Z-score images were generated at a threshold of $Z = 2.3$ with corrected cluster significance of $p \leq 0.05$ (Worsley, 2001). We excluded one subject from the analysis of cerebral perfusion in the sensitised state because we failed to acquire adequate calibration images to estimate blood magnetisation in S2.

Registration to structural and standard space was carried out using BBR (Greve and Fischl, 2009) and FLIRT (Jenkinson et al., 2002). PAG CBF was extracted from a custom mask of the PAG (Figure 6.3), drawn in standard MNI space (with reference from a detailed brainstem atlas (Naidich et al., 2009)).

### 6.1.4 Results

In both sessions, subjects developed secondary mechanical punctate hyperalgesia (SMPH), defined by a significant increase (t-test, $p<0.05$) in punctate intensity ratings to repeated stimuli in the target area, when tested at least an hour after the capsaicin cream was applied. In both sessions, there was no significant difference between the two spontaneous pain ratings recorded (pre- and post- scanning) (S1: $t(18)=0.28$, $p>0.05$; S2: $t(21)=0.09$, $p>0.05$), suggesting a stable spontaneous pain state had been reached. Subjects reported mild-moderate ongoing pain (OGP) and developed punctate unpleasantness hyperalgesia ($\Delta$UNP) during both sessions. Both OGP and $\Delta$UNP are significantly different between the two sessions (Fig 6.2A).

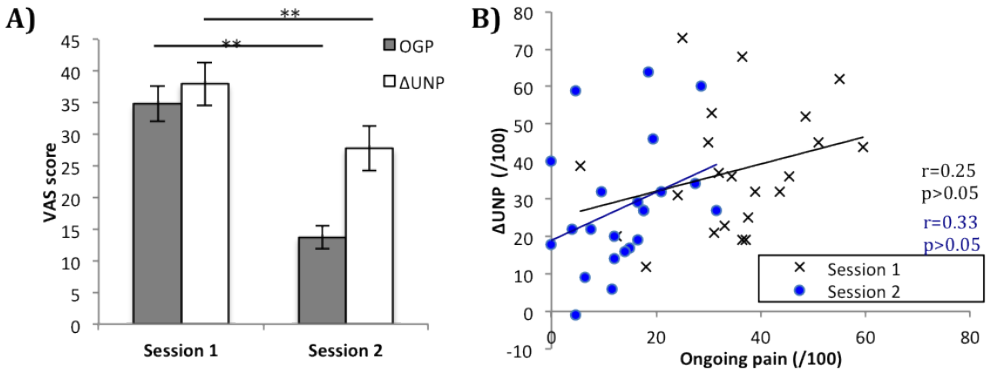


Figure 6.2: **Ongoing pain (OGP) and hyperalgesia ($\Delta$UNP) during both sessions.** OGP was taken as an average of ratings pre and post scanning in Session 1 and pre and post testing in session 2. (a) shows a significant difference between both sessions for both measures ** $p<0.01$ (b) both measures are not correlated in either session.

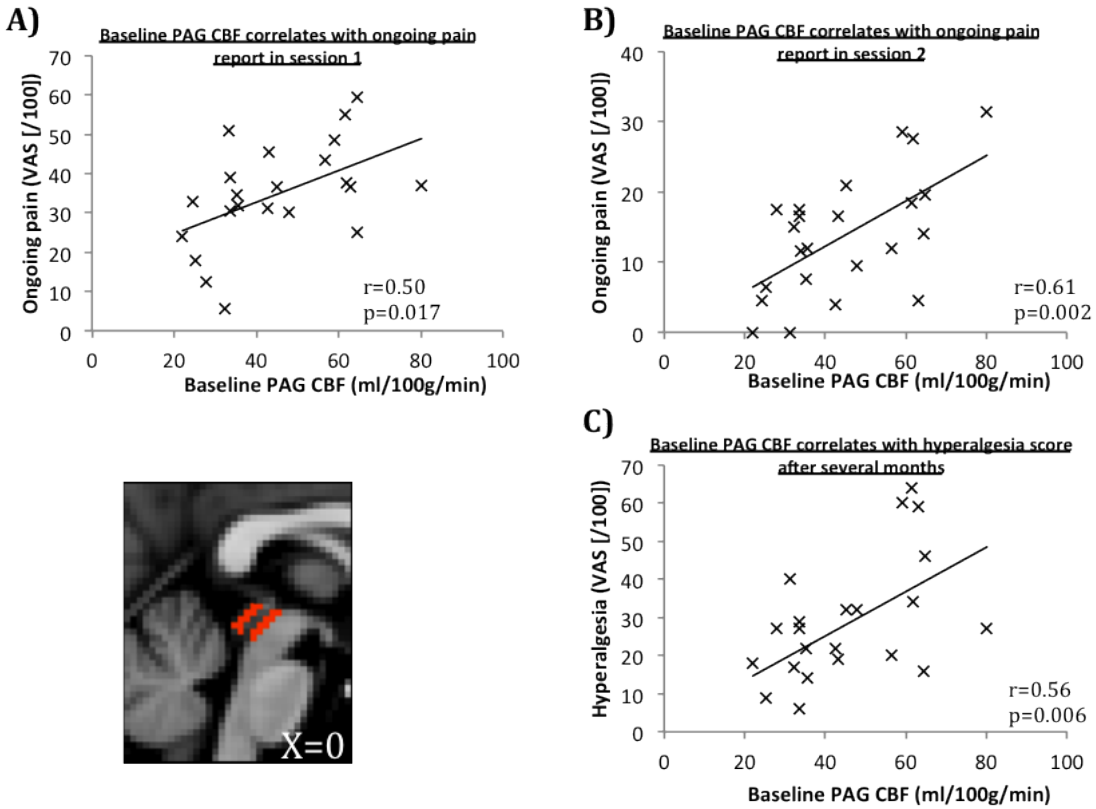


Figure 6.3: **Baseline PAG CBF correlates with pain behaviour in S1 and S2.** Bottom left: CBF was extracted from a PAG anatomical mask drawn in standard space as shown (a) PAG CBF in session 1 correlates with ongoing pain in session 1 (n=22) and (b) session two (n=23) (c) as well as ΔUNP in session 2 (n=23). Pearson correlation analyses were used for all analysis.

We demonstrate that baseline PAG perfusion correlates with ongoing pain on the day of baseline scan (S1) ($r(20)=0.50$, $p=0.017$) and in the subsequent session (S2) several months later ($r(21)=0.61$, $p=0.002$) (Fig 6.3). Furthermore, S1 baseline perfusion in the PAG also correlated with hyperalgesia unpleasantness scores (ΔUNP) during S2 ($r(21)=0.56$, $p=0.006$) (Fig 6.3). There is no significant correlation between OGP in S1 compared to S2 ($r(20)=0.26$, $p>0.05$) and OGP does not correlate with ΔUNP within either session (Fig 6.2B). To validate the specificity of this effect, we showed that mean baseline CBF in a control region (primary visual cortex) and for the whole brain grey

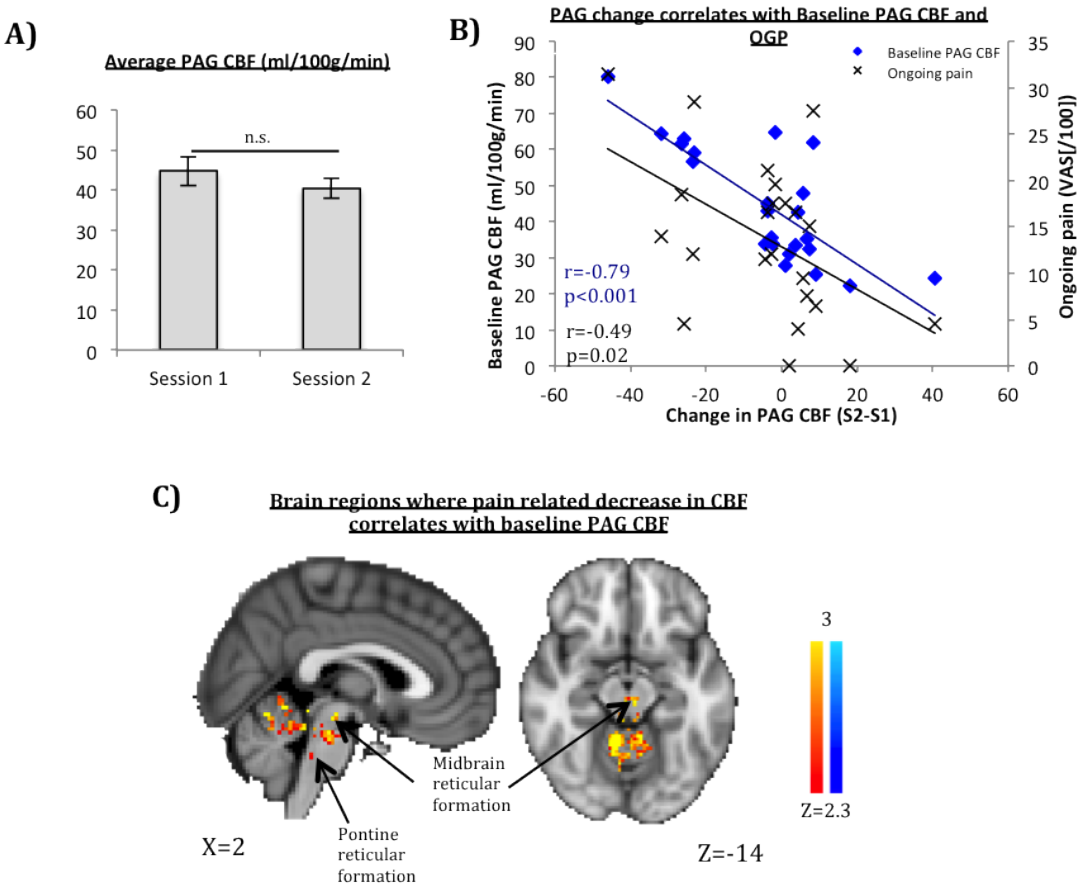


Figure 6.4: **CBF change between S1 and S2 is correlated with pain scores and baseline PAG CBF.** (a) there is a non significant mean decrease in PAG CBF induced during the central sensitised and persistent pain state (b) Inter-session PAG change between subjects is associated with baseline PAG CBF and ongoing pain scores (c) regions of the brainstem reticular formation are functionally coupled with the PAG from baseline to the CS state. Mixed effects, Z=2.3, $p<0.05$.

matter do not predict pain behaviour (Appendix B: Suppl Fig 6.3A). There was also no relationship between the time interval from S1 to S2, and PAG CBF change or pain scores in session 2 (Appendix B: Suppl Fig 6.3B).

We tested the neural mechanisms underlying this effect using perfusion scans acquired in the sensitised state (S2). There was no significant difference in PAG perfusion (Fig 6.4A) or in mean grey matter CBF ($t(20)=0.48$, $p>0.05$)(Fig 6.6B) between the two sessions. However, we demonstrated that PAG perfusion change due to sensitisation (S2-S1) is negatively correlated with baseline PAG CBF ($r(20)=-0.79$, $p<0.001$) and with ongoing pain ($r(20)=-0.49$, $p=0.02$) (Fig. 6.4B). Therefore, individuals with higher baseline PAG not only rated higher ongoing pain, but also had a larger CBF decrease in the PAG during the pain/sensitisation state.

To further assess how basal PAG blood flow indicates pain and hyperalgesic behaviour, we tested for other brain regions where hypoperfusion is functionally connected to the PAG CBF in the baseline conditions- interindividual baseline PAG CBF was used as a covariate in the S1>S2 contrast across the whole brain. We show that PAG baseline CBF correlates with CBF decreases in the midbrain reticular formation and pontine reticular formation (whole-brain cluster corrected, $Z=2.3$, $p<0.05$) (Figure 6.4C). This suggests that in the sensitised state, there is a stronger decrease in perfusion in these regions in individuals with higher PAG blood flow at baseline.

#### 6.1.4.1 Validation in a unique cohort

To further confirm our findings, we tested the ability to predict pain behaviour from baseline PAG blood flow in a separate cohort of 6 subjects ($26.8 \pm 2.27$ years). Subjects were imaged at baseline using an identical pCASL method, several months ($10.6 \pm 0.38$

months) after they had been induced into a central sensitised state. All subjects received capsaicin to an equivalent region in the lower leg bilaterally and spontaneous pain was assessed during a 7T fMRI session, 60 minutes and 90 minutes after capsaicin application (see Chapter 2, Experiment 2). We showed that in this smaller cohort, baseline PAG CBF retrospectively indicates spontaneous pain scores (Pearson's correlation: r(4)=0.84, p=0.035; Spearman's correlation: r(4)=0.83, p=0.042) (Appendix B: Suppl Fig. 6.3C).

### 6.1.5 Discussion

Our findings provide the first in vivo evidence in humans that susceptibility to pain injury is associated with basal PAG blood flow. Furthermore, although the PAG receives ascending nociceptive inputs and is involved in autonomic functions, blood flow imaging in this region may in part reflect descending pain inhibitory drive in the healthy human.

In this study, we report that baseline cerebral blood flow in the PAG predicts individual behavioural responses in the central sensitised (CS) state- individuals with higher PAG activity at baseline report higher spontaneous pain and are more hyperalgesic during CS. We demonstrate this effect at two distinct timepoints separated by several months- where subjective ratings are not influenced by the time interval between sessions (Appendix B: Suppl Fig 6.3). Importantly, the behavioural measures used (ongoing pain and hyperalgesia) are significantly different between both sessions supporting the robustness of the prediction of individual pain reports over different pain levels. The difference between session pain scores is likely due to the first-time exposure to capsaicin for most of the subjects in S1 and the slightly different experimental conditions in S2 (see Methods). Additionally, the two measures do not correlate with each other in either session. While this may be due to insufficient subjects numbers, it may also reflect two distinct but overlapping mechanisms underlying spontaneous and evoked components of the CS

phenotype, which are associated with baseline PAG activity.

We confirmed the specificity of this result by showing that a control region and the mean grey matter CBF are not associated with behavioural reports. We also show that the effect is reproducible in a separate cohort of subjects (Suppl Fig 6.3). In this latter experiment, baseline CBF measures are taken up to 11 months following CS-related injury. This suggests that the relationship between PAG activity and pain behaviour manifests in different subject groups under different experimental conditions, supporting its relevance beyond our preliminary findings.

Our analysis of metabolic change in the PAG induced by central sensitisation suggests that decreased perfusion in the region is indicated by higher baseline activity and is associated with increased pain reports. This suggests that an individual with high susceptibility to pain on injury has high PAG metabolic activity at baseline, which decreases upon injury. We propose that this indicates a loss of inhibitory drive in these individuals. We further show that baseline PAG CBF is negatively correlated with CBF changes in the midbrain reticular formation and pontine reticular formation, regions that are structurally and functionally connected with the PAG.

Our findings are unexpected given our hypothesis that increased facilitatory drive underlies the development and manifestation of central sensitisation. In particular, RVM control of spinal processing has been suggested to have a predominantly pain facilitatory influence in normal anaesthetised animals (Bee and Dickenson, 2007). However we note that the mechanisms underlying the 'on-off' balance within the DPMS are not well understood in man. While the metabolic change we measure with ASL does not allow us to fully disentangle the distinct contributions of inhibitory and facilitatory mechanisms, it is conceivable that the development of central sensitisation is driven by reduced in-

hibitory drive, in tandem with a more subtle increase in facilitatory drive. Importantly, this would alter the balance between these two pathways, increasing the dominance of the facilitatory system and supporting a CS phenotype (Porreca et al., 2002; Wang et al., 2013).

The response of the PAG-RVM system to nerve injury is not straightforward (Vanegas and Schaible, 2004). Silencing of the RVM has been shown to reverse allodynia in nerve-injured hypersensitive rats, but also to induce hypersensitivity in nerve-injured rats that do not exhibit mechanical hypersensitivity (De Felice et al., 2011; Wang et al., 2013). This implies that the balance of inhibitory and facilitatory RVM drive can differentially influence the manifestation of the central sensitisation phenotype, and that descending inhibition may protect against the transition from acute to persistent pain.

There is evidence for dominance of inhibitory mechanisms in the PAG-RVM system in both preclinical and human studies. It is well established that stimulation of the medial brainstem leads to analgesia in experimental animals (Mayer and Price, 1976) and in man (Bittar et al., 2005). This has often been attributed to opioid related mechanisms (Hosobuchi et al., 1977). In a rodent inflammatory pain model, thoracic spinal block by intrathecal lidocaine was shown to increase dorsal horn receptive fields, suggesting a net descending inhibitory effect (Ren and Dubner, 1996). Preclinical electrophysiological studies investigating the activity of RVM neuronal populations in rodent models of neuropathic pain further suggest that spontaneous RVM OFF cell activity dominates at baseline (Silva et al., 2013) and decreases in post-injury persistent pain observed by a second-phase formalin response (De Felice et al., 2011). Taken together, these findings suggest that baseline activity in the midbrain may reflect OFF cell activity and tonic inhibitory drive, which decreases on injury in susceptible individuals. Increased PAG activity at baseline in susceptible individuals may therefore indicate a requisite for

greater tonic inhibition to maintain a normal state in these individuals.

An important implication of these findings is that they support the use of functional imaging in the assessment of individuals' risk of developing persistent pain. This may have important clinical implications, particularly in the peri-operative setting where pre-surgical assessment of susceptibility to persistent post-surgical pain has practical applications (Deumens et al., 2013; Kehlet et al., 2006). It will be prudent to test the influence of baseline PAG activity on pain behaviour in larger groups, different experimental settings, as well as in clinical populations in order to validate its utility for risk assessment in such settings.

## 6.2 Experiment 2

The efficacy of gabapentin as an analgesic is established for some neuropathic pain conditions, including postherpetic neuralgia and painful diabetic neuropathy (Backonja et al., 1998; Rowbotham et al., 1998). However, its neural effects and central mechanism of analgesia are not well understood. In particular, few imaging studies have assessed its pain-relieving effect in the context of persistent pain. In the previous chapter, we identify a set of neural structures that are consistently recruited in persistent pain. In this study, we use the experimental design from chapter 3 to directly investigate the effect of gabapentin on regional cerebral blood flow in the context of ongoing pain relief. We are also able to assess the utility of arterial spin labelling as a tool for detecting drug efficacy in a model of central sensitisation.

### 6.2.1 Introduction

Gabapentin is an effective analgesic, anti-anxiolytic and anti-epileptic agent. Although a GABA-mimetic, it acts on the central nervous system without directly binding to GABA receptors. Its analgesic effect is thought to be related to suppression of voltage gated calcium channels in spinal dorsal horn presynaptic terminals, as well as activation of descending noradrenergic systems supraspinally (Dooley et al., 2007; Hayashida et al., 2007; Tanabe et al., 2008). Its wider effects on cerebral metabolism are not known. In a model of central sensitisation, Iannetti and colleagues (Iannetti et al., 2005b) reported that gabapentin has measurable antinociceptive and antihyperalgesic effects by showing associated BOLD signal reductions. Interestingly, the authors note that the strongest antihyperalgesic effect of gabapentin was in suppressing or reversing stimulus induced deactivations in several bilateral brain regions including the medial prefrontal cortex, precuneus, parieto-temporo-occipital junction, caudate and hippocampus.

To our knowledge, no studies have quantified gabapentin's effect on cerebral blood flow in vivo, although we note two clinical cases which report reversal of pain related CBF abnormalities after 1-2 weeks of gabapentin treatment using single-photon emission computed tomography (SPECT) imaging (Ness et al., 1998; Wu et al., 2011).

### 6.2.2 Aim

We tested the effect of gabapentin (as compared to placebo and ibuprofen) on cerebral blood flow in the central sensitised (CS) and persistent pain state using ASL. To validate previous findings with BOLD imaging, we also tested the influence of gabapentin on stimulus related deactivations in the context of dynamic mechanical allodynia (DMA).

We hypothesised that gabapentin would suppress neural activity to persistent pain as it does with more brief stimuli (Chapter 3). In line with previous reports in an acute pain paradigm (Iannetti et al., 2005b), we also expected that gabapentin will have a reversal effect on brain regions showing decreased cerebral perfusion in the persistent pain state.

### 6.2.3 Methods

The data described here was collected as described in Chapter 3 Methods.

#### 6.2.3.1 Subjects

24 healthy subjects (mean $\pm$ s.e.m. $= 23.79 \pm 0.83$ years) participated in the experiment.

#### 6.2.3.2 Experimental design

This was a crossover, double-blinded, randomised study as described in chapter 3. In two of the sessions, subjects were dosed with either placebo (PL) or 1200mg gabapentin (GB) 1 hour prior to application of topical capsaicin to the right lower leg. The baseline scan session (no capsaicin) took place on the 1st visit, and the capsaicin only (no drug) scan took place on the 5th visit. The experimental paradigm was identical for all study visits (Figs 3.1, 3.2).

#### 6.2.3.3 Stimulation paradigm

Topical capsaicin was applied as described in Chapter 3. Dynamic mechanical stimulation (using a calibrated brush) included 15 identical 6-second long stimuli, with three 2-second strokes across the leg in the medio-lateral direction. The inter-stimulus interval (ISI) was jittered between 28 and 46 seconds (average 38 seconds). Subjects were instructed to fixate on a cross that was displayed on a projector, during the stimulation. Ongoing pain scores were rated with a computerised visual analogue scale (VAS) 120 and 180 minutes after dosing (before and after scanning). Average unpleasantness and pain intensity of the brush stimulation were rated 12 seconds and 18 seconds after the final brush stimulation using a VAS scale.

#### 6.2.3.4 fMRI scanning protocol

Functional scanning began 1 hour after capsaicin application (Figure 3.1). Brush stimuli were applied in the first BOLD functional scan (over a 10 minute period). Scan parameters are described in Chapter 3. Resting ASL data was acquired 20 minutes after functional scanning began (Figure 3.2). The pCASL implementation was as described in Experiment 1 of this chapter.

#### 6.2.3.5 Data analysis

Psychophysical statistical analysis, including analysis of variance (ANOVA) tests and t-tests were implemented using IBM SPSS Statistics, version 18 (IBM, Armonk, NY, USA). Post-hoc correction for multiple comparisons was performed using *Bonferroni* adjustments. Normality testing was performed using the Shapiro-Wilk test.

For the analysis of neural responses to brush stimuli, only subjects who developed dynamic mechanical allodynia (DMA) (18/24, see Table 3.1) in the baseline session were included. BOLD data was analysed as described in Chapter 3. pCASL data was analysed and absolute perfusion maps generated as described in Experiment 1.

For BOLD data, group means and a paired t-test were calculated for subjects' statistical maps to test for an effect of session on allodynic neural responses. Group level statistical maps were thresholded at $Z=2.3$, $p<0.05$.

For pCASL data, paired t-tests were performed to test the effect of CS related persistent pain on cerebral blood flow, and its modulation by gabapentin as compared to placebo. Pairwise ASL statistical comparison maps were thresholded at $Z=2$, $p<0.05$.

For ROI and correlation analyses, we used a non-parametric permutation method with the *Randomise* tool integrated within FSL (Hayasaka and Nichols, 2003). Ongoing pain ratings were added as a covariate in the GLM design. Test statistics were generated using cluster correction at $Z=2.3$, $p<0.05$. For illustration of perfusion change, the functional mask generated from a pairwise comparison was used.

### 6.2.4 Results

There was no significant difference between subject ratings of pain and unpleasantness to brush stimuli between placebo and gabapentin sessions (Pain $t(19)=1.52$, $p>0.05$; Unpleasantness $t(21)=0.54$, $p>0.05$) (see Figure 3.4). For both sessions, group means comparing BOLD neural responses to the brush stimulus predominantly show stimulus-related deactivations across the brain- including the prefrontal cortex, posterior cingulate cortex, precuneus, hippocampal formation, motor and sensory cortices (Fig 6.5). These decreases appear to be attenuated in the gabapentin session compared to placebo- we show significant suppression of deactivation in regions of the prefrontal cortex (Fig 6.5). There is also a cluster of increased activity in the posterior cingulate cortex in the gabapentin session when compared to placebo.

We report significantly lower ongoing pain scores between the placebo and gabapentin sessions ($t(22)=2.35$, $p=0.028$). The gabapentin session ongoing pain scores have previously been shown not to be associated with gabapentin session mental sedation scores (Fig. 3.5). There was no significant difference between capsaicin session ongoing pain ratings and the placebo ($p=0.076$) or gabapentin ($p=0.631$) sessions (Fig 6.6A). To test for habituation effects, a visit by pain ANOVA was performed to test for an effect of visit order on pain ratings. We show that there is a significant effect of visit order on pain report ($F[20]=1.82$, $p<0.05$) (Appendix B: Suppl Fig 6.6).

In a 4-way repeated measures ANOVA (PL, GB, BL, CAPS), there is no significant effect of session on mean grey matter CBF ($F(19)=0.262$, $p>0.05$) (Fig 6.6B).

In a paired comparison between baseline and capsaicin sessions (mixed effects, $Z=2$, $p<0.05$), we report decreased perfusion in the persistent pain condition in a number of pain-related brain areas including the bilateral thalamus and insula cortex, ipsilateral

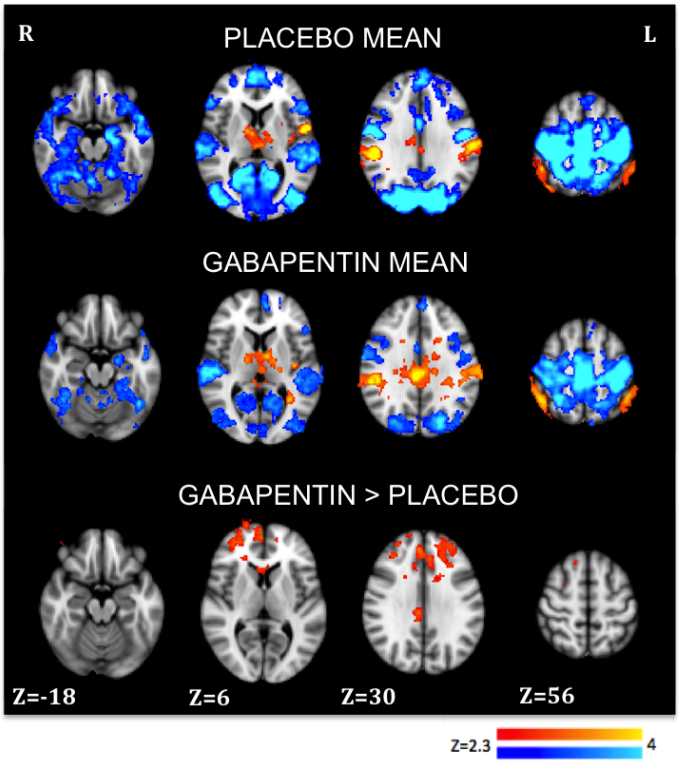


Figure 6.5: **Gabapentin suppression of deactivation to allodynic stimuli.** n=18, Mixed effects, Z=2.3, p<0.05. For mean images, orange indicates regions showing BOLD activation and blue indicates regions showing BOLD deactivation to the stimuli. Images are in radiological convention.

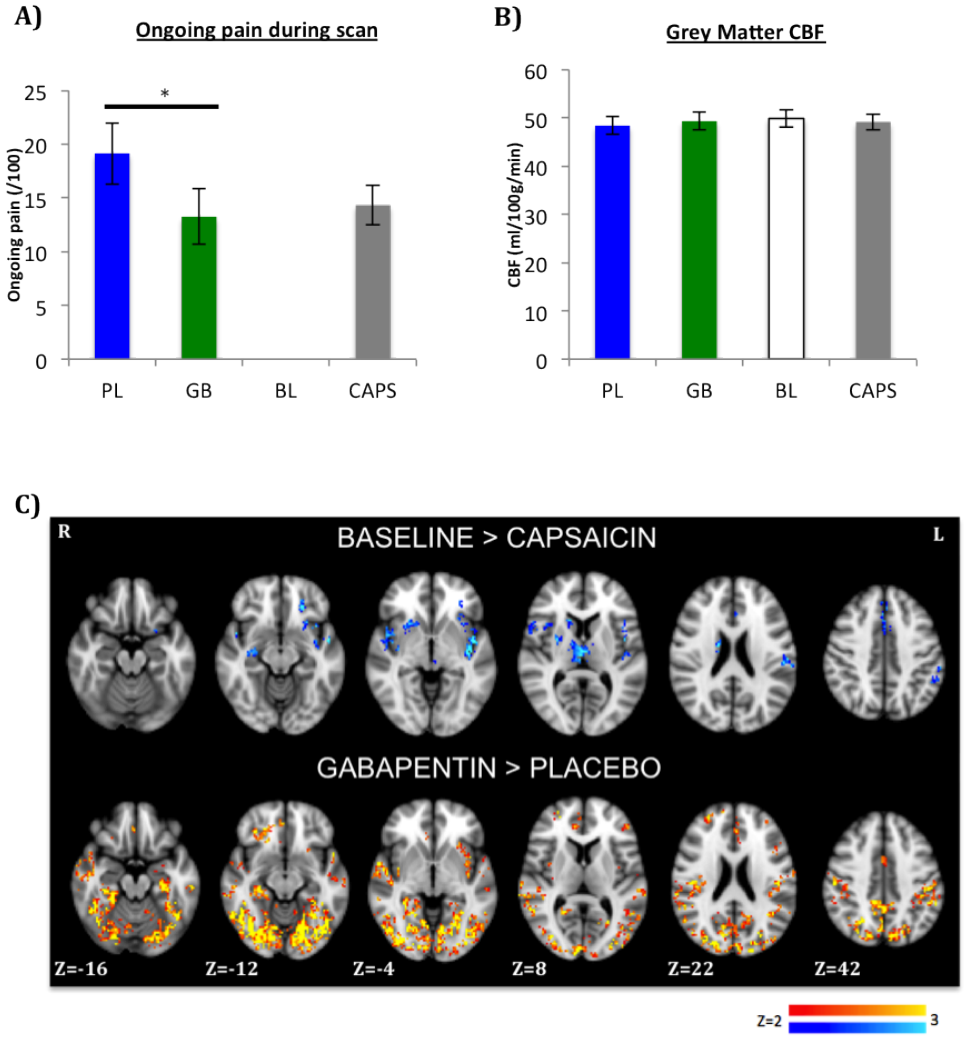


Figure 6.6: **Gabapentin suppression of pain and hypoperfusion.** (a) Ongoing pain across all sessions (average of pre and post scan) * $p<0.05$. (b) Mean Grey matter CBF does not differ between sessions (c) Top shows decreased perfusion in the capsaicin session when compared to baseline (n=22) Bottom shows increased perfusion in the gabapentin session when compared to placebo (n=24). Mixed effects, Z=2, $p<0.05$. Images are in radiological convention.

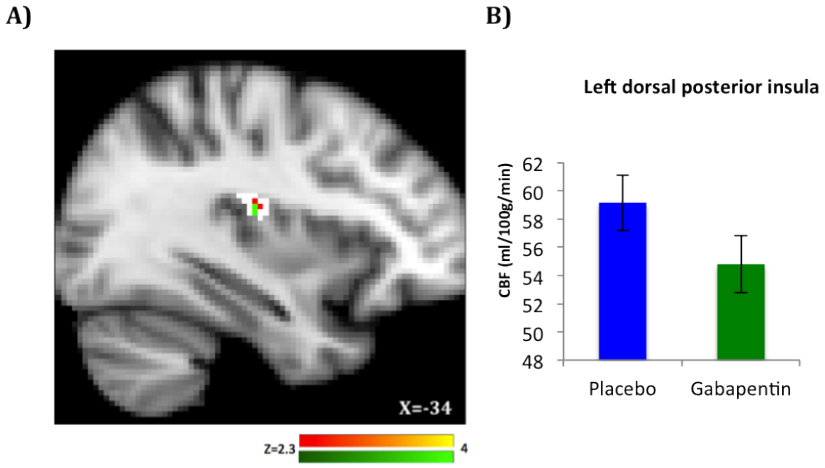


Figure 6.7: **Gabapentin suppression of posterior insula activity.** (a) shows mask of functional region encoding capsaicin pain from Chapter 5 (white) used in ROI analysis, region where there is decreased CBF in gabapentin session when compared to placebo (orange) and region where decreased CBF correlates with gabapentin suppression of ongoing pain (green). Z=2.3, p<0.05 (b) illustrates CBF change in functional region of gabapentin CBF suppression shown in orange in (a).

hippocampus and putamen, and anterior cingulate cortex (Fig 6.6C). We see no regions with increased perfusion during the pain condition.

In a paired comparison between placebo and gabapentin sessions (mixed effects, Z=2, p<0.05), we report increased perfusion induced by gabapentin in a wide range of brain areas. Some of these regions overlap regions that show decreased perfusion in the pain condition (compared to baseline)- including in the hippocampus, insula and anterior cingulate cortex (Fig 6.6C). We suggest that gabapentin suppresses pain-induced hypoperfusion in these regions. In a whole brain corrected analysis, we see no regions where gabapentin causes a decrease in perfusion.

To test whether gabapentin's suppression of behavioural pain reports is reflected in its neural modulation of pain, we performed an ROI analysis using the functional mask of the contralateral dorsal posterior insula, which was shown in chapter 5 to be activated in

early capsaicin induced persistent pain compared to baseline. We show that gabapentin suppresses perfusion within this functional region when compared to placebo (Fig 6.7A, B) and that this suppression is correlated with behavioural suppression of ongoing pain ratings (Fig 6.7A).

### 6.2.5 Discussion

In a cohort of healthy subjects, we quantify for the first time the effects of gabapentin on regional cerebral blood flow in the central sensitised and persistent pain state. We show that gabapentin reverses pain-induced hypoperfusion in several pain-related brain areas, and also decreases perfusion in a region of the brain that we shown to be recruited during the persistent pain state in a previous study. We further parallel gabapentin's suppression of hypoperfusion during persistent pain with its suppression of deactivation to acute allodynic stimuli in the same subject group.

Gabapentin has been shown to be efficacious in reducing daily pain scores in neuropathic pain conditions (Serpell et al., 2002). We show a similar effect on spontaneous pain in our human model of central sensitisation with a small healthy cohort (Fig 6.6A). There is also a large but non-significant decrease in spontaneous pain scores between the placebo session and the capsaicin-only session. This is shown to result from a habituation effect due to our study design where all drug/placebo sessions were randomised, while capsaicin-only sessions took place at the end after subjects had been exposed to capsaicin multiple times in the same leg region (Appendix B: Suppl 6.6). As a result, the comparison of ongoing pain scores between the gabapentin session and the capsaicin-only session is not easily interpretable. Interestingly, pre-emptive gabapentin dosing does not have an effect on the development of dynamic mechanical allodynia (DMA) in this model. A single 900mg dose of gabapentin has been previously shown to reduce pain severity and

allodynia in patients with post-herpetic neuralgia (Berry and Petersen, 2005). The lack of efficacy against DMA may therefore reflect inadequacies in our model or in subject numbers.

Despite the evidence of incomplete behavioural efficacy, we identify distinct neural response patterns to gabapentin administration. We have previously reported that gabapentin suppresses hyperalgesia-related BOLD activity in the posterior insula and brainstem, when compared to placebo or ibuprofen (see Chapter 3). However, previous findings have also suggested that gabapentin's antihyperalgesic effect is predominantly represented neurally by its suppression of BOLD deactivation in a number of brain regions (Iannetti et al., 2005b). We corroborate these findings by showing that gabapentin suppresses stimulus related BOLD deactivations to allodynic stimuli- significantly in the medial prefrontal cortex, but also non-significantly in the precuneus, hippocampal formation and temporal lobes (Fig 6.5). We do not see any regions of decreased BOLD activity to the allodynic stimuli after gabapentin dosing. These findings suggest that in the gabapentin session, there is a reversal of changes in neural activity induced by pain behaviour- regions which show increases in response to pain decrease in activity, while regions which show decreases to pain increase in activity.

Deactivations in response to a range of stimuli have been commonly reported in a network of largely medial brain structures (including the medial prefrontal cortex, posterior cingulate, precuneus and parieto-temporo-occipital junction). Such signal decreases are task-independent, parametrically modulated and are thought to underlie a 'default mode' network, which is active at rest but deactivates to a goal-oriented task (Gusnard et al., 2001; Kong et al., 2010; McKiernan et al., 2003). While we see suppression of deactivation in part of this network in the gabapentin session when compared to placebo (Fig 6.5), the lack of a perceptual between-session difference in allodynia suggests a more

pertinent neural relevance for functional deactivations in the context of gabapentin dosing.

In light of these findings, we investigated the effect of gabapentin on cerebral blood flow, with the hypothesis that it may reverse blood flow changes elicited by a persistent pain state. We find that the brain response to mild persistent pain is represented by decreased perfusion in a network of pain-related brain areas including the thalamus, insula, hippocampus and anterior cingulate cortex (Fig 6.6C). Furthermore, the predominant effect of gabapentin on CBF in the capsaicin model is shown to be an increase in perfusion (or suppression of hypoperfusion) in several regions overlapping the network described above- including the insula, hippocampus and anterior cingulate cortex (Fig 6.6C). Analysis of mean grey matter CBF across session suggests that these effects are not attributable to global physiological effects of gabapentin (Fig 6.6B). In the literature, there is some evidence for gabapentin's reversal of pain-induced CBF change in two clinical reports (Ness et al., 1998; Wu et al., 2011). Gabapentin's effect on CBF in the hippocampal formation is also in line with in vitro studies suggesting its direct action on hippocampal cells (Cheng et al., 2006), and may be associated with its anxiolytic effects (Siok et al., 2009). Gabapentin's reversal of decreased perfusion may partially reflect the neural representation of decreased pain perception, or may be modulated in a different way to networks underlying increased perfusion to pain stimuli.

In the pain vs. baseline contrast, we find no regions of increased perfusion in response to pain. We previously identified widespread decreased perfusion together with more localised increased perfusion in response to a strong persistent pain stimulus (see Chapter 5). In the associated discussion, we proposed that the brain response to persistent pain is dominated by decreased perfusion but includes a more localised increase in perfusion in brain areas that respond directly to the pain stimulus. We confirm this by showing in

a ROI analyses that gabapentin suppresses perfusion in the region of the contralateral dorsal posterior insula shown to be active during strong persistent pain in a similar paradigm design (Fig 6.7). This suppression is further shown to be associated with pain reports (Fig 6.7), suggesting that the dorsal posterior insula provides a neural correlate for gabapentin-induced modulation of pain perception. The comparatively low CBF change seen in this study, and the need for a region of interest approach, may be explained by the lower intensity/percept of the baseline (placebo condition) pain stimulus when compared to the early pain state in the previous study.

These findings underline the significance of stimulus related deactivations and decreases in perfusion in the neural representation of pain. We parallel both phenomena in the modulation of acute and persistent pain by pre-emptive gabapentin dosing. While the default mode hypothesis is described for BOLD responses to brief stimuli, there is little understanding of the implications of decreased perfusion. Given that we report effects in a lower stimulus frequency condition (i.e. in a 'resting' pain state) than previously assessed in experimental pain paradigms, it is less likely that the regions where decreased perfusion is evident are subserving an immediate shift in subjective focus. This challenges the view that pain related decreases in perfusion are an epiphenomenon of alterations in attention (Owen et al., 2012; Thunberg et al., 2005), and suggests a potential functional relevance for hypoperfusion in the assessment of pain and its pharmacological modulation.

In conclusion, the quantification of perfusion changes provides an exciting opportunity to assess pain perception and analgesic effects. A major challenge is that current healthy human models of persistent pain do not allow assessment of strong persistent pain stimuli over long time frames. This is problematic for the inherently low-SNR ASL technique, and at this stage means it may be suboptimal for direct assessment of pharmacological

efficacy using experimental models. However, CBF abnormalities in default-mode regions have been suggested to be predictive of inter-individual gabapentin responsiveness in fibromyalgia patients (Usui et al., 2010). Quantifying the neural response to persistent pain and its analgesic modulation will be important in defining the mechanisms underlying responsiveness to treatment in neuropathic pain conditions.

# Chapter 7

# Investigating the Neural Correlates of Transcranial Direct Current Stimulation (TDCS) therapy in Phantom Limb Pain

In the previous chapters, we have validated the use of fMRI techniques for evaluating the potency of analgesics in a healthy human model of central sensitisation. In this chapter we will use these techniques to assess the efficacy of a novel neuro-stimulatory therapy for the treatment of neuropathic pain in a cohort of phantom limb pain patients. We aim to validate the behavioural efficacy of this treatment, and to demonstrate the sensitivity of fMRI to the neural representation of any analgesic effect.

## 7.1 Introduction

Amputation of a limb is usually followed by the continued perception of the missing limb in affected individuals. This perception manifests as largely ubiquitous non-painful kinaesthetic 'phantom sensations', as well as chronic painful sensations that are reported by up to 80% of amputees (Nikolajsen, 2013; Weeks et al., 2010). Phantom limb pain (PLP) is distinct from pain arising from the remaining part of the limb (stump pain) and

is likely mediated by a separate neural mechanism (Flor et al., 2006). PLP is unresponsive to many conventional pain management approaches and can lead to a significantly impoverished quality of life (Knotkova et al., 2012; Lindner et al., 2010). Over the past few decades, increasing understanding of the peripheral and central mechanisms underlying the development of this condition has highlighted potential innovative interventions aimed at alleviating PLP. Further, PLP has become an important model for studying plasticity-driven chronic pain in a range of symptomatic pain conditions such as complex regional pain syndrome and back pain (Gustin et al., 2012).

### 7.1.1 Pathophysiology of phantom limb pain

PLP is a neuropathic pain syndrome that occurs secondary to amputation or deafferentation. PLP is more common in females, upper limb amputees and individuals with pre-existing or pre-operative pain (Bosmans et al., 2010; Flor et al., 2006). Pain onset can be immediate following amputation or after several years (Nikolajsen, 2013). Furthermore, PLP is more frequent when amputation occurs in adulthood, less common when amputation occurs in childhood and very rare in congenital amputees. The influence of emotional factors such as depression has also been reported (Ephraim et al., 2005).

The development of pain following amputation is thought to involve both peripheral and central pathophysiological mechanisms. Peripheral mechanisms may include aberrant ectopic discharges from stump neuromas (swellings of nerve terminals and axonal sprouting) and dorsal root ganglion neurons that act to maintain spontaneous pain and abnormal evoked pain (Flor et al., 2006; Fried et al., 1991; Nikolajsen, 2013; Wall and Gutnick, 1974). However anaesthetic blockade or removal of peripheral neuromas only eliminates spontaneous and evoked pain related to the stump and not necessarily PLP

(Birbaumer et al., 1997; Nikolajsen et al., 2010; Nyström and Hagbarth, 1981), indicating the involvement of more central mechanisms.

In the central nervous system, spinal mediated central sensitisation can be triggered by nerve injury in animals (Woolf, 2011) and may have a role in PLP in humans, although direct evidence is lacking. The prevailing theory of a central contribution to the development of PLP is that of supraspinal (largely cortical) maladaptive plasticity. This view purports that the deprivation of sensory input following amputation results in striking brain plasticity, where primary sensorimotor (M1/SI) representations of cortically neighbouring body parts (e.g. face) take over the area previously devoted to the missing limb (Knotkova et al., 2012; Pons et al., 1991). Such cortical reorganisation has been shown to be correlated with PLP (Flor et al., 1995, 2006; Lotze et al., 2001) and is proposed to trigger sensory and pain representations in the missing hand by responding to inputs to the neighbouring cortical regions (Flor et al., 2006; Ramachandran et al., 1992). Such central reorganisation may also be influenced by peripheral factors such as aberrant neuroma firing and C-fibre loss (Calford and Tweedale, 1991; Spitzer et al., 1995).

Interestingly, a recent study from our group has challenged the role of maladaptive plasticity in the development of PLP (Makin et al., 2013). While the maladaptive plasticity model would predict decreased cortical representations of the phantom hand in individuals with more severe PLP, the authors showed the opposite effect with phantom hand movements in unilateral upper limb amputees. Further, they showed that phantom hand representation in the amputee group was similar to non-dominant hand representation in a control group, although the amputee group showed structural degeneration of the phantom cortex. This suggests that cortical representations of the phantom hand are not only maintained in PLP (also see Bogdanov et al. (2012); Raffin et al. (2012b)), but

also indicate more severe pain. Therefore, the decrease in phantom limb representation during cortical remapping may not be maladaptive as it is associated with decreased PLP perception.

Using functional connectivity analyses of resting state scans, Makin and colleagues (2013) also demonstrate reduced inter-hemispheric connectivity between the phantom and intact hand areas in amputees, as compared to healthy controls- perhaps due to the lack of co-activation between both intact and deprived cortices following amputation. This decreased connectivity was further shown to be associated with higher PLP scores. The 'persistent representation' model proposed by Makin and colleagues (2013) therefore suggests that both sensory deprivation and phantom pain experience have modulatory effects- sensory deprivation is associated with decreased local functional and structural representations, while coexisting phantom pain experience is associated with maintained local cortical representations and functional inter-hemispheric decoupling.

The major limiting factor to the development of effective treatments for PLP is the poor understanding of its underlying causes (Knotkova et al., 2012). By targeting these newly defined disease mechanisms, we may be able to provide novel therapies for PLP.

### 7.1.2 Stimulation induced plasticity as an intervention in PLP

Current pharmacological, physical and surgical treatment approaches to PLP only provide partial relief and often cause significant side-effects due to the non-specific nature of their neural targeting. More recently, behavioural therapies aimed at normalising the representation of the phantom hand, show partial short-term symptomatic benefit (Moseley and Flor, 2012). Non-invasive brain stimulation techniques such as transcranial direct current stimulation (tDCS) provide a means by which such representations

can be modulated safely.

TDCS alters cortical excitability by delivering a low-intensity electric current (1-2 mA) through the skull to the underlying cortex via two large electrodes powered by a battery. Its effects are polarity dependent (Nitsche and Paulus, 2000), with the 'active' electrode placed on the scalp overlying the cortex (e.g. M1) and the 'return' electrode typically placed above the contralateral supraorbital ridge. Anodal stimulation is facilitatory, leading to neuronal depolarisation and decreases in GABA; conversely cathodal stimulation leads to hyperpolarisation of neurons and diminished cortical excitability (Nitsche et al., 2005; Stagg et al., 2009). Stimulatory effects of tDCS are due to polarity-dependent shifts in the resting membrane potential while lasting effects may be mediated by long-term potentiation and inhibition (Stagg and Nitsche, 2011). Notably, current modelling and field estimation of the spatial distribution of tDCS has suggested its effects to be widespread in cortical and subcortical structures (Parazzini et al., 2011). The after effects of tDCS stimulation are typically brief following a single session but are longer-lasting with serial stimulation paradigms.

The mechanisms underlying the maladaptive changes seen in phantom limb pain may be related to a loss of GABAergic inhibition (Lefaucheur et al., 2006), glutamate-mediated long-term potentiation-like changes (Zhuo, 2012) and structural alterations such as axonal sprouting. These mechanisms can therefore be directly targeted using tDCS therapy (Stagg and Nitsche, 2011). As well as its role in motor learning and plasticity across a range of neuropathological conditions (e.g. stroke, tinnitus) (Stagg et al., 2012; Vanneste et al., 2010), tDCS has also been shown to have some efficacy in chronic pain (Antal et al., 2010; Lefaucheur et al., 2008). A recent study has also reported short-lasting analgesia in PLP after a single session of passive anodal tDCS (2mA, 15 minutes) to the deprived sensorimotor cortex in a small cohort of phantom limb pain patients (Bolognini

et al., 2013). The neural correlates of such analgesia remains to be investigated.

Given the ease of tDCS application, its low cost, and established safety, this technique offers a promising and attractive method by which to modulate cortical plasticity in chronic neuropathic pain, with the aim of alleviating pain.

## 7.2 Aim

In this study we aimed to test whether modification of cortical representations in phantom limb patients can effectively reduce PLP and to assess the neural mechanisms and representation underlying any analgesia. We use a pseudo-randomised, double-blind, sham-controlled crossover design to assess the effectiveness of tDCS therapy against PLP.

TDCS has been particularly successful at inducing long-term gains in learning when combined with a behavioural task (Cohen Kadosh et al., 2010). Interestingly, amputees have been reported to have motor control over their phantom hands (Reilly et al., 2006), which has been demonstrated by detection of stump contractions (using electromyography) and motor cortex (M1) activation (using fMRI) to be separate from imaginary movements (Raffin et al., 2012a,b). We therefore performed tDCS while asking amputees to execute a range of movements with their phantom hands, allowing us to target appropriate neural pathways.

Following from previous findings by Makin and colleagues (2013) and Bolognini and colleagues (2013), we use three separate montages to target putative pain mechanisms:

1) Anodal tDCS to M1/SI of the intact cortex, to increase interhemispheric connectivity between primary sensorimotor cortices.
2) Cathodal tDCS to M1/SI of the deprived cortex, to decrease maintained phantom hand representation.
3) Anodal tDCS to M1/SI of the deprived cortex, as is shown to be effective at relieving PLP in a single session by Bolognini and colleagues (2013).

We used fMRI (in particular ASL) for detecting both the presence of and neural mechanism underpinning any analgesic effect of tDCS therapy in PLP, in addition to a range of behavioural measures and pain reporting.

## 7.3 Methods

### 7.3.1 Subjects

Eleven unilateral upper limb amputees (mean age ± s.e.m. = 44.27 ± 0.93, four right-arm amputees) completed the study. All participants were recruited through the Oxford Centre for Enablement and Opcare. The amputees comprised a heterogeneous population with different causes of amputation and different time periods since amputation (see Table 7.1). Approval was granted by the NHS National Research Ethics Service and written informed consent was obtained from all subjects.

Amputees were regarded as suitable to participate if they fulfilled the following inclusion criteria: 1) between 18 to 70 years of age; 2) unilateral upper-limb amputation, undergone at least 6 months before study enrolment; 3) frequent presence of phantom limb pain in the preceding month (more than once a week).

Exclusion criteria were: 1) simultaneous enrolment in other brain stimulation experiments; 2) use of medication known to effect GABA receptors in the brain. 3) contraindications to tDCS or MRI as according to MRI and tDCS safety guidelines.

Subjects that were perceived as having an increased theoretical risk of seizure from tDCS (i.e., due to specific medication intake) consulted with a medical doctor prior to being enrolled in the study.

### 7.3.2 Experimental design

Subjects attended four identical sessions separated by at least 1 week, each lasting around 4 hours and consisting of behavioural testing prior to and following MRI scanning with concurrent tDCS stimulation (see Fig 7.1). The tDCS montage used for the sessions was pseudo-randomised between anodal to the ipsilateral/intact M1/S1 (AI), anodal to the contralateral/deprived M1/SI (AD), cathodal to the deprived M1/S1 (CD), and sham stimulation to the intact M1/S1 (SI). Both the experimenter and subject were blinded to the treatment.

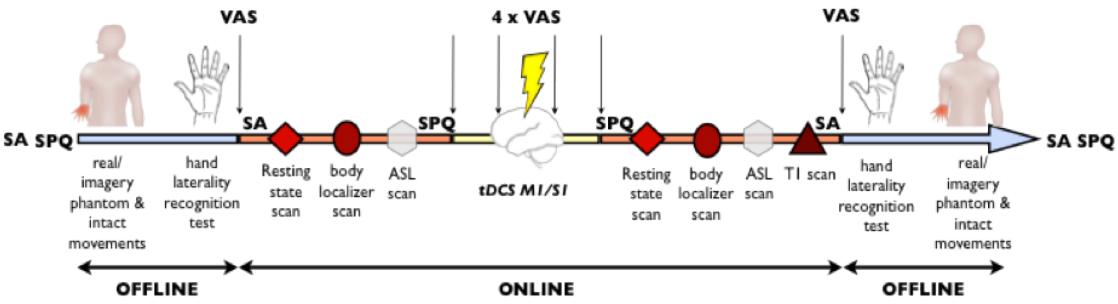


Figure 7.1: **Experimental setup for a single session.** SA- state anxiety questionnaire; SPQ - short pain questionnaire; VAS - visual analogue scale; ASL, arterial spin labelling; online - inside MRI scanner; offline - outside MRI scanner. Pain thresholds were also tested using punctate probes at the start and end of each session (not shown).

### 7.3.3 Questionnaires

Prior to the first experimental visit, subjects completed a detailed questionnaire to record details of amputation (cause of amputation, time since amputation, amputation level), PLP features, stump pain features, features of non-painful phantom limb sensation, prosthesis use, and any other subjective descriptions related to the phantom limb. Subjects also completed a PainDETECT questionnaire (Freynhagen et al., 2006) to assess whether there were neuropathic elements to their pain.

During each session, subjects completed four state anxiety questionnaires (SA) (Spielberger, 1983) - on arrival, at the start of scanning and at the end of scanning (while lying in the scanner), and at the end of the session, to measure changes in anxiety that may influence pain perception (Ploghaus et al., 1999) (see Fig 7.1).

Analysis of these questionnaires is not discussed in this thesis, as preliminary results showed no significant differences across treatments.

### 7.3.4 Pain ratings

Prior to the first session, subjects were asked to rate the maximum intensity of painful sensations of the phantom hand and stump as well as the intensity of non-painful sensations of the phantom hand, as experienced in a typical week prior to study onset (scale 0 - 100; no pain at all - worst pain imaginable). Chronic phantom and stump pain magnitude was calculated by dividing worst pain intensity by pain frequency (1- all the time; 2- daily; 3- weekly), as performed by Makin and colleagues (2013).

Ongoing pain ratings were recorded in three ways- by text message, with short pain questionnaires and with visual analogue scales. Daily pain fluctuations were recorded

Table 7.1: **Amputee clinical details.** For 11 amputees studied (numbered A01-A11). Amp., amputation; telesc., telescoping; amputation level: 5- wrist; 4- below elbow; 3- through elbow; 2- above elbow; 1- through shoulder; Side- missing hand side; dominant-dominant hand prior to amputation; phantom pain magnitude- worst phantom pain experienced in a typical week prior to study onset /frequency (1- all the time; 2- daily; 3- weekly). R, right; L, left; Y, yes; N, no.

| | Age | Age at amp. | Amp. level | Side/ Dominant | Chronic phantom pain magnitude | Chronic stump pain magnitude | Voluntary finger mov. | Telesc. | Brachial plexus injury | Cause of amp. |
|---|---|---|---|---|---|---|---|---|---|---|
| A01 | 47 | 27 | 2 | R/R | 45 | 0 | Y | N | Y | Trauma |
| A02 | 23 | 18 | 4 | R/R | 25 | 0 | Y | Y | N | Trauma |
| A03 | 49 | 18 | 2 | L/R | 50 | 0 | Y | Y | Y | Trauma |
| A04 | 48 | 44 | 2 | L/L | 70 | 10 | Y | N | N | Tumour |
| A05 | 46 | 17 | 2 | L/R | 15 | 3.3 | Y | Y | | Trauma |
| A06 | 45 | 37 | 4 | L/R | 92 | 0 | Y | Y | N | Trauma |
| A07 | 55 | 19 | 5 | L/L | 70 | 0 | Y | N | N | Trauma |
| A08 | 40 | 27 | 2 | R/L | 80 | 26.7 | Y | Y | Y | Trauma |
| A09 | 54 | 53 | 2 | L/R | 10 | 20 | Y | Y | N | Vascular disease |
| A10 | 28 | 23 | 1 | L/R | 26.7 | 5 | Y | Y | Y | Trauma |
| A11 | 52 | 28 | 4 | R/L | 35 | 10 | Y | Y | N | Trauma |

via responses to automated text messages twice a day over a 6 week period (starting 1 week before the first session and ending one week after the final session). At 10am, subjects were instructed to rate the pain they felt 'at this moment in time' (0-100; 'No pain at all' - 'Worst pain imaginable'); while at 8pm subjects were asked to give their average, minimum and maximum PLP intensity ratings for the day.

Short pain questionnaires (SPQ) were used to record subjects' verbal ratings (0-100) of ongoing phantom sensation, stump pain and phantom limb pain. The SPQ was completed at four timepoints in each session- at the start of the session, just prior to tdcs, just after tdcs, at the end of the session (about 90 minutes after tDCS onset) (Fig 7.1). Computerised visual analogue scales (VAS) were used to assess ongoing phantom limb pain magnitude (anchors: 'No pain at all', 'Worst pain imaginable'). These were assessed at several timepoints- at the start of the scanning, during tDCS (x4) and at the end of scanning (Fig 7.1).

In this thesis we will focus on data from the SPQ, for which the most complete dataset was collected. Although the computerised VAS allowed assessment of PLP intensity during the scanning phases when we could not speak to the subjects, it was more difficult for subjects to use; several subjects reported that they were unable to manipulate the visual display adequately in the time provided. These computerised scales are also likely to be less directly comparable to other numerical/verbal pain ratings collected (i.e. text messages and chronic pain magnitude).

### 7.3.5 Behavioural measures

A range of behavioural measures were also collected (see Supplementary Methods in Appendix C) but these do not directly address the effect of tDCS on ongoing pain

perception and so do not fall under the scope of this thesis.

### 7.3.6 Transcranial direct current stimulation

A DC-Stimulator (Magstim) was used to deliver electric current to the brain via two 5 x 7 cm electrodes (Easycap), fitted with 5 kΩ resistors for safe use in the MRI environment. High-chloride electrolyte EEG gel was used as a conducting medium between the scalp and electrodes. Electrode position was determined according to the EEG 10-20 system. For anodal stimulation centred over M1/S1, the anodal electrode was positioned 5 cm lateral to $C_z$ (corresponding to C3/C4), with the cathode electrode placed over the contralateral supraorbital area. For cathodal S1/M1 stimulation, the cathodal electrode was positioned 5 cm lateral to $C_z$, with the anode over the contralateral supraorbital area. TDCS stimulation lasted 20 minutes (fade-in/fade-out phases = 10 s), with an intensity of 1 mA. We use a 1mA current in conjunction with a longer stimulation period given recent concerns about the effectiveness of blinding with 2mA intensities (O'Connell et al., 2012). Similar electrode arrangement and stimulation parameters were used for sham tDCS as in the anodal tDCS montage, but the stimulator was turned off after the impedance was stable (after approximately 30 s).

### 7.3.7 fMRI acquisition

In this thesis, we will focus on the ASL scan data as it is most relevant to verifying the utility of fMRI for detecting changes in the perception of spontaneous pain. All other scan protocols are described in the Supplementary Methods (Appendix C).

ASL scanning used the resting scan protocol exactly as described in Chapter 4. Two scans were performed (prior to tDCS and 20 minutes after tDCS ended) while subjects

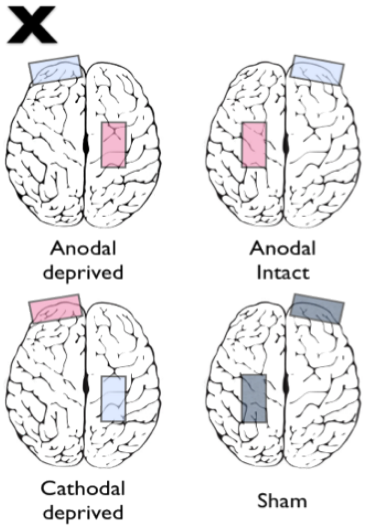


Figure 7.2: **tDCS setup for various sessions.** X - amputation side; red - anodal electrode; blue - cathodal electrode; grey - sham electrode.

were instructed to stay awake and focus on a fixation cross projected on the screen.

A high-resolution T1-weighted anatomical image (TR: 2040 ms; TE: 4.7 ms; flip angle 8; voxel size: 1mm isotropic resolution) was acquired for registration. Field maps were obtained in order to reduce spatial distortion of the EPI and multiband images.

### 7.3.8 Analysis of pain ratings

Statistical analysis was carried out using SPSS version 21. As PLP generally decreases once participants enter the MRI scanner and increases during the performance of phantom movements, PLP ratings were contrasted with ratings acquired in the sham condition to control for these general effects. The pain ratings were not expected to be normally distributed, because of large variability in PLP experiences across subjects. The Shapiro-Wilk test was used to test for normality and indeed revealed a violation of

the normality assumption ($p<0.05$). Analysis of PLP relief was thus carried out using non-parametric statistical tests. A two-tailed related-sampled Friedman's two-way analysis of variance by ranks was used to investigate potential baseline differences (both raw and controlled values). Pain relief following each stimulation protocol was investigated using non-parametric related-samples Wilcoxon Signed Rank Tests.

### 7.3.9 ASL analysis

Due to scanner malfunction and time restraints, both pCASL images were not collected in three sessions (two anodal deprived (AD) sessions, one cathodal deprived (CD) sessions).

For subjects A01, A02, A08 and A11, raw perfusion images (and structural images) were flipped along the x-axis, such that the right cortex represented the deprived cortex while the left cortex represented the intact cortex for all subjects. PCASL images were pre-processed and quantified as described in Chapter 4. All CBF map outputs from quantification were registered to MNI space (see Chapter 4) and concatenated to generate a CBF timecourse for the entire experimental period. For paired comparisons between scan blocks, averaged CBF maps were also generated for all scan blocks for each subject using a mixed effects model.

To compare CBF changes induced by tDCS, a paired t-test was performed between the pre-tdcs and post-tdcs scans using a mixed effects linear model across all subjects. Statistical significance was determined by performing cluster correction at a Z threshold of 2 and significance of $p<0.05$. CBF values were extracted from a conjunction region between functionally active voxels and appropriate anatomical masks taken from the Harvard-Oxford cortical and subcortical atlases.

In order to explore the relationship between regional CBF, pain ratings, and subject demographics, pairwise correlations were performed. Non-parametric statistics (Spearman's rank-order correlation) were used where the assumptions of normality were violated (Shapiro-Wilk test, $p<0.05$).

## 7.4 Results

### 7.4.1 Changes in pain scores

There was no significant difference between the raw pre-tDCS pain ratings either offline (Friedman $X_2(3,10) = 1.209$, $p = 0.75$) or in the scanner (Friedman $X_2(3,10) = 6.389$, $p = 0.10$), indicating no consistent deviations in baseline pain rating across stimulation sessions.

In a paired comparison controlling for sham effects, phantom limb pain was significantly decreased following anodal tDCS to deprived M1/S1 (AD) ($Z(9) = -2.209$, $p = 0.03$) and a weak trend in pain reduction was observed following cathodal tDCS to deprived M1/S1 (CD) ($Z(10) = -1.604$, $p = 0.11$) (Fig 7.3). This effect of tDCS on pain relief disappeared after approximately 70 minutes (AP: $Z(10) = -0.845$, $p = 0.40$; CP: $Z(9) = -0.406$, $p = 0.68$) (Fig 7.3).

Anodal tDCS to intact M1/S1 (AI) did not cause a significant difference in pain immediately after ($Z(9) = -.281$, $p = 0.78$) or 70 minutes following tDCS therapy ($Z(9) = -0.595$, $p = 0.55$).

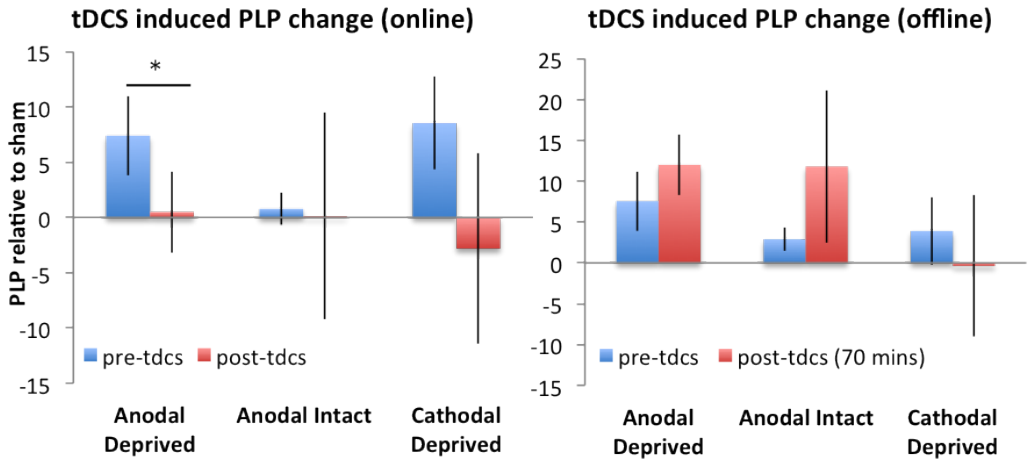


Figure 7.3: **tDCS induced change in phantom limb pain (PLP).** Measured using a verbal numerical rating scale (0-100) as part of the short pain questionnaire. Normalised to sham session (stimulation - sham). * $p<0.05$, Online- inside the scanner, Offline- outside the scanner. Error bars represent SEM

### 7.4.2 Cerebral blood flow changes

In paired t-tests comparing the effects of tDCS stimulation across the whole brain (post versus pre scans), there was no significant effect of SI stimulation or CD stimulation on CBF ($p>0.05$).

Following AD stimulation, we report a decrease in CBF in the posterior insula, secondary somatosensory cortex and hippocampus ipsilateral to the amputated limb (contralateral to stimulation site) (Fig 7.4). CBF values extracted from these functional regions in stimulation and sham sessions are displayed for illustration purposes. We also report a decrease in CBF following AI stimulation in the secondary somatosensory cortex and supramarginal gyrus, contralateral to the amputated limb (contralateral to stimulation side) (Fig 7.4A). These changes did not survive when an ANOVA between stimulation condition and sham was performed (not shown).

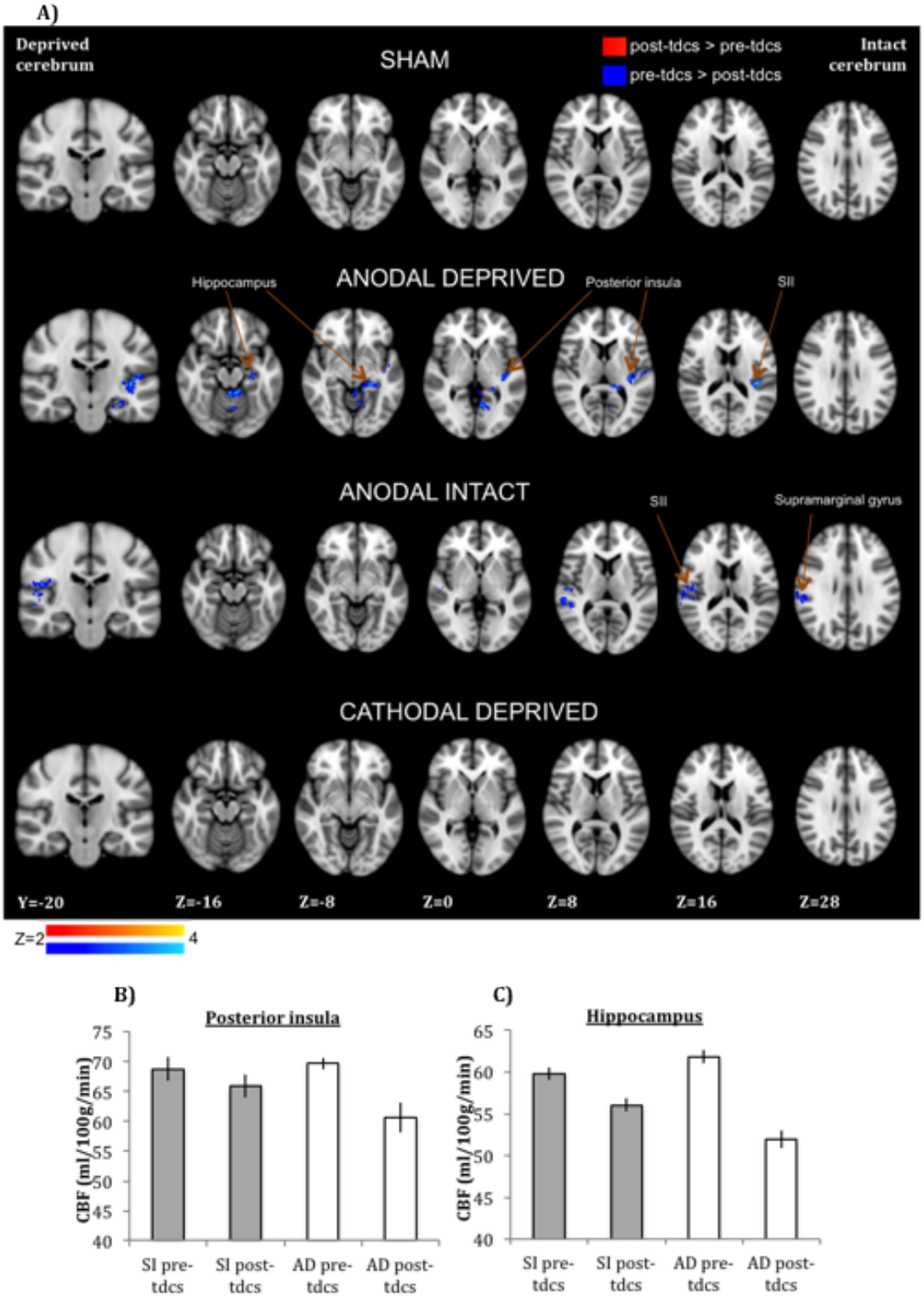


Figure 7.4: **tDCS induced change in cerebral blood flow.** Mixed effects, Z=2 p<0.05. A) shows changes induced by each tDCS stimulation montage- sham (n=11), anodal deprived (n=9), anodal intact (n=11), cathodal deprived (n=10); B) and C) illustrates CBF measurements in functional ROIs defined from the ADpre>ADpost contrast (masked by anatomical masks).

### 7.4.3 Correlations between variables

To test the relationship between decreases in subjective pain scores and AD tDCS induced CBF decreases in the posterior insula and hippocampus, we extracted the sham controlled CBF change (ADpre-post - SIpre-post) in the two regions. We show that there is no significant correlation between PLP relief and CBF decrease in the posterior insula (Spearman's r(7)=0.48 p=0.19) or hippocampus (Spearman's r(7)=0.39 p= 0.30).

Length of time since amputation may reflect many different variables (e.g. stump and prosthetic usage, remaining function of the phantom cortex and in turn effectiveness of stimulation) contributing to the overall variability across participants. Therefore, we further tested the effect of time since amputation on subjective pain relief and on AD tDCS induced CBF changes in the posterior insula and hippocampus. We report that subjects who have had their amputation for a shorter time have significantly more reduced CBF in the hippocampus (Pearson's r(7)=-0.836, p<0.01) following AD tDCS. We also observed a similar trend towards a relationship between time since amputation and CBF change in the posterior insula (Pearson's r(7)=-0.58, p=0.10). There was no significant effect of time since amputation on subjective pain relief (Spearman's r(9)=-0.085, p=0.81) or chronic phantom pain magnitude (Spearman's r(9)= 0.078, p=0.84).

## 7.5 Discussion

We show that anodal tDCS to the deprived cortex is effective at reducing phantom limb associated pain and that this may be reflected by neural blood flow changes in the posterior insula and hippocampus.

### 7.5.1 Changes in pain scores

A growing body of evidence suggests that anodal tDCS to the M1 hand area is efficacious against chronic neuropathic pain syndromes (Antal et al., 2010; Fregni et al., 2007; Lefaucheur et al., 2008). However only a single study to date has directly assessed this effect in amputees with phantom limb pain. Bolognini and colleagues (2013) reported that a single session of passive anodal tDCS (2mA, 15 minutes) to the deprived motor cortex led to a significant short-lasting decrease in the magnitude of phantom limb pain. Although the tDCS sessions were separated by only 3 hours, and the small cohort of 8 amputees (comprising of 7 lower limb amputees) were on medications that interacted with tDCS, these results provided preliminary evidence that AD tDCS may be an effective therapy against PLP. Our results corroborate these early findings in a well-controlled study of a larger group of upper limb amputees without interacting medications. In line with the aforementioned study, we also report a short-lasting pain relieving effect, which disappears by 70 minutes post stimulation. Our use of an active stimulation protocol, where subjects performed phantom movements that increased PLP in some cases, limits our interpretation of the reported analgesic effect to an interaction between stimulation and sham sessions. However, this effect together with previous findings suggests that AD tDCS is an appropriate potential treatment for more targeted serial use against PLP.

Although we hypothesised that we could reduce PLP by reinstating the deprived cortex into the sensorimotor network (with AI tDCS), this treatment appears to have no efficacy in our cohort. This may be because we were ineffective at increasing the functional connectivity between both sensorimotor cortices, or it may indicate that restoring their connectivity does not have an analgesic effect. Further investigation of the functional association between the cortices will enable us to elucidate this. We also hypothesised that abolishing the maladaptive representation of the phantom hand (with CD tDCS) would reduce PLP. Cathodal tDCS has also been shown to reduce experimentally induced

pain when delivered to the somatosensory cortex contralateral to the pain stimulus (Antal et al., 2008). We do not observe changes in CBF here, but we note a trend in pain relief, suggesting that there may be an analgesic effect to be realised with a larger subject cohort.

### 7.5.2 Neural changes detected by ASL

Anodal tDCS to M1 increases cortical excitability and its more general analgesic effects have been associated with direct restoration of defective intracortical inhibitory processes (Antal et al., 2010; Lefaucheur et al., 2006) or indirect effects on other pain modulating structures such as the thalamus (Lang et al., 2005; Polanía et al., 2012). Therefore the reduction in PLP following AD tDCS may reflect these general effects, or may be associated with mechanisms more specific to PLP. While some authors have suggested that an increase in the motor representation of the phantom hand may lead to this decrease (Bolognini et al., 2013), recent findings suggest that this could have the opposite effect (Makin et al., 2013). Nevertheless, no studies have directly assessed the neural representation of tDCS therapy against PLP.

Following AD tDCS, we report cerebral blood flow decreases in the posterior insula, secondary somatosensory cortex (SII) and hippocampus contralateral to the stimulation side. Given that we also report decreases in the contralateral SII following AI tDCS, it is possible that SII decreased perfusion may reflect a more general effect of anodal tDCS to the sensorimotor area. CBF decreases in the posterior insula and hippocampus may therefore indicate changes associated with pain relief or with plasticity specific to PLP. While there is no significant association between these CBF decreases and pain relief across subjects, a moderate correlation is seen for the posterior insula. A wealth of evidence, including our previous findings in Chapter 5, suggests that the posterior

insula may be an appropriate region to serve as a biomarker for nociceptive-driven pain perception (see Chapter 5 discussion). Although the relative peripheral and central contributions to PLP are as yet unknown, our findings of reduced CBF in the posterior insula may reflect decreased pain perception resulting from top-down modulation by stimulation induced cortical plasticity. The potential mechanisms of plasticity underlying this analgesic effect are not explored in this thesis but will be an important subsequent investigation.

The hippocampus is also an important limbic region, which is structurally altered in persistent pain (Duric and McCarson, 2006; Mutso et al., 2012), and is associated with pain-related anxiety (Bingel et al., 2011; Ploghaus et al., 2001). Its role in PLP may therefore be more associated with plasticity and affective aspects of pain perception, as compared to sensory aspects coded by the posterior insula. Interestingly, we report that subjects who had their amputations more recently had more reduced CBF in the hippocampus following anodal stimulation to the deprived cortex. Notably, this does not appear to reflect changes in chronic pain magnitude with time following amputation. Given the importance of the hippocampus in learning and memory, the effects of AD tDCS may be dependent on the development of amputation related neural plasticity in this region over time.

### 7.5.3 Limitations

The first major limitation of this study is the small sample size; studying more amputees will be important to validate our current findings and to reveal any underlying trends.

Another key limitation of our study is the use of an active stimulation protocol during which subjects performed movements that increased their phantom pain. As a result, our

findings by necessity reflected the interaction between the sham and stimulation sessions to elucidate any therapeutic effects. Given that there was no apparent effect of AI tDCS (for which active stimulation was essential to increase bi-hemispheric sensorimotor connectivity), the use of passive stimulation may be more appropriate in future studies with AD or CD tDCS.

Finally, we report a short lasting analgesic effect following single session therapy; to assess the clinical viability of such therapy in patient groups, it will be important to test the effects of multiple tDCS sessions (Monte-Silva et al., 2012).

### 7.5.4 Conclusions

The findings reported above suggest that tDCS to the anodal deprived cortex is an effective and promising treatment for phantom limb pain. Importantly, we show that the ASL technique can measure the neural representation of this analgesic effect and that this is reflected in the secondary somatosensory cortex, posterior insula and hippocampus.

Future work will help elucidate the mechanisms underlying this analgesic effect and optimise the use of AD tDCS as a therapy in PLP.

# Chapter 8

# Conclusion

This thesis has focused on the use of fMRI as a tool to investigate the neural correlates of acute and persistent pain, and its modulation using pharmacological and non-invasive neuromodulatory interventions. We have validated the utility of neuroimaging techniques for defining a neural biomarker, against which the efficacy of analgesic therapies can be tested. This improves our knowledge of the mechanistic basis of neuropathic conditions, and is important for development efforts aimed at identifying successful novel treatments against chronic pain.

## 8.1 Thesis overview

Previous findings have highlighted the importance of supraspinal involvement in the development of pain-related hypersensitivity following nerve injury in animals (De Felice et al., 2011; Porreca et al., 2002; Woolf, 2011). Work has also defined a healthy human brainstem correlate of such phenomena (Iannetti et al., 2005b; Lee et al., 2008; Zambreanu et al., 2005). However, prior to this thesis no study had directly challenged the use of this neural 'biomarker' to detect the pharmacological efficacy of an analgesic effective in neuropathic pain, when controlled with an ineffective active compound. Moreover, the development of clinically viable therapies has in part been hindered by the lack

of appropriate experimental models for persistent pain (Blackburn-Munro, 2004); while persistent pain is the primary complaint in neuropathic pain and the primary outcome measure used in most clinical trials (Backonja and Stacey, 2004; Finnerup et al., 2010). Importantly, few studies have attempted to translate the utility of pain-related neural changes as therapeutic markers from healthy populations to neuropathic patient groups. This thesis set out to address these important issues.

In an initial set of experiments described in Chapter 2, we optimised BOLD fMRI analysis and acquisition methods for imaging the supraspinal correlates of pain by applying physiological noise modelling (PNM) to an axially oriented acquisition protocol. We further confirmed the suitability of the topical capsaicin model of central sensitisation (CS) for assessing the behavioural and neural correlates of hypersensitivity and spontaneous persistent pain in a crossover design. In the first study directly comparing the merits of 7T over 3T whole-brain imaging of pain hypersensitivity using PNM, we identified immediate cortical benefits of improved z-statistics with ultra-high field imaging. As the subcortical benefits of 7T imaging at this stage were not overwhelming, and access difficult, we decided to use the 3T for the subsequent experiments. Further sequence optimisation will be required to reduce the effect of increased distortions in the inferior brain at 7T and subsequently to improve imaging of subcortical structures.

By combining the topical capsaicin model with optimised imaging parameters in a double-blind placebo-controlled crossover paradigm in Chapter 3, we tested the pharmacological modulation of hyperalgesia-related BOLD activity in the midbrain, which had been previously shown to be specifically associated with CS (Lee et al., 2008). Our findings validated that fMRI can be used to detect the efficacy of an analgesic which is effective against neuropathic pain (gabapentin) when compared to an analgesic which has no proven efficacy against neuropathic pain (ibuprofen). Furthermore, we demon-

strate that the use of fMRI is more sensitive than subjective reports for assessing such efficacy. These findings support the use of neuroimaging in the early phase of pharmacological development, to confirm the mechanistic and pharmacodynamic action of novel compounds in humans, before larger scale clinical trials (Chizh et al., 2008; Wartolowska and Tracey, 2011; Wise and Preston, 2010).

Having demonstrated the utility of BOLD fMRI for the assessment of drug potency against evoked hypersensitivity associated with neuropathic pain, we then developed and optimised a novel arterial spin labelling (ASL) imaging and analysis pipeline for the assessment of tonic states (e.g. persistent pain) in Chapter 4. The use of a multi-inversion time pseudo-continuous ASL (pCASL) sequence enabled accurate estimation and quantification of absolute cerebral blood flow (CBF) across the whole brain (Chappell et al., 2010). We were therefore able to optimise an fMRI pipeline for resting and long visual activation states that is adequately sensitive and highly reproducible across several timepoints, supporting its application in the imaging of persistent pain states.

Using the optimised pCASL pipeline developed in Chapter 4 together with the topical capsaicin model of tonic/persistent pain validated in Chapter 2, we were able to directly investigate the neural correlates of a mutable C-fibre nociceptor-driven persistent pain experience in Chapter 5. A wealth of past and recent convergent evidence has suggested a key role for the posterior insula and adjoining medial operculum in the encoding of sensory aspects of pain perception (Craig, 2013; Garcia-Larrea, 2012). In this study, we confirmed this hypothesis by quantifying significant changes in CBF in this region in association with moderate persistent pain, and by demonstrating that this region is the only brain area where CBF is correlated with changing pain percept over a 3-hour experimental timecourse. Our findings also attest to the importance of the anterior insula in more general interoception and state awareness (Craig, 2009); we show that

activity in the anterior insula in relation to persistent pain is binary and not correlated to pain percept. Given that the region remains active when the affective valence of the stimulus is switched from pain to relief by cooling, we propose that its role is likely related to high order homeostatic monitoring. Interestingly, we also report that a region of the dorsolateral prefrontal cortex (DLPFC) is anti-correlated to the perception of persistent pain. This is in line with findings that suggest a vital role for the DLPFC in top-down pain inhibition (Boggio et al., 2008; Lorenz et al., 2003).

In the two experiments described in Chapter 6, we used the ASL technique to investigate the physiological basis underlying pain vulnerability, and to assess the pharmacological modulation of persistent pain from topical capsaicin. Previous animal studies have highlighted a role for bidirectional pain modulation from the periaqueductal grey (PAG) and rostral ventromedial medulla (RVM) in the maintenance of spontaneous pain and hyperalgesia (De Felice et al., 2011; Wang et al., 2013), and likely the development of chronic neuropathic pain states (Heinricher et al., 2009; Suzuki et al., 2004). We performed the first study in humans assessing the role of baseline activity in the PAG on subsequent development of spontaneous pain and hyperalgesia. Our findings suggest that higher baseline activity in the PAG as indicated by increased CBF is associated with greater vulnerability to spontaneous pain and hyperalgesia following CS related injury. We further demonstrated that increased vulnerability is associated with decreased PAG CBF in the pain state, suggesting that PAG CBF may in part reflect descending pain inhibitory drive. These important findings provide a basis for further assessment of physiological markers of inter-individual vulnerability to pain following injury. In a second experiment described in Chapter 6, we tested the modulation of CBF changes related to persistent pain by gabapentin, as compared to placebo. We show that gabapentin suppresses neural activity in an overlapping functional region of the posterior insula that was hyperperfused to a similar pain stimulus in a different subject cohort in Chap-

ter 5, and that this suppression correlated with the suppression of subjective ongoing pain scores by gabapentin. This provided further evidence that the posterior insula can be used as a neural biomarker in the assessment of pharmacological efficacy against nociceptive-driven pain in the healthy human. Interestingly, we also reported (both in Chapter 5 and this experiment) that the largest part of the neural response to persistent pain was a widespread decrease in CBF in several brain regions, which was partially reversed by gabapentin therapy. While the functional interpretation of pain related deactivations and hypoperfusion remains debated (Iannetti et al., 2005b; Kong et al., 2010; Owen et al., 2010; Thunberg et al., 2005), our evidence suggests that these changes may provide an important readout for assessing drug efficacy in the context of persistent pain.

In Chapter 7, we translated the use of our optimised ASL pipeline to the assessment of ongoing pain and its relief through neurostimulation in a cohort of phantom limb pain (PLP) patients. By targeting putative PLP mechanisms of maladaptive plasticity in the deprived sensorimotor cortex (Flor et al., 2006), we demonstrated that anodal transcranial direct current stimulation (tDCS) to the deprived sensorimotor cortex has a short-lasting analgesic effect, and that this effect is reflected in the brain by decreased activity in the posterior insula and hippocampus. These findings suggest that activity in the posterior insula may also serve as an important marker of pain percept in neuropathic patient cohorts. Furthermore, we show that tDCS therapy is a promising intervention in the management of PLP, and that more extensive study of its mechanisms and longer-term analgesic effects is appropriate.

## 8.2 Summary

This thesis provides two major novel additions to the pain field. Firstly, we confirm over a series of experiments that the use of fMRI to image acute and persistent pain can

provide important biomarkers for the assessment of analgesic efficacy. We repeatedly demonstrate the importance of the posterior insula as a neural readout of persistent pain, and suggest that activity in this region can be used in the assessment of efficacy of novel therapies in both healthy volunteers and neuropathic pain patient groups. Future work should aim to link activity in the posterior insula with integrative functional networks underlying the emergence of the pain experience from ongoing nociceptive afferent input. It will also be important to validate the role of fMRI for testing analgesic efficacy of known compounds in larger clinical populations, and of novel therapies in more homogenous healthy subject groups.

Secondly, we identified a physiological marker of susceptibility to nociceptive-driven pain and CS related hypersensitivity by highlighting a specific relationship between PAG baseline CBF and subsequent pain reports. Given that only a proportion patients go on to develop chronic pain after nerve injury (Helgason et al., 2000; Kehlet et al., 2006), the assessment of vulnerability to immediate post-injury pain (a strong prognostic indicator for chronic pain) may have important clinical implications, particularly in the perioperative setting (Deumens et al., 2013). To appropriately investigate this, subsequent studies should address the relationship between pre-surgical baseline PAG activity and post-surgical incidence and severity of persistent pain.

# References


Aguirre, G. K. G., Detre, J. A. J., Zarahn, E. E., and Alsop, D. C. D. (2002). Experimental Design and the Relative Sensitivity of BOLD and Perfusion fMRI. *NeuroImage*, 15(3):13–13. 111

Albanese, M.-C., Duerden, E. G., Rainville, P., and Duncan, G. H. (2007). Memory traces of pain in human cortex. *The Journal of neuroscience : the official journal of the Society for Neuroscience*, 27(17):4612–4620. 169

Ali, Z., Meyer, R. A., and Campbell, J. N. (1996). Secondary hyperalgesia to mechanical but not heat stimuli following a capsaicin injection in hairy skin. *Pain*, 68(2-3):401–411. 57

Andersson, J., Jenkinson, M., and Smith, S. (2007). Non-linear registration, aka Spatial normalisation FMRIB technical report TR07JA2. *FMRIB Analysis Group*. 44, 66, 92, 124, 126

Andrew, D. and Greenspan, J. D. (1999a). Mechanical and heat sensitization of cutaneous nociceptors after peripheral inflammation in the rat. *Journal of Neurophysiology*, 82(5):2649–2656. 21

Andrew, D. and Greenspan, J. D. (1999b). Peripheral coding of tonic mechanical cutaneous pain: comparison of nociceptor activity in rat and human psychophysics. *Journal of Neurophysiology*, 82(5):2641–2648. 151

Antal, A., Brepohl, N., Poreisz, C., Boros, K., Csifcsak, G., and Paulus, W. (2008). Transcranial direct current stimulation over somatosensory cortex decreases experimentally induced acute pain perception. *The Clinical Journal of Pain*, 24:56–63. 223

Antal, A., Terney, D., Kühnl, S., and Paulus, W. (2010). Anodal Transcranial Direct Current Stimulation of the Motor Cortex Ameliorates Chronic Pain and Reduces Short Intracortical Inhibition. *Journal of pain and symptom management*, 39(5):890–903. 208, 222, 223

Apkarian, A., Bushnell, M., and Schweinardt, P. (2013). Representation of Pain in the Brain. In *Wall and Melzack's Textbook of Pain*, pages 111–128. Elsevier Saunders. 6

Apkarian, A. V., Bushnell, M. C., Treede, R.-D., and Zubieta, J.-K. (2005). Human brain mechanisms of pain perception and regulation in health and disease. *European Journal of Pain*, 9(4):463–484. 6, 105, 110, 148, 152, 168

Apkarian, A. V., Sosa, Y., Sonty, S., Levy, R. M., Harden, R. N., Parrish, T. B., and Gitelman, D. R. (2004). Chronic back pain is associated with decreased prefrontal and thalamic gray matter density. *Journal of Neuroscience*, 24(46):10410–10415. 174

Aslan, S., Xu, F., Wang, P. L., Uh, J., Yezhuvath, U. S., van Osch, M., and Lu, H. (2010). Estimation of labeling efficiency in pseudocontinuous arterial spin labeling. *Magnetic Resonance*

*in Medicine*, 63(3):765–771. 123, 124, 145

Attal, N., Bouhassira, D., Baron, R., Dostrovsky, J., Dworkin, R. H., Finnerup, N., Gourlay, G., Haanpaa, M., Raja, S., Rice, A. S. C., Simpson, D., and Treede, R.-D. (2011). Assessing symptom profiles in neuropathic pain clinical trials: can it improve outcome? *European Journal of Pain*, 15(5):441–443. 83

Attwell, D., Buchan, A. M., Charpak, S., Lauritzen, M., Macvicar, B. A., and Newman, E. A. (2010). Glial and neuronal control of brain blood flow. *Nature*, 468(7321):232–243. 31, 148

Backonja, M., Beydoun, A., and Edwards, K. R. (1998). Gabapentin for the symptomatic treatment of painful neuropathy in patients with diabetes mellitus. *JAMA*. 191

Backonja, M.-M. and Stacey, B. (2004). Neuropathic pain symptoms relative to overall pain rating. *The Journal of Pain*, 5(9):7–7. 32, 147, 227

Baliki, M. N., Chialvo, D. R., Geha, P. Y., Levy, R. M., Harden, R. N., Parrish, T. B., and Apkarian, A. V. (2006). Chronic pain and the emotional brain: specific brain activity associated with spontaneous fluctuations of intensity of chronic back pain. *Journal of Neuroscience*, 26(47):12165–12173. 8, 150

Baliki, M. N., Petre, B., Torbey, S., Herrmann, K. M., Huang, L. L., Schnitzer, T. J., Fields, H. L., and Apkarian, A. V. (2012). Corticostriatal functional connectivity predicts transition to chronic back pain. *Nature Neuroscience*, 15(8):1117–1119. 13

Bandettini, P. A., Wong, E. C., Hinks, R. S., Tikofsky, R. S., and Hyde, J. S. (1992). Time course EPI of human brain function during task activation. *Magnetic Resonance in Medicine*, 25(2):390–397. 110

Bantick, S. J., Wise, R. G., Ploghaus, A., Clare, S., Smith, S. M., and Tracey, I. (2002). Imaging how attention modulates pain in humans using functional MRI. *Brain*, 125(Pt 2):310–319. 32

Baron, R. (2006). Mechanisms of disease: neuropathic pain–a clinical perspective. *Nature Clinical Practice. Neurology*, 2(2):95–106. 23, 56

Bauer, H. C., Duarte, F. L., Horliana, A. C. R. T., Tortamano, I. P., Perez, F. E. G., Simone, J. L., and Jorge, W. A. (2012). Assessment of preemptive analgesia with ibuprofen coadministered or not with dexamethasone in third molar surgery: a randomized double-blind controlled clinical trial. *Oral and maxillofacial surgery*. 83

Baumgärtner, U., Iannetti, G. D., Zambreanu, L., Stoeter, P., Treede, R.-D., and Tracey, I. (2010). Multiple somatotopic representations of heat and mechanical pain in the operculo-insular cortex: a high-resolution fMRI study. *Journal of Neurophysiology*, 104(5):2863–2872. 7, 169

Bayer, K., Ahmadi, S., and Zeilhofer, H. U. (2004). Gabapentin may inhibit synaptic transmission in the mouse spinal cord dorsal horn through a preferential block of P/Q-type Ca2+ channels. *Neuropharmacology*, 46(5):743–749. 106

Bee, L. A. and Dickenson, A. H. (2007). Rostral ventromedial medulla control of spinal sensory processing in normal and pathophysiological states. *Neuroscience*, 147(3):8–8. 188

Berge, O.-G. O. (2011). Predictive validity of behavioural animal models for chronic pain. *British Journal of Pharmacology*, 164(4):1195–1206. 28

Bergström, M., Hargreaves, R. J., Burns, H. D., Goldberg, M. R., Sciberras, D., Reines, S. A.,

Petty, K. J., Ogren, M., Antoni, G., Långström, B., Eskola, O., Scheinin, M., Solin, O., Majumdar, A. K., Constanzer, M. L., Battisti, W. P., Bradstreet, T. E., Gargano, C., and Hietala, J. (2004). Human positron emission tomography studies of brain neurokinin 1 receptor occupancy by aprepitant. *Biological Psychiatry*, 55(10):1007–1012. 79

Berna, C., Leknes, S., Holmes, E. A., Edwards, R. R., Goodwin, G. M., and Tracey, I. (2010). Induction of depressed mood disrupts emotion regulation neurocircuitry and enhances pain unpleasantness. *Biological Psychiatry*, 67(11):1083–1090. 32, 88

Bernard, J. F. and Besson, J. M. (1990). The spino(trigemino)pontoamygdaloid pathway: electrophysiological evidence for an involvement in pain processes. *Journal of Neurophysiology*, 63(3):473–490. 6

Berry, J. D. and Petersen, K. L. (2005). A single dose of gabapentin reduces acute pain and allodynia in patients with herpes zoster. *Neurology*, 65(3):444–447. 200

Bevan, S. and Szolcsányi, J. (1990). Sensory neuron-specific actions of capsaicin: mechanisms and applications. *Trends in Pharmacological Sciences*, 11(8):330–333. 58

Bingel, U., Gläscher, J., Weiller, C., and Büchel, C. (2004a). Somatotopic representation of nociceptive information in the putamen: an event-related fMRI study. *Cerebral Cortex*, 14(12):1340–1345. 172

Bingel, U., Lorenz, J., Glauche, V., Knab, R., Gläscher, J., Weiller, C., and Büchel, C. (2004b). Somatotopic organization of human somatosensory cortices for pain: a single trial fMRI study. *NeuroImage*, 23(1):9–9. 7

Bingel, U. and Tracey, I. (2008). Imaging CNS modulation of pain in humans. *Physiology (Bethesda, Md.)*, 23:371–380. 12

Bingel, U., Wanigasekera, V., Wiech, K., Ni Mhuircheartaigh, R., Lee, M. C., Ploner, M., and Tracey, I. (2011). The effect of treatment expectation on drug efficacy: imaging the analgesic benefit of the opioid remifentanil. *Science translational medicine*, 3(70):70ra14. 224

Birbaumer, N., Lutzenberger, W., Montoya, P., Larbig, W., Unertl, K., Töpfner, S., Grodd, W., Taub, E., and Flor, H. (1997). Effects of regional anesthesia on phantom limb pain are mirrored in changes in cortical reorganization. *Journal of Neuroscience*, 17(14):5503–5508. 206

Birklein, F., Rolke, R., and Müller-Forell, W. (2005). Isolated insular infarction eliminates contralateral cold, cold pain, and pinprick perception. *Neurology*, 65(9):1381–1381. 8

Birn, R. M., Diamond, J. B., Smith, M. A., and Bandettini, P. A. (2006). Separating respiratory-variation-related fluctuations from neuronal-activity-related fluctuations in fMRI. *NeuroImage*, 31(4):1536–1548. 37

Bittar, R. G., Kar-Purkayastha, I., Owen, S. L., Bear, R. E., Green, A., Wang, S., and Aziz, T. Z. (2005). Deep brain stimulation for pain relief: a meta-analysis. *Journal of Clinical Neuroscience*, 12(5):515–519. 189

Blackburn-Munro, G. (2004). Pain-like behaviours in animals - how human are they? *Trends in Pharmacological Sciences*, 25(6):299–305. 79, 227

Bland, J. M. and Altman, D. G. (1986). Statistical methods for assessing agreement between two methods of clinical measurement. *Lancet*, 1(8476):307–310. 67, 74

Bland, J. M. J. and Altman, D. G. D. (1996). Measurement error proportional to the mean. *BMJ*, 313(7049):106–106. 128

Blockley, N. P. N., Griffeth, V. E. M. V., and Buxton, R. B. R. (2012). A general analysis of calibrated BOLD methodology for measuring CMRO2 responses: comparison of a new approach with existing methods. *NeuroImage*, 60(1):279–289. 111

BNF (2007). *British National Formulary 54th Ed.* London: British Medical Association and Royal Pharmaceutical Society of Great Britain. 86

Boccard, S. G. J., Pereira, E. A. C., Moir, L., Aziz, T. Z., and Green, A. L. (2013). Long-term outcomes of deep brain stimulation for neuropathic pain. *Neurosurgery*, 72(2):221–231. 27, 175

Bockbrader, H. N., Wesche, D., Miller, R., Chapel, S., Janiczek, N., and Burger, P. (2010). A comparison of the pharmacokinetics and pharmacodynamics of pregabalin and gabapentin. *Clinical pharmacokinetics*, 49(10):661–669. 82

Bogdanov, S., Smith, J., and Frey, S. H. (2012). Former hand territory activity increases after amputation during intact hand movements, but is unaffected by illusory visual feedback. *Neurorehabilitation and Neural Repair*, 26(6):604–615. 206

Boggio, P. S., Zaghi, S., Lopes, M., and Fregni, F. (2008). Modulatory effects of anodal transcranial direct current stimulation on perception and pain thresholds in healthy volunteers. *European Journal of Neurology*, 15(10):1124–1130. 13, 229

Boivie, J. J. and Meyerson, B. A. B. (1982). A correlative anatomical and clinical study of pain suppression by deep brain stimulation. *Pain*, 13(2):113–126. 10

Bokkers, R. P., Bremmer, J. P., van Berckel, B. N., Lammertsma, A. A., Hendrikse, J., Pluim, J. P., Kappelle, L. J., Boellaard, R., and Klijn, C. J. (2010). Arterial spin labeling perfusion MRI at multiple delay times: a correlative study with H(2)(15)O positron emission tomography in patients with symptomatic carotid artery occlusion. *Journal of Cerebral Blood Flow and Metabolism*, 30(1):222–222. 119

Bollen, K. and Jackman, R. (1990). Regression diagnostics: An expository treatment of outliers and influential cases. In *Modern Methods of Data Analysis*, pages 257–291. 91

Bolognini, N., Olgiati, E., Maravita, A., Ferraro, F., and Fregni, F. (2013). Motor and parietal cortex stimulation for phantom limb pain and sensations. *Pain*, 154(8):1274–1280. 208, 209, 210, 222, 223

Bond, A. J., James, D. C., and Lader, M. H. (1974). Physiological and psychological measures in anxious patients. *Psychological Medicine*, 4(4):364–373. 88

Bornhövd, K., Quante, M., Glauche, V., Bromm, B., Weiller, C., and Büchel, C. C. (2002). Painful stimuli evoke different stimulus-response functions in the amygdala, prefrontal, insula and somatosensory cortex: a single-trial fMRI study. *Brain*, 125(Pt 6):1326–1336. 7, 169

Borsook, D., Becerra, L., and Hargreaves, R. (2006). A role for fMRI in optimizing CNS drug development. *Nature Reviews: Drug Discovery*, 5(5):411–424. 80

Borsook, D., Upadhyay, J., Chudler, E. H., and Becerra, L. (2010). A key role of the basal ganglia in pain and analgesia - insights gained through human functional imaging. *Molecular Pain*, 6(1):27–27. 170, 171

Bosmans, J. C., Geertzen, J., and Post, W. J. (2010). Factors associated with phantom limb pain: a 3-year prospective study. *Clinical ...*. 205

Breivik, H., Collett, B., Ventafridda, V., Cohen, R., and Gallacher, D. (2006). Survey of chronic pain in Europe: prevalence, impact on daily life, and treatment. *European Journal of Pain*, 10:287–333. 1

Brodersen, K. H., Wiech, K., Lomakina, E. I., Lin, C.-S., Buhmann, J. M., Bingel, U., Ploner, M., Stephan, K. E., and Tracey, I. (2012). Decoding the perception of pain from fMRI using multivariate pattern analysis. *NeuroImage*, 63(3):1162–1170. 13, 170, 176

Brooks, J. C. W., Beckmann, C. F., Miller, K. L., Wise, R. G., Porro, C. A., Tracey, I., and Jenkinson, M. (2008). Physiological noise modelling for spinal functional magnetic resonance imaging studies. *NeuroImage*, 39(2):680–692. 38, 44, 65

Brooks, J. C. W., Zambreanu, L., Godinez, A., Craig, A. D. B., and Tracey, I. (2005). Somatotopic organisation of the human insula to painful heat studied with high resolution functional imaging. *NeuroImage*, 27(1):201–209. 7, 169

Buxton, R., Frank, L., Wong, E., Siewert, B., Warach, S., and Edelman, R. (1998). A general kinetic model for quantitative perfusion imaging with arterial spin labeling. *Magnetic Resonance in Medicine*, 40(3):383–396. 113, 125

Buxton, R. B. and Frank, L. R. (1997). A model for the coupling between cerebral blood flow and oxygen metabolism during neural stimulation. *Journal of Cerebral Blood Flow and Metabolism*, 17(1):64–72. 111, 148

Buxton, R. B., Uludağ, K., Dubowitz, D. J., and Liu, T. T. (2004). Modeling the hemodynamic response to brain activation. *NeuroImage*, 23 Suppl 1:S220–33. 110

Calford, M. B. and Tweedale, R. (1991). C-fibres provide a source of masking inhibition to primary somatosensory cortex. *Proceedings of the Royal Society B: Biological Sciences*, 243(1308):269–275. 206

Carpenter, D., Engberg, I., and Lundberg, A. (1965). Differential supra spinal control of inhibitory and excitatory actions from the FRA to ascending spinal pathways. *Acta Physiologica Scandinavica*, 63:103–110. 9

Carver, C. S. and White, T. L. (1994). Behavioral inhibition, behavioral activation, and affective responses to impending reward and punishment: The BIS/BAS Scales. *Journal of personality and social psychology*. 85

Caterina, M. J. and Julius, D. (2001). The vanilloid receptor: a molecular gateway to the pain pathway. *Annual review of neuroscience*, 24:487–517. 58

Caterina, M. J., Rosen, T. A., Tominaga, M., Brake, A. J., and Julius, D. (1999). A capsaicin-receptor homologue with a high threshold for noxious heat. *Nature*, 398(6726):436–441. 3

Caterina, M. J., Schumacher, M. A., Tominaga, M., Rosen, T. A., Levine, J. D., and Julius, D. (1997). The capsaicin receptor: a heat-activated ion channel in the pain pathway. *Nature*, 389(6653):816–824. 3

Cavanaugh, D. J., Lee, H., Lo, L., Shields, S. D., Zylka, M. J., Basbaum, A. I., and Anderson, D. J. (2009). Distinct subsets of unmyelinated primary sensory fibers mediate behavioral responses to noxious thermal and mechanical stimuli. *Audio, Transactions of the IRE Professional Group on*, 106(22):9075–9080. 4

Cerliani, L., Thomas, R. M., Jbabdi, S., Siero, J. C. W., Nanetti, L., Crippa, A., Gazzola, V., D'Arceuil, H., and Keysers, C. (2012). Probabilistic tractography recovers a rostrocaudal trajectory of connectivity variability in the human insular cortex. *Human Brain Mapping*, 33(9):2005–2034. 169

Chang, C., Cunningham, J. P., and Glover, G. H. (2009). Influence of heart rate on the BOLD signal: the cardiac response function. *NeuroImage*, 44(3):857–869. 38

Chappell, M. A., Groves, A. R., and Whitcher, B. (2009). Variational Bayesian inference for a nonlinear forward model. *... IEEE Transactions on*. 125

Chappell, M. A., MacIntosh, B. J., Donahue, M. J., Günther, M., Jezzard, P., and Woolrich, M. W. (2010). Separation of macrovascular signal in multi-inversion time arterial spin labelling MRI. *Magnetic Resonance in Medicine*, 63(5):1357–1365. 117, 119, 125, 182, 228

Chen, Y. Y., Wang, D. J. J. D., and Detre, J. A. J. (2011). Test-retest reliability of arterial spin labeling with common labeling strategies. *Journal of Magnetic Resonance Imaging*, 33(4):940–949. 119, 142

Cheng, V. Y., Bonin, R. P., Chiu, M. W., Newell, J. G., MacDonald, J. F., and Orser, B. A. (2006). Gabapentin increases a tonic inhibitory conductance in hippocampal pyramidal neurons. *Anesthesiology*, 105(2):325–333. 201

Chizh, B. A., Greenspan, J. D., Casey, K. L., Nemenov, M. I., and Treede, R.-D. (2008). Identifying biological markers of activity in human nociceptive pathways to facilitate analgesic drug development. *Pain*, 140(2):249–253. 80, 228

Chudler, E. H. and Dong, W. K. (1995). The role of the basal ganglia in nociception and pain. *Pain*, 60(1):3–38. 171

Clarke, H. H., Bonin, R. P. R., Orser, B. A. B., Englesakis, M. M., Wijeysundera, D. N. D., and Katz, J. J. (2012). The prevention of chronic postsurgical pain using gabapentin and pregabalin: a combined systematic review and meta-analysis. *Anesthesia and analgesia*, 115(2):428–442. 108

Cloutman, L. L., Binney, R. J., Drakesmith, M., Parker, G. J. M., and Lambon Ralph, M. A. (2012). The variation of function across the human insula mirrors its patterns of structural connectivity: evidence from in vivo probabilistic tractography. *NeuroImage*, 59(4):3514–3521. 169

Coghill, R. C. R., Sang, C. N. C., Berman, K. F. K., Bennett, G. J. G., and Iadarola, M. J. M. (1998). Global cerebral blood flow decreases during pain. *Journal of Cerebral Blood Flow and Metabolism*, 18(2):141–147. 149, 150

Coghill, R. C. R., Sang, C. N. C., Maisog, J. M. J., and Iadarola, M. J. M. (1999). Pain intensity processing within the human brain: a bilateral, distributed mechanism. *Journal of Neurophysiology*, 82(4):1934–1943. 7, 169

Cohen, E. R., Ugurbil, K., and Kim, S.-G. (2002). Effect of basal conditions on the magnitude and dynamics of the blood oxygenation level-dependent fMRI response. *Journal of Cerebral Blood Flow and Metabolism*, 22(9):1042–1053. 111

Cohen Kadosh, R., Soskic, S., Iuculano, T., Kanai, R., and Walsh, V. (2010). Modulating Neuronal Activity Produces Specific and Long-Lasting Changes in Numerical Competence. *Current Biology*, 20(22):2016–2020. 209

Cook and Dennis, R. (1977). Detection of Influential Observations in Linear Regression. *Technometrics*, 19:15–18. 91

Craig, A. (2013). Topographically organized projection to posterior insular cortex from the posterior portion of the ventral medial nucleus (VMpo) in the long-tailed macaque monkey. *The Journal of comparative neurology*. 8, 152, 171, 173, 228

Craig, A. D. (2009). How do you feel — now? The anterior insula and human awareness. *Nature Reviews Neuroscience*, 10(1):59–70. 169, 173, 228

Craig, A. D. B. A. (2003). Pain mechanisms: labeled lines versus convergence in central processing. *Neuroscience*, 26:1–30. 5

Crawford, J. R. and Henry, J. D. (2004). The positive and negative affect schedule (PANAS): construct validity, measurement properties and normative data in a large non-clinical sample. *The British journal of clinical psychology / the British Psychological Society*, 43(Pt 3):245–265. 85

Culp, W. J., Ochoa, J., Cline, M., and Dotson, R. (1989). Heat and mechanical hyperalgesia induced by capsaicin. Cross modality threshold modulation in human C nociceptors. *Brain*, 112:1317–1331. 168

Curros-Criado, M. M. and Herrero, J. F. (2007). The antinociceptive effect of systemic gabapentin is related to the type of sensitization-induced hyperalgesia. *Journal of Neuroinflammation*, 4:15–15. 82

Dai, W., Garcia, D., de Bazelaire, C., and Alsop, D. C. (2008). Continuous flow-driven inversion for arterial spin labeling using pulsed radio frequency and gradient fields. *Magnetic Resonance in Medicine*, 60(6):1488–1497. 115

Davies, N. M. (1998). Clinical pharmacokinetics of ibuprofen. The first 30 years. *Clinical pharmacokinetics*, 34(2):101–154. 86

De Felice, M., Sanoja, R., Wang, R., Vera-Portocarrero, L., Oyarzo, J., King, T., Ossipov, M. H., Vanderah, T. W., Lai, J., Dussor, G. O., Fields, H. L., Price, T. J., and Porreca, F. (2011). Engagement of descending inhibition from the rostral ventromedial medulla protects against chronic neuropathic pain. *Pain*, 152(12):2701–2709. 16, 23, 189, 226, 229

De Martino, F., Esposito, F., van de Moortele, P.-F., Harel, N., Formisano, E., Goebel, R., Ugurbil, K., and Yacoub, E. (2011). Whole brain high-resolution functional imaging at ultra high magnetic fields: an application to the analysis of resting state networks. *NeuroImage*, 57(3):1031–1044. 60

Derbyshire, S. W. G. and Osborn, J. (2009). Offset analgesia is mediated by activation in the region of the periaqueductal grey and rostral ventromedial medulla. *NeuroImage*, 47(3):1002–1006. 177

Derbyshire, S. W. G. S., Whalley, M. G. M., Stenger, V. A. V., and Oakley, D. A. D. (2004). Cerebral activation during hypnotically induced and imagined pain. *NeuroImage*, 23(1):10–10. 32

Derry, S., Lloyd, R., Moore, R. A., and McQuay, H. J. (2009). Topical capsaicin for chronic neuropathic pain in adults. *Cochrane database of systematic reviews (Online)*, (4):CD007393. 58

Derry, S., Moore, R. A., and Rabbie, R. (2012). Topical NSAIDs for chronic musculoskeletal

pain in adults. *Cochrane database of systematic reviews (Online)*, 9:CD007400. 83

Detre, J. A. J., Wang, J. J., Wang, Z. Z., and Rao, H. H. (2009). Arterial spin-labeled perfusion MRI in basic and clinical neuroscience. *Current Opinion in Neurology*, 22(4):348–355. 112, 113

Deumens, R., Steyaert, A., Forget, P., Schubert, M., Lavand'homme, P., Hermans, E., and De Kock, M. (2013). Prevention of chronic postoperative pain: cellular and molecular insights for mechanisms-based treatment approaches. *Progress in Neurobiology*, pages –. 190, 231

Deyama, S., Nakagawa, T., Kaneko, S., Uehara, T., and Minami, M. (2007a). Involvement of the bed nucleus of the stria terminalis in the negative affective component of visceral and somatic pain in rats. *Behavioural Brain Research*, 176(2):367–371. 14

Deyama, S., Takishita, A., Tanimoto, S., Ide, S., Nakagawa, T., Satoh, M., and Minami, M. (2010). Roles of - and 2-adrenoceptors within the central nucleus of the amygdala in the visceral pain-induced aversion in rats. *Journal of Pharmacological Sciences (Print Edition)*, 114(1):123–126. 14

Deyama, S. S., Yamamoto, J. J., Machida, T. T., Tanimoto, S. S., Nakagawa, T. T., Kaneko, S. S., Satoh, M. M., and Minami, M. M. (2007b). Inhibition of glutamatergic transmission by morphine in the basolateral amygdaloid nucleus reduces pain-induced aversion. *Neuroscience Research*, 59(2):199–204. 11, 14

Di Piero, V. V., Jones, A. K. A., Iannotti, F. F., Powell, M. M., Perani, D. D., Lenzi, G. L. G., and Frackowiak, R. S. R. (1991). Chronic pain: a PET study of the central effects of percutaneous high cervical cordotomy. *Pain*, 46(1):9–12. 148

Dirks, J., Petersen, K. L., Rowbotham, M. C., and Dahl, J. B. (2002). Gabapentin suppresses cutaneous hyperalgesia following heat-capsaicin sensitization. *Anesthesiology*, 97(1):102–107. 82

Donahue, M. J. M., Strother, M. K. M., and Hendrikse, J. J. (2012). Novel MRI approaches for assessing cerebral hemodynamics in ischemic cerebrovascular disease. *Stroke*, 43(3):903–915. 116

Dooley, D. J., Taylor, C. P., Donevan, S., and Feltner, D. (2007). Ca2+ channel alpha2delta ligands: novel modulators of neurotransmission. *Trends in Pharmacological Sciences*, 28(2):75–82. 25, 82, 191

Dostrovsky, J. and Craig, A. (2013). Ascending Projection Systems. In *Wall and Melzack's Textbook of Pain*, pages 182–197. Elsevier Saunders. 5, 6

Drummond, P. D. P. (2001). The effect of sympathetic activity on thermal hyperalgesia in capsaicin-treated skin during body cooling and warming. *European Journal of Pain*, 5(1):9–9. 151

Dum, R. P., Levinthal, D. J., and Strick, P. L. (2009). The spinothalamic system targets motor and sensory areas in the cerebral cortex of monkeys. *Journal of Neuroscience*, 29(45):14223–14235. 8

Dunckley, P., Wise, R. G., Fairhurst, M., Hobden, P., Aziz, Q., Chang, L., and Tracey, I. (2005). A comparison of visceral and somatic pain processing in the human brainstem using functional magnetic resonance imaging. *Journal of Neuroscience*, 25(32):7333–7341. 18, 36, 38, 54

Duric, V. and McCarson, K. E. (2006). Persistent Pain Produces Stress-like Alterations in

Hippocampal Neurogenesis and Gene Expression. *The journal of pain : official journal of the American Pain Society*, 7(8):12–12. 224

Dworkin, R. H., O'Connor, A. B., Backonja, M., Farrar, J. T., Finnerup, N. B., Jensen, T. S., Kalso, E. A., Loeser, J. D., Miaskowski, C., Nurmikko, T. J., Portenoy, R. K., Rice, A. S. C., Stacey, B. R., Treede, R.-D., Turk, D. C., and Wallace, M. S. (2007). Pharmacologic management of neuropathic pain: evidence-based recommendations. *Pain*, 132(3):237–251. 25, 27, 82

Edelman, R. R. R. and Chen, Q. Q. (1998). EPISTAR MRI: multislice mapping of cerebral blood flow. *Magnetic Resonance in Medicine*, 40(6):800–805. 115

Eippert, F., Bingel, U., Schoell, E. D., Yacubian, J., Klinger, R., Lorenz, J., and BUchel, C. (2009). Activation of the Opioidergic Descending Pain Control System Underlies Placebo Analgesia. *Neuron*, 63(4):533–543. 10, 11, 177

Eisenberger, N. I., Lieberman, M. D., and Williams, K. D. (2003). Does rejection hurt? An FMRI study of social exclusion. *Science*, 302(5643):290–292. 32

Ephraim, P. L., Wegener, S. T., MacKenzie, E. J., Dillingham, T. R., and Pezzin, L. E. (2005). Phantom Pain, Residual Limb Pain, and Back Pain in Amputees: Results of a National Survey. *Archives of Physical Medicine and Rehabilitation*, 86(10):1910–1919. 205

Feinberg, D. A., Moeller, S., Smith, S. M., Auerbach, E., Ramanna, S., Glasser, M. F., Miller, K. L., Ugurbil, K., and Yacoub, E. (2010). Multiplexed echo planar imaging for sub-second whole brain FMRI and fast diffusion imaging. *PLoS ONE*, 5(12):e15710–e15710. 155, 268

Fera, F., Yongbi, M. N., van Gelderen, P., Frank, J. A., Mattay, V. S., and Duyn, J. H. (2004). EPI-BOLD fMRI of human motor cortex at 1.5 T and 3.0 T: sensitivity dependence on echo time and acquisition bandwidth. *Journal of Magnetic Resonance Imaging*, 19(1):19–26. 60

Fernández-Seara, M. A. M., Wang, Z. Z., Wang, J. J., Rao, H.-Y. H., Guenther, M. M., Feinberg, D. A. D., and Detre, J. A. J. (2005). Continuous arterial spin labeling perfusion measurements using single shot 3D GRASE at 3 T. *Magnetic Resonance in Medicine*, 54(5):1241–1247. 117

Field, M. J., Cox, P. J., Stott, E., Melrose, H., Offord, J., Su, T.-Z., Bramwell, S., Corradini, L., England, S., Winks, J., Kinloch, R. A., Hendrich, J., Dolphin, A. C., Webb, T., and Williams, D. (2006). Identification of the alpha2-delta-1 subunit of voltage-dependent calcium channels as a molecular target for pain mediating the analgesic actions of pregabalin. *Proceedings of the National Academy of Sciences of the United States of America*, 103(46):17537–17542. 82

Fields, H., Basbaum, A., and Heinricher, M. (2006). Central nervous system mechanisms of pain modulation. In *Wall and Melzack's Textbook of Pain*, pages 125–142. Elsevier Saunders. 15, 19

Fields, H. L., Bry, J., Hentall, I., and Zorman, G. (1983). The activity of neurons in the rostral medulla of the rat during withdrawal from noxious heat. *Journal of Neuroscience*, 3(12):2545–2552. 17, 106, 176

Fields, H. L. H., Heinricher, M. M. M., and Mason, P. P. (1991). Neurotransmitters in nociceptive modulatory circuits. *Neuroscience*, 14:219–245. 16

Finnerup, N. B., Sindrup, S. H., and Jensen, T. S. (2010). The evidence for pharmacological treatment of neuropathic pain. *Pain*, 150(3):573–581. 27, 28, 82, 227

Finnerup, N. B. N. and Jensen, T. S. T. (2006). Mechanisms of disease: mechanism-based classi-

fication of neuropathic pain-a critical analysis. *Nature Clinical Practice. Neurology*, 2(2):107–115. 25

Fleiss, J. L., Levin, B., Paik, M. C., and Fleiss, J. (2003). *Statistical Methods for Rates & Proportions*. Wiley-Interscience, 3rd edition. 129, 135, 136

Flor, H., Elbert, T., Knecht, S., Wienbruch, C., Pantev, C., Birbaumer, N., Larbig, W., and Taub, E. (1995). Phantom-limb pain as a perceptual correlate of cortical reorganization following arm amputation. *Nature*, 375(6531):482–484. 206

Flor, H., Nikolajsen, L., and Jensen, T. S. (2006). Phantom limb pain: a case of maladaptive CNS plasticity? *Nature Reviews Neuroscience*, 7(11):873–881. 205, 206, 230

Floyd, T. F., Ratcliffe, S. J., and Wang, J. (2003). Precision of the CASLperfusion MRI technique for the measurement of cerebral blood flow in whole brain and vascular territories. *Journal of Magnetic ....* 142

Fox, P. T. P. and Raichle, M. E. M. (1986). Focal physiological uncoupling of cerebral blood flow and oxidative metabolism during somatosensory stimulation in human subjects. *Proceedings of the National Academy of Sciences of the United States of America*, 83(4):1140–1144. 111

Fregni, F., Freedman, S., and Pascual-Leone, A. (2007). Recent advances in the treatment of chronic pain with non-invasive brain stimulation techniques. *The Lancet Neurology*, 6(2):188–191. 27, 222

Freynhagen, R., Baron, R., Gockel, U., and Tölle, T. R. (2006). painDETECT: a new screening questionnaire to identify neuropathic components in patients with back pain. *Current Medical Research and Opinion*, 22(10):1911–1920. 212

Friebel, U., Eickhoff, S. B., and Lotze, M. (2011). Coordinate-based meta-analysis of experimentally induced and chronic persistent neuropathic pain. *NeuroImage*, 58(4):1070–1080. 93, 131

Fried, K., Govrin-Lippmann, R., Rosenthal, F., Ellisman, M. H., and Devor, M. (1991). Ultrastructure of afferent axon endings in a neuroma. *Journal of Neurocytology*, 20(8):682–701. 205

Friese, S., Hamhaber, U., Erb, M., Kueker, W., and Klose, U. (2004). The influence of pulse and respiration on spinal cerebrospinal fluid pulsation. *Investigative radiology*, 39(2):120–130. 38

Frot, M., Feine, J. S., and Bushnell, M. C. (2004). Sex differences in pain perception and anxiety. A psychophysical study with topical capsaicin. *Pain*, 108(3):7–7. 167

Frot, M. M., Mauguière, F. F., Magnin, M. M., and Garcia-Larrea, L. L. (2008). Parallel processing of nociceptive A-delta inputs in SII and midcingulate cortex in humans. *Journal of Neuroscience*, 28(4):944–952. 8

Gallichan, D. and Jezzard, P. (2009). Variation in the shape of pulsed arterial spin labeling kinetic curves across the healthy human brain and its implications for CBF quantification. *Magnetic Resonance in Medicine*, 61(3):686–695. 117

Gao, K. K. and Mason, P. P. (2000). Serotonergic Raphe magnus cells that respond to noxious tail heat are not ON or OFF cells. *Journal of Neurophysiology*, 84(4):1719–1725. 18

Garcia-Larrea, L. (2012). The posterior insular-opercular region and the search of a primary cortex for pain. *Neurophysiologie Clinique/Clinical Neurophysiology*. 6, 8, 152, 169, 173, 228

Garcia-Larrea, L., Maarrawi, J., Peyron, R., Costes, N., Mertens, S., Magnin, M., and Laurent, B. (2006). On the relation between sensory deafferentation, pain and thalamic activity in Wallenberg's syndrome: a PET-scan study before and after motor cortex stimulation. *European Journal of Pain*, 10:677–688. 148

Garcia-Larrea, L. L., Frot, M. M., and Valeriani, M. M. (2003). Brain generators of laser-evoked potentials: from dipoles to functional significance. *Neurophysiologie Clinique/Clinical Neurophysiology*, 33(6):279–292. 8

Garcia-Larrea, L. L., Peyron, R. R., Mertens, P. P., Gregoire, M. C. M., Lavenne, F. F., Le Bars, D. D., Convers, P. P., Mauguière, F. F., Sindou, M. M., and Laurent, B. B. (1999). Electrical stimulation of motor cortex for pain control: a combined PET-scan and electrophysiological study. *Pain*, 83(2):259–273. 148

Geber, C., Fondel, R., Krmer, H., Rolke, R., Treede, R., Sommer, C., and Birklein, F. (2007). Psychophysics, flare, and neurosecretory function in human pain models: capsaicin versus electrically evoked pain. *The Journal of Pain*, 8:503–514. 151

Gebhart, G. F. (2004). Descending modulation of pain. *Neuroscience & Biobehavioral Reviews*, 27(8):729–737. 106

Gee, N. S., Brown, J. P., Dissanayake, V. U., Offord, J., Thurlow, R., and Woodruff, G. N. (1996). The novel anticonvulsant drug, gabapentin (Neurontin), binds to the alpha2delta subunit of a calcium channel. *The Journal of biological chemistry*, 271(10):5768–5776. 82

Geers, A. L., Helfer, S. G., Kosbab, K., Weiland, P. E., and Landry, S. J. (2005). Reconsidering the role of personality in placebo effects: dispositional optimism, situational expectations, and the placebo response. *Journal of psychosomatic research*, 58(2):121–127. 85

Gevers, S. S., van Osch, M. J. M., Bokkers, R. P. H. R., Kies, D. A. D., Teeuwisse, W. M. W., Majoie, C. B. C., Hendrikse, J. J., and Nederveen, A. J. A. (2011). Intra- and multicenter reproducibility of pulsed, continuous and pseudo-continuous arterial spin labeling methods for measuring cerebral perfusion. *Journal of Cerebral Blood Flow and Metabolism*, 31(8):1706–1715. 119, 135, 136, 142, 145

Gilron, I. (2007). Gabapentin and pregabalin for chronic neuropathic and early postsurgical pain: current evidence and future directions. *Current opinion in anaesthesiology*, 20(5):456–472. 82

Glover, G. H., Li, T. Q., and Ress, D. (2000). Image-based method for retrospective correction of physiological motion effects in fMRI: RETROICOR. *Magnetic Resonance in Medicine*, 44(1):162–167. 37, 44

Goddard, G., Karibe, H., and McNeill, C. (2004). Reproducibility of visual analog scale (VAS) pain scores to mechanical pressure. *Cranio : the journal of craniomandibular practice*, 22(3):250–256. 74

Gøransson, L. G., Mellgren, S. I., Lindal, S., and Omdal, R. (2004). The effect of age and gender on epidermal nerve fiber density. *Neurology*, 62(5):774–777. 167

Granot, M. and Ferber, S. G. (2005). The roles of pain catastrophizing and anxiety in the prediction of postoperative pain intensity: a prospective study. *The Clinical journal of pain*, 21(5):439–445. 85

Greenspan, J. D., Lee, R. R., and Lenz, F. A. (1999). Pain sensitivity alterations as a function of lesion location in the parasylvian cortex. *Pain*, 81(3):273–282. 8, 169

Greffrath, W., Baumgärtner, U., and Treede, R.-D. (2007). Peripheral and central components of habituation of heat pain perception and evoked potentials in humans. *Pain*, 132(3):11–11. 151, 168

Greve, D. N. and Fischl, B. (2009). Accurate and robust brain image alignment using boundary-based registration. *NeuroImage*, 48(1):63–72. 36, 40, 44, 66, 92, 126, 183

Gusnard, D. A., Raichle, M. E., and Raichle, M. E. (2001). Searching for a baseline: functional imaging and the resting human brain. *Nature Reviews Neuroscience*, 2(10):685–694. 200

Gustin, S. M., Peck, C. C., Cheney, L. B., Macey, P. M., Murray, G. M., and Henderson, L. A. (2012). Pain and plasticity: is chronic pain always associated with somatosensory cortex activity and reorganization? *Journal of Neuroscience*, 32(43):14874–14884. 205

Hadjipavlou, G., Dunckley, P., Behrens, T. E., and Tracey, I. (2006). Determining anatomical connectivities between cortical and brainstem pain processing regions in humans: a diffusion tensor imaging study in healthy controls. *Pain*, 123(1-2):169–178. 13

Hagbarth, K. E. and Kerr, D. I. (1954). Central influences on spinal afferent conduction. *Journal of Neurophysiology*, 17(3):295–307. 9

Haghparast, A., Naderi, N., Khani, A., Lashgari, R., and Motamedi, F. (2010). Formalin-induced differential activation of nucleus cuneiformis neurons in the rat: an electrophysiological study. *The Journal of Pain*, 11(1):32–43. 19

Haghparast, A. A., Gheitasi, I.-P. I., and Lashgari, R. R. (2007). Involvement of glutamatergic receptors in the nucleus cuneiformis in modulating morphine-induced antinociception in rats. *European Journal of Pain*, 11(8):8–8. 19

Hahn, A., Kranz, G. S., Seidel, E.-M., Sladky, R., Kraus, C., Küblböck, M., Pfabigan, D. M., Hummer, A., Grahl, A., Ganger, S., Windischberger, C., Lamm, C., and Lanzenberger, R. (2013). Comparing neural response to painful electrical stimulation with functional MRI at 3 and 7T. *NeuroImage*, 82C:336–343. 60

Han, J. S. and Neugebauer, V. (2004). Synaptic plasticity in the amygdala in a visceral pain model in rats. *Neuroscience Letters*, 361(1-3):4–4. 14

Harvey, A. K., Pattinson, K. T. S., Brooks, J. C. W., Mayhew, S. D., Jenkinson, M., and Wise, R. G. (2008). Brainstem functional magnetic resonance imaging: Disentangling signal from physiological noise. *Journal of Magnetic Resonance Imaging*, 28(6):1337–1344. 36, 38, 44, 52

Hasenbring, M. I., Hallner, D., and Rusu, A. C. (2009). Fear-avoidance- and endurance-related responses to pain: development and validation of the Avoidance-Endurance Questionnaire (AEQ). *European Journal of Pain*, 13(6):620–628. 85

Haws, C. M. C., Williamson, A. M. A., and Fields, H. L. H. (1989). Putative nociceptive modulatory neurons in the dorsolateral pontomesencephalic reticular formation. *Brain Research*, 483(2):272–282. 18, 106

Hayasaka, S. and Nichols, T. E. (2003). Validating cluster size inference: random field and permutation methods. *NeuroImage*, 20(4):2343–2356. 92, 194

Hayashida, K.-I., DeGoes, S., Curry, R., and Eisenach, J. C. (2007). Gabapentin activates spinal noradrenergic activity in rats and humans and reduces hypersensitivity after surgery. *Anesthesiology*, 106(3):557–562. 191

Head, H. and Holmes, G. (1911). Sensory disturbances from cerebral lesions. *Brain*. 6

Heinricher, M. M., Tavares, I., Leith, J. L., and Lumb, B. M. (2009). Descending control of nociception: Specificity, recruitment and plasticity. *Brain Research Reviews*, 60(1):214–225. 10, 16, 17, 175, 177, 229

Heinricher, M. M. M. and Neubert, M. J. M. (2004). Neural basis for the hyperalgesic action of cholecystokinin in the rostral ventromedial medulla. *Journal of Neurophysiology*, 92(4):1982–1989. 16

Heinricher, M. M. M. and Tortorici, V. V. (1994). Interference with GABA transmission in the rostral ventromedial medulla: disinhibition of off-cells as a central mechanism in nociceptive modulation. *Neuroscience*, 63(2):533–546. 17

Helgason, S., Petursson, G., Gudmundsson, S., and Sigurdsson, J. (2000). Prevalence of postherpetic neuralgia after a first episode of herpes zoster: prospective study with long term follow up. *BMJ*, 321:794–796. 231

Hempenstall, K., Nurmikko, T. J., Johnson, R. W., A'Hern, R. P., and Rice, A. S. C. (2005). Analgesic therapy in postherpetic neuralgia: a quantitative systematic review. *PLoS medicine*, 2(7):e164. 83

Henderson, L. A. L., Rubin, T. K. T., and Macefield, V. G. V. (2011). Within-limb somatotopic representation of acute muscle pain in the human contralateral dorsal posterior insula. *Human Brain Mapping*, 32(10):1592–1601. 7

Herbert, H. and Saper, C. B. (1992). Organization of medullary adrenergic and noradrenergic projections to the periaqueductal gray matter in the rat. *Journal of Comparative Neurology*, 315(1):34–52. 15

Hermes, M. M., Hagemann, D. D., Britz, P. P., Lieser, S. S., Rock, J. J., Naumann, E. E., and Walter, C. C. (2007). Reproducibility of continuous arterial spin labeling perfusion MRI after 7 weeks. *Magnetic Resonance Materials in Biology, Physics, and Medicine*, 20(2):103–115. 119, 144

Hill, R. (2000). NK1 (substance P) receptor antagonists–why are they not analgesic in humans? *Trends in Pharmacological Sciences*, 21(7):244–246. 5, 79

Hosobuchi, Y. Y., Adams, J. E. J., and Linchitz, R. R. (1977). Pain relief by electrical stimulation of the central gray matter in humans and its reversal by naloxone. *Science*, 197(4299):183–186. 189

Howard, M. A., Krause, K., Khawaja, N., Massat, N., Zelaya, F., Schumann, G., Huggins, J. P., Vennart, W., Williams, S. C. R., and Renton, T. F. (2011). Beyond Patient Reported Pain: Perfusion Magnetic Resonance Imaging Demonstrates Reproducible Cerebral Representation of Ongoing Post-Surgical Pain. *PLoS ONE*, 6(2):e17096. 131, 149

Howard, M. A., Sanders, D., Krause, K., O'Muircheartaigh, J., Fotopoulou, A., Zelaya, F., Thacker, M., Massat, N., Huggins, J. P., Vennart, W., Choy, E., Daniels, M., and Williams, S. C. R. (2012). Alterations in resting cerebral blood flow demonstrate ongoing pain in osteoarthritis: An arterial spin labelled magnetic resonance imaging study. *Arthritis and Rheumatism*. 149

Hsieh, J. C. J., Belfrage, M. M., Stone-Elander, S. S., Hansson, P. P., and Ingvar, M. M. (1995). Central representation of chronic ongoing neuropathic pain studied by positron emission to-

mography. *Pain*, 63(2):225–236. 148, 171

Huettel, S. A., Song, A. W., and McCarthy, G. (2008). *Functional Magnetic Resonance Imaging, Second Edition*. Sinauer Associates, 2nd edition. 30

Hunt, S. P. and Rossi, J. (1985). Peptide- and non-peptide-containing unmyelinated primary afferents: the parallel processing of nociceptive information. *Audio and Electroacoustics Newsletter, IEEE*, 308(1136):283–289. 3

Iadarola, M. J. M., Max, M. B. M., Berman, K. F. K., Byas-Smith, M. G. M., Coghill, R. C. R., Gracely, R. H. R., and Bennett, G. J. G. (1995). Unilateral decrease in thalamic activity observed with positron emission tomography in patients with chronic neuropathic pain. *Pain*, 63(1):55–64. 148, 149, 171

Iannetti, G., Zambreanu, L., Cruccu, G., and Tracey, I. (2005a). Operculoinsular cortex encodes pain intensity at the earliest stages of cortical processing as indicated by amplitude of laser-evoked potentials in humans. *Neuroscience*, 131(1):10–10. 8, 173

Iannetti, G. D., Zambreanu, L., Wise, R. G., Buchanan, T. J., Huggins, J. P., Smart, T. S., Vennart, W., and Tracey, I. (2005b). Pharmacological modulation of pain-related brainactivity during normal and central sensitizationstates in humans. *PNAS*, pages 1–6. 33, 38, 81, 82, 86, 105, 191, 192, 200, 226, 230

IASP (1986). International Association for the Study of Pain: Classification of chronic pain. *Pain*, Suppl 3:S1–S226. 1

Institute of Medicine (2011). *Relieving Pain in America: A Blueprint for Transforming Prevention, Care, Education, and Research*. The National Academies Collection: Reports funded by National Institutes of Health. National Academies Press (US), Washington (DC), 1 edition. 1

Ito, H., Kanno, I., and Fukuda, H. (2005). Human cerebral circulation: positron emission tomography studies. *Annals of Nuclear Medicine*, 19(2):65–74. 118

Jain, V. V., Duda, J. J., Avants, B. B., Giannetta, M. M., Xie, S. X. S., Roberts, T. T., Detre, J. A. J., Hurt, H. H., Wehrli, F. W. F., and Wang, D. J. J. D. (2012). Longitudinal reproducibility and accuracy of pseudo-continuous arterial spin-labeled perfusion MR imaging in typically developing children. *Radiology*, 263(2):527–536. 119, 142, 144

Jenkinson, M., Bannister, P., Brady, M., and Smith, S. (2002). Improved optimization for the robust and accurate linear registration and motion correction of brain images. *NeuroImage*, 17(2):825–841. 43, 65, 66, 92, 124, 183

Jenkinson, M. M., Beckmann, C. F. C., Behrens, T. E. J. T., Woolrich, M. W. M., and Smith, S. M. S. (2012). FSL. *NeuroImage*, 62(2):782–790. 123, 182

Jenkinson, M. M. and Smith, S. S. (2001). A global optimisation method for robust affine registration of brain images. *Medical Image Analysis*, 5(2):143–156. 44, 92, 124

Jensen, M. P., Turner, J. A., Romano, J. M., and Fisher, L. D. (1999). Comparative reliability and validity of chronic pain intensity measures. *Pain*, 83(2):157–162. 29

Jensen, M. P. M., Chodroff, M. J. M., and Dworkin, R. H. R. (2007). The impact of neuropathic pain on health-related quality of life: review and implications. *Neurology*, 68(15):1178–1182. 24

Jensen, T. S. T., Baron, R. R., Haanpää, M. M., Kalso, E. E., Loeser, J. D. J., Rice, A. S. C. A.,

and Treede, R.-D. R. (2011). A new definition of neuropathic pain. *Pain*, 152(10):2204–2205. 1

Jezzard, P. and Balaban, R. S. (1995). Correction for geometric distortion in echo planar images from B0 field variations. *Magnetic Resonance in Medicine*, 34(1):65–73. 60

Ji, R.-R., Kohno, T., Moore, K. A., and Woolf, C. J. (2003). Central sensitization and LTP: do pain and memory share similar mechanisms? *Trends in Neurosciences*, 26(12):696–705. 57

Johansen, J. P. and Fields, H. L. (2004). Glutamatergic activation of anterior cingulate cortex produces an aversive teaching signal. *Nature Neuroscience*, 7(4):398–403. 11

Jones, S. L. S. and Gebhart, G. F. G. (1988). Inhibition of spinal nociceptive transmission from the midbrain, pons and medulla in the rat: activation of descending inhibition by morphine, glutamate and electrical stimulation. *Brain Research*, 460(2):281–296. 20

Jun, J. H. and Yaksh, T. L. (1998). The effect of intrathecal gabapentin and 3-isobutyl gamma-aminobutyric acid on the hyperalgesia observed after thermal injury in the rat. *Anesthesia and analgesia*, 86(2):348–354. 82

Kahnt, T., Heinzle, J., Park, S. Q., and Haynes, J.-D. (2010). The neural code of reward anticipation in human orbitofrontal cortex. *Proceedings of the National Academy of Sciences of the United States of America*, 107(13):6010–6015. 13

Karrer, T. T. and Bartoshuk, L. L. (1991). Capsaicin desensitization and recovery on the human tongue. *Physiology & Behavior*, 49(4):757–764. 58

Kehlet, H., Jensen, T. S., and Woolf, C. J. (2006). Persistent postsurgical pain: risk factors and prevention. *Lancet*, 367(9522):1618–1625. 190, 231

Kety, S. and Schmidt, C. (1945). The determination of cerebral blood flow in man by the use of nitrous oxide in low concentrations. *American Journal of Physiology*, 143:53–66. 111

Kilo, S., Schmelz, M., Koltzenburg, M., and Handwerker, H. O. (1994). Different patterns of hyperalgesia induced by experimental inflammation in human skin. *Brain*, 117 ( Pt 2):385–396. 58

Kim, D.-H. D., Adalsteinsson, E. E., Glover, G. H. G., and Spielman, D. M. D. (2002). Regularized higher-order in vivo shimming. *Magnetic Resonance in Medicine*, 48(4):715–722. 122

Kim, S. G. S. (1995). Quantification of relative cerebral blood flow change by flow-sensitive alternating inversion recovery (FAIR) technique: application to functional mapping. *Magnetic Resonance in Medicine*, 34(3):293–301. 115

King, T., Vera-Portocarrero, L., Gutierrez, T., Vanderah, T. W., Dussor, G., Lai, J., Fields, H. L., and Porreca, F. (2009). Unmasking the tonic-aversive state in neuropathic pain. *Nature Neuroscience*, 12(11):1364–1366. 147

Kishima, H. H., Saitoh, Y. Y., Oshino, S. S., Hosomi, K. K., Ali, M. M., Maruo, T. T., Hirata, M. M., Goto, T. T., Yanagisawa, T. T., Sumitani, M. M., Osaki, Y. Y., Hatazawa, J. J., and Yoshimine, T. T. (2010). Modulation of neuronal activity after spinal cord stimulation for neuropathic pain; H(2)15O PET study. *NeuroImage*, 49(3):2564–2569. 148

Klein, T., Magerl, W., Rolke, R., and Treede, R.-D. (2005). Human surrogate models of neuropathic pain. *Pain*, 115(3):227–233. 28, 57, 81, 147

Knotkova, H., Cruciani, R. A., Tronnier, V. M., and Rasche, D. (2012). Current and future

options for the management of phantom-limb pain. *Journal of Pain Research*, 5:39–49. 205, 206, 207

Koltzenburg, M. M., Torebjörk, H. E. H., and Wahren, L. K. L. (1994). Nociceptor modulated central sensitization causes mechanical hyperalgesia in acute chemogenic and chronic neuropathic pain. *Brain*, 117 ( Pt 3):579–591. 151

Kong, J., Loggia, M. L., Zyloney, C., Tu, P., Laviolette, P., and Gollub, R. L. (2010). Exploring the brain in pain: activations, deactivations and their relation. *Pain*, 148(2):257–267. 200, 230

Kong, Y., Jenkinson, M., Andersson, J., Tracey, I., and Brooks, J. C. W. (2012). Assessment of physiological noise modelling methods for functional imaging of the spinal cord. *NeuroImage*, 60(2):1538–1549. 44

Koyama, T., Kato, K., and Mikami, A. (2000). During pain-avoidance neurons activated in the macaque anterior cingulate and caudate. *Neuroscience Letters*, 283(1):17–20. 172

Krueger, G. and Glover, G. (2001). Physiological noise in oxygenation-sensitive magnetic resonance imaging. *Magnetic Resonance in Medicine*, 46:631–637. 60

Kuo, C. C. C., Chen, R. S. R., Lu, L. L., and Chen, R. C. R. (1997). Carbamazepine inhibition of neuronal Na+ currents: quantitative distinction from phenytoin and possible therapeutic implications. *Molecular Pharmacology*, 51(6):1077–1083. 27

Kurth, F., Zilles, K., Fox, P. T., Laird, A. R., and Eickhoff, S. B. (2010). A link between the systems: functional differentiation and integration within the human insula revealed by meta-analysis. *Brain structure & function*, 214(5-6):519–534. 169

Kwong, K. K., Belliveau, J. W., Chesler, D. A., Goldberg, I. E., Weisskoff, R. M., Poncelet, B. P., Kennedy, D. N., Hoppel, B. E., Cohen, M. S., and Turner, R. (1992). Dynamic magnetic resonance imaging of human brain activity during primary sensory stimulation. *Proceedings of the National Academy of Sciences of the United States of America*, 89(12):5675–5679. 110

Kwong, K. K. K., Chesler, D. A. D., Weisskoff, R. M. R., Donahue, K. M. K., Davis, T. L. T., Ostergaard, L. L., Campbell, T. A. T., and Rosen, B. R. B. (1995). MR perfusion studies with T1-weighted echo planar imaging. *Magnetic Resonance in Medicine*, 34(6):878–887. 114, 115

LaMotte, R. H., Shain, C. N., Simone, D. A., and Tsai, E. F. (1991). Neurogenic hyperalgesia: psychophysical studies of underlying mechanisms. *Journal of Neurophysiology*, 66(1):190–211. 23, 58

Lang, N., Siebner, H. R., Ward, N. S., Lee, L., Nitsche, M. A., Paulus, W., Rothwell, J. C., Lemon, R. N., and Frackowiak, R. S. (2005). How does transcranial DC stimulation of the primary motor cortex alter regional neuronal activity in the human brain? *European Journal of Neuroscience*, 22(2):495–504. 223

Langford, D. J., Bailey, A. L., Chanda, M. L., Clarke, S. E., Drummond, T. E., Echols, S., Glick, S., Ingrao, J., Klassen-Ross, T., Lacroix-Fralish, M. L., Matsumiya, L., Sorge, R. E., Sotocinal, S. G., Tabaka, J. M., Wong, D., van den Maagdenberg, A. M. J. M., Ferrari, M. D., Craig, K. D., and Mogil, J. S. (2010). Coding of facial expressions of pain in the laboratory mouse. *Nature methods*, 7(6):447–449. 170

Larson, K. B. K., Markham, J. J., and Raichle, M. E. M. (1987). Tracer-kinetic models for measuring cerebral blood flow using externally detected radiotracers. *Journal of Cerebral*

*Blood Flow and Metabolism*, 7(4):443–463. 111

Lautenbacher, S. S., Roscher, S. S., and Strian, F. F. (1995). Tonic pain evoked by pulsating heat: temporal summation mechanisms and perceptual qualities. *Somatosensory & Motor Research*, 12(1):59–70. 151

Lee, M. C., Ploner, M., Wiech, K., Bingel, U., Wanigasekera, V., Brooks, J., Menon, D. K., and Tracey, I. (2013). Amygdala activity contributes to the dissociative effect of cannabis on pain perception. *Pain*, 154(1):124–134. 14

Lee, M. C., Zambreanu, L., Menon, D. K., and Tracey, I. (2008). Identifying Brain Activity Specifically Related to the Maintenance and Perceptual Consequence of Central Sensitization in Humans. *Journal of Neuroscience*, 28(45):11642–11649. 17, 23, 28, 36, 39, 54, 58, 59, 75, 76, 81, 99, 105, 106, 226, 227

Lee, M. C. M., Mouraux, A. A., and Iannetti, G. D. G. (2009). Characterizing the cortical activity through which pain emerges from nociception. *Journal of Neuroscience*, 29(24):7909–7916. 8, 173

Lefaucheur, J.-P., Antal, A., Ahdab, R., Ciampi de Andrade, D., Fregni, F., Khedr, E. M., Nitsche, M., and Paulus, W. (2008). The use of repetitive transcranial magnetic stimulation (rTMS) and transcranial direct current stimulation (tDCS) to relieve pain. *Brain stimulation*, 1(4):337–344. 208, 222

Lefaucheur, J. P., Drouot, X., Ménard-Lefaucheur, I., Keravel, Y., and Nguyen, J. P. (2006). Motor cortex rTMS restores defective intracortical inhibition in chronic neuropathic pain. *Neurology*, 67(9):1568–1574. 208, 223

Legrain, V. V., Iannetti, G. D. G., Plaghki, L. L., and Mouraux, A. A. (2011). The pain matrix reloaded. *Progress in Neurobiology*, 93(1):14–14. 32

Li, T. Q. T., Kastrup, A. A., Moseley, M. E. M., and Glover, G. H. G. (2000). Changes in baseline cerebral blood flow in humans do not influence regional cerebral blood flow response to photic stimulation. *Journal of Magnetic Resonance Imaging*, 12(5):757–762. 111

Limbrick-Oldfield, E. H. E., Brooks, J. C. W. J., Wise, R. J. S. R., Padormo, F. F., Hajnal, J. V. J., Beckmann, C. F. C., and Ungless, M. A. M. (2012). Identification and characterisation of midbrain nuclei using optimised functional magnetic resonance imaging. *NeuroImage*, 59(2):1230–1238. 37, 38, 44

Lindner, H. Y. N., Nätterlund, B. S., and Hermansson, L. M. N. (2010). Upper limb prosthetic outcome measures: review and content comparison based on International Classification of Functioning, Disability and Health. *Prosthetics and Orthotics International*, 34(2):109–128. 205

Linnman, C. C., Moulton, E. A. E., Barmettler, G. G., Becerra, L. L., and Borsook, D. D. (2012). Neuroimaging of the periaqueductal gray: state of the field. *NeuroImage*, 60(1):505–522. 15, 177

Liu, J. J., Hao, Y. Y., Du, M. M., Wang, X. X., Zhang, J. J., Manor, B. B., Jiang, X. X., Fang, W. W., and Wang, D. D. (2013). Quantitative cerebral blood flow mapping and functional connectivity of postherpetic neuralgia pain: A perfusion fMRI study. *Pain*, 154(1):110–118. 149

Liu, M., Max, M. B., Robinovitz, E., Gracely, R. H., and Bennett, G. J. (1998). The human cap-

saicin model of allodynia and hyperalgesia: sources of variability and methods for reduction. *Journal of pain and symptom management*, 16(1):10–20. 58, 63, 86

Logothetis, N. K., Pauls, J., Augath, M., Trinath, T., and Oeltermann, A. (2001). Neurophysiological investigation of the basis of the fMRI signal. *Nature*, 412(6843):150–157. 31

Lorenz, J. J., Minoshima, S. S., and Casey, K. L. K. (2003). Keeping pain out of mind: the role of the dorsolateral prefrontal cortex in pain modulation. *Brain*, 126(Pt 5):1079–1091. 13, 174, 229

Lotze, M., Flor, H., Grodd, W., Larbig, W., and Birbaumer, N. (2001). Phantom movements and pain. An fMRI study in upper limb amputees. *Brain*, 124(Pt 11):2268–2277. 206

Luppi, P. H. P., Aston-Jones, G. G., Akaoka, H. H., Chouvet, G. G., and Jouvet, M. M. (1995). Afferent projections to the rat locus coeruleus demonstrated by retrograde and anterograde tracing with cholera-toxin B subunit and Phaseolus vulgaris leucoagglutinin. *Neuroscience*, 65(1):119–160. 20

Machin, D., Campbell, M. J., Tan, S.-B., and Tan, S.-H. (2011). *Sample Size Tables for Clinical Studies*. John Wiley & Sons. 131

MacIntosh, B. J., Filippini, N., Chappell, M. A., Woolrich, M. W., Mackay, C. E., and Jezzard, P. (2010). Assessment of arterial arrival times derived from multiple inversion time pulsed arterial spin labeling MRI. *Magnetic Resonance in Medicine*, 63(3):641–647. 117

MacIntosh, B. J., Pattinson, K. T. S., Gallichan, D., Ahmad, I., Miller, K. L., Feinberg, D. A., Wise, R. G., and Jezzard, P. (2008). Measuring the effects of remifentanil on cerebral blood flow and arterial arrival time using 3D GRASE MRI with pulsed arterial spin labelling. *Journal of Cerebral Blood Flow and Metabolism*, 28(8):1514–1522. 124

Magerl, W., Wilk, S. H., and Treede, R. D. (1998). Secondary hyperalgesia and perceptual wind-up following intradermal injection of capsaicin in humans. *Pain*, 74(2-3):257–268. 58, 81

Magnusson, B. M. B. and Koskinen, L. D. L. (2000). In vitro percutaneous penetration of topically applied capsaicin in relation to in vivo sensation responses. *International Journal of Pharmaceutics*, 195(1-2):55–62. 167

Maier, C., Baron, R., Tölle, T. R., Binder, A., Birbaumer, N., Birklein, F., Gierthmühlen, J., Flor, H., Geber, C., Huge, V., Krumova, E. K., Landwehrmeyer, G. B., Magerl, W., Maihöfner, C., Richter, H., Rolke, R., Scherens, A., Schwarz, A., Sommer, C., Tronnier, V., Uçeyler, N., Valet, M., Wasner, G., and Treede, R. D. (2010). Quantitative sensory testing in the German Research Network on Neuropathic Pain (DFNS): somatosensory abnormalities in 1236 patients with different neuropathic pain syndromes. *Pain*, 150(3):439–450. 57

Makin, T. R., Scholz, J., Filippini, N., Slater, D. H., Tracey, I., and Johansen-Berg, H. (2013). Phantom pain is associated with preserved structure and function in the former hand area. *Nature Communications*, 4:1570–1570. 206, 207, 209, 223

Maleki, N., Brawn, J., Barmettler, G., Borsook, D., and Becerra, L. (2013). Pain response measured with arterial spin labeling. *NMR in Biomedicine*, pages –. 113, 148, 168

Mansfield, P. P. and Maudsley, A. A. A. (1977). Medical imaging by NMR. *British Journal of Radiology*, 50(591):188–194. 31

Mason, P. (1997). Physiological identification of pontomedullary serotonergic neurons in the rat. *Journal of Neurophysiology*, 77(3):1087–1098. 17

Mayer, D. J. and Price, D. D. (1976). Central nervous system mechanisms of analgesia. *Pain*, 2(4):379–404. 9, 189

Mazzola, L., Isnard, J., Peyron, R., Guénot, M., and Mauguière, F. (2009). Somatotopic organization of pain responses to direct electrical stimulation of the human insular cortex. *Pain*, 146(1-2):99–104. 8, 173

McDermott, A. M. A., Toelle, T. R. T., Rowbotham, D. J. D., Schaefer, C. P. C., and Dukes, E. M. E. (2006). The burden of neuropathic pain: results from a cross-sectional survey. *European Journal of Pain*, 10(2):9–9. 24

McGaraughty, S. S. and Heinricher, M. M. M. (2002). Microinjection of morphine into various amygdaloid nuclei differentially affects nociceptive responsiveness and RVM neuronal activity. *Pain*, 96(1-2):153–162. 17

McKelvey, L., Shorten, G. D., and O'Keeffe, G. W. (2013). Nerve growth factor-mediated regulation of pain signalling and proposed new intervention strategies in clinical pain management. *Journal of Neurochemistry*, 124(3):276–289. 23

McKiernan, K. A., Kaufman, J. N., Kucera-Thompson, J., and Binder, J. R. (2003). A parametric manipulation of factors affecting task-induced deactivation in functional neuroimaging. *Journal of Cognitive Neuroscience*, 15(3):394–408. 200

McQuay, H. J. H. (2002). Neuropathic pain: evidence matters. *European Journal of Pain*, 6 Suppl A:8–8. 1, 24

Melzack, R. and Casey, K. (1968). Sensory, motivational and central control determinants of pain. A new conceptual model. In *The Skin Senses*, pages 423–443. Springfield. 6, 7

Melzack, R. and Wall, P. D. (1965). Pain mechanisms: a new theory. *Science*, 150(3699):971–979. 9

Mendell, L. M. and Wall, P. D. (1965). Responses of single dorsal cord cells to peripheral cutaneous unmyelinated fibres. *Nature*, 206:97–99. 21

Menon, V. and Uddin, L. Q. (2010). Saliency, switching, attention and control: a network model of insula function. *Brain structure & function*, 214(5-6):655–667. 169

Mesulam, M. M. and Mufson, E. J. (1982). Insula of the old world monkey. III: Efferent cortical output and comments on function. *Journal of Comparative Neurology*, 212(1):38–52. 169

Meyer, E. (1989). Simultaneous correction for tracer arrival delay and dispersion in CBF measurements by the H215O autoradiographic method and dynamic PET. *Audio and Electroacoustics Newsletter, IEEE*, 30(6):1069–1078. 112

Millan, M. J. (1999). The induction of pain: an integrative review. *Progress in Neurobiology*, 57(1):1–164. 3, 4

Mitchell, D. G. (2011). The nexus between decision making and emotion regulation: A review of convergent neurocognitive substrates. *Behavioural Brain Research*, 217(1):215–231. 13

Mitsis, G. D., Iannetti, G. D., Smart, T. S., Tracey, I., and Wise, R. G. (2008). Regions of interest analysis in pharmacological fMRI: how do the definition criteria influence the inferred result? *NeuroImage*, 40(1):121–132. 32

Moeller, S., Yacoub, E., Olman, C. A., Auerbach, E., Strupp, J., Harel, N., and Ugurbil, K. (2010). Multiband multislice GE-EPI at 7 tesla, with 16-fold acceleration using partial parallel

imaging with application to high spatial and temporal whole-brain fMRI. *Magnetic Resonance in Medicine*, 63(5):1144–1153. 155, 268

Mogil, J. S. J., Graham, A. C. A., Ritchie, J. J., Hughes, S. F. S., Austin, J.-S. J., Schorscher-Petcu, A. A., Langford, D. J. D., and Bennett, G. J. G. (2010). Hypolocomotion, asymmetrically directed behaviors (licking, lifting, flinching, and shaking) and dynamic weight bearing (gait) changes are not measures of neuropathic pain in mice. *Molecular Pain*, 6:34–34. 147

Monte-Silva, K., Kuo, M.-F., Hessenthaler, S., Fresnoza, S., Liebetanz, D., Paulus, W., and Nitsche, M. A. (2012). Induction of late LTP-like plasticity in the human motor cortex by repeated non-invasive brain stimulation. *Brain stimulation*, pages 424–432. 225

Moseley, G. (2004). Why do people with complex regional pain syndrome take longer to recognize their affected hand? *Neurology*, 62:2182–2186. 268

Moseley, G. (2006). Graded motor imagery for pathologic pain: A randomized controlled trial. *Neurology*, 67:2129–2134. 268

Moseley, G. L. and Flor, H. (2012). Targeting cortical representations in the treatment of chronic pain: a review. *Neurorehabilitation and Neural Repair*, 26(6):646–652. 207

Mouraux, A., Diukova, A., Lee, M. C., Wise, R. G., and Iannetti, G. D. (2011). A multisensory investigation of the functional significance of the "pain matrix". *NeuroImage*, 54(3):2237–2249. 32, 150

Mufson, E. J. and Mesulam, M. M. (1982). Insula of the old world monkey. II: Afferent cortical input and comments on the claustrum. *Journal of Comparative Neurology*, 212(1):23–37. 169

Mutso, A. A., Radzicki, D., Baliki, M. N., Huang, L., Banisadr, G., Centeno, M. V., Radulovic, J., Martina, M., Miller, R. J., and Apkarian, A. V. (2012). Abnormalities in hippocampal functioning with persistent pain. *Journal of Neuroscience*, 32(17):5747–5756. 224

Naidich, T. P., Duvernoy, H. M., Delman, B. N., Sorensen, A. G., Kollias, S. S., and Haacke, E. M. (2009). *Duvernoy's Atlas of the Human Brain Stem and Cerebellum*. Springer, 1st edition. 39, 41, 45, 52, 99, 183

Ness, T. J., Pedro, E. C. S., Richards, J. S., Kezar, L., Liu, H. G., and Mountz, J. M. (1998). A case of spinal cord injury-related pain with baseline rCBF brain SPECT imaging and beneficial response to gabapentin. *Pain*, 78(2):139–143. 192, 201

Neubert, M. J., Kincaid, W., and Heinricher, M. M. (2004). Nociceptive facilitating neurons in the rostral ventromedial medulla. *Pain*, 110(1-2):158–165. 17

Neugebauer, V. V., Li, W. W., Bird, G. C. G., and Han, J. S. J. (2004). The amygdala and persistent pain. *Neuroscientist*, 10(3):221–234. 13, 14

NICE (2010). Neuropathic pain: The pharmacological management of neuropathic pain in adults in non-specialist settings. *NICE clinical guideline 96*. 82

Nikolajsen, L. (2013). Phantom Limb. In *Wall and Melzack's Textbook of Pain*, pages 915–925. Elsevier Saunders. 204, 205

Nikolajsen, L., Black, J. A., Kroner, K., Jensen, T. S., and Waxman, S. G. (2010). Neuroma removal for neuropathic pain: efficacy and predictive value of lidocaine infusion. *The Clinical journal of pain*, 26(9):788–793. 206

Nitsche, M. A. and Paulus, W. (2000). Excitability changes induced in the human motor cortex

by weak transcranial direct current stimulation. *Journal of Physiology*, 527 Pt 3:633–639. 208

Nitsche, M. A. M., Seeber, A. A., Frommann, K. K., Klein, C. C., Rochford, C., Nitsche, M. S., Fricke, K., Liebetanz, D. D., Lang, N. N., Antal, A. A., Paulus, W. W., and Tergau, F. (2005). Modulating parameters of excitability during and after transcranial direct current stimulation of the human motor cortex. *Journal of Physiology*, 568(Pt 1):291–303. 208

Nyström, B. and Hagbarth, K. E. (1981). Microelectrode recordings from transected nerves in amputees with phantom limb pain. *Neuroscience Letters*, 27(2):211–216. 206

Ochsner, K. N., Ray, R. D., Cooper, J. C., Robertson, E. R., Chopra, S., Gabrieli, J. D. E., and Gross, J. J. (2004). For better or for worse: neural systems supporting the cognitive down- and up-regulation of negative emotion. *NeuroImage*, 23(2):483–499. 11

O'Connell, N. E., Cossar, J., Marston, L., Wand, B. M., Bunce, D., Moseley, G. L., and De Souza, L. H. (2012). Rethinking clinical trials of transcranial direct current stimulation: participant and assessor blinding is inadequate at intensities of 2mA. *PLoS ONE*, 7(10):e47514–e47514. 215

Oertel, B. G., Preibisch, C., Martin, T., Walter, C., Gamer, M., Deichmann, R., and Lötsch, J. (2012). Separating brain processing of pain from that of stimulus intensity. *Human Brain Mapping*, 33(4):883–894. 169, 171

Ogawa, S. S., Lee, T. M. T., Kay, A. R. A., and Tank, D. W. D. (1990). Brain magnetic resonance imaging with contrast dependent on blood oxygenation. *Proceedings of the National Academy of Sciences of the United States of America*, 87(24):9868–9872. 31, 110

Okell, T. W., Chappell, M. A., Kelly, M. E., and Jezzard, P. (2013). Cerebral blood flow quantification using vessel-encoded arterial spin labeling. *Journal of Cerebral Blood Flow and Metabolism*. 122, 127

O'Neill, J. J., Brock, C. C., Olesen, A. E. A., Andresen, T. T., Nilsson, M. M., and Dickenson, A. H. A. (2012). Unravelling the mystery of capsaicin: a tool to understand and treat pain. *Pharmacological Reviews*, 64(4):939–971. 151

Ostrowsky, K. K., Magnin, M. M., Ryvlin, P. P., Isnard, J. J., Guenot, M. M., and Mauguière, F. F. (2002). Representation of pain and somatic sensation in the human insula: a study of responses to direct electrical cortical stimulation. *Cerebral Cortex*, 12(4):376–385. 8

Owen, D. G., Bureau, Y., Thomas, A. W., Prato, F. S., and St Lawrence, K. S. (2008). Quantification of pain-induced changes in cerebral blood flow by perfusion MRI. *Pain*, 136(1-2):85–96. 148

Owen, D. G., Clarke, C. F., Bureau, Y., Ganapathy, S., Prato, F. S., and St Lawrence, K. S. (2012). Measuring the neural response to continuous intramuscular infusion of hypertonic saline by perfusion MRI. *Journal of Magnetic Resonance Imaging*, 35(3):669–677. 149, 150, 151, 202

Owen, D. G., Clarke, C. F., Ganapathy, S., Prato, F. S., and Lawrence, K. S. S. (2010). Using perfusion MRI to measure the dynamic changes in neural activation associated with tonic muscular pain. *Pain*, 148(3):375–386. 149, 150, 170, 171, 230

Parazzini, M. M., Fiocchi, S. S., Rossi, E. E., Paglialonga, A. A., and Ravazzani, P. P. (2011). Transcranial direct current stimulation: estimation of the electric field and of the current density in an anatomical human head model. *Biomedical Engineering, IEEE Transactions on*,

58(6):1773–1780. 208

Parepally, J. M. R. J., Mandula, H. H., and Smith, Q. R. Q. (2006). Brain uptake of nonsteroidal anti-inflammatory drugs: ibuprofen, flurbiprofen, and indomethacin. *Pharmaceutical Research*, 23(5):873–881. 105

Parkes, L. M. L., Rashid, W. W., Chard, D. T. D., and Tofts, P. S. P. (2004). Normal cerebral perfusion measurements using arterial spin labeling: reproducibility, stability, and age and gender effects. *Magnetic Resonance in Medicine*, 51(4):736–743. 121, 145

Peltz, E., Seifert, F., DeCol, R., Dörfler, A., Schwab, S., and Maihöfner, C. (2011). Functional connectivity of the human insular cortex during noxious and innocuous thermal stimulation. *NeuroImage*, 54(2):1324–1335. 13, 169

Penfield, W. and Boldrey, E. (1937). Somatic motor and sensory representation in the cerebral cortex of man as studied by electrical stimulation. *Brain*, 60(4):389–443. 6

Petersen, E. T., Zimine, I., Ho, Y.-C. L., and Golay, X. (2006). Non-invasive measurement of perfusion: a critical review of arterial spin labelling techniques. *British Journal of Radiology*, 79(944):688–701. 116

Petersen, E. T. E., Mouridsen, K. K., and Golay, X. X. (2010). The QUASAR reproducibility study, Part II: Results from a multi-center Arterial Spin Labeling test-retest study. *NeuroImage*, 49(1):104–113. 119, 145

Petrovic, P. (2002). Placebo and Opioid Analgesia– Imaging a Shared Neuronal Network. *Science*, 295(5560):1737–1740. 10, 11

Petrovic, P., Kalso, E., Petersson, K. M., Andersson, J., Fransson, P., and Ingvar, M. (2010). A prefrontal non-opioid mechanism in placebo analgesia. *Pain*, 150(1):59–65. 11

Peyron, R., Laurent, B., and Garcia-Larrea, L. (2000). Functional imaging of brain responses to pain. A review and meta-analysis (2000). *Neurophysiologie Clinique/Clinical Neurophysiology*, 30(5):263–288. 112, 148

Pfeuffer, J. J., Adriany, G. G., Shmuel, A. A., Yacoub, E. E., Van De Moortele, P.-F. P., Hu, X. X., and Ugurbil, K. K. (2002). Perfusion-based high-resolution functional imaging in the human brain at 7 Tesla. *Magnetic Resonance in Medicine*, 47(5):903–911. 110, 111, 169

Phan, K. L., Fitzgerald, D. A., Nathan, P. J., Moore, G. J., Uhde, T. W., and Tancer, M. E. (2005). Neural substrates for voluntary suppression of negative affect: A functional magnetic resonance imaging study. *Biological Psychiatry*, 57(3):210–219. 11

Phelps, E. A. and LeDoux, J. E. (2005). Contributions of the amygdala to emotion processing: from animal models to human behavior. *Neuron*, 48(2):175–187. 13

Ploghaus, A., Narain, C., Beckmann, C. F., Clare, S., Bantick, S., Wise, R., Matthews, P. M., Rawlins, J. N., and Tracey, I. (2001). Exacerbation of pain by anxiety is associated with activity in a hippocampal network. *Journal of Neuroscience*, 21(24):9896–9903. 63, 88, 224

Ploghaus, A., Tracey, I., Gati, J. S., Clare, S., Menon, R. S., Matthews, P. M., and Rawlins, J. N. J. (1999). Dissociating pain from its anticipation in the human brain. *Science*, 284(5422):1979–1981. 32, 169, 212

Ploner, M., Lee, M. C., Wiech, K., Bingel, U., and Tracey, I. (2010). Prestimulus functional connectivity determines pain perception in humans. *Proceedings of the National Academy of*

*Sciences of the United States of America*, 107(1):355–360. 176

Ploner, M., Lee, M. C., Wiech, K., Bingel, U., and Tracey, I. (2011). Flexible cerebral connectivity patterns subserve contextual modulations of pain. *Cerebral Cortex*, 21(3):719–726. 169

Plow, E. B., Pascual-Leone, A., and Machado, A. (2012). Brain stimulation in the treatment of chronic neuropathic and non-cancerous pain. *The Journal of Pain*, 13(5):411–424. 174

Polanía, R., Paulus, W., and Nitsche, M. A. (2012). Modulating cortico-striatal and thalamo-cortical functional connectivity with transcranial direct current stimulation. *Human Brain Mapping*, 33(10):2499–2508. 223

Poncelet, B. P., Wedeen, V. J., Weisskoff, R. M., and Cohen, M. S. (1992). Brain parenchyma motion: measurement with cine echo-planar MR imaging. *Radiology*, 185(3):645–651. 37

Pons, T. P., Garraghty, P. E., Ommaya, A. K., Kaas, J. H., Taub, E., and Mishkin, M. (1991). Massive cortical reorganization after sensory deafferentation in adult macaques. *Science*, 252(5014):1857–1860. 206

Porreca, F., Ossipov, M. H., and Gebhart, G. F. (2002). Chronic pain and medullary descending facilitation. *Trends in Neurosciences*, 25(6):319–325. 16, 23, 106, 177, 189, 226

Portas, C. M., Rees, G., Howseman, A. M., Josephs, O., Turner, R., and Frith, C. D. (1998). A specific role for the thalamus in mediating the interaction of attention and arousal in humans. *Journal of Neuroscience*, 18(21):8979–8989. 142

Price, D. D., Greenspan, J. D., and Dubner, R. (2003). Neurons involved in the exteroceptive function of pain. *Pain*, 106(3):215–219. 4

Price, D. D., McGrath, P. A., Rafii, A., and Buckingham, B. (1983). The validation of visual analogue scales as ratio scale measures for chronic and experimental pain. *Pain*, 17(1):45–56. 29

Proudfit, H. K. (1988). Pharmacologic evidence for the modulation of nociception by noradrenergic neurons. *Progress in brain research*, 77:357–370. 20

Proudfit, H. K. H. and Clark, F. M. F. (1991). The projections of locus coeruleus neurons to the spinal cord. *Progress in brain research*, 88:123–141. 20

Raffin, E., Giraux, P., and Reilly, K. T. (2012a). The moving phantom: motor execution or motor imagery? *Cortex*, 48(6):746–757. 209, 268

Raffin, E. E., Mattout, J. J., Reilly, K. T. K., and Giraux, P. P. (2012b). Disentangling motor execution from motor imagery with the phantom limb. *Brain*, 135(Pt 2):582–595. 206, 209

Raichle, M. E. M., Martin, W. R. W., Herscovitch, P. P., Mintun, M. A. M., and Markham, J. J. (1983). Brain blood flow measured with intravenous H2(15)O. II. Implementation and validation. *Journal of Nuclear Medicine*, 24(9):790–798. 112, 118

Raij, T. T. T., Numminen, J. J., Närvänen, S. S., Hiltunen, J. J., and Hari, R. R. (2005). Brain correlates of subjective reality of physically and psychologically induced pain. *Proceedings of the National Academy of Sciences of the United States of America*, 102(6):2147–2151. 7, 169

Rainville, P., Duncan, G. H., Price, D. D., Carrier, B., and Bushnell, M. C. (1997). Pain affect encoded in human anterior cingulate but not somatosensory cortex. *Science*, 277(5328):968–971. 7

Raj, D., Anderson, A. W., and Gore, J. C. (2001). Respiratory effects in human functional magnetic resonance imaging due to bulk susceptibility changes. *Physics in medicine and biology*, 46(12):3331–3340. 37

Ramachandran, V. S., Rogers-Ramachandran, D., and Stewart, M. (1992). Perceptual correlates of massive cortical reorganization. *Science*, 258(5085):1159–1160. 206

Raoult, H. H., Petr, J. J., Bannier, E. E., Stamm, A. A., Gauvrit, J.-Y. J., Barillot, C. C., and Ferré, J.-C. J. (2011). Arterial spin labeling for motor activation mapping at 3T with a 32-channel coil: reproducibility and spatial accuracy in comparison with BOLD fMRI. *NeuroImage*, 58(1):157–167. 112

Rasmussen, P. V. P., Sindrup, S. H. S., Jensen, T. S. T., and Bach, F. W. F. (2004). Symptoms and signs in patients with suspected neuropathic pain. *Pain*, 110(1-2):9–9. 23

Redgrave, P. P., Prescott, T. J. T., and Gurney, K. K. (1999). The basal ganglia: a vertebrate solution to the selection problem? *Neuroscience*, 89(4):1009–1023. 172

Reilly, K. T., Mercier, C., Schieber, M. H., and Sirigu, A. (2006). Persistent hand motor commands in the amputees' brain. *Brain*, 129(Pt 8):2211–2223. 209

Ren, K. and Dubner, R. (1996). Enhanced descending modulation of nociception in rats with persistent hindpaw inflammation. *Journal of Neurophysiology*, 76(5):3025–3037. 189

Rennefeld, C., Wiech, K., Schoell, E. D., Lorenz, J., and Bingel, U. (2010). Habituation to pain: Further support for a central component. *Pain*, 148(3):6–6. 151

Reynolds, D. V. D. (1969). Surgery in the rat during electrical analgesia induced by focal brain stimulation. *Science*, 164(878):444–445. 9

Rhudy, J. L. and Meagher, M. W. (2000). Fear and anxiety: divergent effects on human pain thresholds. *Pain*, 84(1):65–75. 85

Rice, A. S., Maton, S., and Postherpetic Neuralgia Study Group (2001). Gabapentin in postherpetic neuralgia: a randomised, double blind, placebo controlled study. *Pain*, 94(2):215–224. 82

Ringkamp, M., Raja, S., Campbell, J., and Meyer, R. (2013). Peripheral Mechanisms of Cutaneous Nociception. In *Textbook of Pain*, pages 1–30. Elsevier Saunders. 3

Roelofs, P. D. D. M., Deyo, R. A., Koes, B. W., Scholten, R. J. P. M., and van Tulder, M. W. (2008). Non-steroidal anti-inflammatory drugs for low back pain. *Cochrane database of systematic reviews (Online)*, (1):CD000396. 83

Rose, M. A. and Kam, P. C. A. (2002). Gabapentin: pharmacology and its use in pain management. *Anaesthesia*, 57(5):451–462. 86

Rosier, E. M., Iadarola, M. J., and Coghill, R. C. (2002). Reproducibility of pain measurement and pain perception. *Pain*, 98(1-2):205–216. 29, 74

Rowbotham, M., Harden, N., Stacey, B., Bernstein, P., and Magnus-Miller, L. (1998). Gabapentin for the treatment of postherpetic neuralgia: a randomized controlled trial. *JAMA*, 280(21):1837–1842. 191

Ruscheweyh, R., Marziniak, M., Stumpenhorst, F., Reinholz, J., and Knecht, S. (2009). Pain sensitivity can be assessed by self-rating: Development and validation of the Pain Sensitivity Questionnaire. *Pain*, 146(1-2):65–74. 85

Ruscheweyh, R., Stumpenhorst, F., Knecht, S., and Marziniak, M. (2010). Comparison of the cold pressor test and contact thermode-delivered cold stimuli for the assessment of cold pain sensitivity. *The Journal of Pain*, 11(8):728–736. 151

Salomons, T., Johnstone, T., Backonja, M., Shackman, A., and Davidson, R. (2007). Individual differences in the effects of perceived controllability on pain perception: critical role of the prefrontal cortex. *Journal of Cognitive Neurosciences*, 19:993–1003. 11

Sandkühler, J. J. and Gebhart, G. F. G. (1984). Relative contributions of the nucleus raphe magnus and adjacent medullary reticular formation to the inhibition by stimulation in the periaqueductal gray of a spinal nociceptive reflex in the pentobarbital-anesthetized rat. *Brain Research*, 305(1):77–87. 16

Sawynok, J., Esser, M. J., and Reid, A. R. (2001). Antidepressants as analgesics: an overview of central and peripheral mechanisms of action. *Journal of psychiatry & neuroscience : JPN*, 26(1):21–29. 25

Sawynok, J. J., Reid, A. A., and Meisner, J. J. (2006). Pain Behaviors Produced by Capsaicin: Influence of Inflammatory Mediators and Nerve Injury. *The Journal of Pain*, 7(2):8–8. 151

Scheier, M. F., Carver, C. S., and Bridges, M. W. (1994). Distinguishing optimism from neuroticism (and trait anxiety, self-mastery, and self-esteem): a reevaluation of the Life Orientation Test. *Journal of personality and social psychology*, 67(6):1063–1078. 85

Schweinhardt, P., Glynn, C., Brooks, J., McQuay, H., Jack, T., Chessell, I., Bountra, C., and Tracey, I. (2006). An fMRI study of cerebral processing of brush-evoked allodynia in neuropathic pain patients. *NeuroImage*, 32(1):10–10. 170

Segerdahl, A., Xie, J., and Tracey, I. (2011). Development of a whole brain ASL approach for use in fMRI investigations of tonic pain states. In *DPhil Thesis: Investigation of the neural correlates of ongoing pain states using quantitative perfusion arterial spin labelling.* 117

Seifert, F., Bschorer, K., De Col, R., Filitz, J., Peltz, E., Koppert, W., and Maihöfner, C. (2009). Medial prefrontal cortex activity is predictive for hyperalgesia and pharmacological antihyperalgesia. *Journal of Neuroscience*, 29(19):6167–6175. 13

Serpell, M. G., Others, and Neuropathic pain study group (2002). Gabapentin in neuropathic pain syndromes: a randomised, double-blind, placebo-controlled trial. *Pain*, 99(3):557–566. 82, 199

Sherrington, C. S. (1906). *The Integrative Action of the Nervous System.* Oxford UP. 2, 9

Shmueli, K., van Gelderen, P., de Zwart, J. A., Horovitz, S. G., Fukunaga, M., Jansma, J. M., and Duyn, J. H. (2007). Low-frequency fluctuations in the cardiac rate as a source of variance in the resting-state fMRI BOLD signal. *NeuroImage*, 38(2):306–320. 37

Shrout, P. E. and Fleiss, J. L. (1979). Intraclass correlations: uses in assessing rater reliability. *Psychological bulletin*, 86(2):420–428. 129

Silva, M., Amorim, D., Almeida, A., Tavares, I., Pinto-Ribeiro, F., and Morgado, C. (2013). Pronociceptive changes in the activity of rostroventromedial medulla (RVM) pain modulatory cells in the streptozotocin-diabetic rat. *Brain Research Bulletin*, 96:39–44. 189

Simons, L. E., Moulton, E. A., Linnman, C., Carpino, E., Becerra, L., and Borsook, D. (2012). The human amygdala and pain: Evidence from neuroimaging. *Human Brain Mapping*, pages –. 14

Simpson, D. M., Schifitto, G., Clifford, D. B., Murphy, T. K., Durso-De Cruz, E., Glue, P., Whalen, E., Emir, B., Scott, G. N., Freeman, R., and 1066 HIV Neuropathy Study Group (2010). Pregabalin for painful HIV neuropathy: a randomized, double-blind, placebo-controlled trial. *Neurology*, 74(5):413–420. 83

Singer, T. T., Seymour, B. B., O'Doherty, J. J., Kaube, H. H., Dolan, R. J. R., and Frith, C. D. C. (2004). Empathy for pain involves the affective but not sensory components of pain. *Science*, 303(5661):1157–1162. 7, 32

Siok, C. J., Taylor, C. P., and Hajós, M. (2009). Anxiolytic profile of pregabalin on elicited hippocampal theta oscillation. *Neuropharmacology*, 56(2):7–7. 201

Sivilotti, L. G., Thompson, S. W., and Woolf, C. J. (1993). Rate of rise of the cumulative depolarization evoked by repetitive stimulation of small-caliber afferents is a predictor of action potential windup in rat spinal neurons in vitro. *Journal of Neurophysiology*, 69(5):1621–1631. 21

Smith, A. M. A., Lewis, B. K. B., Ruttimann, U. E. U., Ye, F. Q. F., Sinnwell, T. M. T., Yang, Y. Y., Duyn, J. H. J., and Frank, J. A. J. (1999). Investigation of Low Frequency Drift in fMRI Signal. *NeuroImage*, 9(5):8–8. 111

Smith, S. M. (2002). Fast robust automated brain extraction. *Human Brain Mapping*, 17(3):143–155. 43, 65, 123

Snider, W. D. W. and McMahon, S. B. S. (1998). Tackling pain at the source: new ideas about nociceptors. *Neuron*, 20(4):629–632. 3, 4

Sokolski, K. N., Green, C., Maris, D. E., and DeMet, E. M. (1999). Gabapentin as an adjunct to standard mood stabilizers in outpatients with mixed bipolar symptomatology. *Annals of Clinical Psychiatry*, 11(4):217–222. 88

Spielberger, C. D. (1983). *Manual for the State-trait anxiety inventory (form Y) ("self-evaluation questionnaire")*. Consulting Psychologists Press. 85, 88, 212

Spitzer, M., Böhler, P., Weisbrod, M., and Kischka, U. (1995). A neural network model of phantom limbs. *Biological Cybernetics*, 72:197–206. 206

Stagg, C. J., Bachtiar, V., O'Shea, J., Allman, C., Bosnell, R. A., Kischka, U., Matthews, P. M., and Johansen-Berg, H. (2012). Cortical activation changes underlying stimulation-induced behavioural gains in chronic stroke. *Brain*, 135(Pt 1):276–284. 208

Stagg, C. J., Best, J. G., Stephenson, M. C., O'Shea, J., Wylezinska, M., Kincses, Z. T., Morris, P. G., Matthews, P. M., and Johansen-Berg, H. (2009). Polarity-Sensitive Modulation of Cortical Neurotransmitters by Transcranial Stimulation. *Journal of Neuroscience*, 29(16):5202–5206. 208

Stagg, C. J. and Nitsche, M. A. (2011). Physiological basis of transcranial direct current stimulation. *Neuroscientist*, 17(1):37–53. 208

Stanfa, L. C., Singh, L., Williams, R. G., and Dickenson, A. H. (1997). Gabapentin, ineffective in normal rats, markedly reduces C-fibre evoked responses after inflammation. *Neuroreport*, 8(3):587–590. 82

Steeds (2009). The anatomy and physiology of pain. *Surgery (Oxford)*, 27(12):5–5. 2

Stephenson, D. T. D. and Arneric, S. P. S. (2008). Neuroimaging of Pain: Advances and Future

Prospects. *The Journal of Pain*, 9(7):13–13. 6

Sullivan, M., Bishop, S. R., and Pivik, J. (1995). The pain catastrophizing scale: development and validation. *Psychological assessment*. 85

Sullivan, M. J., Thorn, B., Haythornthwaite, J. A., Keefe, F., Martin, M., Bradley, L. A., and Lefebvre, J. C. (2001). Theoretical perspectives on the relation between catastrophizing and pain. *The Clinical journal of pain*, 17(1):52–64. 85

Suzuki, R., Morcuende, S., Webber, M., Hunt, S. P., and Dickenson, A. H. (2002). Superficial NK1-expressing neurons control spinal excitability through activation of descending pathways. *Nature Neuroscience*, 5(12):1319–1326. 59, 76, 106

Suzuki, R., Rygh, L. J., and Dickenson, A. H. (2004). Bad news from the brain: descending 5-HT pathways that control spinal pain processing. *Trends in Pharmacological Sciences*, 25(12):613–617. 16, 18, 24, 177, 229

Talagala, S. L. S., Ye, F. Q. F., Ledden, P. J. P., and Chesnick, S. S. (2004). Whole-brain 3D perfusion MRI at 3.0 T using CASL with a separate labeling coil. *Magnetic Resonance in Medicine*, 52(1):131–140. 114

Tanabe, M., Takasu, K., Takeuchi, Y., and Ono, H. (2008). Pain relief by gabapentin and pregabalin via supraspinal mechanisms after peripheral nerve injury. *Journal of Neuroscience Research*, 86(15):3258–3264. 191

Taylor, A. M. W. A., Peleshok, J. C. J., and Ribeiro-da Silva, A. A. (2009). Distribution of P2X(3)-immunoreactive fibers in hairy and glabrous skin of the rat. *Journal of Comparative Neurology*, 514(6):555–566. 3

Thunberg, J., Lyskov, E., Korotkov, A., Ljubisavljevic, M., Pakhomov, S., Katayeva, G., Radovanovic, S., Medvedev, S., and Johansson, H. (2005). Brain processing of tonic muscle pain induced by infusion of hypertonic saline. *European Journal of Pain*, 9(2):185–194. 149, 150, 202, 230

Tjandra, T., Brooks, J. C. W., Figueiredo, P., Wise, R., Matthews, P. M., and Tracey, I. (2005). Quantitative assessment of the reproducibility of functional activation measured with BOLD and MR perfusion imaging: Implications for clinical trial design. *NeuroImage*, 27(2):9–9. 111, 112, 169

Torebjörk, H. E., Lundberg, L. E., and LaMotte, R. H. (1992). Central changes in processing of mechanoreceptive input in capsaicin-induced secondary hyperalgesia in humans. *Journal of Physiology*, 448:765–780. 23

Torrance, N., Smith, B. H., Bennett, M. I., and Lee, A. J. (2006). The epidemiology of chronic pain of predominantly neuropathic origin. Results from a general population survey. *The Journal of Pain*, 7(4):281–289. 24

Tracey, I. (2010). Getting the pain you expect: mechanisms of placebo, nocebo and reappraisal effects in humans. *Nature Medicine*, 16(11):1277–1283. 11

Tracey, I. and Mantyh, P. W. (2007). The Cerebral Signature for Pain Perception and Its Modulation. *Neuron*, 55(3):377–391. 7, 107

Tracey, I., Ploghaus, A., Gati, J. S., Clare, S., Smith, S., Menon, R. S., and Matthews, P. M. (2002). Imaging attentional modulation of pain in the periaqueductal gray in humans. *Journal of Neuroscience*, 22(7):2748–2752. 10

Treede, R. D., Rolke, R., Andrews, K., and Magerl, W. (2002). Pain elicited by blunt pressure: neurobiological basis and clinical relevance. *Pain*, 98(3):235–240. 58

Treede, R. D. R., Kenshalo, D. R. D., Gracely, R. H. R., and Jones, A. K. A. (1999). The cortical representation of pain. *Pain*, 79(2-3):105–111. 6

Triantafyllou, C., Hoge, R. D., Krueger, G., Wiggins, C. J., Potthast, A., Wiggins, G. C., and Wald, L. L. (2005). Comparison of physiological noise at 1.5 T, 3 T and 7 T and optimization of fMRI acquisition parameters. *NeuroImage*, 26(1):243–250. 61

Tsuruoka, M. M. and Willis, W. D. W. (1996). Bilateral lesions in the area of the nucleus locus coeruleus affect the development of hyperalgesia during carrageenan-induced inflammation. *Brain Research*, 726(1-2):233–236. 20

Uh, J., Lewis-Amezcua, K., Varghese, R., and Lu, H. (2009). On the measurement of absolute cerebral blood volume (CBV) using vascular-space-occupancy (VASO) MRI. *Magnetic Resonance in Medicine*, 61(3):659–667. 111

Usui, C., Hatta, K., Doi, N., Nakanishi, A., Nakamura, H., and Nishioka, K. (2010). Brain perfusion in fibromyalgia patients and its differences between responders and poor responders to gabapentin. *Arthritis Research and Therapy*, 12(2):R64. 203

Valet, M., Sprenger, T., Boecker, H., Willoch, F., Rummeny, E., Conrad, B., Erhard, P., and Tolle, T. R. (2004). Distraction modulates connectivity of the cingulo-frontal cortex and the midbrain during pain-an fMRI analysis. *Pain*, 109(3):10–10. 10

Vanegas, H. and Schaible, H.-G. (2004). Descending control of persistent pain: inhibitory or facilitatory? *Brain Research Reviews*, 46(3):15–15. 189

Vanneste, S., Plazier, M., Ost, J., van der Loo, E., Van de Heyning, P., and De Ridder, D. (2010). Bilateral dorsolateral prefrontal cortex modulation for tinnitus by transcranial direct current stimulation: a preliminary clinical study. *Experimental Brain Research*, 202(4):779–785. 208

Veit, R., Singh, V., Sitaram, R., Caria, A., Rauss, K., and Birbaumer, N. (2012). Using real-time fMRI to learn voluntary regulation of the anterior insula in the presence of threat-related stimuli. *Social Cognitive and Affective Neuroscience*, 7(6):623–634. 13

Viisanen, H. and Pertovaara, A. (2010). Roles of the rostroventromedial medulla and the spinal 5-HT"1"A receptor in descending antinociception induced by motor cortex stimulation in the neuropathic rat. *Neuroscience Letters*, 476(3):5–5. 16

Vo, T., Rice, A. S. C., and Dworkin, R. H. (2009). Non-steroidal anti-inflammatory drugs for neuropathic pain: how do we explain continued widespread use? *Pain*, 143(3):169–171. 83

von Hehn, C. A. C., Baron, R. R., and Woolf, C. J. C. (2012). Deconstructing the neuropathic pain phenotype to reveal neural mechanisms. *Neuron*, 73(4):638–652. 21, 23

Wager, T. D., Atlas, L. Y., Lindquist, M. A., Roy, M., Woo, C.-W., and Kross, E. (2013). An fMRI-based neurologic signature of physical pain. *The New England journal of medicine*, 368(15):1388–1397. 7

Wager, T. D. T., Rilling, J. K. J., Smith, E. E. E., Sokolik, A. A., Casey, K. L. K., Davidson, R. J. R., Kosslyn, S. M. S., Rose, R. M. R., and Cohen, J. D. J. (2004). Placebo-induced changes in FMRI in the anticipation and experience of pain. *Science*, 303(5661):1162–1167. 11, 32, 169

Wall, P. D. and Gutnick, M. (1974). Ongoing activity in peripheral nerves: the physiology and pharmacology of impulses originating from a neuroma. *Experimental neurology*, 43(3):580–593. 205

Wang, D. J. J., Chen, Y., Fernández-Seara, M. A., and Detre, J. A. (2011). Potentials and challenges for arterial spin labeling in pharmacological magnetic resonance imaging. *Journal of Pharmacology and Experimental Therapeutics*, 337(2):359–366. 113

Wang, J. J., Aguirre, G. K. G., Kimberg, D. Y. D., Roc, A. C. A., Li, L. L., and Detre, J. A. J. (2003). Arterial spin labeling perfusion fMRI with very low task frequency. *Magnetic Resonance in Medicine*, 49(5):796–802. 113

Wang, R., King, T., De Felice, M., Guo, W., Ossipov, M. H., and Porreca, F. (2013). Descending facilitation maintains long-term spontaneous neuropathic pain. *The Journal of Pain*, 14(8):845–853. 16, 24, 177, 189, 229

Wang, Z. Z., Wang, J. J., Connick, T. J. T., Wetmore, G. S. G., and Detre, J. A. J. (2005). Continuous ASL (CASL) perfusion MRI with an array coil and parallel imaging at 3T. *Magnetic Resonance in Medicine*, 54(3):732–737. 117

Wanigasekera, V., Lee, M. C., Rogers, R., Kong, Y., Leknes, S., Andersson, J., and Tracey, I. (2012). Baseline reward circuitry activity and trait reward responsiveness predict expression of opioid analgesia in healthy subjects. *PNAS*, 109(43):17705–17710. 14, 85

Wartolowska, K. and Tracey, I. (2011). Neuroimaging as a tool for pain diagnosis and analgesic development. *Neurotherapeutics*, pages 755–760. 80, 228

Wasan, A. D., Loggia, M. L., Chen, L. Q., Napadow, V., Kong, J., and Gollub, R. L. (2011). Neural Correlates of Chronic Low Back Pain Measured by Arterial Spin Labeling. *Anesthesiology*, 115(2):364–374. 149

Weeks, S. R., Anderson-Barnes, V. C., and Tsao, J. W. (2010). Phantom limb pain: theories and therapies. *Neurologist*, 16(5):277–286. 204

Whiteside, G. T., Adedoyin, A., and Leventhal, L. (2008). Predictive validity of animal pain models? A comparison of the pharmacokinetic-pharmacodynamic relationship for pain drugs in rats and humans. *Neuropharmacology*, 54(5):767–775. 79

Wiberg, M. M., Westman, J. J., and Blomqvist, A. A. (1987). Somatosensory projection to the mesencephalon: an anatomical study in the monkey. *Journal of Comparative Neurology*, 264(1):92–117. 6

Wible, J. H., Tata, P. N. V., Napoli, A. M., Lowe, L. H., and Kearns, G. L. (2009). Pharmacokinetics of gadoversetamide injection, a gadolinium-based contrast agent, in pediatric patients. *Magnetic Resonance Imaging*, 27(4):7–7. 112

Wiech, K., Lin, C.-S., Brodersen, K. H., Bingel, U., Ploner, M., and Tracey, I. (2010). Anterior insula integrates information about salience into perceptual decisions about pain. *The Journal of neuroscience : the official journal of the Society for Neuroscience*, 30(48):16324–16331. 170, 173

Wiech, K., Ploner, M., and Tracey, I. (2008). Neurocognitive aspects of pain perception. *Trends in Cognitive Sciences*, 12(8):8–8. 7, 11, 32

Wiech, K. and Tracey, I. (2009). The influence of negative emotions on pain: Behavioral effects and neural mechanisms. *NeuroImage*, 47(3):8–8. 7, 11

Williams, D. S., Detre, J. A., Leigh, J. S., and Koretsky, A. P. (1992). Magnetic resonance imaging of perfusion using spin inversion of arterial water. *Proceedings of the National Academy of Sciences of the United States of America*, 89(1):212–216. 112, 114

Willis, W. D. (1985). Nociceptive Pathways: Anatomy and Physiology of Nociceptive Ascending Pathways. *Philosophical Transactions of the Royal Society B: Biological Sciences*, 308(1136):253–268. 5

Wise, R. G. and Preston, C. (2010). What is the value of human FMRI in CNS drug development? *Drug Discovery Today*, 15(21-22):8–8. 80, 228

Wise, R. G. and Tracey, I. (2006). The role of fMRI in drug discovery. *Journal of Magnetic Resonance Imaging*, 23(6):862–876. 33

Wong, E. C. E., Buxton, R. B. R., and Frank, L. R. L. (1998). A theoretical and experimental comparison of continuous and pulsed arterial spin labeling techniques for quantitative perfusion imaging. *Magnetic Resonance in Medicine*, 40(3):348–355. 115

Woolf, C. J. (1983). Evidence for a central component of post-injury pain hypersensitivity. *Nature*, pages 1–3. 23, 57

Woolf, C. J. (2010). What is this thing called pain? *The Journal of clinical investigation*, 120(11):3742–3744. 24, 26

Woolf, C. J. (2011). Central sensitization: Implications for the diagnosis and treatment of pain. *Pain*, 152(S):S2–S15. 22, 23, 58, 59, 206, 226

Woolf, C. J. and Mannion, R. J. (1999). Neuropathic pain: aetiology, symptoms, mechanisms, and management. *Lancet*, 353(9168):6–6. 59

Woolf, C. J. and Salter, M. W. (2000). Neuronal plasticity: increasing the gain in pain. *Science*, 288(5472):1765–1769. 21, 23

Worsley, K. J. (2001). Statistical analysis of activation images. *Functional MRI: an introduction to methods*. 32, 45, 66, 92, 182

Wu, B., Lou, X., Wu, X., and Ma, L. (2013). Intraand interscanner reliability and reproducibility of 3D wholebrain pseudocontinuous arterial spinlabeling MR perfusion at 3T. *Journal of Magnetic Resonance ...*. 119, 143, 144

Wu, W.-C. W., Fernández-Seara, M. M., Detre, J. A. J., Wehrli, F. W. F., and Wang, J. J. (2007). A theoretical and experimental investigation of the tagging efficiency of pseudocontinuous arterial spin labeling. *Magnetic Resonance in Medicine*, 58(5):1020–1027. 115

Wu, Y.-T. Y., Lai, M.-H. M., Lu, S.-C. S., and Chang, S.-T. S. (2011). Beneficial response to gabapentin portraying with interval change of brain SPECT imaging in a case with failed back surgery syndrome. *Journal of Clinical Pharmacy and Therapeutics*, 36(4):525–528. 192, 201

Xie, J., Clare, S., Gallichan, D., and Gunn, R. N. (2010). Realtime adaptive sequential design for optimal acquisition of arterial spin labeling MRI data. *Magnetic Resonance ...*. 144

Xie, J. J., Gallichan, D. D., Gunn, R. N. R., and Jezzard, P. P. (2008). Optimal design of pulsed arterial spin labeling MRI experiments. *Magnetic Resonance in Medicine*, 59(4):826–834. 122

Xu, B., Descalzi, G., Ye, H.-R., Zhuo, M., and Wang, Y.-W. (2012). Translational investigation and treatment of neuropathic pain. *Molecular Pain*, 8:15–15. 27

Yacoub, E., Duong, T. Q., van de Moortele, P.-F., Lindquist, M., Adriany, G., Kim, S.-G., Ugurbil, K., and Hu, X. (2003). Spin-echo fMRI in humans using high spatial resolutions and high magnetic fields. *Magnetic Resonance in Medicine*, 49(4):655–664. 59

Yacoub, E., Shmuel, A., Pfeuffer, J., Van De Moortele, P. F., Adriany, G., Andersen, P., Vaughan, J. T., Merkle, H., Ugurbil, K., and Hu, X. (2001). Imaging brain function in humans at 7 Tesla. *Magnetic Resonance in Medicine*, 45(4):588–594. 59

Yaksh, T. L. and Rudy, T. A. (1978). Narcotic analgestics: CNS sites and mechanisms of action as revealed by intracerebral injection techniques. *Pain*, 4(4):299–359. 10, 16, 176

Yarnitsky, D., Sprecher, E., Zaslansky, R., and Hemli, J. A. (1996). Multiple session experimental pain measurement. *Pain*, 67(2-3):327–333. 74

Zambreanu, L., Wise, R. G., Brooks, J. C. W., Iannetti, G. D., and Tracey, I. (2005). A role for the brainstem in central sensitisation in humans. Evidence from functional magnetic resonance imaging. *Pain*, 114(3):397–407. 17, 19, 36, 38, 54, 58, 59, 75, 99, 106, 177, 226

Zemlan, F. P. and Behbehani, M. M. (1988). Nucleus cuneiformis and pain modulation: anatomy and behavioral pharmacology. *Brain Research*, 453(1-2):89–102. 19, 106

Zhang, W.-T., Mainero, C., Kumar, A., Wiggins, C. J., Benner, T., Purdon, P. L., Bolar, D. S., Kwong, K. K., and Sorensen, A. G. (2006). Strategies for improving the detection of fMRI activation in trigeminal pathways with cardiac gating. *NeuroImage*, 31(4):1506–1512. 37

Zhang, Y., Brady, M., and Smith, S. (2001). Segmentation of brain MR images through a hidden Markov random field model and the expectation-maximization algorithm. *Medical Imaging, IEEE Transactions on*, 20(1):45–57. 124

Zhuo, M. (2012). Cortical depression and potentiation: basic mechanisms for phantom pain. *Experimental Neurobiology*, 21(4):129–135. 208

Zhuo, M. and Gebhart, G. F. (1990). Characterization of descending inhibition and facilitation from the nuclei reticularis gigantocellularis and gigantocellularis pars alpha in the rat. *Pain*, 42(3):337–350. 16

Zhuo, M. and Gebhart, G. F. (1992). Characterization of descending facilitation and inhibition of spinal nociceptive transmission from the nuclei reticularis gigantocellularis and gigantocellularis pars alpha in the rat. *Journal of Neurophysiology*, 67(6):1599–1614. 16

Zhuo, M. and Gebhart, G. F. (1997). Biphasic modulation of spinal nociceptive transmission from the medullary raphe nuclei in the rat. *Journal of Neurophysiology*, 78(2):746–758. 16

Ziegler, E. A., Magerl, W., Meyer, R. A., and Treede, R. D. (1999). Secondary hyperalgesia to punctate mechanical stimuli. Central sensitization to A-fibre nociceptor input. *Brain*, 122 ( Pt 12):2245–2257. 23, 58, 86, 179

# Appendix A

## Supplementary Results to Chapter 4

**Supplementary Table 4.1**: Top: Grey matter (GM) absolute CBF during rest. Bottom: Absolute CBF for key ROIs during rest. CBF values represent the group mean extracted from anatomical masks generated as described in Chapter 4 Methods. ROI, region of interest; GM, grey matter; WM, white matter; CBF, cerebral blood flow; SD, standard deviation of the group mean.

| **GM CBF (ml/100g/min)** | | | |
|---|---|---|---|
| Subject | Session1 | Session 2 | Session 3 |
| 1 | 46.48 | 42.90 | 40.62 |
| 2 | 41.65 | 40.70 | 44.69 |
| 3 | 50.87 | 45.31 | 39.40 |
| 4 | 45.74 | 48.33 | 45.16 |
| 5 | 44.33 | 50.72 | 55.81 |
| 6 | 53.79 | 49.48 | 49.65 |
| 7 | 48.40 | 46.24 | 49.91 |
| 8 | 38.09 | 38.40 | 36.30 |
| **Mean** | **46.17** | **45.25** | **45.20** |
| SD | 4.99 | 4.32 | 6.42 |

| **Mean CBF (ml/100g/min)** | | | | | | |
|---|---|---|---|---|---|---|
| ROI | Session 1 | *SD* | Session 2 | *SD* | Session 3 | *SD* |
| GM | 46.17 | 4.99 | 45.25 | 4.34 | 45.20 | 6.42 |
| WM | 25.20 | 3.07 | 24.08 | 2.29 | 24.20 | 3.50 |
| Frontal lobe | 39.76 | 5.43 | 40.27 | 3.77 | 38.97 | 5.07 |
| Temporal lobe | 38.84 | 4.02 | 36.86 | 4.52 | 37.63 | 5.65 |
| Parietal lobe | 43.85 | 5.08 | 43.15 | 4.37 | 42.89 | 6.74 |
| Occipital lobe | 41.49 | 6.09 | 40.42 | 4.88 | 40.61 | 10.33 |
| Insular cortex | 58.84 | 6.98 | 55.13 | 5.48 | 55.37 | 6.85 |
| Thalamus | 52.21 | 9.45 | 46.85 | 7.40 | 50.15 | 9.42 |
| Caudate | 37.62 | 7.61 | 37.95 | 6.84 | 38.01 | 5.60 |
| Putamen | 44.41 | 6.50 | 43.85 | 4.58 | 45.15 | 4.47 |

**Supplementary Table 4.2**: Top: Grey matter (GM) arterial arrival time during rest scans. Bottom: Absolute CBF for key ROIs during rest. Arterial arrival time values represent the group mean extracted from anatomical masks generated as described in Chapter 4 Methods. ROI, region of interest; GM, grey matter; WM, white matter; AAT, arterial arrival time; SD, standard deviation of the group mean.

| **GM AAT (s)** | | | |
|---|---|---|---|
| Subject | Session1 | Session 2 | Session 3 |
| 1 | 1.27 | 1.26 | 1.26 |
| 2 | 1.26 | 1.20 | 1.20 |
| 3 | 1.24 | 1.24 | 1.23 |
| 4 | 1.21 | 1.22 | 1.24 |
| 5 | 1.28 | 1.24 | 1.25 |
| 6 | 1.19 | 1.20 | 1.18 |
| 7 | 1.19 | 1.22 | 1.23 |
| 8 | 1.25 | 1.20 | 1.23 |
| **Mean** | **1.20** | **1.23** | **1.23** |
| SD | 0.04 | 0.02 | 0.02 |

| **Mean AAT (s)** | | | | | | |
|---|---|---|---|---|---|---|
| ROI | Session 1 | *SD* | Session 2 | *SD* | Session 3 | *SD* |
| GM | 1.23 | 0.04 | 1.23 | 0.02 | 1.23 | 0.02 |
| WM | 1.29 | 0.01 | 1.29 | 0.01 | 1.29 | 0.01 |
| Frontal lobe | 1.21 | 0.04 | 1.23 | 0.02 | 1.22 | 0.02 |
| Temporal lobe | 1.21 | 0.03 | 1.21 | 0.03 | 1.19 | 0.04 |
| Parietal lobe | 1.25 | 0.03 | 1.26 | 0.02 | 1.26 | 0.02 |
| Occipital lobe | 1.26 | 0.05 | 1.25 | 0.02 | 1.26 | 0.03 |
| Insular cortex | 1.23 | 0.03 | 1.23 | 0.02 | 1.22 | 0.02 |
| Thalamus | 1.28 | 0.04 | 1.28 | 0.02 | 1.27 | 0.03 |
| Caudate | 1.24 | 0.04 | 1.24 | 0.03 | 1.24 | 0.04 |
| Putamen | 1.21 | 0.04 | 1.21 | 0.03 | 1.19 | 0.04 |

**Supplementary Table 4.3**: Regional F-test statistics comparing all three sessions. ROI, region of interest; GM, grey matter; WM, white matter. CBF, cerebral blood flow; AAT, arterial arrival time. * *Bonferroni* adjusted p-value

**F-tests**

| | **CBF** | | **AAT** | |
|---|---|---|---|---|
| ROI | F | *p-value* | F | *p-value* |
| GM | 0.44 | 0.66 | 0.51 | 0.62 |
| WM | 1.35 | 0.32 | 0.76 | 0.50 |
| Frontal lobe | 0.94 | 0.44 | 0.97 | 0.43 |
| Temporal lobe | 2.63 | 0.14 | 1.57 | 0.27 |
| Parietal lobe | 0.31 | 0.74 | 0.46 | 0.65 |
| Occipital lobe | 0.10 | 0.90 | 0.46 | 0.65 |
| Insular cortex | 1.74 | 0.25 | 0.14 | 0.87 |
| Thalamus | 3.90 | 0.08 | 0.23 | 0.80 |
| Caudate | 0.02 | 0.99 | 6.19 | 0.32* |
| Putamen | 0.37 | 0.71 | 3.66 | 0.09 |

# Appendix B

## Supplementary Results to Chapter 6

### 6.1: Experiment 1

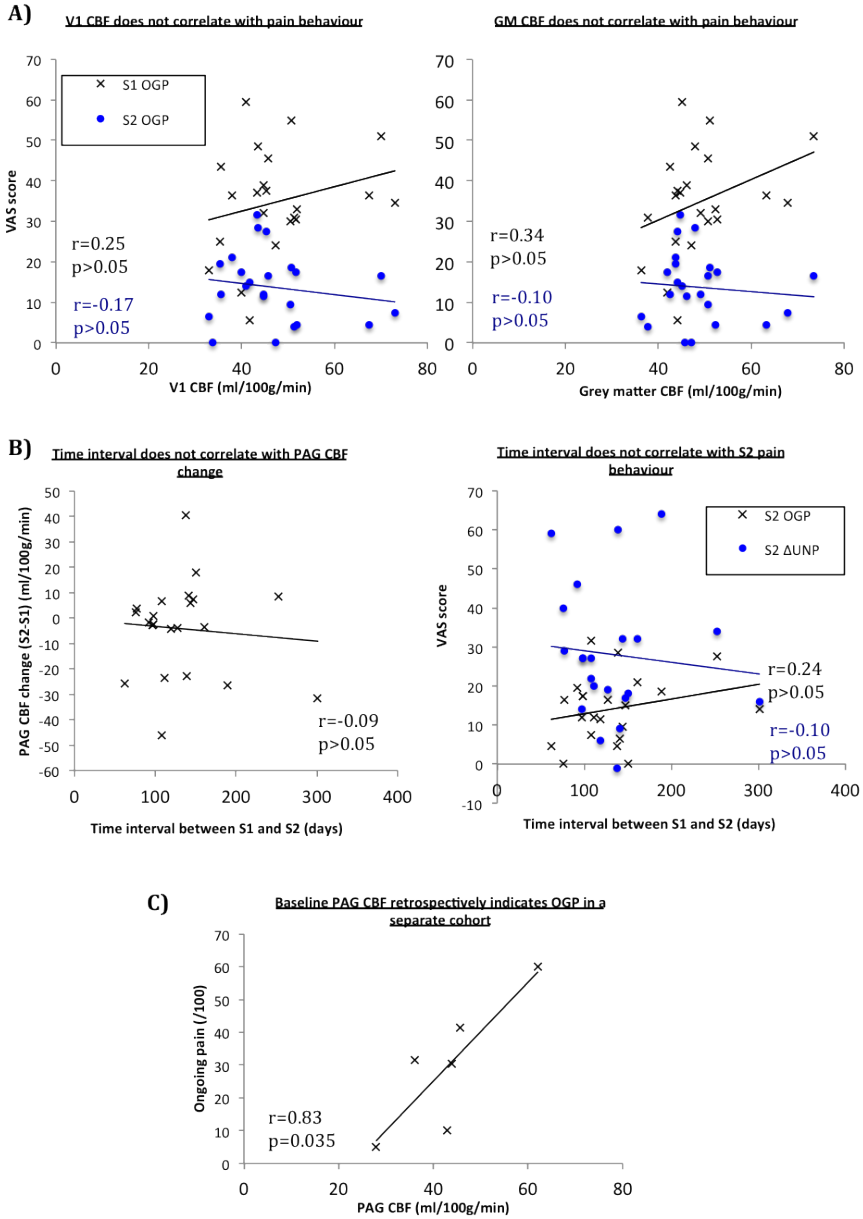


Supplementary to Figure 6.3: **Validation of baseline PAG CBF prediction of pain behaviour.** (a) Primary visual cortex (V1) and grey matter (GM) CBF are not associated with ongoing pain in either session (b) Time interval between sessions 1 and 2 is not associated with session 2 pain scores (c) In a repeated study design with a separate cohort, we reproduce the correlation between ongoing pain scores and baseline PAG CBF measured months later (n=6)

## 6.2: Experiment 2

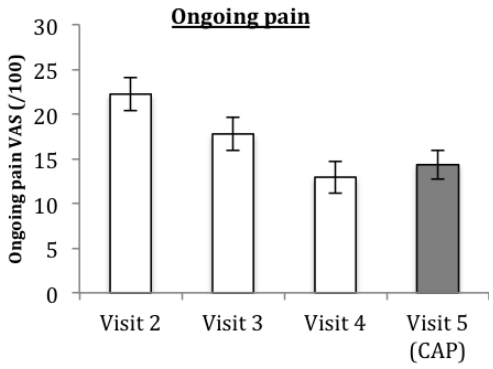


Supplementary to Figure 6.6: **Ongoing pain across all visits in order of visit (average of pre and post scan).** In a time by pain ANOVA between visits 2-4, there is a main effect of visit number on pain ratings (F[21]=6.781,p=0.002). CAP., capsaicin visit.

# Appendix C

## Supplementary Methods to Chapter 7

### Methods

#### Behavioural measures

Behavioural measures were taken prior to and after the scanning/tDCS phase on each visit. These measures included a hand laterality recognition task, an imagery task and pain threshold detection. The hand laterality task tested implicit motor imagery (Moseley, 2004, 2006) by requiring subjects to verbally indicate whether a rotated hand presented to them on a computer screen (Presentation software, version 16.4) was a right or a left hand. The imagery task assessed the ability of subjects to perform or imagine phantom hand and intact hand movements quickly and accurately (Raffin et al., 2012a). Pain thresholds were detected by testing ratings of sharpness of punctate stimulation (8, 16, 32, 64, 128, 256 and 512 mN) on the stump and corresponding area of the intact limb.

#### MRI acquisition

Body localiser scans (7 minutes) were performed while subjects moved their feet, lips, intact hand and phantom hands in a counterbalanced paradigm alternating 4 blocks of 12 s movement with 12 s rest. Resting state scans (5 minutes) were acquired while subjects focused on the fixation cross. Both body localiser and resting state BOLD-EPI scans were collected using a multiband T2*-weighted pulse sequence (Feinberg et al., 2010; Moeller et al., 2010)- TR: 1300 ms; TE: 40 ms; flip angle: 66; FOV: 212x212 mm, 72 2-mm transversal slices for full brain coverage.

During stimulation (20 minutes) subjects were visually instructed to perform five different types of movement (i.e., wrist flexing, hand opening/closing, index finger flexing, ring finger flexing, and fingers adduction), in a block design fashion. Each movement block was repeated four times, twice using the phantom hand only, and twice bimanually. In the bimanual blocks subjects were requested to mirror phantom movement using the intact hand. The protocol consisted of 45 s periods of movement alternated with 15 s of rest. Every 5 minutes subjects were requested to provide a subjective pain rating using a

visually presented analogue scale (VAS). Subjects were videotaped during stimulation sessions, and the degree of volitional movement of the phantom was quantified offline, based on the bimanual (mirror) trials, by a blinded experimenter. Here, an echo-planar T2*-weighted pulse sequence was used to record images based on the BOLD signal (TR: 2000 ms; TE: 30ms; flip angle: 90; volumes 608; FOV: 192mm transversal slices; 35 slices with slice thickness 3.0 mm, with partial cerebellum coverage).